Prepared for
Montana Resources, LLC
600 Shields Avenue
Butte, Montana
USA, 59701

Prepared by
Knight Piésold Ltd.
Suite 1400 - 750 West Pender Street
Vancouver, British Columbia
Canada, V6C 2T8

VA101-126/24-7

MONTANA RESOURCES
YANKEE DOODLE TAILINGS IMPOUNDMENT - DAM BREACH INUNDATION STUDY FOR THE 6,560 AMENDMENT DESIGN DOCUMENT

Rev	Description	Date
0	Issued in Final	December 20, 2024

Knight Piésold CONSULTING

Management System Certified By:
bsi
ISO 9001 Quality Management Systems CERTIFIED FS 64925
ISO 14001 Environmental Management CERTIFIED EMS 550121
ISO 45001 Occupational Health and Safety Management CERTIFIED OHS 550122

EXECUTIVE SUMMARY

Montana Resources, LLC (MR) is in the process of preparing a permit amendment application (the 6,560 Amendment Application) for continued development of the Yankee Doodle Tailings Impoundment (YDTI) above the currently permitted maximum embankment crest elevation of 6,450 ft. The proposed amendment considers raising the crest elevation (EL.) in two or more lifts to EL. 6,560 ft to facilitate continued mining until the mid-2050s. The permit amendment application process requires the permit applicant (MR) to submit a design document related to the proposed facility expansion. Knight Piésold Ltd. (KP) prepared this dam breach inundation study to estimate the potential consequences of a hypothetical dam failure at the ultimate proposed configuration (prior to closure) of the YDTI to support the 6,560 Amendment Design Document. This dam breach inundation study is not a risk assessment and explicitly does not include an assessment of the likelihood of a dam breach occurrence.

The information for the facility used in this study included the YDTI embankment design, recent and projected topography around the mine site area, and cone penetration test (CPT) and rheology data to characterize the tailings, as recommended in the Global Industry Standard on Tailings Management (GISTM, 2020). The applied methodology followed the current state of practice outlined in recent and most comprehensive guidelines on this topic such as the Technical Bulletin on Tailings Dam Breach Analysis (CDA, 2021) and Bulletin No. 194, Version 1.0, Tailings Dam Safety (ICOLD, 2022). The modeling results are intended to assist in characterizing the potential physical impacts in terms of inundation and inform the assessment of risk of this proposed future facility arrangement.

The breach analysis was conducted for a hypothetical erosional Flood Induced scenario through evaluating possible ranges for various breach parameters to understand the sensitivity of the peak discharge and the shape of the breach outflow hydrograph. Breach hydrographs were simulated using the U.S. Army Corps of Engineers Hydrologic Engineering Center River Analysis System (HEC-RAS) Version 6.2 software, which can model non-Newtonian tailings flows. The selected outflow hydrographs for the Flood Induced scenario were then used as inputs for the downstream flood routing, which was also completed using HEC-RAS. Concurrent flows from the catchments surrounding the YDTI were assumed to be equivalent to the probable maximum flood (PMF) event generated by the 24-hour probable maximum precipitation (PMP) combined with a complete melt of the 1 in 100-year snowpack.

The components of the breach outflow volume considered the volume of free water in the YDTI (i.e., supernatant pond), the mobilized tailings through erosion and/or liquefaction, and the eroded dam materials. Where appropriate, the impact of the tailings rheology on the breach runout characteristics were considered by using the non-Newtonian fluid approximation. The uncertainties related to the selection of the breach parameters, the rheological parameters, or the Manning's roughness parameter were all evaluated through sensitivity analyses to understand the impact on the results. It was found that some parameters were more sensitive than others; however, the overall impact on the outcome of the study was found not to be substantial and the findings remain unchanged.

The inundation results downstream of the dam were presented on inundation maps in terms of maximum inundation extents, maximum inundation depths, peak discharges, as well as flood wave and peak discharge arrival times. The results of the Flood Induced scenario demonstrate that the hypothetical breach outflow could impact structures around the Horseshoe Bend (HsB) area, including the HsB Water Treatment Plant, as well as pipelines, access roads, and open pits within the mine property boundary. The flood wave was predicted to be fully contained within the Berkeley and Continental Pits without reaching the city of Butte.

Considering that the study indicates the inundation limits of the Flood Induced scenario would be contained within the mine site boundary, it was deemed reasonable to exclude modeling of the Fair Weather scenario. An erosional Fair Weather dam breach occurring in the same location could reasonably be expected to result in similar potential impacts around the site, but with less outflow from the YDTI and correspondingly less volume entering the Berkeley and Continental Pits.

The modeled inundation extent is largely controlled by the presence of the Berkeley Pit and the expanded limits of the Continental Pit, which allows the pits to intercept the potential outflow from the hypothetical breach. The expanded footprint of the Continental Pit is made possible by continued mining at the site.

TABLE OF CONTENTS

PAGE

Executive Summary I

Table of Contents i

1.0 Introduction 1
1.1 Overview 1
1.2 Scope of Work 3
1.3 Limitations 3

2.0 Project Background 4
2.1 Yankee Doodle Tailings Impoundment 4
2.1.1 General 4
2.1.2 Tailings Dam Hazard Classification 4
2.2 Areas of Potential Impacts 7
2.3 Site Hydrology 7
2.3.1 General 7
2.3.2 Upstream and Downstream Drainage Network 7
2.3.3 Initial Pond Conditions in the YDTI 9
2.3.4 Initial Conditions in the Pits 10
2.4 Tailings Characteristics and Rheology 11
2.4.1 General 11
2.4.2 Tailings Characterization 11
2.4.3 Tailings Liquefaction Potential 13
2.4.4 Tailings Rheology 15

3.0 Failure Scenarios and Failure Modes 19
3.1 Failure Scenarios 19
3.2 Physical Processes During Dam Failure 19
3.3 Failure Modes and Failure Mechanisms 21
3.3.1 Failure Modes 21
3.3.2 Flood Induced Failure Mechanism and Assumptions 22

4.0 Dam Breach Analysis 23
4.1 General 23
4.2 Volume of Mobilized Water and Tailings 23
4.2.1 Overview 23
4.2.2 Flood Induced Breach Volume 24
4.3 Breach Outflow Hydrographs 26
4.3.1 Dam Breach Parameters 26
4.3.2 Breach Outflow Hydrograph Development and Sensitivity 27

4.3.3 Comparison of Breach Parameters to Past Failures 30
4.4 Breach Outflow Characteristics 34

5.0 Flood Routing Model Development 35
5.1 General 35
5.2 Elevation Data 35
5.3 Flood Routing Model Setup 37

6.0 Flood Induced Scenario Modeling Results 38
6.1 General 38
6.2 Breach Flood Routing Results 38
6.3 Impacts to Open Pits 42
6.4 Sensitivity Analysis 43
6.4.1 General 43
6.4.2 Breach Hydrograph 43
6.4.3 Tailings Rheology 45
6.4.4 Manning's n 47

7.0 Conclusions 49

8.0 References 51

9.0 Certification 55

TABLES

Table 2.1 Yield Stress and Viscosity for C_v used for Modeling 18
Table 2.2 Yield Stress and Viscosity as a Function of C_v used for Modeling 18
Table 4.1 Estimated Water and Tailings Volumes in the Flood Induced Breach Outflows 25
Table 4.2 Breach Parameters and Peak Discharge Estimates for YDTI Flood Induced Breach 27
Table 4.3 Peak Discharge and Selected Breach Parameters 29

FIGURES

Figure 1.1 Yankee Doodle Tailings Impoundment – Project Arrangement 2
Figure 2.1 Yankee Doodle Tailings Impoundment – Life of Mine Design 5
Figure 2.2 Yankee Doodle Tailings Impoundment – North-South Embankment Typical Section 6
Figure 2.3 Yankee Doodle Tailings Impoundment – Catchment Areas 8
Figure 2.4 YDTI Supernatant Pond Elevation-Capacity Curve 9
Figure 2.5 Berkeley Pit Elevation-Capacity Curve – Initial Conditions 10
Figure 2.6 Continental Pit Elevation-Capacity Curve – Initial Conditions 10
Figure 2.7 Rheology and CPT Testing Locations in the YDTI 11
Figure 2.8 Grain Size Distribution for YDTI Tailings (P&C, 2022) 12
Figure 2.9 Micro-Photographs of the +300 μm Size Fraction (P&C, 2022) 13
Figure 2.10 CPT Analysis for SCPT21-S1 14

Figure 2.11 CPT Analysis for SCPT21-S4 14
Figure 2.12 YDTI Tailings Yield Stress and Viscosity (P&C, 2022) 16
Figure 2.13 Yield Stress and Viscosity Data Comparison Based on Literature 17
Figure 3.1 Conceptual TDBA Cases (CDA, 2021) 19
Figure 3.2 Post-Failure Cone of Depression for the Merriespruit Dam Failure (CDA, 2021) 21
Figure 4.1 Schematic of Mobilized Materials in a Tailings Dam Breach Event 24
Figure 4.2 Breach Geometry for the Flood Induced Failure 25
Figure 4.3 Comparison of Predicted Outflow Volume to Observed Outflow Volumes in Past Failures of Tailings Dams (adapted from Rana et al., 2021a) 26
Figure 4.4 Breach Parameters Sensitivity Analysis 28
Figure 4.5 Flood Induced Breach Outflow Hydrographs 29
Figure 4.6 Comparison to Observed Breach Heights and Breach Formation Times for Past Failures of Water and Tailings Dams 30
Figure 4.7 Comparison to Observed Breach Heights and Breach Widths for Past Failures of Water and Tailings Dams 32
Figure 4.8 Comparison of Observed Eroded Dam Volumes and Predicted Eroded Dam Volumes for Past Failures of Water and Tailings Dams 33
Figure 4.9 Flow Behavior as a Function of Solids Concentration (CDA, 2021) 34
Figure 5.1 Overview of the Terrain used in the Breach Flood Routing Models 36
Figure 6.1 Flood Induced Scenario – Maximum Inundation and Flow Depth Map 39
Figure 6.2 Flood Induced Scenario – Maximum DV Map 40
Figure 6.3 Flood Induced Scenario – Flood Wave Arrival Times Map 41
Figure 6.4 Berkeley Pit Elevation-Capacity Curve with Breach Inflow 42
Figure 6.5 Continental Pit Elevation-Capacity Curve with Breach Inflow 43
Figure 6.6 Flood Induced Scenario Inundation Extent – Breach Hydrograph Sensitivity 44
Figure 6.7 Flood Induced Scenario Inundation Extent – Rheology Sensitivity 46
Figure 6.8 Flood Induced Scenario Inundation Extent – Manning's n Sensitivity 48

APPENDICES

Appendix A Montana Resources Rheology: Test Work Report
Appendix B Inundation Maps for Flood Induced Dam Breach

ABBREVIATIONS

2D ..... two-dimensional
ac-ft ..... acre-ft
ACC ..... Anaconda Copper Company
CDA ..... Canadian Dam Association
CPT ..... cone penetration test
CS ..... Capture System
C_v, %v ..... solids concentration by volume
C_w, %m ..... solids concentration by weight
DEM ..... digital elevation model
DV ..... depth-velocity product
EL. ..... elevation
FEMA ..... Federal Emergency Management Agency
FERC ..... Federal Energy Regulatory Commission
FS ..... Factor of Safety
ft ..... feet, foot
GISTM ..... Global Industry Standard on Tailings Management
h:mm ..... hours:minutes
H:V ..... horizontal distance to vertical rise
HEC-RAS ..... Hydrologic Engineering Center River Analysis System
hr ..... hour
HsB ..... Horseshoe Bend
ICOLD ..... International Commission on Large Dams
KP ..... Knight Piésold Ltd.
LiDAR ..... Light Detection and Ranging
LLA ..... Loss of Life Analysis
m ..... meter
M m^3 ..... million cubic meters
MDEQ ..... Montana Department of Environmental Quality
min ..... minute
MR ..... Montana Resources, LLC
Pa·s ..... Pascal·second
PMF ..... probable maximum flood
PMP ..... probable maximum precipitation
PSD ..... particle size distribution
RDS ..... rock disposal site
TDBA ..... Tailings Dam Breach Analysis
the Design Document ..... 6,560 Amendment Design Document
TSF ..... Tailings Storage Facility
USACE ..... U.S. Army Corps of Engineers
USBR ..... U.S. Bureau of Reclamation
WTP ..... Water Treatment Plant
YDTI ..... Yankee Doodle Tailings Impoundment

1.0 INTRODUCTION

1.1 OVERVIEW

Montana Resources, LLC (MR) operates an open pit copper and molybdenum mine located in Butte, Montana. The tailings from ore processing are conveyed to the Yankee Doodle Tailings Impoundment (YDTI) for disposal and permanent storage. The mine is located in Silver Bow County and is bounded by Interstate 15 and the Continental Divide on the east, Moulton Reservoir Road on the west, and Farrell Street, Continental Drive, and Shields Avenue to the south.

The key components of the MR mine site facilities, as shown on Figure 1.1, include the following:

- Yankee Doodle Tailings Impoundment
- Berkeley Pit
- Continental Pit
- Mill and processing facilities
- Horseshoe Bend (HsB) area and associated facilities

Coordinates and elevations in this report are referenced to the site coordinate system known as the 'Anaconda Mine Grid' established by The Anaconda Company in 1957. The Anaconda Mine Grid is based on the Anaconda Copper Company (ACC) Datum established in 1915. All elevations are stated in Anaconda Mine Grid coordinates with respect to the ACC Vertical Datum utilizing International Feet unless specifically stated otherwise.

There are two open pits within the mine boundary, the Berkeley Pit and the Continental Pit. Mining of the Berkeley Pit began in 1955 and ceased in 1982. When mining and dewatering of the Berkeley Pit concluded, the water levels in the pit began to rise due to inflows from the surrounding aquifers and surface water runoff. The maximum level in the Berkeley Pit is currently limited to an elevation (EL.) of 5,466 ft that represents the Protective Water Level; however, the current operating level is managed via pumping at a constant elevation of approximately 5,412 ft. Mining of the Continental Pit started in 1986 and is currently projected to continue until the mid-2050s. The mine operation incorporates a mill ore throughput of approximately 49,000 tons per day.

The tailings dam breach analysis (TDBA) presented in this report considers a hypothetical failure of the YDTI with embankments raised to EL. 6,560 ft to determine the potential inundation extent at the end of operations. Knight Piésold Ltd. (KP) prepared this dam breach inundation study to estimate the potential consequences of a hypothetical dam failure at the ultimate proposed configuration (prior to closure) of the YDTI to support the 6,560 Amendment Design Document (the Design Document). This study uses current information for the facility, including the embankment design, recent and projected topography around the mine site area that includes future Continental Pit expansion and preliminary waste rock placement plans. Available cone penetration test (CPT) data and tailings rheology data from the YDTI were used to characterize the tailings, as recommended in the Global Industry Standard on Tailings Management (GISTM, 2020). The applied methodology in this study follows the current state of practice for TDBA based on International Commission on Large Dams (ICOLD) guidelines (ICOLD, 2022) and Canadian Dam Association (CDA) guidelines (CDA, 2021), which includes considering potential tailings runout as a non-Newtonian fluid or mudflow where appropriate. This dam breach inundation study is not a risk assessment and explicitly does not include an assessment of the likelihood of a dam breach occurrence.

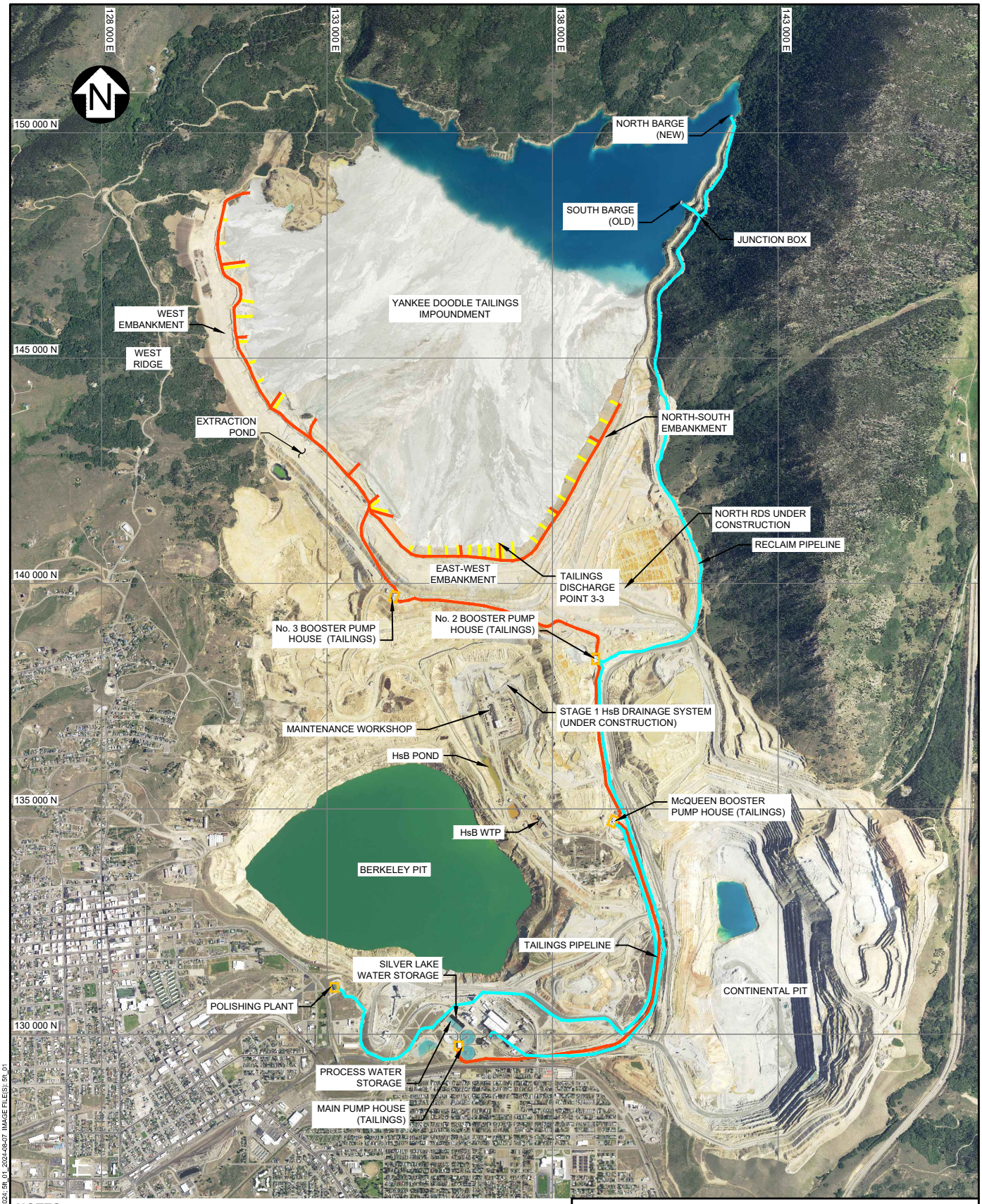

NOTES:

1. COORDINATE SYSTEM AND ELEVATIONS ARE BASED ON ANACONDA MINE GRID.
2. AERIAL IMAGE PROVIDED BY MONTANA RESOURCES, LLC ON AUGUST 7, 2024.

SCALE A: 1500 0 1500 3000 4500 6000 7500 ft

REV	DATE	DESCRIPTION	DESIGNED	DRAWN	REVIEWED
0	19DEC'24	ISSUED WITH REPORT	DBM	RMM	DDF

MONTANA RESOURCES, LLC

MONTANA RESOURCES

YANKEE DOODLE TAILINGS IMPOUNDMENT PROJECT ARRANGEMENT

Knight Piésold CONSULTING

P/A NO. VA101-126/24

REF NO. 7

FIGURE 1.1

REV 0

SAVED: M:\1\101\00126\24\AA\acad\FIGS\A59_12/18/2024 9:35:50 AM_RLI PRINTED: 12/18/2024 9:36:19 AM, FIG 1.1, RLI
XREF FILE(S): Tailings Spigots and Reclaim Pipelines - June 2024_5ft_01_2024-08-07 IMAGE FILE(S): 5ft_01

1.2 SCOPE OF WORK

Two hydrologic conditions are typically considered for a dam breach assessment, as outlined in the Federal Emergency Management Agency (FEMA) guidelines (FEMA, 2013), which are consistent with guidelines from ICOLD (2022) and CDA (CDA, 2013, 2019, and 2021):

1. Flood Induced (hydrologic or Rainy Day) scenario assuming failure due to an extreme flood event.
2. Fair Weather (non-hydrologic or Sunny Day) scenario assuming failure occurs during normal operations and may be caused by an earthquake, internal erosion/piping, foundation failure, mis-operation of the facility, or other event.

This report only considers an erosional failure of the Flood Induced scenario at the end of operations for a dam crest elevation of 6,560 ft. The study indicates that the inundation limits of the Flood Induced scenario are contained within the mine site boundary. Therefore, it was considered reasonable to exclude detailed modeling of an erosional Fair Weather scenario with a much smaller supernatant pond and breach outflow volume occurring at the same location, as it could be reasonably expected to result in similar potential impacts around the site, but with correspondingly less volume predicted to enter the Berkeley and Continental Pits.

A detailed dam breach assessment includes dam breach analysis, hydrodynamic modeling of the dam breach flood wave propagation, deposition analysis for the liquefied tailings runout where appropriate, and inundation and deposition mapping. Potential inundation results are presented in terms of maximum inundation extents, peak discharges, breach flood wave arrival times, and changes in maximum depths at locations of interest. Hydrographs are provided for various points of interest depicting flood wave propagation and attenuation. The modeling results are intended to assist in characterizing the potential physical impacts in terms of inundation and inform the assessment of risk of this proposed future facility arrangement. TDBAs are also commonly used to confirm the dam hazard potential consequence classification and support emergency response planning.

1.3 LIMITATIONS

This study is not intended to be a risk assessment for the tailings dam, and as such, the likelihood of the failure demonstrated with dam breach modeling presented herein was specifically ignored. The results of this analysis do not reflect on the structural integrity or safety of the facility. This study does not account for the design safety measures, management practices, or regulatory requirements implemented to prevent a failure from occurring. Rather, it was assumed that a hypothetical failure of the YDTI could occur, so that the area of impact could be determined. Furthermore, this study does not include a detailed evaluation of downstream consequences (e.g., potential loss of life, or economic values) within the inundation extents; however, the results of this study can be used to undertake these additional assessments, as required.

There are limitations in accurately modeling the effects of a dam breach, primarily because the science is still evolving and some of the physical mechanisms that are represented in the models are not completely understood. The numerous uncertainties inherent to dam breach and inundation modeling are treated in this study in a way that the resulting inundation limits are approximate, but conservative. This study follows the general guidelines from internationally respected institutions, such as the CDA and the ICOLD, and follows the requirements outlined in the GISTM (2020), such as using site specific tailings characterization data.

2.0 PROJECT BACKGROUND

2.1 YANKEE DOODLE TAILINGS IMPOUNDMENT

2.1.1 GENERAL

The YDTI is the tailings storage facility (TSF) for the mine. It comprises a valley-fill style impoundment created by a continuous rockfill embankment as shown on Figure 2.1. The YDTI embankment was originally constructed in 1963 using rockfill from the Berkeley Pit and has been continuously raised to EL. 6,450 ft using rockfill from the Berkeley Pit (until 1982) and from the Continental Pit (since 1986). This dam breach study specifically considers the proposed ultimate arrangement at the end of mining operations with the YDTI constructed to EL. 6,560 ft. The embankment is divided into three rockfill embankments according to the general geometry of each limb of the continuous embankment for descriptive purposes. These embankments are the:

- North-South Embankment – forms the eastern to southeastern limb of the YDTI and runs approximately north to south in orientation. The North-South Embankment abuts onto the base of Rampart Mountain, forming the eastern limit of the MR mine site.
- East-West Embankment – forms the southwestern limb of the YDTI and runs approximately east to west in orientation. The East-West Embankment is constructed upstream of the HsB area and of the Berkeley Pit.
- West Embankment – forms the western limb of the YDTI and runs approximately north to south in orientation. The West Embankment is constructed along the side of the West Ridge and forms the western battery limit of the facility.

A plan view showing the current YDTI general arrangement and downstream facilities is shown on Figure 1.1. The YDTI plan view and a typical cross section for the North-South Embankment for the facility arrangement at EL. 6,560 ft are shown on Figure 2.1 and Figure 2.2, respectively.

2.1.2 TAILINGS DAM HAZARD CLASSIFICATION

The jurisdiction for regulation of tailings impoundments resides with the Montana Department of Environmental Quality (MDEQ), as noted in the Design Basis Report (KP, 2024a). Dams for tailings impoundments and water reservoirs subject to permits issued by MDEQ are specifically exempt from provisions of the Montana Dam Safety Act (MCA 85-15-107), and therefore are not subject to dam hazard potential classification within the state (MCA 85-15-209). Hazard potential classification is not specifically required for the YDTI because the governing legislation for new TSFs requires that the design be sufficient to manage (unless approved otherwise by the Independent Review Panel):

- The Probable Maximum Flood (PMF)
- The Maximum Credible Earthquake or 1 in 10,000-year return period event, whichever is larger.

The corresponding YDTI design criteria are consistent with the above requirements.

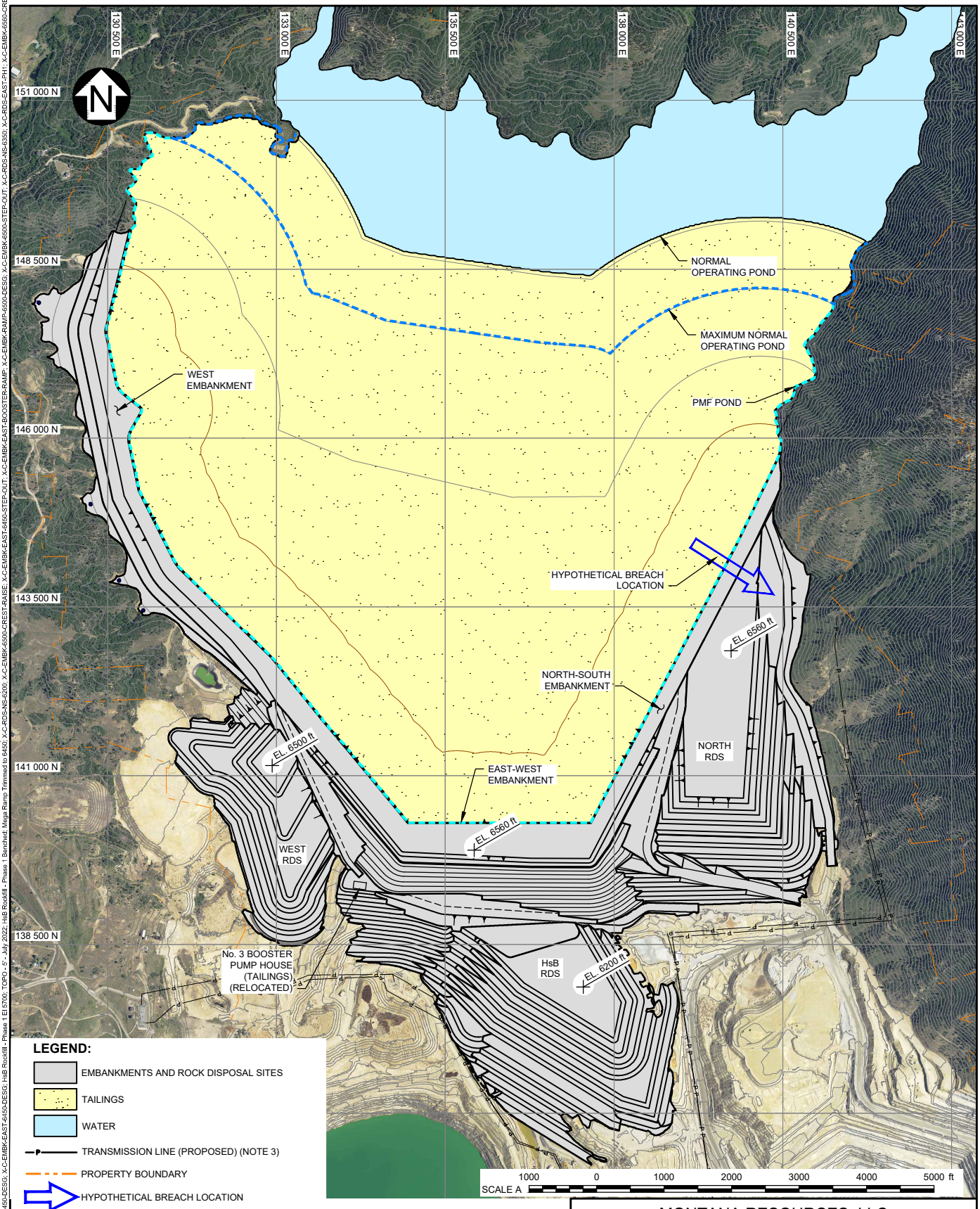

LEGEND:

- EMBANKMENTS AND ROCK DISPOSAL SITES
- TAILINGS
- WATER
- TRANSMISSION LINE (PROPOSED) (NOTE 3)
- PROPERTY BOUNDARY
- HYPOTHETICAL BREACH LOCATION

NOTES:

1. COORDINATE SYSTEM AND ELEVATIONS BASED ON ANACONDA MINE GRID.
2. AERIAL IMAGE PROVIDED BY MONTANA RESOURCES, LLC ON AUGUST 7, 2024.
3. HIGH VOLTAGE TRANSMISSION LINE IS APPROXIMATE AS PROVIDED BY MR IN SEPTEMBER 2023. LAYOUT BY NORTHWEST ENERGY.

REV	DATE	DESCRIPTION	DESIGNED	DRAWN	REVIEWED
0	19DEC'24	ISSUED WITH REPORT	DBM	RMM/PP	DDF

MONTANA RESOURCES, LLC

MONTANA RESOURCES

YANKEE DOODLE TAILINGS IMPOUNDMENT LIFE OF MINE DESIGN

Knight Piésold CONSULTING

P/A NO. VA101-126/24

REF NO. 7

FIGURE 2.1

REV 0

SAVED: M:\1\101\00126\24\AA\acad\FIGS\A56, 12/19/2024 2:54:39 PM, HWONG, PRINTED: 12/19/2024 3:00:24 PM, FIG 2.1, RLI ACAD VERSION: 25.0S (LMS TECH)
XREF FILE(S): X-C-PROP-BND~2020; X-C-EMBK-WEST-6450-DESG; HsB Rockfill - Phase 1 El 6700; TOPO - 5' - July 2022; HsB Rockfill - Phase 1 Benched; Mega Ramp Trimmed to 6450; X-C-RDS-NS-6200; X-C-EMBK-6500-CREST-RAISE; X-C-EMBK-EAST-6450-STEP-OUT; X-C-EMBK-EAST-BOOSTER-RAMP; X-C-EMBK-RAMP-6800-DESG; X-C-EMBK-6800-STEP-OUT; X-C-RDS-NS-6350; X-C-RDS-EAST-PH1; X-C-EMBK-6680-CREST-I

SAVED: M:\1\01\00126\24\A\Acad\FIGS\A57, 11/20/2024 9:17:09 AM , RMCLELLAN PRINTED: 12/18/2024 9:49:04 AM, FIG 2.2, RLI ACAD VERSION: 25.0S (LMS TECH)
XREF FILE(S): Sections IMAGE FILE(S):

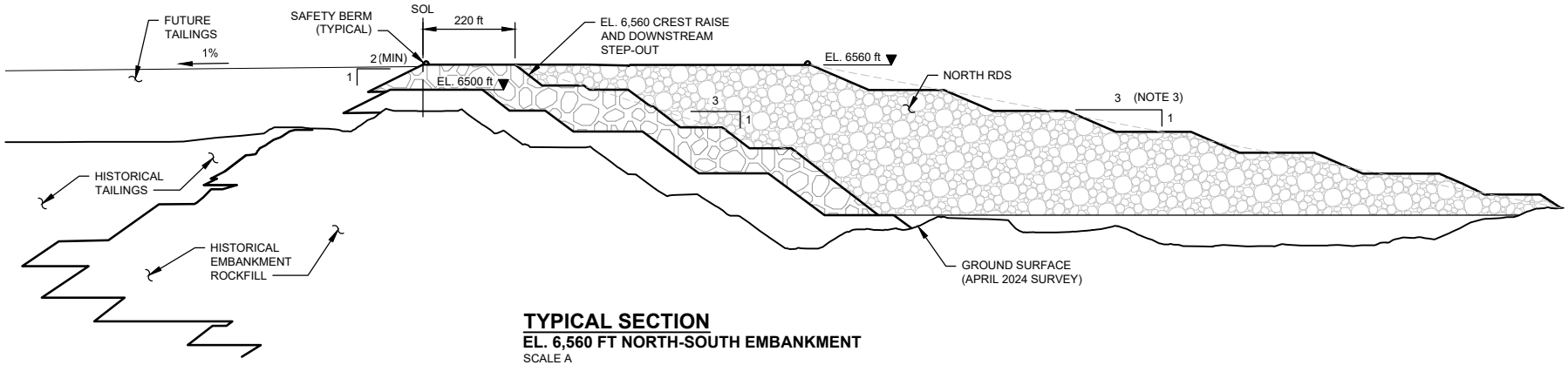

TYPICAL SECTION
EL. 6,560 FT NORTH-SOUTH EMBANKMENT
SCALE A

LEGEND:

- EMBANKMENT ROCKFILL
- ROCK DISPOSAL SITE / RAMPS / OTHER
- OUTLINE FOR CONCEPTUAL FUTURE CONSTRUCTION AREAS

NOTES:

1. COORDINATE SYSTEM AND ELEVATIONS ARE BASED ON ANACONDA MINE GRID.
2. APRIL 2024 TOPOGRAPHY (EXISTING GROUND) PROVIDED BY MONTANA RESOURCES, LLC IN MAY 2024.
3. RDS IS LAID OUT WITH AN OVERALL DOWNSTREAM SLOPE OF 3H:1V. SECTION SHOWN IS NOT PERPENDICULAR TO RDS CREST.

SCALE A: 200 0 200 400 600 800 1000 ft

REV	DATE	DESCRIPTION	DESIGNED	DRAWN	REVIEWED
0	19DEC'24	ISSUED WITH REPORT	DBM	RMM/PP	DDF

MONTANA RESOURCES, LLC

MONTANA RESOURCES

YANKEE DOODLE TAILINGS IMPOUNDMENT
NORTH-SOUTH EMBANKMENT
TYPICAL SECTION

Knight Piésold CONSULTING

P/A NO. VA101-126/24 | REF NO. 7

FIGURE 2.2 | REV 0

2.2 AREAS OF POTENTIAL IMPACTS

The flood wave generated due to a hypothetical dam breach would flow south towards Berkeley and Continental Pits. The mine site areas potentially impacted between the YDTI and open pits include the HsB Water Treatment Plant (HsB WTP), HsB Capture System (HsB CS) pump house, Precipitation Plant, and the McQueen and No. 2 tailings booster pump houses. The tailings distribution and reclaim water pipelines and various mine access roads also run through the potentially affected area. The HsB area, which currently contains several facilities and buildings, including the truck maintenance workshop, is planned to be infilled with rockfill as part of the proposed life of mine design (KP, 2024b).

The mine Concentrator Area and the city of Butte are located to the south of the open pits, approximately three miles away from the hypothetical North-South Embankment breach location. If the breach outflow was to flow past the open pits, it would have the potential to reach these areas; however, the pits are predicted to fully intercept the breach flood wave, as discussed in detail in Section 6.

2.3 SITE HYDROLOGY

2.3.1 GENERAL

The following Flood Induced hydrologic conditions were considered for this dam breach study:

- The initial conditions in the YDTI including the elevation, volume, and configuration of the supernatant pond.
- The initial flow conditions associated with the drainage area upstream of the YDTI that may contribute flows to the YDTI.
- The initial flow conditions from the drainage areas that contribute to the Berkeley and Continental Pits located directly downstream of the YDTI, as the capacity of these pits will determine whether the breach outflow may reach Butte.

The initial flow conditions in the contributing catchment areas are associated with the PMF event, which is generated by a combined occurrence of both the 24-hour probable maximum precipitation (PMP) and the complete melt of the 1 in 100-year snowpack (KP, 2024a). These hydrologic conditions are used for determining the potential breach outflow volumes, as well as for conducting the downstream flood routing, inundation mapping, and consequence evaluation.

2.3.2 UPSTREAM AND DOWNSTREAM DRAINAGE NETWORK

The mine is located in the northeastern part of the city of Butte, Montana. The future life of mine YDTI design configuration and the surrounding catchments are shown on Figure 2.3. The catchments directly above the YDTI contributing inflows to the YDTI are Moulton Reservoir Watershed, Yankee Doodle Creek Watershed, Yankee Doodle Tributary Watershed, West YDTI, Silver Bow Creek Watershed, and Dixie Creek Watershed.

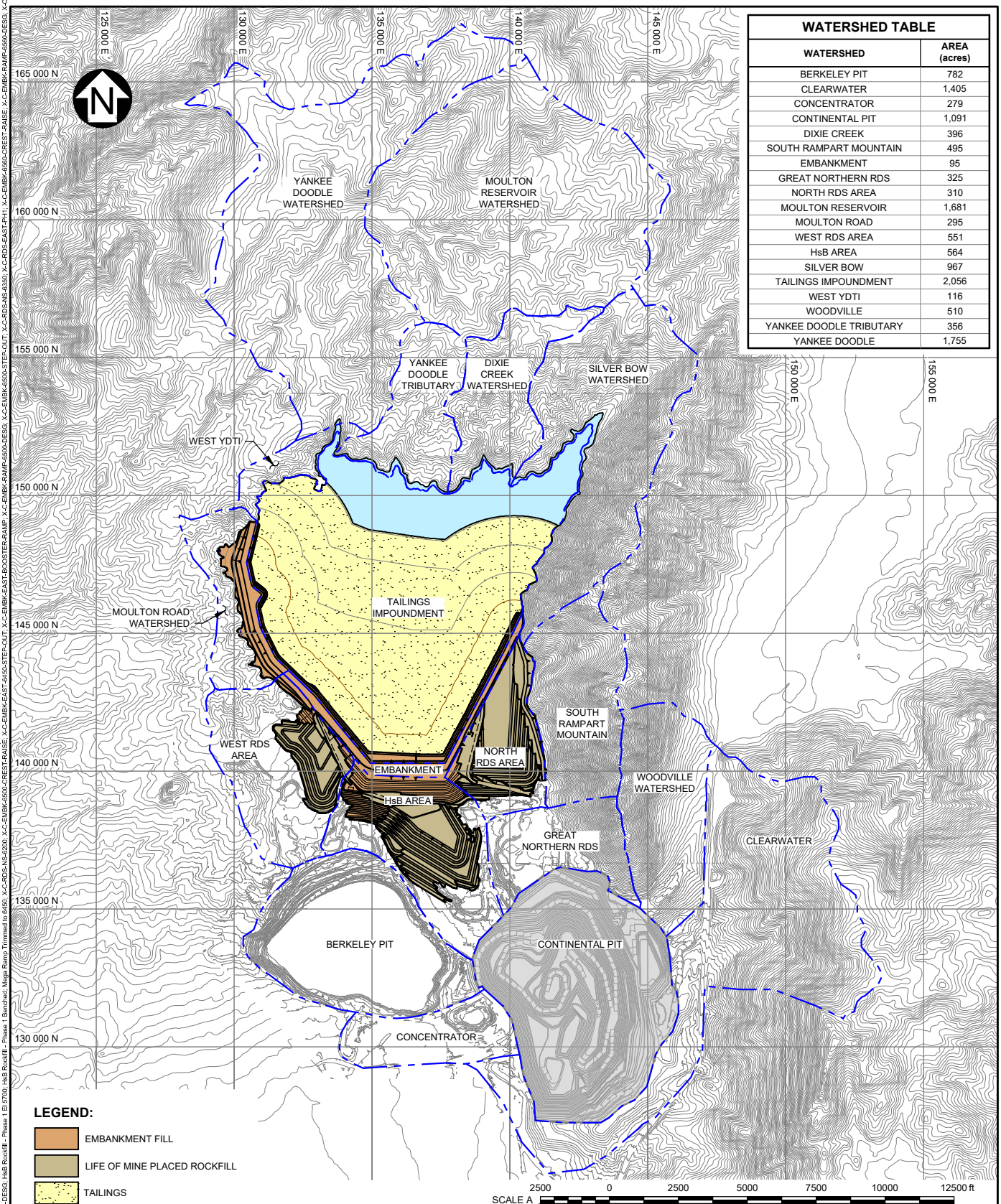

WATERSHED TABLE

WATERSHED	AREA (acres)
BERKELEY PIT	782
CLEARWATER	1,405
CONCENTRATOR	279
CONTINENTAL PIT	1,091
DIXIE CREEK	396
SOUTH RAMPART MOUNTAIN	495
EMBANKMENT	95
GREAT NORTHERN RDS	325
NORTH RDS AREA	310
MOULTON RESERVOIR	1,681
MOULTON ROAD	295
WEST RDS AREA	551
HsB AREA	564
SILVER BOW	967
TAILINGS IMPOUNDMENT	2,056
WEST YDTI	116
WOODVILLE	510
YANKEE DOODLE TRIBUTARY	356
YANKEE DOODLE	1,755

NOTES:

1. COORDINATE SYSTEM AND ELEVATIONS BASED ON ANACONDA MINE GRID.
2. TOPOGRAPHY PROVIDED BY MONTANA RESOURCES, LLC IN SEPTEMBER 2023.

REV	DATE	DESCRIPTION	DESIGNED	DRAWN	REVIEWED
0	19DEC'24	ISSUED WITH REPORT	DBM	RMM/PP	RSD

MONTANA RESOURCES, LLC

MONTANA RESOURCES

YANKEE DOODLE TAILINGS IMPOUNDMENT CATCHMENT AREAS

Knight Piésold CONSULTING

P/A NO. VA101-126/24

REF NO. 7

FIGURE 2.3

REV 0

SAVED: M:\1\101\00126\24\AAcad\FIGS\A58, 11/27/2024 5:24:26 PM, DMCGUIRE, PRINTED: 12/18/2024 9:51:15 AM, FIG 2.3, RLI ACAD VERSION: 25.0S (LMS TECH)
XREF FILE(S): X-C-EMBK-WEST-6450-DESG, X-C-EMBK-EAST-6450-DESG, HsB Rockfill - Phase 1 El 5700, HsB Rockfill - Phase 1 Benched, Mega Ramp Trimmed to 6450, X-C-RDS-NS-8200, X-C-EMBK-6600-CREST-RAISE, X-C-EMBK-EAST-6450-STEP-OUT, X-C-EMBK-EAST-BOOSTER-RAMP, X-C-EMBK-RAMP-6600-DESG, X-C-EMBK-6500-STEP-OUT, X-C-RDS-NS-6350, X-C-RDS-EAST-PH1, X-C-EMBK-6560-CREST-RAISE, X-C-EMBK-RAMP-6560-DESG, X-C-RD

The catchments downstream of the YDTI shown on Figure 2.3 contribute inflows to either the HsB area (which can drain passively to the Berkley Pit), the Berkeley Pit, or the Continental Pit. The pits are directly in the flood path of a potential dam breach of the selected breach location in this study. The downstream catchments shown on Figure 2.3 were used to calculate the inflows and the starting water levels in the pits. The inflow contributions to the pits will be somewhat different once the rock disposal sites (RDS) associated with the life of mine design are in place. The Berkeley Pit would receive somewhat less and the larger Continental Pit would receive somewhat more inflow as the Continental Pit limit expands. However, the difference in inflows is very small compared to the inflows from the hypothetical breach, and it would have no material impact on the results of this study.

The Berkeley and Continental Pits are approximately two miles from the potential breach location, while the mine boundary to the city of Butte is located approximately three miles away. The drainage area contributing to the YDTI is approximately 7,300 acres and the sum of the sub-catchment drainage areas which flow into the Berkeley and Continental Pits are 2,100 acres and 4,600 acres, respectively.

2.3.3 INITIAL POND CONDITIONS IN THE YDTI

The initial supernatant pond volume and the location of the supernatant pond with respect to the dam (near, far, or against the dam) will have a notable impact on the breach outflow volume, peak discharge of the breach outflow, and the extent of the downstream inundation (CDA, 2021).

The maximum operating pond volume is typically used as the initial pond condition for the Flood Induced scenario. According to the Design Document, the maximum normal operating pond volume for the YDTI is approximately 18,000 acre-ft (ac-ft), comprising a nominal operating pond volume of 15,000 ac-ft plus up to 3,000 ac-ft for seasonal fluctuation (KP, 2024a). The PMF volume of 20,000 ac-ft (KP, 2024a) was added to the maximum operating pond volume, corresponding to a total pond volume of 38,000 ac-ft. The YDTI is designed to safely store tailings plus this pond volume with required freeboard for wave runup. The elevation-capacity curve for the supernatant pond up to 38,000 ac-ft is shown on Figure 2.4.

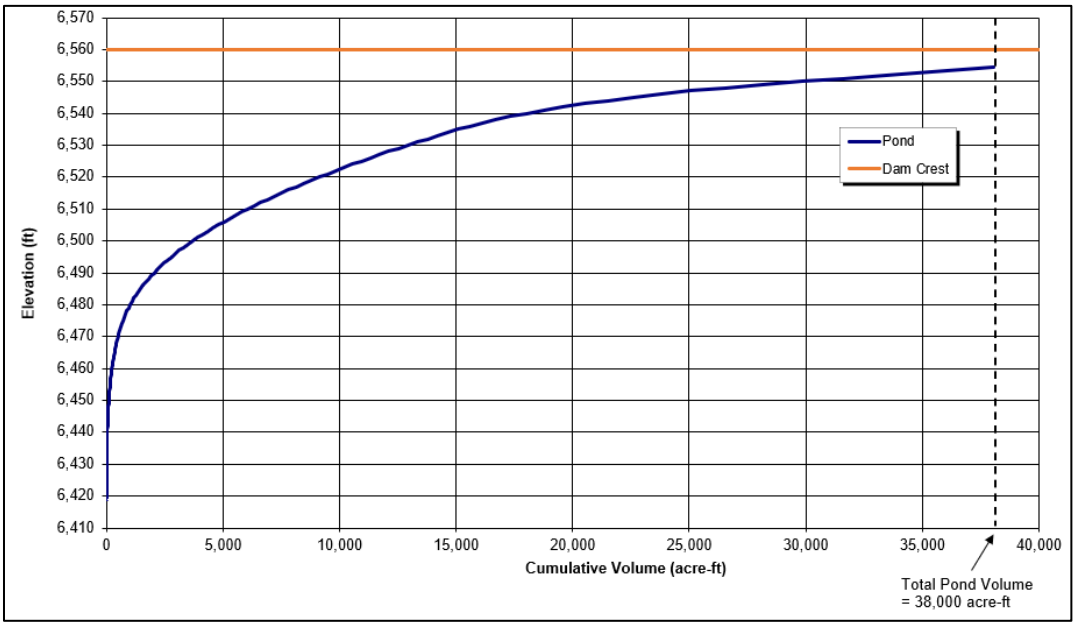

Figure 2.4 YDTI Supernatant Pond Elevation-Capacity Curve

2.3.4 INITIAL CONDITIONS IN THE PITS

The initial condition in the Berkeley and Continental Pits for the Flood Induced scenario includes the PMF volume as well as any pre-existing water volume in the pits. The Berkeley Pit has a current operating level of EL. 5,412 ft, which is being maintained at a relatively steady-state, and the Continental Pit is empty other than a negligible volume required to facilitate dewatering pump system operation.

The estimated PMF inflow volumes to Berkeley and Continental Pits are approximately 5,230 ac-ft and 10,350 ac-ft, respectively, as shown using the elevation-capacity curves on Figure 2.5 and Figure 2.6.

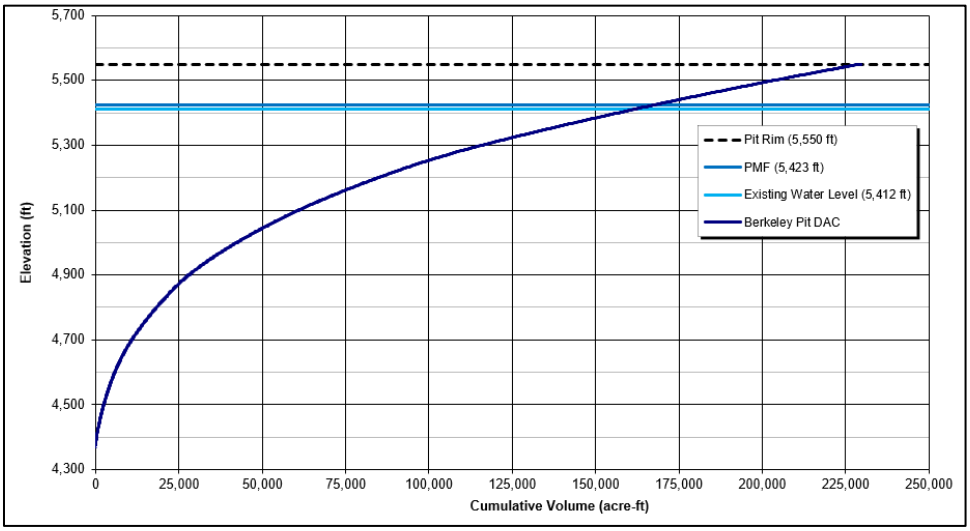

Note(s):
1. Bottom of pit is at EL. 4,370 ft.

Figure 2.5 Berkeley Pit Elevation-Capacity Curve – Initial Conditions

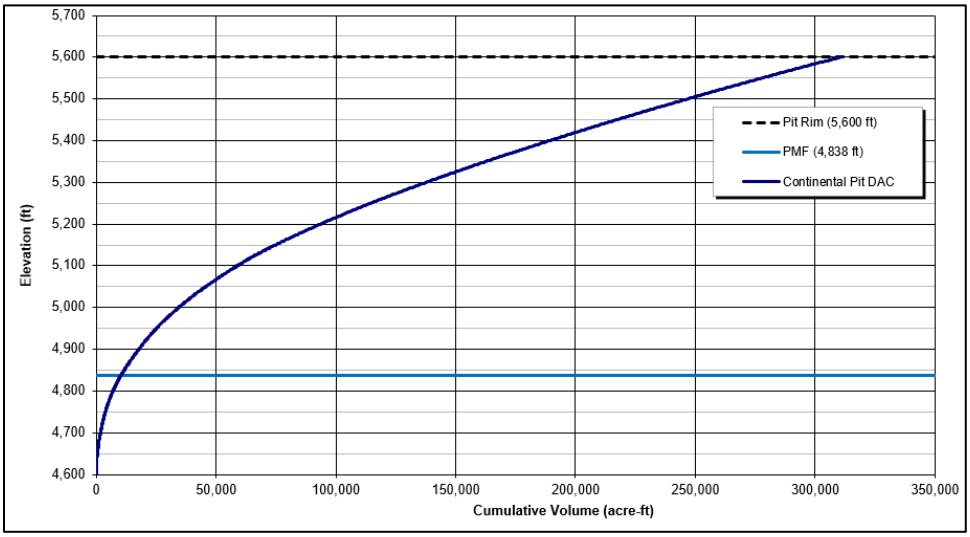

Note(s):
1. Bottom of pit is at EL. 4,600 ft.

Figure 2.6 Continental Pit Elevation-Capacity Curve – Initial Conditions

2.4 TAILINGS CHARACTERISTICS AND RHEOLOGY

2.4.1 GENERAL

The CPT locations used for tailings characterization (Section 2.4.2), analyzing the tailings strength relevant to the dam breach study (Section 2.4.3), and rheology testing (Section 2.4.4) are shown on Figure 2.7. The locations marked in green as “Rheology testing” were also used for tailings characterization.

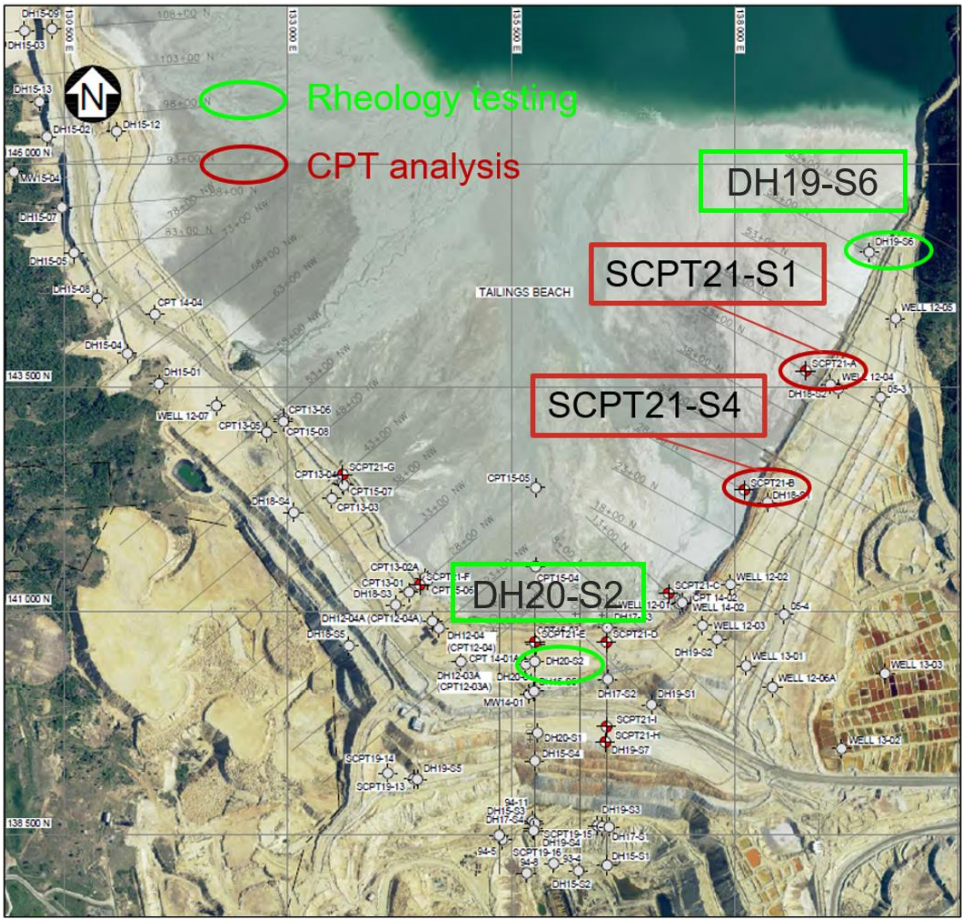

Figure 2.7 Rheology and CPT Testing Locations in the YDTI

2.4.2 TAILINGS CHARACTERIZATION

Solids densities, particle size distribution (PSD), and mineralogy were tested on six samples collected at different depths from drillholes DH19-S6 and DH20-S2 (locations shown on Figure 2.7) by Paterson & Cooke (P&C, 2022). The test work report is provided in Appendix A. Two of the six samples that cover the full range of PSDs were then tested for rheology to evaluate the possible range of behavior and flowability (discussed in Section 2.4.4).

The solids densities were determined using a 0.001-gram accuracy balance and a helium gas pycnometer, which measures solids volume. Three tests were performed on each sample and the average solids densities ranged from 2,663 kg/m^3 to 2,725 kg/m^3 (P&C, 2022). A value of 2,700 kg/m^3 (i.e., a specific gravity of 2.7) was used in the dam breach analysis.

PSDs were determined by wet sieving according to the method detailed in ASTM D422-63 (2007) "Standard Test Method for Particle Size Analysis of Soils", and by laser diffraction using a Microtrac Model S1500 (P&C, 2022). The PSDs of the six tailings samples collected from the two drillholes (DH19-S6 and DH20-S2) are shown on Figure 2.8 and include samples from various depths (as indicated in the legend, e.g., DH19 22-32 is 22-32 ft below the tailings surface and DH19 56-70 is 56-70 ft below). The samples shown on this figure are representative of the range of tailings deposited in the YDTI. The tailings are characterized as silty to sandy, with D10 ranging from approximately 7 - 25 μm, D50 ranging from approximately 45 - 250 μm, D90 ranging from approximately 200 - 700 μm, and the fraction of clay sized particles smaller than 4 μm being generally less than 5%.

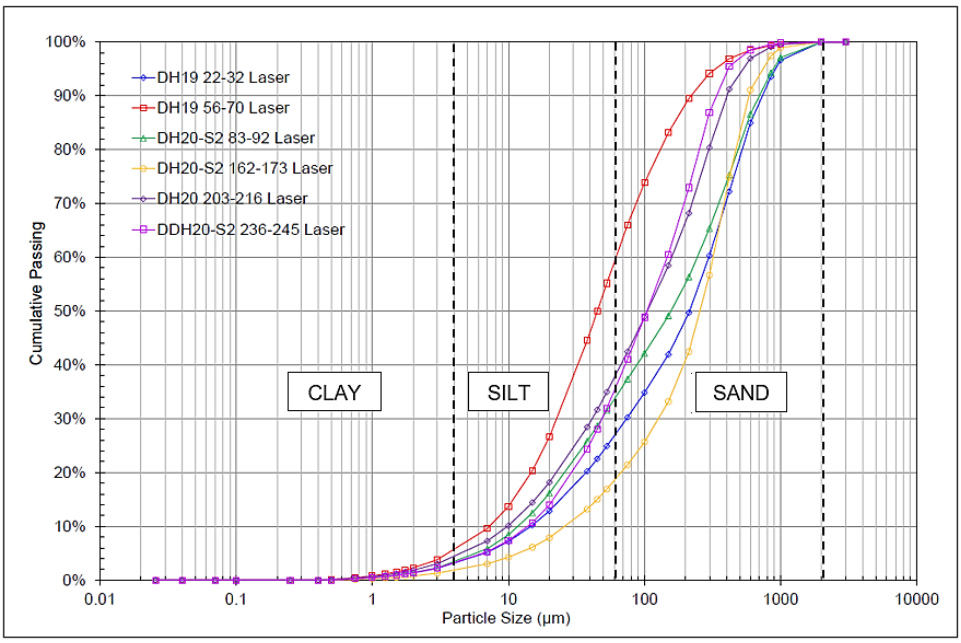

Figure 2.8 Grain Size Distribution for YDTI Tailings (P&C, 2022)

Sub-samples were sent to DCM Science in Wheat Ridge, Colorado, for mineral and clay analysis using X-ray diffraction with reference intensity ratio. The mineralogy of the tested tailings samples indicates the main components are quartz, K-feldspar, and mica (approximately totaling 70%), with total clay minerals ranging from approximately 15-25%. Micro-photographs were taken of the sieved particle size fractions for each sample using a Leica microscope to provide a qualitative view of particle shape (P&C, 2022). Photos of the 300 μm size fraction for the samples that were selected for rheology testing (DH19-S6 56-70 and DH20-S2 162-173) are presented on Figure 2.9.

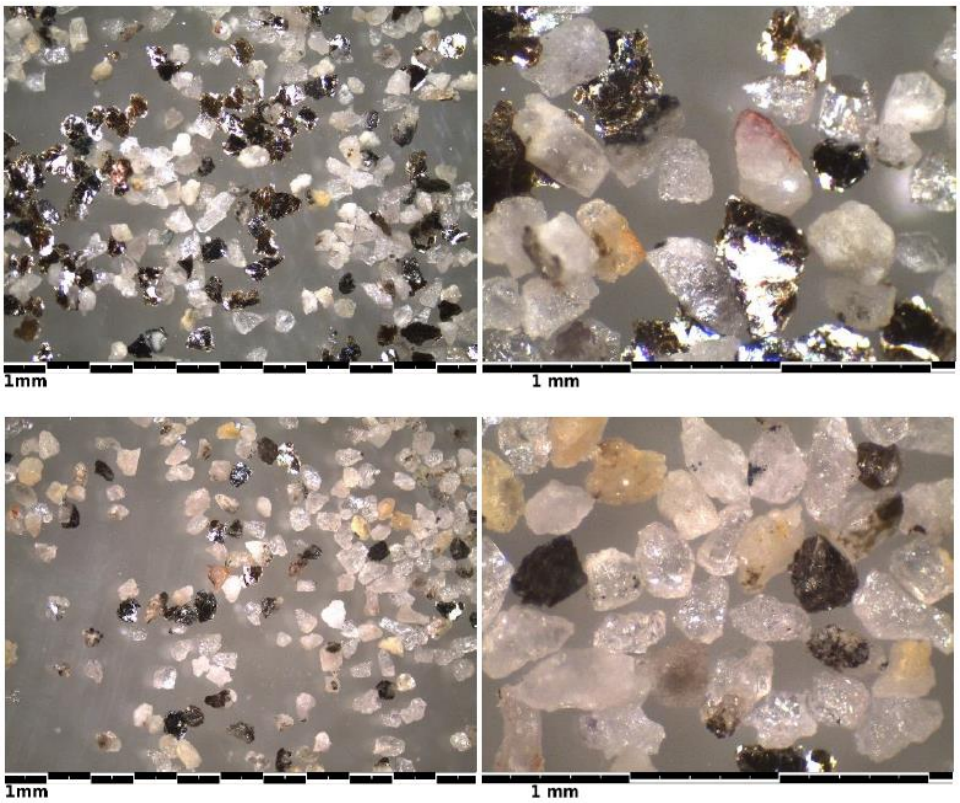

Note(s):

1. The top two images are from drillhole DH19-S6 56-70 ft. The bottom two images are from drillhole DH20-S2 162-173 ft.
2. The left images are x10 magnification, and the right images are x35 magnification.

Figure 2.9 Micro-Photographs of the +300 μm Size Fraction (P&C, 2022)

2.4.3 TAILINGS LIQUEFACTION POTENTIAL

CPT data from locations SCPT21-S1 and SCPT21-S4 shown on Figure 2.7 were analyzed to determine the tailings liquefaction potential and the tailings strengths relevant for this dam breach study. The initial analysis of CPT data was completed using the CPeT-IT software (Geologismiki Geotechnical Software, 2019). The residual tailings strengths were estimated using Robertson (2010 and 2021), the peak undrained shear strengths were determined based on Olson and Stark (2003) for soil behavior type index (Ic) < 3.0 and on the Nkt method for Ic > 3.0, while the soil behavior type was determined based on Robertson (2021). Selected summary results for SCPT21-S1 are shown on Figure 2.10 and for SCPT21-S4 on Figure 2.11.

Bulk densities were estimated using relationships by Robertson and Cabal (2010) and Mayne (2007). For tailings below the water table, reported dry densities (Figure 2.10 and Figure 2.11) were calculated assuming 100% saturation and a specific gravity of 2.7 (P&C, 2022).

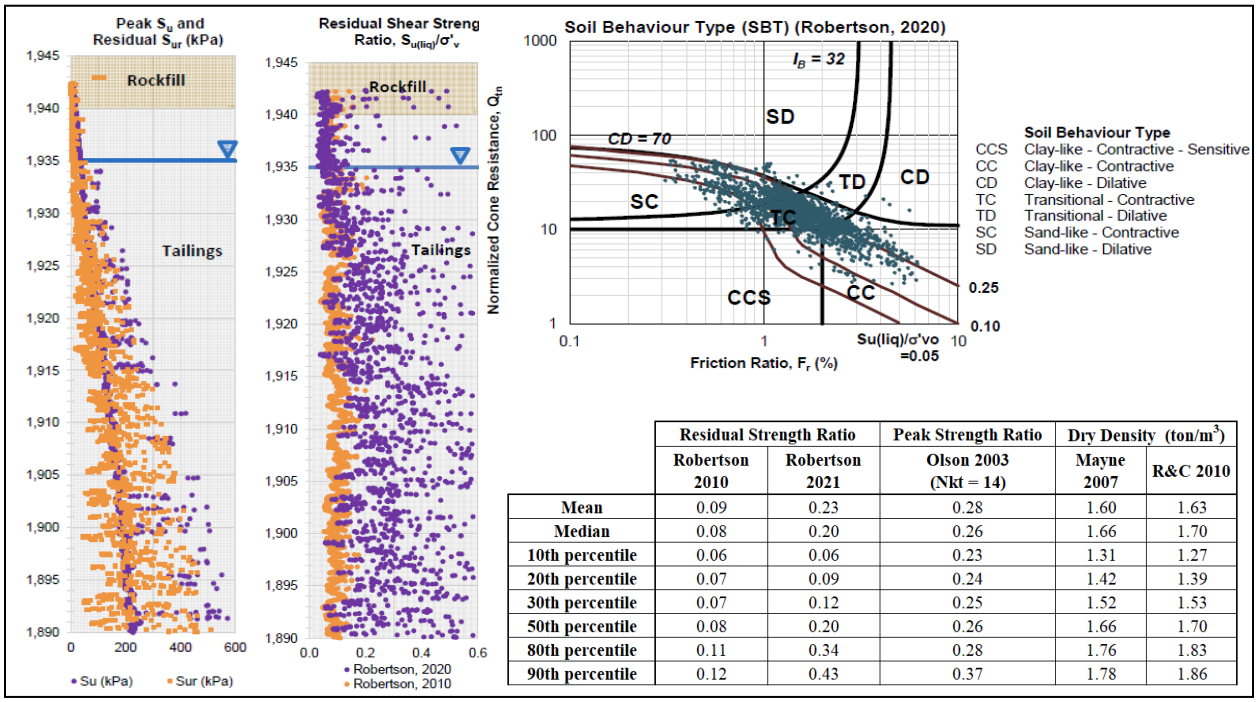

	Residual Strength Ratio		Peak Strength Ratio	Dry Density (ton/m^3)	
	Robertson 2010	Robertson 2021	Olson 2003 (Nkt = 14)	Mayne 2007	R&C 2010
Mean	0.09	0.23	0.28	1.60	1.63
Median	0.08	0.20	0.26	1.66	1.70
10th percentile	0.06	0.06	0.23	1.31	1.27
20th percentile	0.07	0.09	0.24	1.42	1.39
30th percentile	0.07	0.12	0.25	1.52	1.53
50th percentile	0.08	0.20	0.26	1.66	1.70
80th percentile	0.11	0.34	0.28	1.76	1.83
90th percentile	0.12	0.43	0.37	1.78	1.86

Note(s):

1. The depths are shown in meters, where 1,945 m = 6,381 ft

Figure 2.10 CPT Analysis for SCPT21-S1

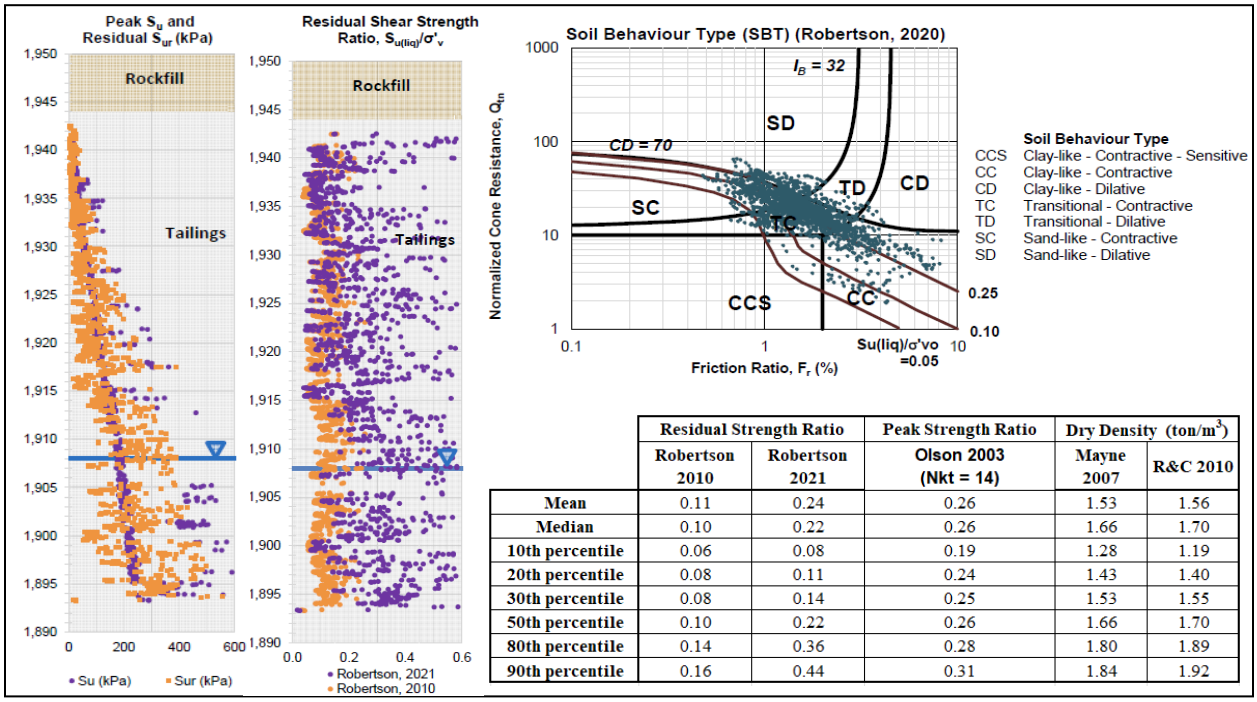

	Residual Strength Ratio		Peak Strength Ratio	Dry Density (ton/m^3)	
	Robertson 2010	Robertson 2021	Olson 2003 (Nkt = 14)	Mayne 2007	R&C 2010
Mean	0.11	0.24	0.26	1.53	1.56
Median	0.10	0.22	0.26	1.66	1.70
10th percentile	0.06	0.08	0.19	1.28	1.19
20th percentile	0.08	0.11	0.24	1.43	1.40
30th percentile	0.08	0.14	0.25	1.53	1.55
50th percentile	0.10	0.22	0.26	1.66	1.70
80th percentile	0.14	0.36	0.28	1.80	1.89
90th percentile	0.16	0.44	0.31	1.84	1.92

Note(s):

1. The depths are shown in meters, where 1,950 m = 6,398 ft

Figure 2.11 CPT Analysis for SCPT21-S4

The CPT data indicate that tailings have a site-specific residual undrained shear strength ratio of 0.12 to 0.14 based on the 30th percentile using Robertson, 2021 (tables on Figure 2.10 and Figure 2.11). The estimated residual undrained shear strength ratios are in line with values observed in case histories, which ranged from 0.04 to 0.16 (Robertson, 2021).

To evaluate the stable post-failure slope angle, an infinite slope analysis can be used, corresponding to a Factor of Safety (FS) of 1.0, for materials with different strength ratios using the following equation (Adams et al., 2022):

$$FS = \frac{\gamma'}{\gamma_{sat}} \frac{tan\ \emptyset'}{tan\ \beta}$$

Where:

- FS = factor of safety
- γ' [kN/m^3] = buoyant unit weight
- γsat [kN/m^3] = saturated unit weight
- *tan φ'* = tangent of the friction angle, equivalent to the peak undrained shear strength ratio (S_u/σ'_{vo}), or the residual undrained strength ratio (S_r/σ'_{vo})
- *tan β* = tangent of the slope angle

For most geological materials, the ratio of the buoyant unit weight (γ') to the saturated unit weight (γ_{sat}) is approximately 1:2. Using this approach, the stable slope angle with FS = 1.0 for the saturated tailings with a residual undrained shear strength ratio (S_r/σ'_{vo}) of 0.12 to 0.14 would be approximately 6 to 7% (3.5 to 4°). Therefore, a slope of 6% was selected as the stable post-failure tailings slope following a Flood Induced hypothetical breach of the YDTI. In comparison, references to the Mochikoshi gold mine dam failure in Japan in 1978 (Lucia et al., 1981) indicate that a final tailings surface slope within the facility was at 4 to 5° (7 to 8.5%), while the Merriespruit tailings dam failure in 1994 in South Africa resulted in a final tailings surface slope of 3.5° or 6% (Blight and Fourie, 2003).

2.4.4 TAILINGS RHEOLOGY

The rheological characteristics of the tailings mass (i.e., yield stress and dynamic viscosity) depend on the solids concentration, type of the tailings material (i.e., hard rock versus soft rock mines), method of deposition, age and consolidation, saturation, and other factors.

P&C tested two of the six samples, namely DH19-S6 from a depth of 56-70 ft and DH20-S2 from a depth of 162-173 ft for rheological characterization. Yield stress and viscosity were tested using a tube viscometer, and the results are shown on Figure 2.12. Superimposed on this figure is the assumed solids concentration by weight (C_w) and volume (C_v) that was used in this study as a “boundary” at which the flow behavior transitions between Newtonian and non-Newtonian. This is further discussed in Section 4.4.

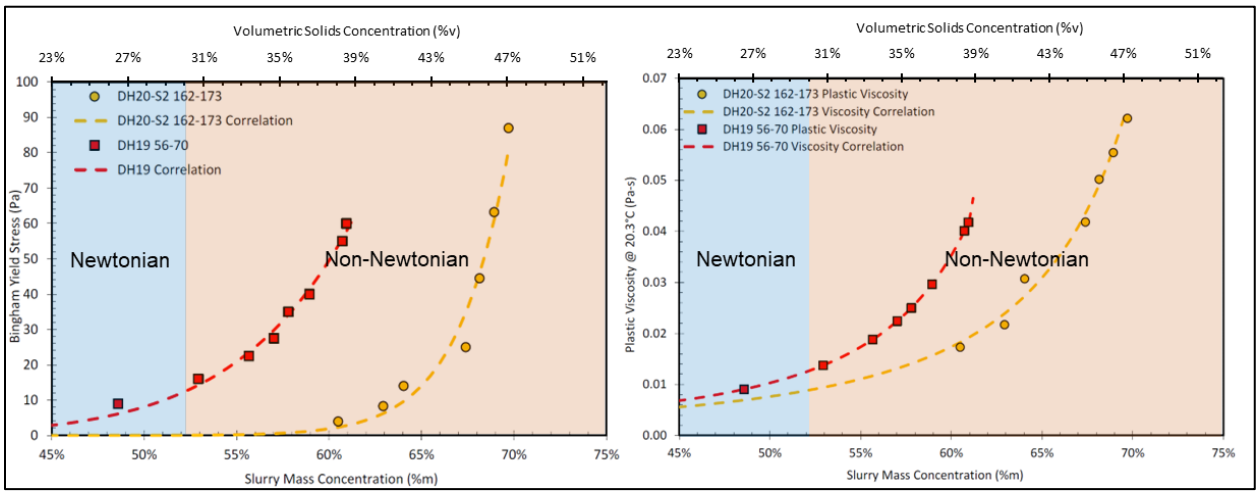

Note(s):

1. The assumed boundary between Newtonian and non-Newtonian flow behavior is superimposed for reference.

Figure 2.12 YDTI Tailings Yield Stress and Viscosity (P&C, 2022)

The rheology data from the YDTI was superimposed on Figure 2.13, which includes the rheological properties of other known materials from literature. These data include mudflow samples in Colorado (Glenwood, Aspen and Natural Soil) presented in O'Brien and Julien (1988), various samples (Bentonite, Coussot, Kaolinite, St. Helens, and Quick Clays) presented in Julien (2010), NA Tailings samples from a copper / gold mine (yield stress only) presented in Adams et al. (2017), and samples from the deposited tailings runout of the Fundão failure in Brazil in 2015 presented in Días (yield stress only) (2017) and Machado (2017). Generally, more yield stress data are available in various literature than viscosity data.

Tailings from hard rock mines (e.g., copper, nickel, gold) behave differently at similar solids concentrations than tailings from soft rock mines (e.g., coal), or tailings with high content of clay sized particles. For example, NA Tailings with higher clay content (> 25%) and Quick Clays shown on Figure 2.13, have a higher yield stress at lower solids concentrations than NA Tailings with a lower clay content (< 15%), or the YDTI samples that also have a low content of clay sized particles (< 5%). Similarly, the Glenwood samples of O'Brien and Julien (1988) were coarser with lower clay content than the Aspen samples. The authors found that samples with lower percentage of clay had lower yield stress values (Glenwood), when compared to the samples with higher clay content (Aspen), but that this same trend was not observed for the viscosity.

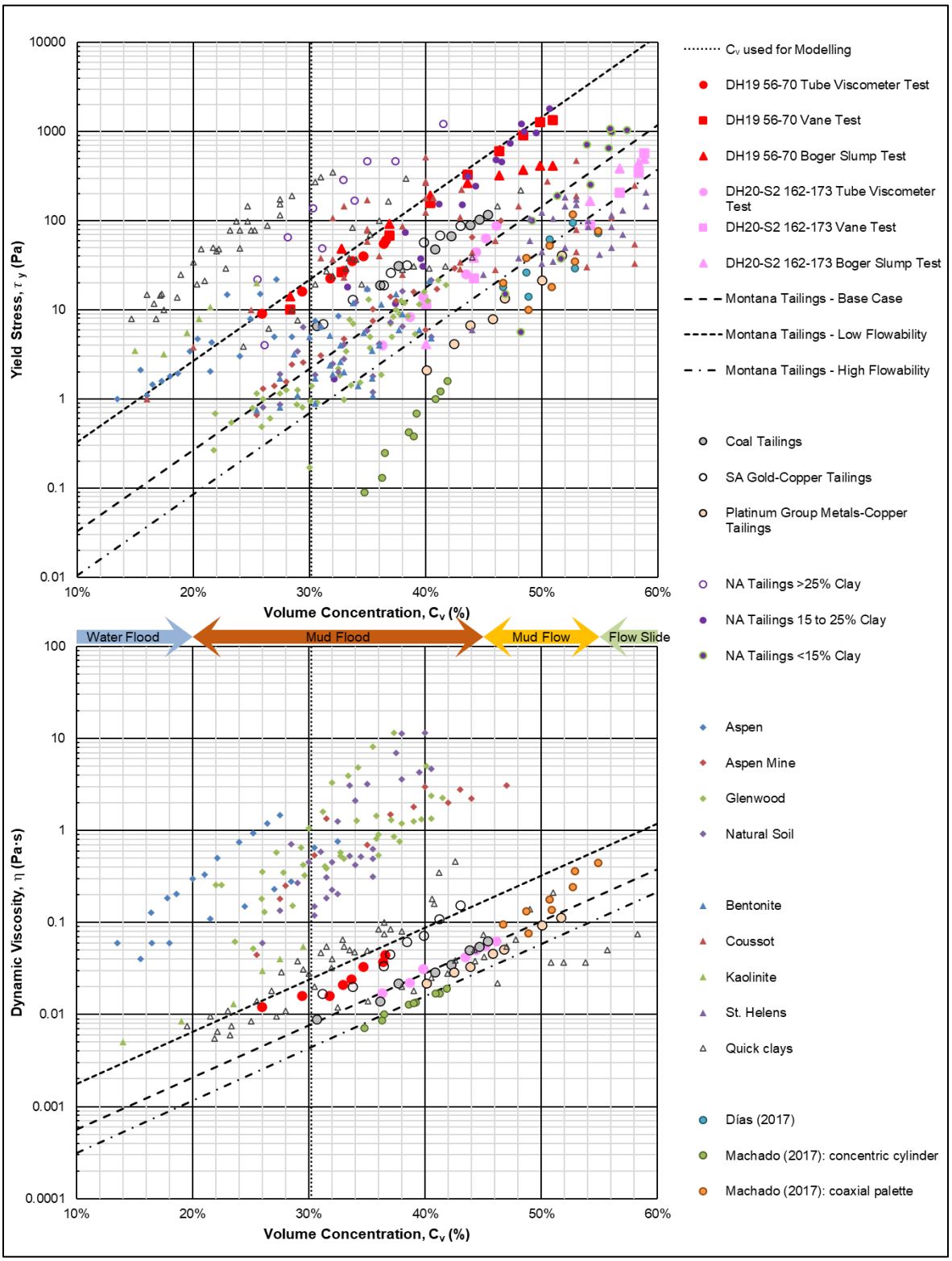

Figure 2.13 Yield Stress and Viscosity Data Comparison Based on Literature

Another finding noted by O'Brien and Julien (1988) was that adding sand particles to the mudflow mixture had a negligible effect on viscosity if the sand content was below 20% by volume. However, the viscosity of the mixture increased rapidly if the sand concentration was beyond 20%. Low viscosity was measured for the YDTI tailings samples, and the coarser sample resulted in lower viscosities and yield stresses.

The iron tailings samples from the Fundão failure exhibit very high flowability with low yield stress and low viscosity at high solids contents, which could likely be attributed to the very high specific gravity of about 4 and the high brittleness of the tailings. The samples were collected from the tailings runout at different locations downstream of the breach location.

Selected yield stress and viscosity values used for modeling the various dam breach scenarios in this study are shown in Table 2.1 along with the Low and High Flowability values used in the sensitivity analysis. The equations and coefficients for the yield stress and viscosity trendlines shown on Figure 2.13 that were used in the dam breach and flood routing modeling are summarized in Table 2.2.

The Base Case trendline was selected conservatively and is representative of the tailings rheology for the sandier/coarser tailings based on the P&C testing (P&C, 2022) as discussed above. The coarser sample was considered to be more representative of the tailings deposited closer to the dam, which would be more likely to mobilize during a breach runout based on how tailings are distributed in the facility with the deposition strategy that has been used in recent years and will continue to be used in the future. The Low and High Flowability was used to estimate the variability due to uncertainties related to the rheological parameters and evaluate their impact on the modeling results, which is discussed further in Section 6.4.3. The Low and High Flowability sensitivity range envelopes the measured data and is equivalent to +1.0 and -0.5 an order of magnitude for the yield stress, and +0.5 and -0.25 an order of magnitude for the viscosity.

Table 2.1 Yield Stress and Viscosity for C_v used for Modeling

C_v (%)	Base Case		Low Flowability		High Flowability	
	Yield Stress (Pa)	Viscosity (Pa·s)	Yield Stress (Pa)	Viscosity (Pa·s)	Yield Stress (Pa)	Viscosity (Pa·s)
30	2.18	0.007619	21.8	0.0241	0.689	0.00429

Table 2.2 Yield Stress and Viscosity as a Function of C_v used for Modeling

Parameter	Yield Stress (Pa)	Viscosity (Pa·s)
Equation	$\tau_y = \alpha \exp(\beta C_v)$	$\eta = \alpha \exp(\beta C_v)$
β	21.0	13.0
α **(Base Case)**	0.00400	0.000153
α **(Low Flowability)**	0.0400 (i.e., +1.0 Magnitude)	0.000485 (i.e., +0.5 Magnitude)
α **(High Flowability**	0.00126 (i.e., -0.5 Magnitude)	0.0000862 (i.e., -0.25 Magnitude)

In conclusion, the yield stress for the YDTI tailings sample seems to fall in the middle of the range of values from literature, while the viscosity appears to be on the lower end of the range, indicating a material that would have a potential to flow relatively easily once mobilized.

3.0 FAILURE SCENARIOS AND FAILURE MODES

3.1 FAILURE SCENARIOS

Failure scenarios are typically conducted for two types of hydrologic conditions, as defined in FEMA (2013), ICOLD (2022), and CDA (2021):

- **Fair Weather, Non-Hydrologic, or Sunny Day scenario** – "used to describe a dam failure when there is no existing natural flood occurring in the downstream receiver. The level of the pond in the TSF could be at the normal operating water level or at a high operating water level" (ICOLD, 2022). Failure triggers and mechanisms include extreme earthquake, foundation instability, slope instability, piping/internal erosion, overtopping due to mismanagement, etc.
- **Flood Induced, Hydrologic, or Rainy Day scenario** – "used to describe a dam failure during a natural flooding event where the tailings facility has a maximum water inflow and the dam breach flow is added to the natural flood flow in the receiving environment" (ICOLD, 2022). A failure is triggered by extreme precipitation, snowmelt, and/or flooding. Failure mechanisms include overtopping, foundation instability, slope instability, piping/internal erosion, erosion of the dam face, etc.

3.2 PHYSICAL PROCESSES DURING DAM FAILURE

The physical processes during a dam breach are complex and not fully understood. There are two main factors that drive the breaching process and the total outflow volume, as shown on Figure 3.1 (CDA, 2021):

- The presence of a supernatant pond on the surface of the tailings facility that could be released during a breach
- The potential for saturated tailings to liquefy and flow, where the liquefaction may be triggered by various mechanisms including the breach itself

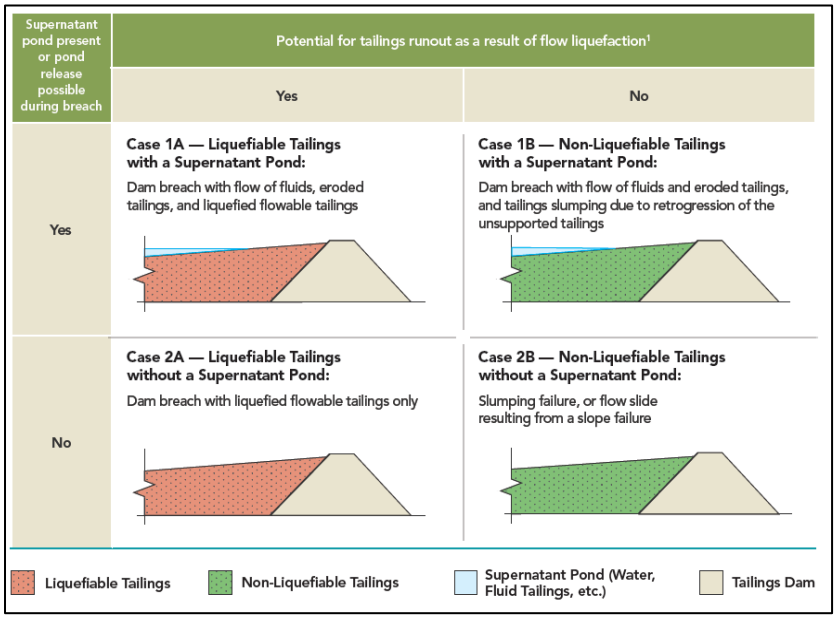

Figure 3.1 Conceptual TDBA Cases (CDA, 2021)

It is reasonable to classify the hypothetical breach scenario of the YDTI as Case 1 for the following reasons:

- There is a supernatant pond present under normal operating conditions (Fair Weather conditions), which would increase in volume due to severe natural flooding (Flood Induced conditions).
- Tailings are present and could be entrained/eroded in the hypothetical breach flows or become mobile/flowable, where saturated, if they become unconfined (Case 1A). Where unsaturated tailings are present, erosion and slumping processes would be more likely to occur (Case 1B).

It is also plausible that a hypothetical Fair Weather failure could occur that does not involve pond release due to the presence of long, drained tailings beaches during normal operations and deficit conditions, which would result in a much smaller remnant pond during closure. Such a failure would likely classify as Case 2A or Case 2B depending on scale; however, that type of breach is not contemplated in this report.

This report only considers an erosional Flood Induced scenario at the end of operations for a dam crest elevation of 6,560 ft for a location where the pond is the closest to the dam. The study indicates that the inundation limits of the Flood Induced scenario are contained within the mine site boundary; therefore, it was considered reasonable to exclude modeling of an erosional Fair Weather (i.e., Sunny Day) scenario, which would have a lower breach volume due to a much smaller supernatant pond. Such a scenario could reasonably be expected to result in similar potential impacts around the site, but with less volume entering the Berkeley and Continental Pits due to less outflow from the YDTI.

For the TDBA purposes, the breach outflow can be understood as two processes that can occur individually, simultaneously, or sequentially. Two conceptual discharge mechanisms or two types of processes may occur during a dam breach event (Martin et al., 2015; CDA, 2021):

- Process I – Initial flood wave
- Process II – Flow of liquefied tailings or progressive slumping of unsupported tailings

These discharge mechanisms are distinctly different in the type of consequence they pose in terms of life safety and potential environmental impacts. The purpose of various dam safety measures during design, construction, operation, and closure of the facility is to prevent release of containment, thereby reducing the risk associated with each consequence to the maximum practical extent. The two discharge mechanisms discussed below implicitly ignore the likelihood of occurrence.

The initial flood wave (Process I) would occur immediately following a failure of containment for TSFs where the pond is sufficiently close to the embankment. The free water within the TSF would start to discharge and mobilize both settled tailings from the impoundment and construction materials from the TSF dam through erosion. Failure of an earth or rockfill dam typically occurs over a matter of minutes to hours with a flood wave rising as the breach develops, peaking at some point during discharge, and then receding as the flood wave subsides. The flood wave would propagate downstream causing erosion and inundating the downstream receiving environment. The extents of inundation are largely driven by the size of the impoundment, rate of breach development, and the downstream topography. The flood wave carries the tailings solids and dam construction materials, as well as floodplain materials scoured along the way. Depending on the volume discharged and the peak discharge magnitude, this initial flood wave could travel downstream for tens to hundreds of miles unless there was a feature present to stop and store the release (e.g., an open pit or large reservoir). The initial flood wave is typically modeled as water, or a Newtonian fluid, due to a relatively low solids concentration in the outflows with relatively weak rheological parameters (as shown in Section 2.4.4).

The flow of liquefied or slumped tailings (Process II) would occur following or in combination with the initial flood wave, as a portion of the tailings mass would be expected to mobilize due to the change in confinement following the dam breach. Tailings that are not mobilized in the initial flood wave may liquefy or slump, and flow through the breach in a paste-like or mud flow fashion until the tailings mass stabilizes. This process cannot be modeled as water, as the viscosity and the yield stress of mobilized tailings play a much more substantial role, with the tailings behaving like non-Newtonian fluids (Jeyapalan et al., 1983; Seddon, 2010; Kulesza, 2011, CDA, 2021). Modeling non-Newtonian sediment laden fluids requires knowledge of rheology (viscosity and yield stress). The inundation extent from Process II flows would typically be less than from the initial flood wave, but more solids would deposit downstream of the breach location. Conceptually, the tailings mobilized through liquefaction would appear like a cone of depression in the TSF forming a slope equivalent to the post-failure residual tailings strength (as discussed in Section 2.4.3).

An example of a cone of depression in a TSF following the 1994 dam failure at Merriespruit in South Africa is shown on Figure 3.2 (CDA, 2021).

Figure 3.2 Post-Failure Cone of Depression for the Merriespruit Dam Failure (CDA, 2021)

3.3 FAILURE MODES AND FAILURE MECHANISMS

3.3.1 FAILURE MODES

The potential failure modes in this study are examined for the YDTI crest elevation of 6,560 ft.

The CDA Guidelines (2007, 2021) define three general dam failure modes:

- Overtopping – Water flows over the crest of the dam, contrary to design intent
- Collapse – Internal resistance to the applied forces is inadequate (e.g., due to piping/internal erosion, weak foundation, slope instability, earthquake, etc.)

- Contaminated seepage – Contaminated fluid escapes to the natural environment (this failure mode does not result in a physical breach of the dam)

Collapse was considered a potential failure mode for the YDTI that could result in deformation and overtopping of the crest, followed by an erosional breach of the dam under Flood Induced conditions. Only the breach of the North-South Embankment was evaluated, as this section of the dam is typically the closest to the pond. The breach location was selected to be near the abutment adjacent to Rampart Mountain. The specific conditions, the failure mechanism, as well as the governing assumptions for the Flood Induced scenario are discussed in Section 3.3.2.

3.3.2 FLOOD INDUCED FAILURE MECHANISM AND ASSUMPTIONS

Failure mechanism - The dam failure is assumed to be triggered by collapse of the North-South Embankment during an extreme flood event (i.e., the PMF), which results in flow of water over the crest and erosional downcutting through the dam. Collapse could be caused by various triggers including slope or foundation instability causing embankment deformation that results in crest settlement and overtopping of the dam. Despite a very low likelihood of these conditions and triggers occurring, an embankment failure with a full PMF pond was evaluated in this study to understand the potential downstream impacts.

The following key assumptions were made for modeling the Flood Induced breach of the dam:

- The hypothetical breach initiates due instability causing embankment deformation and subsequent overtopping. The breach is estimated to develop down to foundation at the contact with the natural mountain side at the breach location at EL. 6,300 ft.
- The YDTI contains the maximum normal operating pond volume of 18,000 ac-ft at the start of the PMF event, which adds another 20,000 ac-ft to the YDTI for a total pond volume of 38,000 ac-ft (Section 2.3.3).
- The release of the pond mobilizes tailings materials through erosion, forming the Process I outflow (Section 3.2). The volume of tailings mobilized through erosion can be calculated based on natural water floods that can have a C_v up to 20 to 30% (Section 4.2.1 of this report and CDA, 2021).
- The Process I discharge initiates static liquefaction and mobilizes additional tailings. Based on CPT data, a stable slope angle of 6% is selected as an average post-failure residual tailings slope (Section 2.4.3). This slope determines the additional volume of mobilized tailings through liquefaction.
- The volume of additional tailings mobilized through liquefaction is relatively small and is combined with the tailings mobilized through erosion to model the entire breach runout as one process (i.e., combined Process I and Process II) (Section 3.2).
- The volume of breached dam materials is small compared to the breach outflow volume and the eroded dam volume is not tracked separately.
- All materials in the breach outflow are assumed to mix instantaneously. The outflow is expected to behave as a mud flood (CDA, 2021) and the runout is modeled as a non-Newtonian fluid with an average C_v of 30%. The associated yield stress and viscosity values are discussed in Section 2.4.4.
- The PMF concurrently occurs in the catchments surrounding the YDTI and contributes water to the Berkeley and Continental Pits, as discussed in Section 2.3.4. The associated water levels in the pits represent the initial background conditions prior to the breach.

4.0 DAM BREACH ANALYSIS

4.1 GENERAL

Quantitative assessment of the potential consequences of a flood resulting from a dam breach of the YDTI requires an estimate of the volume of water and tailings released in the breach and peak outflow discharge, which is defined by the physical characteristics of the breach (height, width, and side slopes), and how quickly the breach would occur (time of failure). These characteristics are used to develop the dam breach hydrographs, which are subsequently routed through the downstream areas to produce inundation and deposition extents of the flood. The approach used to develop the breach outflow hydrographs is described in the following sections.

4.2 VOLUME OF MOBILIZED WATER AND TAILINGS

4.2.1 OVERVIEW

The total outflow volume for a TDBA will comprise one or more of the following components, depending on the TDBA case, as discussed in Section 3.2:

- Supernatant pond (Cases 1A and 1B) – includes the maximum normal operating pond volume and the additional storm volume or inflow design flood, as required based on the scenario and governing hydrologic conditions.
- Eroded tailings (Cases 1A and 1B) – calculated as a C_v of 20 to 30% (or approximately a C_w of 40 to 50%) based on available pond and interstitial water. This estimate is based on the observations of solids contents in large natural floods that were classified as water floods for solids contents of up to 20 to 30% by volume (O'Brien, 1986; Garcia et al., 2008; CDA, 2021), as well as on back analysis for the Mount Polley TSF failure (Martin et al., 2019).
- Liquefied tailings (Cases 1A and 2A) or non-liquefied/slumped tailings (Cases 1B and 2B) – this represents the volume of tailings that could be mobilized as a result of the removal of the confining embankment and subsequent flow liquefaction or slumping to achieve a stable residual slope angle with a factor of safety of 1 (discussed in Section 2.4.3).
- Dam fill materials (all cases).

The total volume of water and tailings hypothetically released from the YDTI was estimated as the sum of released free water from the supernatant pond at the time of failure and the mobilized tailings volume through erosion and/or liquefaction. The total mobilized tailings volume was estimated as the combined volume that mobilizes through erosion (Process I) and/or static liquefaction (Process II), which is conceptually shown on Figure 4.1. The volume of total outflow in the breach and the breach size are interrelated and were determined through an iterative process. Depending on the rheological properties, Process I flows can sometimes be modeled as Newtonian fluids, whereas Process II flows are always modeled as non-Newtonian due to their yield stress and viscosity being much higher than that of water.

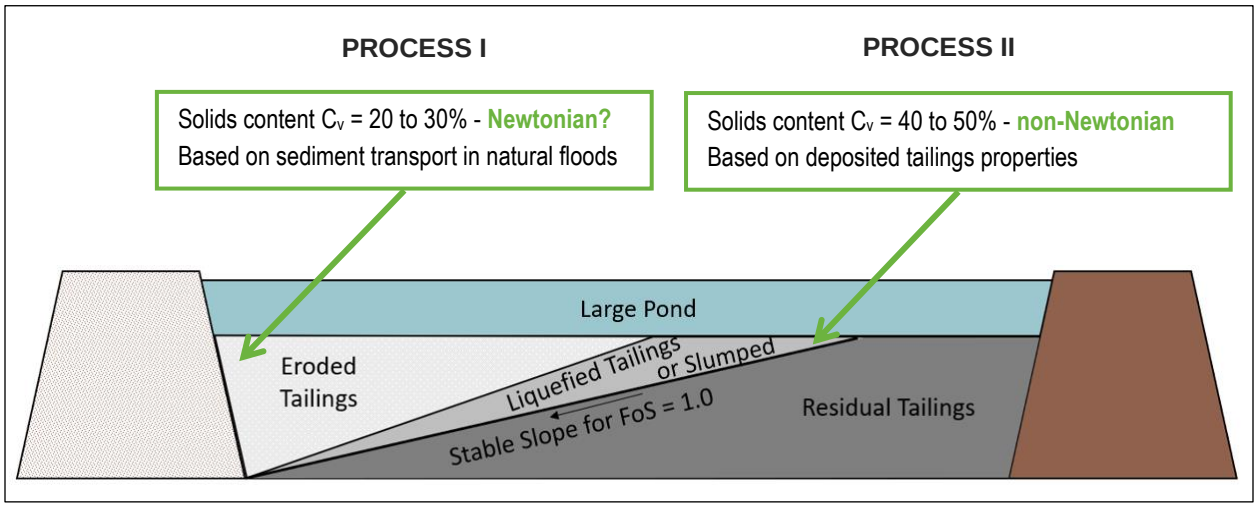

Figure 4.1 Schematic of Mobilized Materials in a Tailings Dam Breach Event

4.2.2 FLOOD INDUCED BREACH VOLUME

The principal driver for the hypothetical breach development contemplated in this study is the release of pond water with a total volume of 38,000 ac-ft, which includes the PMF inflow and the maximum normal operating pond (Section 2.3.3). This volume was bulked with eroded tailings based on the range of C_v equal to 20 to 30% (CDA, 2021), resulting in a mobilization of up to approximately 55,000 ac-ft of tailings (including tailings solids and interstitial water). The discharge of the supernatant pond bulked with eroded tailings represents the estimated Process I outflows (Section 3.2).

At the assumed breach location, the elevation of the natural ground is approximately 6,300 ft where the dam abuts Rampart Mountain. For a breach opening at this elevation, the additional tailings volume that could mobilize due to static liquefaction in the Process II outflows can be estimated by applying a cone of depression with a slope based on the residual undrained shear strength for the tailings. Applying a cone of depression with a post-failure slope of 6% (Section 2.4.3) results in a total mobilizable volume of approximately 50,000 to 55,000 ac-ft (including tailings solids and interstitial water). This volume is roughly equal to the upper end of tailings mobilizable through erosion due to pond discharge, as discussed above.

Consequently, the entire breach outflow was modeled as one process (i.e., combined Process I and Process II). Based on the known characteristics for the tailings (dry density and solids density) and assuming fully saturated conditions, this outflow was estimated to have a C_v of 30%, with additional discussion provided in Section 4.4.

The pond and tailings volumes mobilized in the breach are summarized in Table 4.1. These volumes were used to define the breach parameters and the outflow hydrographs, discussed further in Section 4.3. The breach and the tailings failure surface geometry shown on Figure 4.2 were generated using Muk3D (MineBridge Software Inc., 2023).

Table 4.1 Estimated Water and Tailings Volumes in the Flood Induced Breach Outflows

Mobilized Free Water in Breach[1] (ac-ft)	Mobilized Tailings Volume[2] (ac-ft)	Total Mobilized in the Breach[3] (ac-ft)
38,000	55,000	93,000

Note(s):

1. The released free water volume is the sum of the maximum operating pond volume and the PMF volume.
2. The tailings volume includes tailings solids and interstitial water mobilized through both erosion and liquefaction.
3. The eroded dam volume is small compared to the breach outflow volume and is not tracked separately.

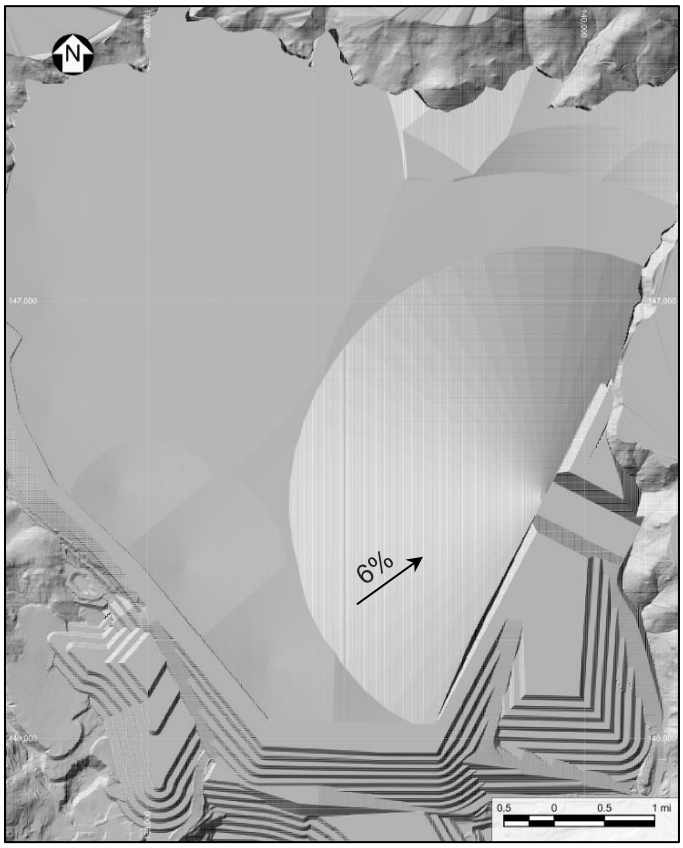

Note(s):

1. Dam and rock disposal sites are projected surfaces at the time of the breach.

Figure 4.2 Breach Geometry for the Flood Induced Failure

The total mobilized breach volume from the YDTI Flood Induced scenario is shown on Figure 4.3, which compares the total outflow volume to the total impounded volume for historic failures of tailings dams, using the database and statistical analysis developed by Rana et al. (2021a, 2021b). The total storage in the YDTI above the breach invert elevation of 6,300 ft is larger than the other case studies shown on Figure 4.3, hence the YDTI breach volume plots outside the range shown in Rana et al. (2021a). However, using simple extrapolation, the predicted Flood Induced breach volume would follow the trend observed in other failures.

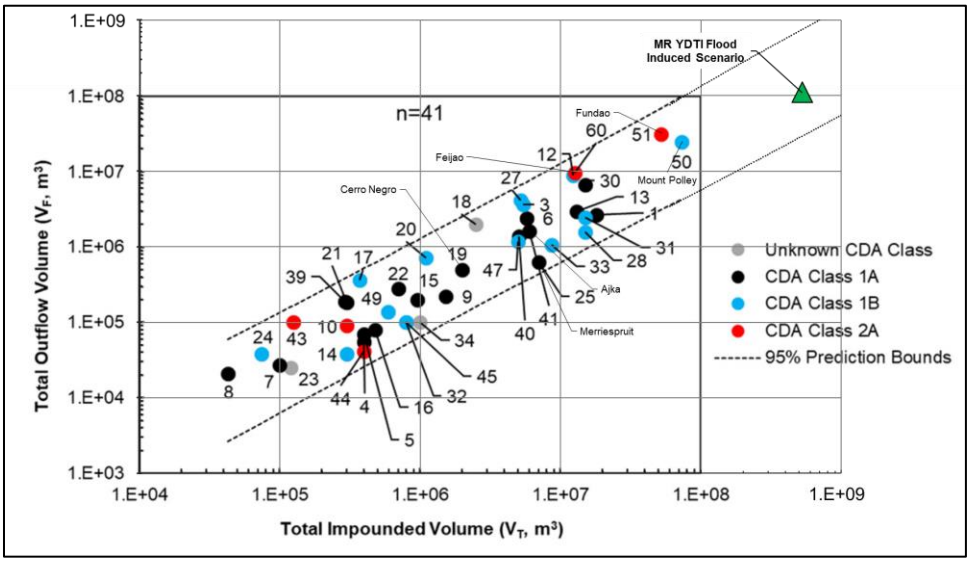

Note(s):

1. The total impounded volume for the YDTI refers to the volume stored above the breach invert elevation of 6,300 ft.

Figure 4.3 Comparison of Predicted Outflow Volume to Observed Outflow Volumes in Past Failures of Tailings Dams (adapted from Rana et al., 2021a)

4.3 BREACH OUTFLOW HYDROGRAPHS

4.3.1 DAM BREACH PARAMETERS

The quantitative assessment of the potential consequences of a flood from a dam breach requires estimates of the peak discharge during the breach, the physical characteristics of the breach defined by the breach parameters (height, width, side slopes), and the breach development time (or time to fail). The peak discharge and the breach parameters were estimated using empirical methods and guidelines, and then applied to develop dam breach hydrographs that were routed downstream to predict the extent of flooding in the downstream area. It is acknowledged that the empirical relationships used for this analysis are based on past failures of water retaining dams; however, these equations are considered applicable for erosional type failures of tailings facilities (CDA, 2021), such as the failure of the North-South Embankment considered in this study.

Several references were used to assess the range of calculated peak discharges and breach parameters. Various empirical equations and guidelines summarized by Wahl (1988) include: Johnson and Illes (1976), Singh and Snorrason (1982), MacDonald and Langridge-Monopolis (1984), Costa (1985), U.S. Bureau of Reclamation (USBR, 1988), Von Thun and Gillette (1990), Federal Energy Regulatory Commission (FERC, 1993), and Froehlich (1995a, 1995b). Other common approaches used in this study include Walder and O'Connor (1997), Rico et al. (2007), Froehlich (2008, 2016), Xu and Zhang (2009), and Pierce et al. (2010). The ranges of calculated peak discharges and breach parameters are summarized in Table 4.2.

Relevant topographic constraints and physical characteristics of the dam design were considered when calculating the breach parameters, including the construction method and the erodibility of the rockfill dam construction materials. Furthermore, some of the empirical methods estimate the volume of dam materials that can be mobilized considering the breach outflow volume (e.g., MacDonald and Langridge-Monopolis, 1984; Washington, 2007; Adria et al., 2023 and 2024). These methods were utilized to confirm a reasonable breach height considering the breach outflow volume.

Table 4.2 Breach Parameters and Peak Discharge Estimates for YDTI Flood Induced Breach

Description	Peak Discharge (ft^3/s)	Bottom Width (ft)	Side Slope (xH:1V)	Time to Fail (hours)
Range(1)	460,000 – 4,200,000	0 – 575	0.25 – 1.40	0.74 – 8
Average Values(1)	1,340,000	265	0.81	2.08
Range using Guidelines(2)	460,000 – 4,200,000	0 – 1,050	0.25 – 1.40	0.74 – 8
Average Values using Guidelines(2)	1,340,000	350	0.81	2.59

Note(s):
1. Values based on calculations using empirical equations only.
2. Values based on calculations using a combination of empirical equations and guidelines (e.g., USBR, 1988; FERC, 1993).
3. Breach bottom elevation is at 6,300 ft, i.e., the dam foundation at the breach location.

The ranges for breach parameters and peak discharge shown in Table 4.2 were used as part of the sensitivity analysis to develop breach hydrographs and select representative hydrographs for downstream routing and evaluation of inundation extents.

4.3.2 BREACH OUTFLOW HYDROGRAPH DEVELOPMENT AND SENSITIVITY

The hypothetical breach outflow hydrographs for the dam failure were simulated using a hydrodynamic modeling software developed by the U.S. Army Corps of Engineers (USACE) Hydrologic Engineering Center River Analysis System (HEC-RAS) Version 6.2. It models the two-dimensional (2D) unsteady flow characteristics by solving the Saint-Venant equations and can also be used to simulate dam breach outflow hydrographs (USACE, 2014).

Data inputs to the breach model include the dam crest elevation, the supernatant pond elevation, the breach bottom elevation, the elevation-capacity curve for the outflow volume above the breach elevation, and the breach parameters (breach bottom width, side slope, and time to fail). In addition, HEC-RAS Version 6.2 is capable of modeling both Newtonian and non-Newtonian flows.

To evaluate the sensitivity of possible peak discharges for the Flood Induced scenario, various combinations of breach parameters within the ranges shown in Table 4.2 were used. A selection of modeled hydrographs is shown on Figure 4.4. Breach hydrographs were developed by varying the breach width and development time to estimate the following conditions:

- Peak discharge based on average breach parameters calculated using empirical equations and guidelines.
- Average peak discharges calculated using empirical equations.
- Average peak discharge plus 1 or 2 standard deviations, which are approximately equal to the 66th or 95th percentile flows based on a normal distribution.

- High peak discharges by having either a very fast downcutting rate of 100 m/hr (330 ft/hr) or higher, or by having a very wide breach. The 100 m/hr downcutting rate is among the fastest observed rates in historical erosional type failures of water retaining dams (Walder and O'Connor, 1997; Xu and Zhang, 2009).
- Low peak discharges by having a slow downcutting rate of 10 m/hr (33 ft/hr).

The sensitivity analysis indicates that the peak discharge is sensitive to the time of failure and the breach width, and much less sensitive to the breach side slopes. The peak of the breach hydrograph developed using average breach parameters is about 1,100,000 ft^3/s. Very wide breaches with bottom widths of over 500 ft resulted in higher peak discharges of over 2,000,000 ft^3/s. However, breaches of this width begin to extend into the heavily buttressed part of the dam. The times of failure of less than 1 hour resulted in similarly high peak discharges. However, given the construction materials, the buttressing, and the height of the dam, such fast failure times are less likely given that it would require downcutting rates of over 250 ft/hr.

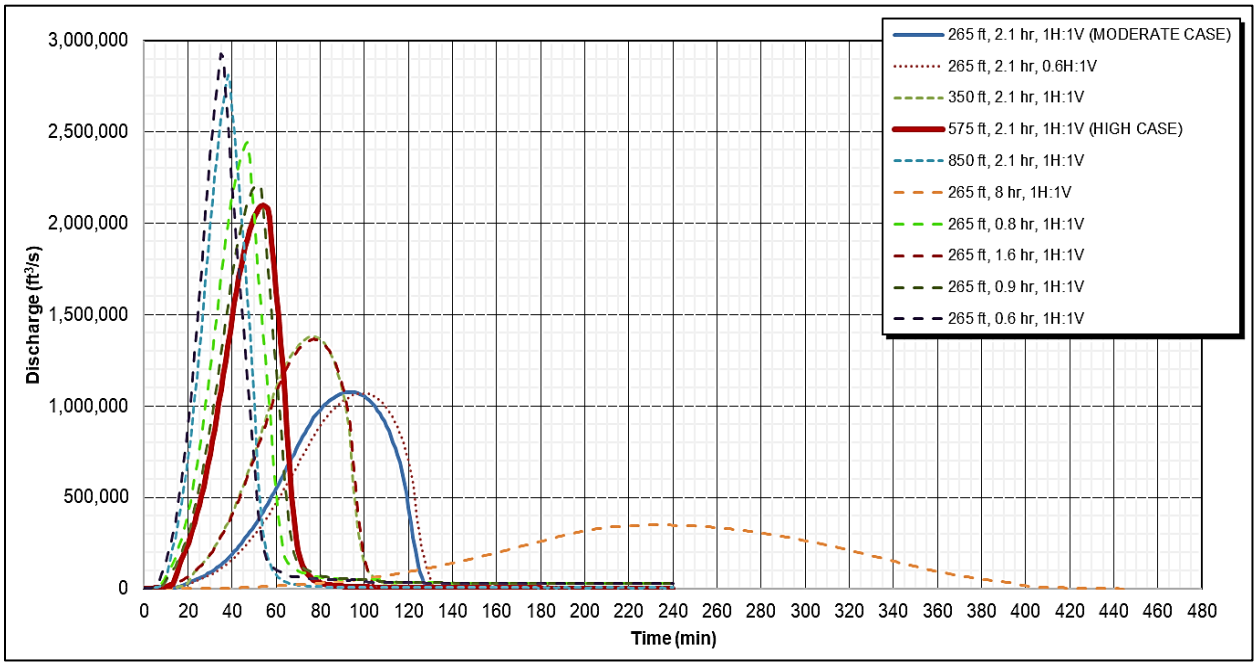

Note(s):

1. The breach parameters shown in the legend represent the bottom width, time to fail, and side slopes.
2. The "Moderate Case" and the "High Case" hydrographs were selected for downstream flood routing, as discussed in the text.

Figure 4.4 Breach Parameters Sensitivity Analysis

The results from the sensitivity analysis were used to inform the final selection of breach parameters and breach hydrographs to carry forward to model the downstream propagation of the breach flood wave. The final selection was based on breach parameters that were conservative, but that physically made sense considering the dam design and topographic constraints. Two hydrographs were selected to evaluate the downstream propagation – a higher peak hydrograph denoted High Case, and a lower peak hydrograph denoted Moderate Case.

The High Case breach hydrograph was developed using a wide breach bottom width of 575 ft with a time to fail of 2.1 hours. A narrower breach of 265 ft with a faster time to fail of 0.9 hours resulted in essentially the same peak magnitude and hydrograph shape as shown on Figure 4.4. Given the dam size and construction with additional buttressing encountered as the breach size increases, both the bottom breach width of 575 ft and a time to fail of 0.9 hours are conservative; therefore, the selected High Case hydrograph is considered to be conservative.

The Moderate Case hydrograph was based on the average breach parameters calculated using empirical equations and had a narrower bottom breach width of 265 ft with the same time to fail of 2.1 hours as the High Case hydrograph. Both hydrographs are based on the same breach outflow volume.

The selected breach parameters are summarized in Table 4.3, while the corresponding breach outflow hydrographs are shown on Figure 4.5. The High Case hydrograph was selected to be the governing case for modeling the downstream impacts, while the Moderate Case was evaluated as part of the sensitivity analysis to evaluate the impact on the timing of the breach flood wave propagation and corresponding inundation extent.

Table 4.3 Peak Discharge and Selected Breach Parameters

Description	Peak Discharge (ft^3/s)	Bottom Width (ft)	Side Slope (xH:1V)	Time to Fail (hr)	Breach Height (ft)
High Case	2,100,000	575	1.00	2.1	260
Moderate Case	1,080,000	265	1.00	2.1	260

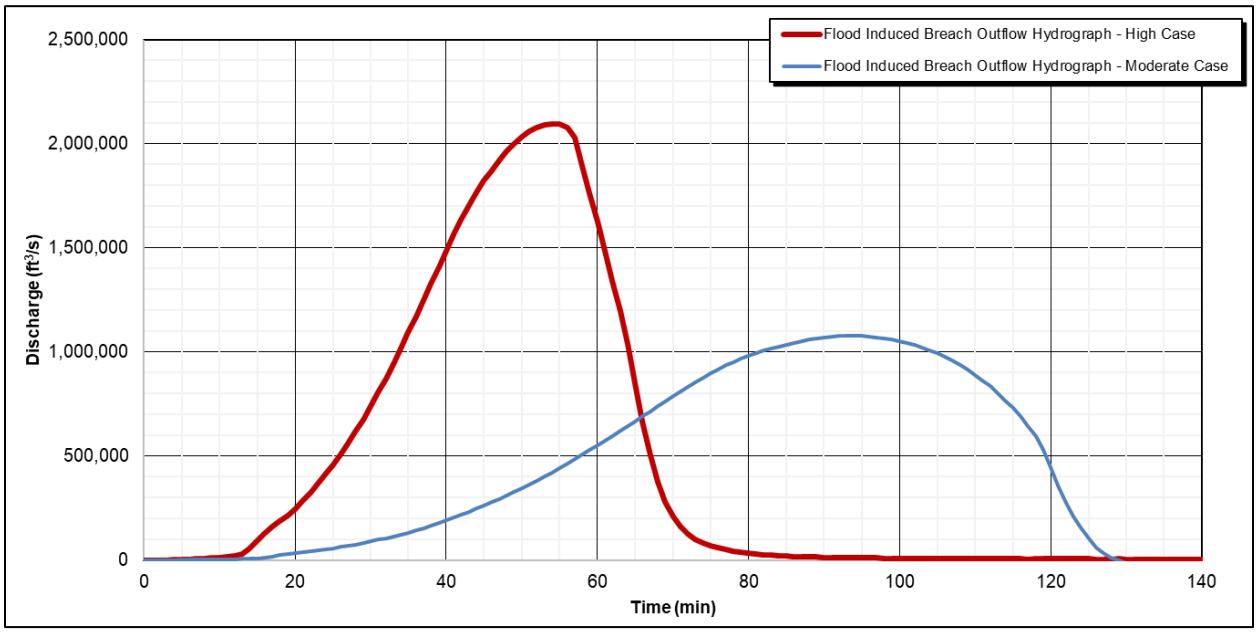

Figure 4.5 Flood Induced Breach Outflow Hydrographs

4.3.3 COMPARISON OF BREACH PARAMETERS TO PAST FAILURES

The selected breach parameters are compared to case studies of past dam breach events of water retaining and tailings embankments to assess their reasonableness and level of conservatism. The case studies are compiled in databases developed by Wahl (2014), Walder & O'Connor (1997), Rana et al. (2021b), and Adria (2022). Figure 4.6 shows the comparison of breach heights to breach formation times for historical failures of water retaining dams and tailings embankments, as well as landslide dams. Figure 4.7 shows the comparison of average breach widths to breach heights for historic failures of water retaining and tailings embankments. Figure 4.8 shows the comparison of observed eroded dam volumes to predicted eroded dam volumes using an empirical equation developed by Adria et al. (2023). The selected breach parameters for the YDTI Flood Induced breach are superimposed on these figures for comparison.

Breach Erosion Rate

Walder & O'Connor (1997) proposed the mean erosion rate (annotated as *k* on Figure 4.6) as a method to normalize formation times by the breach height, with higher mean erosion rates indicating a faster breach for a given breach height. They noted that most erosional breaches experience mean erosion rates between 10 and 100 m/hr (approximately 33 to 330 ft/hr). Several different mean erosion rates are included as colored lines on Figure 4.6 for reference. The erosion rate has a profound impact on the hydrograph shape, where higher rates result in faster time to fail, and consequently a peakier hydrograph. The impact of the hydrograph shape was further evaluated as part of the sensitivity analysis in Section 6.4.2.

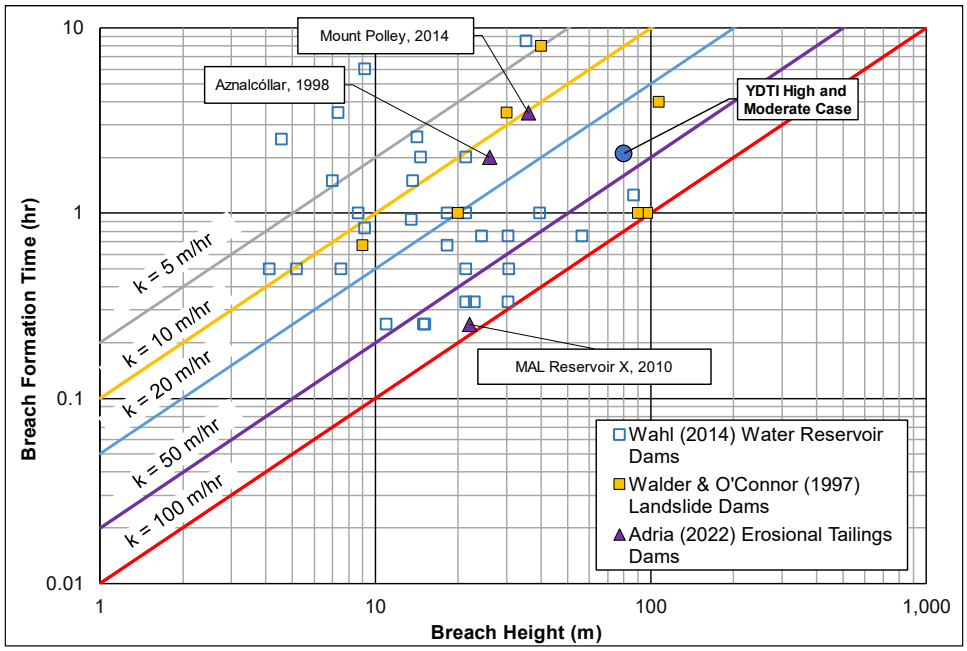

Figure 4.6 Comparison to Observed Breach Heights and Breach Formation Times for Past Failures of Water and Tailings Dams

Dams of all types with mean erosion rates faster than 80 m/hr (262 ft/hr) involved some additional failure mechanism, such as a structural or foundation failure, combined with the erosional type failure mechanism (Wahl, 1998; Wahl 2014). The events that failed primarily through the erosional breach mechanism typically experienced mean erosion rates of about 55 m/hr (180 ft/hr) or less. Walsh (2020) conducted physical modeling breach studies and found that the presence of a tailings beach reduced the severity and speed of a breach by 2 to 3 times compared to a failure without a tailings beach (i.e., a conventional water embankment without a core). This finding is supported by the Mount Polley (in 2010) and Aznalcóllar (also known as Los Frailes in 1998) tailings dam failures (both rockfill) exhibiting mean erosion rates of about 15 m/hr (50 ft/hr), or roughly one quarter of the typical mean erosion rate of 55 m/hr (180 ft/hr) for water dams.

Adria (2022) assessed the MAL Reservoir X tailings dam failure in Hungary in 2010 (commonly known as the Ajka or Kolontár event) to have experienced a combination of foundation, structural, and erosional failure mechanisms, which contributed to a high mean erosion rate of 88 m/hr (290 ft/hr). Most of the constructed water dams or landslide dams of similar breach height to the hypothetical YDTI breach height impounded water volumes 3 to 10 times larger than the YDTI pond volume contemplated in this study. The breadth of the YDTI dam (i.e., the crest width and shallow downstream slopes) is broader than most of the breached dams in the databases, which may result in a lower mean erosion rate for the same breach height and outflow volume. The selected formation time for this study results in a mean erosion rate of approximately 40 m/hr (130 ft/hr), which is considered a more realistic yet conservative estimate for the erosional type breach associated with the assumed failure mode conditions (i.e., more than 2.5 times the erosion rate observed in the Mount Polley and Aznalcóllar failures).

Breach Width

The colored lines shown on Figure 4.7 represent the average breach width as a multiple of the breach height. These have been used in guidelines (USBR, 1988; FERC, 1993) for water dam breach studies, and were included in the breach parameter selection as discussed in Section 4.3.1. An average breach width with a larger multiple of the breach height indicates a larger and more severe breach for the given breach height. Most of the guidelines for water dams generally recommend a multiple between 1 and 5; however, the water dams data from Wahl (2014) indicate that breaches wider than this range were observed for low height dams (i.e., lower than 30 m, or about 100 ft). This can be explained with the breach preferentially developing through materials with lower resistance to erosion, i.e., once the foundation with higher resistance to erosion is reached, the breach starts to widen through the embankment.

The widths presented in Rana et al. (2021b) are based on past failures of tailings dams, where the width was typically measured from aerial photos. These data were not segregated to include consideration of the failure mechanism. Adria (2022) found that the widths in Rana et al. (2021b) generally correspond to the top width of the breach, and are therefore higher than the average width of the breach. The higher number of events assessed in Rana et al. (2021b) compared to Adria (2022) are still useful to consider the scatter and relative trend for tailings dams, while the data from Adria provide further insight on the impact of the failure mechanism on the breach width. Adria (2022) segregated breaches that were considered primarily erosional to those that were primarily driven by non-erosional failure mechanisms. Non-erosional tailings dam failures included those that had a combination of two or more failure mechanisms (e.g., foundation or structural combined with erosional failure mechanism), liquefaction type failures (e.g., the failures in Brazil – Fundão in 2015 and Feijão in 2019), or other failure mechanisms causing a sudden collapse.

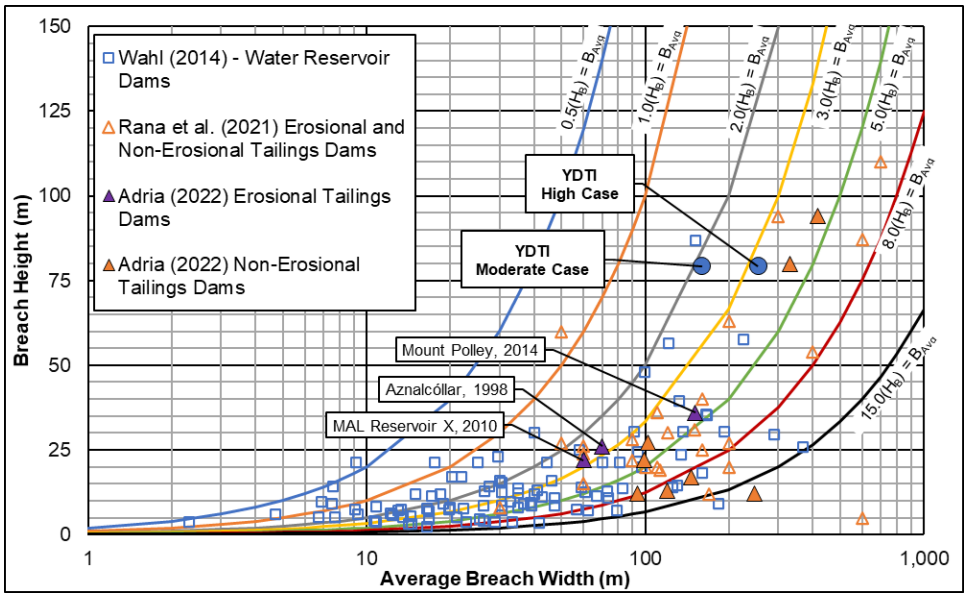

Figure 4.7 Comparison to Observed Breach Heights and Breach Widths for Past Failures of Water and Tailings Dams

The average breach width is generally around 3 times the breach height for water dams, typically ranging from 0.5 to 8 breach heights. The tailings dam widths reported in Rana et al. (2021b) have greater scatter in the data, but generally indicate a larger breach width for a given breach height than observed in water dams. Adria (2022) found that the erosional tailings dam breaches had average breach widths between 3 and 5 breach heights, which is generally less than the non-erosional tailings dam breach events. The breadth of the YDTI dam is much larger than the events in the databases, which would reduce the lateral erosion that could occur during a breach. The selected breach geometry for the hypothetical YDTI failure results in an average breach width of approximately 3 breach heights, which was considered a reasonable estimate for the erosional type breach associated with the assumed failure mode and failure mechanism conditions.

Eroded Dam Volume

To evaluate the eroded dam volume, an empirical equation that uses a multiple linear regression approach was developed by Adria et al. (2023). The best fit empirical equation is based on the databases in Wahl (2014) and Adria (2022), and is shown below:

$$V_{Er} = 1.68{H_B}^{2.08}{V_{Out}}^{0.26}$$

Where:

- V_{Er} [m^3] = Eroded Dam Volume
- H_B [m] = Breach Height
- V_{Out} [m^3] = Outflow Volume of free water and tailings

The eroded dam volume predicted by the best fit empirical equation is compared against the observed eroded dam volume on Figure 4.8 for past failures, with the YDTI values superimposed on it. The 1:1 agreement line, as well as 0.5 order of magnitude dashed lines that roughly represent the upper and lower envelopes to the observed scatter are included on Figure 4.9 for reference.

The best fit empirical equation estimates an eroded dam volume for the YDTI of 2.0 M m^3 (1,600 ac-ft). The calculated eroded dam volume based on the selected breach parameters is equal to 4.2 M m^3 (3,400 ac-ft) for the High Case and 2.5 M m^3 (2,040 ac-ft) for the Moderate Case breach outflow hydrographs. The selected breach parameters would result in a higher eroded dam volume than would be predicted using the best fit empirical equation and fit within the observed scatter from past failures.

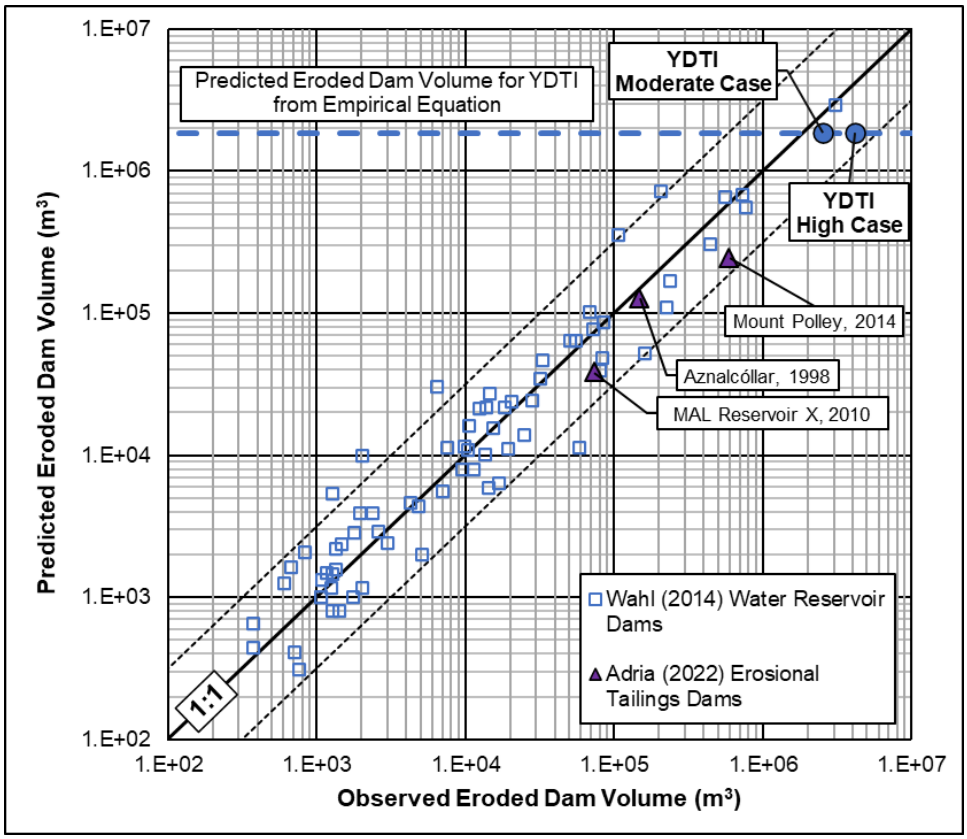

Note(s):

1. The estimated eroded dam volumes calculated using the breach parameters selected for the High Case and Moderate Case breach hydrographs (Table 4.3) were plotted as Observed Eroded Dam Volumes for the YDTI for comparison purposes.

Figure 4.8 Comparison of Observed Eroded Dam Volumes and Predicted Eroded Dam Volumes for Past Failures of Water and Tailings Dams

4.4 BREACH OUTFLOW CHARACTERISTICS

The physical behavior and the flow characteristics for different flow types was investigated by O'Brien (1986) and indicates that lower solids concentrations are associated with water floods and some mud floods, which can be modeled as Newtonian flows. Such flows typically move faster than mudflows, debris flows, or flow slides that need to be modeled as non-Newtonian flows. Consequently, Newtonian flows may result in larger and deeper inundation and faster flood wave propagation. As the concentration of solids continues to increase and reaches approximately 45% by volume (about 70% by weight) at the upper end of mud floods, the flow behavior becomes increasingly impacted by rheological properties of the solids/water mixture. Such flows must be considered as non-Newtonian for which the rheological properties need to be accounted for. Further increase in solids concentration would result in mud flows, and finally in flow slides and debris flows for solids concentrations above approximately 55% by volume.

Figure 4.9 was generated based on research by O'Brien (1986) and adopted in CDA (2021). It shows various flow behavior categories depending on the solids concentration in the flow. The calculated solids concentration in this study was superimposed on Figure 4.9. The figure indicates that the breach outflow is within the mid to lower range of mud floods, which is expected to be moderately affected by the rheology due to the relatively low solids concentration. As such, the outflows were modeled as non-Newtonian flows using the quadratic rheological model with the input parameters summarized in Section 2.4.4.

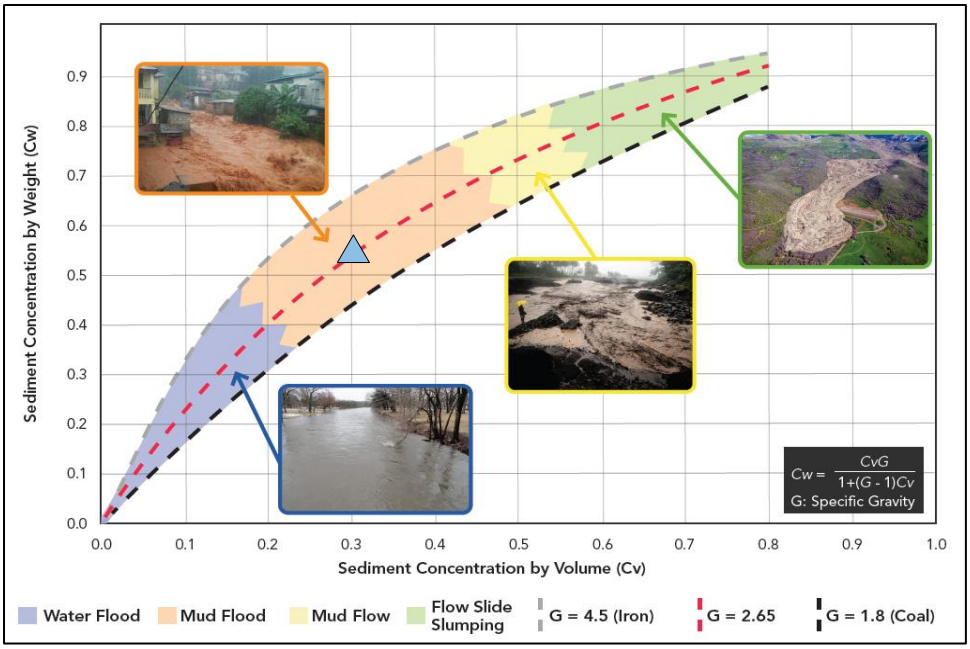

Note(s):

1. The blue triangle indicates the solids concentration by volume (C_v) of 30% for the YDTI Flood Induced scenario.

Figure 4.9 Flow Behavior as a Function of Solids Concentration (CDA, 2021)

5.0 FLOOD ROUTING MODEL DEVELOPMENT

5.1 GENERAL

The downstream routing of the breach flood wave caused by a hypothetical YDTI failure was conducted to estimate the maximum extent of inundation using HEC-RAS Version 6.2. The breach outflows were modeled as non-Newtonian flows using the quadratic rheological model.

The model extended south from the breach location and included the Berkeley and Continental Pits. The initial hydrologic conditions of the hypothetical dam breach are discussed in Section 2.3, and the dam breach outflow hydrographs are defined in Section 4.3.2.

5.2 ELEVATION DATA

The digital elevation model (DEM) used for flood propagation modeling is based on detailed Light Detection and Ranging (LiDAR) data, taken on June 25, 2021, provided by Montana Resources, LLC. The vertical accuracy of the LiDAR data is typically in the order of 0.5 to 0.7 ft. The DEM extended beyond the mine boundary as shown with the photo extent on Figure 5.1, and included the YDTI area, and the Berkeley and Continental Pits, as well as parts of the city of Butte.

Additional high resolution topographic data covering Butte and Ramsay was obtained from PhotoSat Information Ltd. in 2022. This topography would have been used in case the flood wave propagated past the mine boundary.

Surfaces of the life of mine embankment, rock disposal sites, and pits from the Design Document were incorporated over the 2021 LiDAR topography for the purposes of dam breach modeling (as shown on Figure 5.1). The detailed life of mine arrangement of the YDTI and Continental Pit are shown on Figure 2.1. Design details for the continued development of the YDTI are summarized in the design report (KP, 2024b).

The Berkeley Pit was filled to the elevation associated with its current operating level combined with the PMF generated by the PMP combined with the 1 in 100-year snowpack melt. The Continental Pit, which would be empty during operations, was filled with the PMF hydrological event only. In the model, these water levels consist of flat surfaces in the pits at elevations noted in Section 2.3.4.

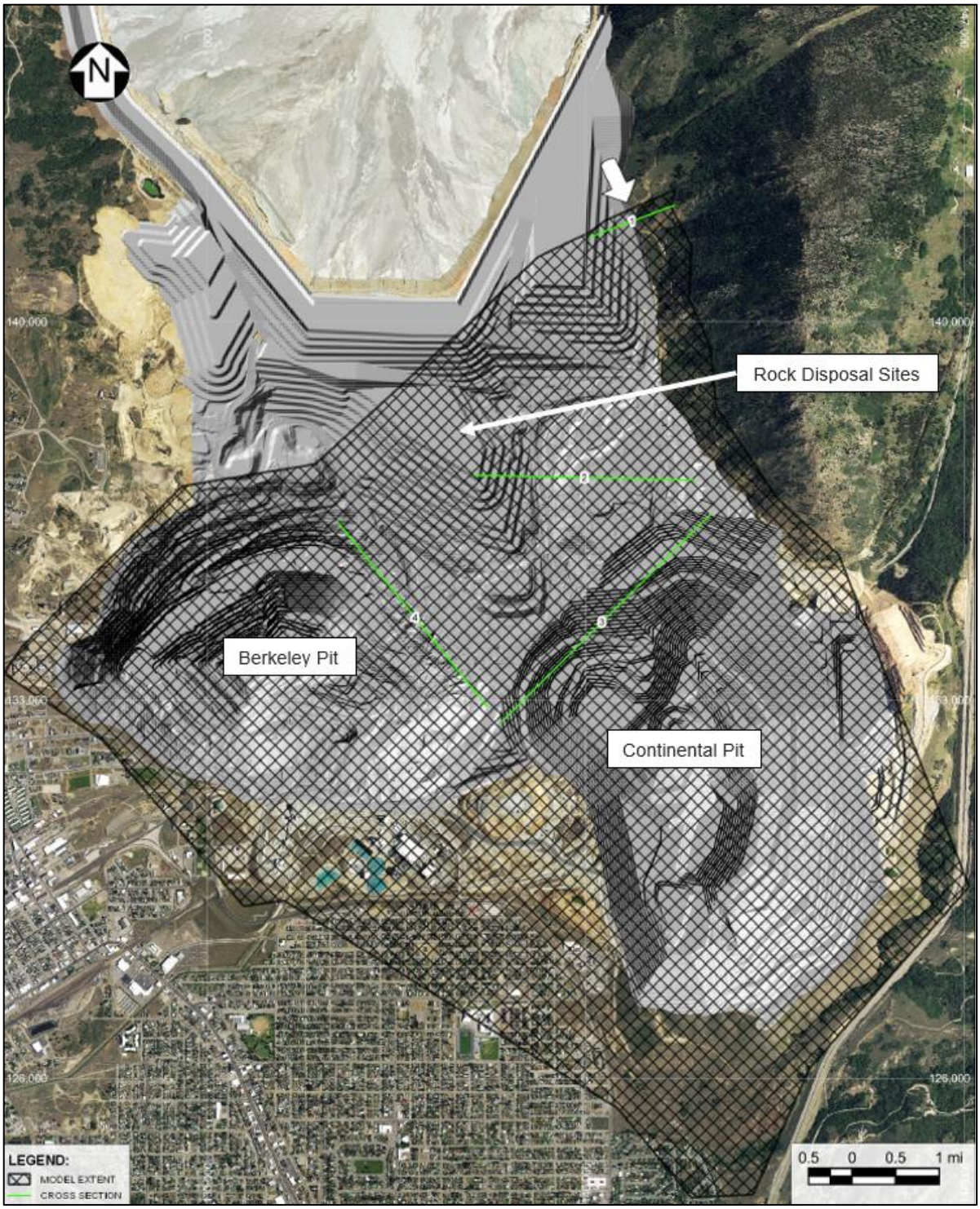

Note(s):

1. Base map provided by Montana Resources, LLC on August 7, 2024.
2. Dam and rock disposal sites are projected surfaces at the time of the breach.

Figure 5.1 Overview of the Terrain used in the Breach Flood Routing Models

5.3 FLOOD ROUTING MODEL SETUP

The 2D hydrodynamic model was developed using HEC-RAS Version 6.2, with the model extent shown on Figure 5.1. The cell size immediately downstream of the dam was selected to be 25 ft, which transitioned to 50 ft farther downstream. This resulted in a total of approximately 75,000 cells for the entire model domain. HEC-RAS utilizes all of the topographic information contained in the DEM by developing hydraulic property tables for each individual cell. The 2D flow areas in HEC-RAS are based on the actual terrain rather than on the mesh cell size (HEC, 2021), which enables maintaining accurate results with larger cell sizes compared to other 2D hydrodynamic modeling software. In other words, the details of the terrain are accurately captured within the mesh cell size, even if the mesh cell size is much larger than the terrain grid size.

Cells near the dam breach location were connected to a storage area that equaled the corresponding breach outflow volume. The breach inflow into the model corresponded to the breach hydrographs shown on Figure 4.5. Models were run to a finish time of 12 hours, which ensured full breach discharge from the YDTI and the inflow into the pits were complete.

The flow path downstream of the North-South Embankment runs along the base of the dam and then into the Continental and Berkeley Pits. The terrain over which the flood wave travels is an active area of the mine site with a variety of access roads. Due to the irregularity of the terrain, a Manning's n value of 0.06 was selected for the entire model domain. This value was estimated from site and aerial photographs and typical values for this terrain type. A sensitivity analysis that evaluated the selected Manning's n value is discussed in Section 6.4.4.

6.0 FLOOD INDUCED SCENARIO MODELING RESULTS

6.1 GENERAL

Results from the Flood Induced dam breach inundation modeling for the North-South Embankment are described in the following sections. The results include inundation extents and information on the breach flood wave propagation in terms of maximum flow depths, peak discharges, and flood front and peak discharge arrival times.

Additional maps that show maximum depth-velocity product (DV) are presented, which are indicative of the flood severity. The DV maps can be used to conduct Loss of Life Analysis (LLA) based on estimated Population at Risk (PAR) (e.g., Montana DNRC, 2010; USBR, 2015). While LLA was not undertaken as part of this dam breach study, the results can be used for such analysis. Generally, a flow with a DV of less than 4.3 ft^2/s (e.g., a flow depth of 4.3 ft with a velocity of 1 ft/s) would be safe for most adults, while a flow with a DV of 15 ft^2/s would be able to sweep away passenger vehicles. Flows with a DV of 54 ft^2/s can be damaging for poorly constructed buildings, while a DV of over 108 ft^2/s can cause damage to well-built timber and masonry buildings.

6.2 BREACH FLOOD ROUTING RESULTS

The inundation areas for the Flood Induced breach outflows are shown on Figure 6.1, Figure 6.2, and Figure 6.3 and include the following information:

- Maximum flow depths (Figure 6.1)
- Maximum DV values (Figure 6.2)
- Flood wave arrival times (Figure 6.3)

The maps shown on these figures are also provided in Appendix B. Due to the short travel path of the flood wave before reaching the Berkeley and Continental Pits, most of the flooded areas are inundated within 1 hour of the breach. The flood arrival times indicated on the maps are relative to the start of the breach rather than the start of the storm event. The modeling indicates the entire breach outflow would be contained in the Berkeley and Continental Pits; hence the inundation boundary does not extend into the city of Butte.

The areas impacted by the breach outflow are between the breach location and the Berkeley and Continental Pits. The potentially affected facilities include the HsB WTP, Precipitation Plant, HsB CS pump house, and the McQueen (tailings) booster pump house. Any tailings distribution and reclaim pipelines, as well as various access roads that run through this area would also be within the inundation zone. The inundated areas upstream of the pits have maximum flooded depths of over 12 to 24 ft as shown on Figure 6.1, and DV values greater than 54 ft^2/s as shown on Figure 6.2. The breach flood wave would reach the pits within approximately 15 to 20 minutes, as shown on Figure 6.1 and Figure 6.3 The impacts to these inundated areas are expected to be severe.

Additional information on the flood routing and potential impacts in the pits can be found in Section 6.3.

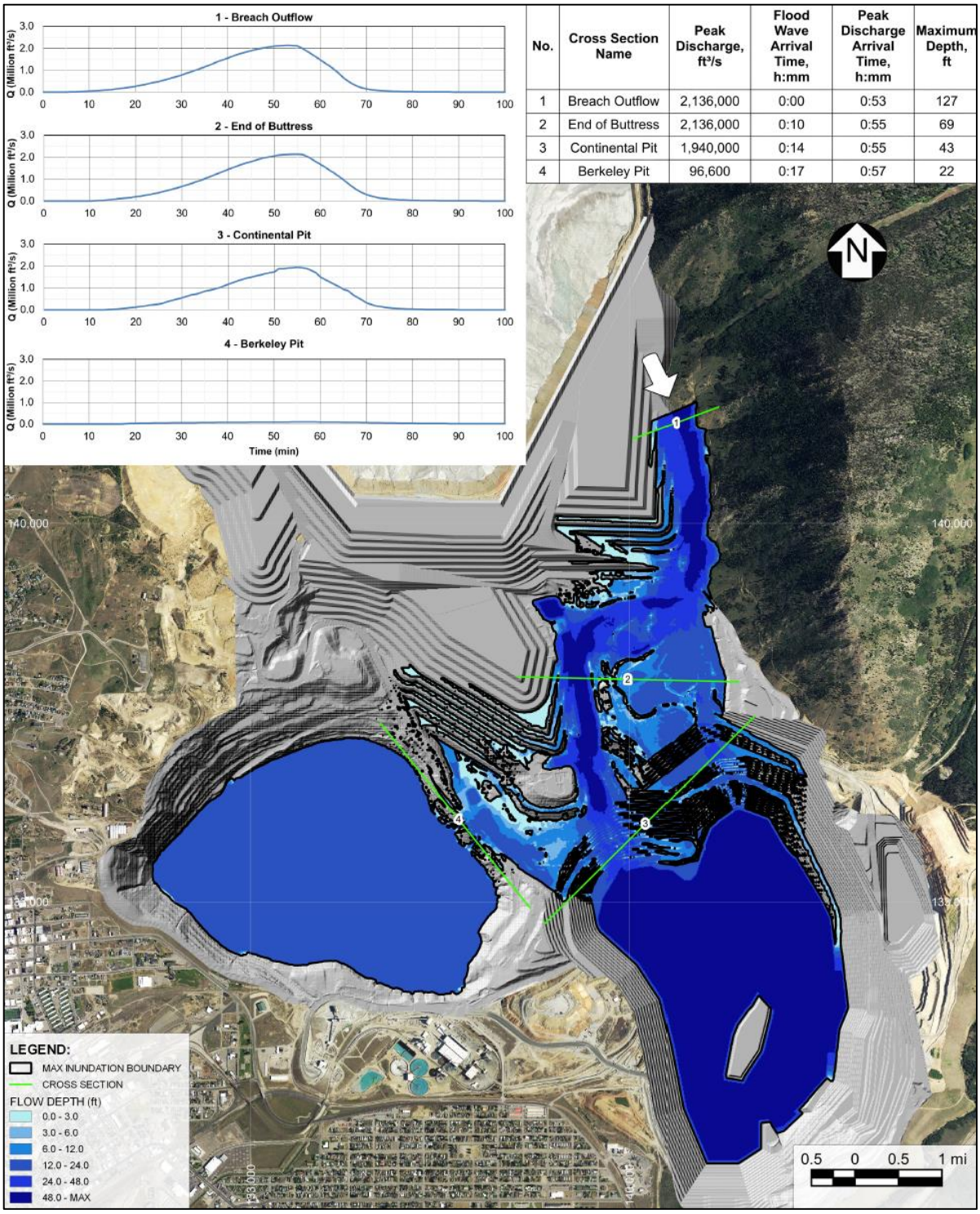

No.	Cross Section Name	Peak Discharge, ft³/s	Flood Wave Arrival Time, h:mm	Peak Discharge Arrival Time, h:mm	Maximum Depth, ft
1	Breach Outflow	2,136,000	0:00	0:53	127
2	End of Buttress	2,136,000	0:10	0:55	69
3	Continental Pit	1,940,000	0:14	0:55	43
4	Berkeley Pit	96,600	0:17	0:57	22

Note(s):

1. Base map provided by Montana Resources, LLC on August 7, 2024.
2. Dam and rock disposal sites are projected surfaces at the time of the breach.

Figure 6.1 Flood Induced Scenario – Maximum Inundation and Flow Depth Map

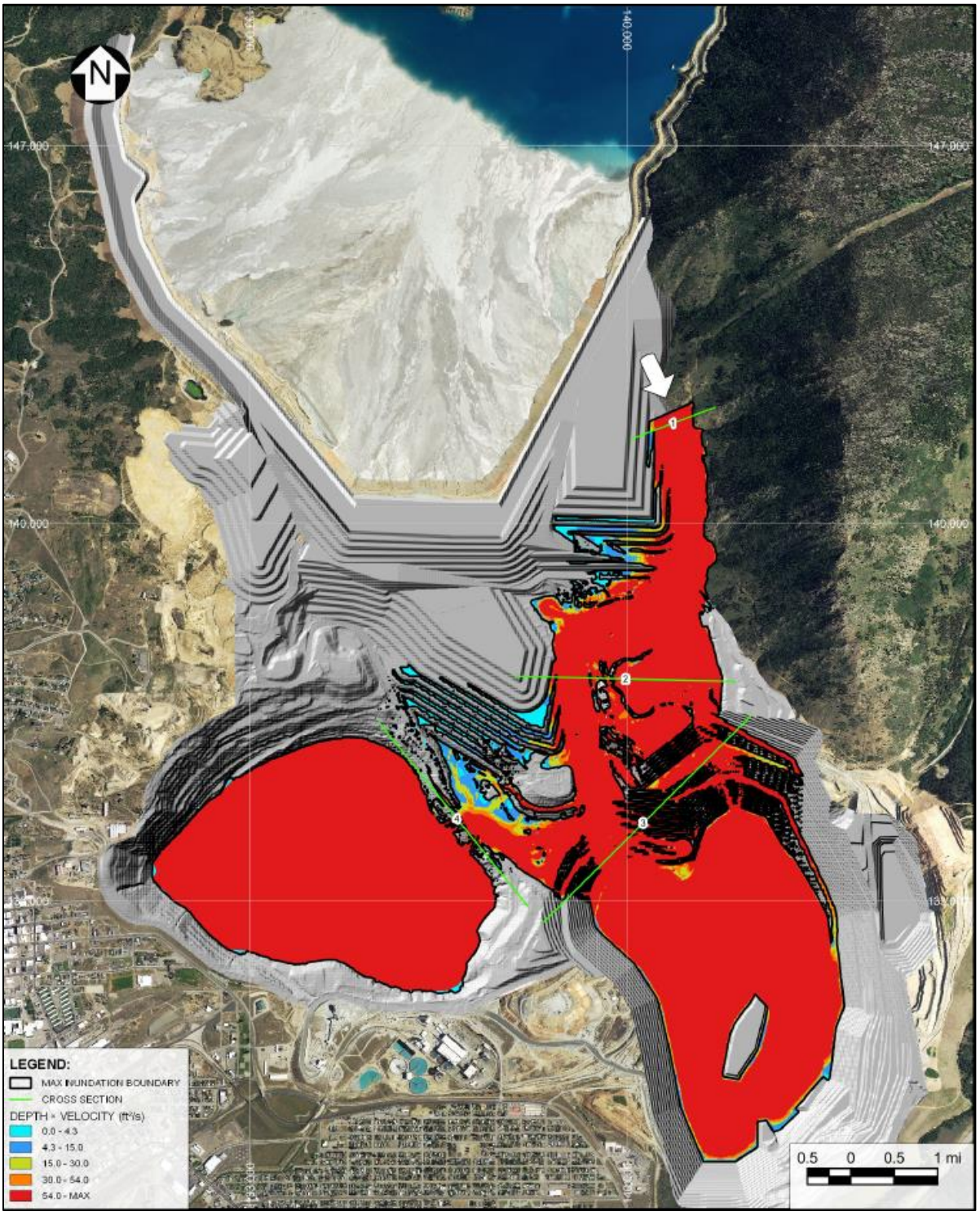

Note(s):

1. Base map provided by Montana Resources, LLC on August 7, 2024.
2. Dam and rock disposal sites are projected surfaces at the time of the breach.

Figure 6.2 Flood Induced Scenario – Maximum DV Map

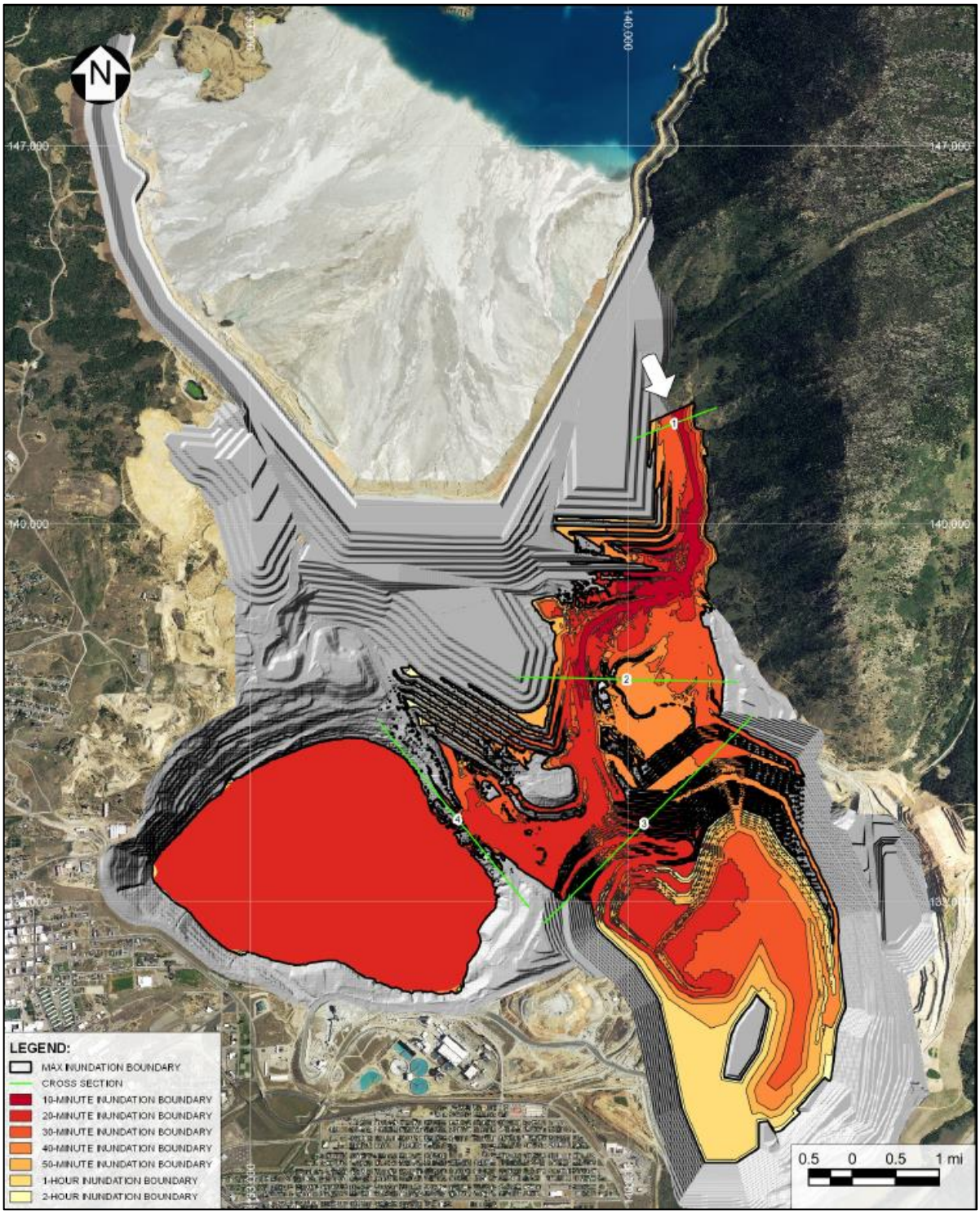

Note(s):

1. Base map provided by Montana Resources, LLC on August 7, 2024.
2. Dam and rock disposal sites are projected surfaces at the time of the breach.

Figure 6.3 Flood Induced Scenario – Flood Wave Arrival Times Map

6.3 IMPACTS TO OPEN PITS

The flood front arrival times, incremental depths, and other flood wave characteristics for selected locations, including the Berkeley and Continental Pits, are summarized in the table on Figure 6.1. The times shown in the table are relative to the start of the breach. The identification numbers for the cross sections are indicated on Figure 6.1.

The breach flood wave hydrographs at different locations are also shown on Figure 6.1. The flood wave first travels downstream of the breach (Cross Section 1) and is contained between the North RDS and the slopes of Rampart Mountain. After it reaches the end of the North RDS (Cross Section 2), the flood wave continues before finally flowing east into the Continental Pit (Cross Section 3) and west into the Berkeley Pit (Cross Section 4). Most of the breach outflow volume enters the Continental Pit with only a small portion predicted to flow into the Berkeley Pit. The elevation-capacity curves of the Berkeley Pit and Continental Pit with noted elevations of interest are shown on Figure 6.4 and Figure 6.5, respectively. The figures depict the existing water level (only applicable for Berkeley Pit), water level including PMF before the breach, and water level with the added breach outflow volume. The entire breach outflow volume is shown to be contained by the two pits.

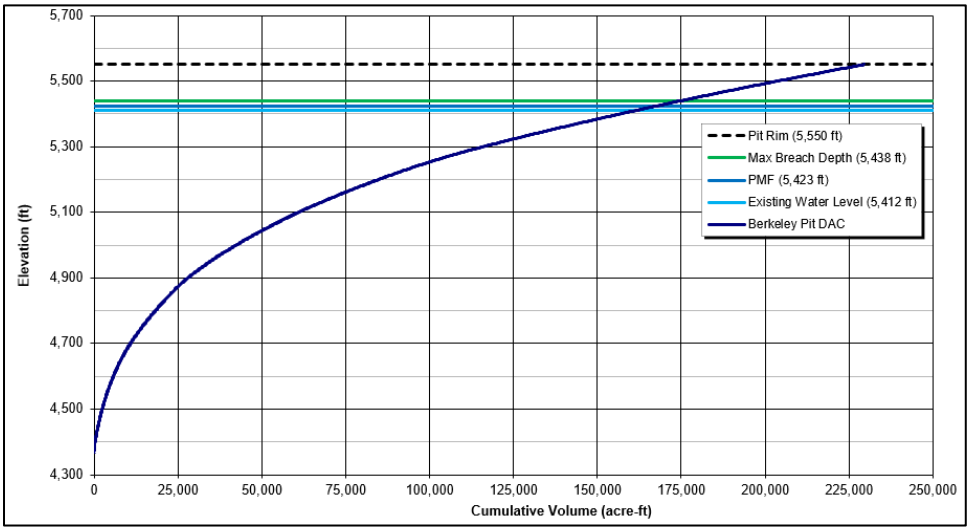

Note(s):

1. Bottom of Berkeley Pit is at EL. 4,370 ft.

Figure 6.4 Berkeley Pit Elevation-Capacity Curve with Breach Inflow

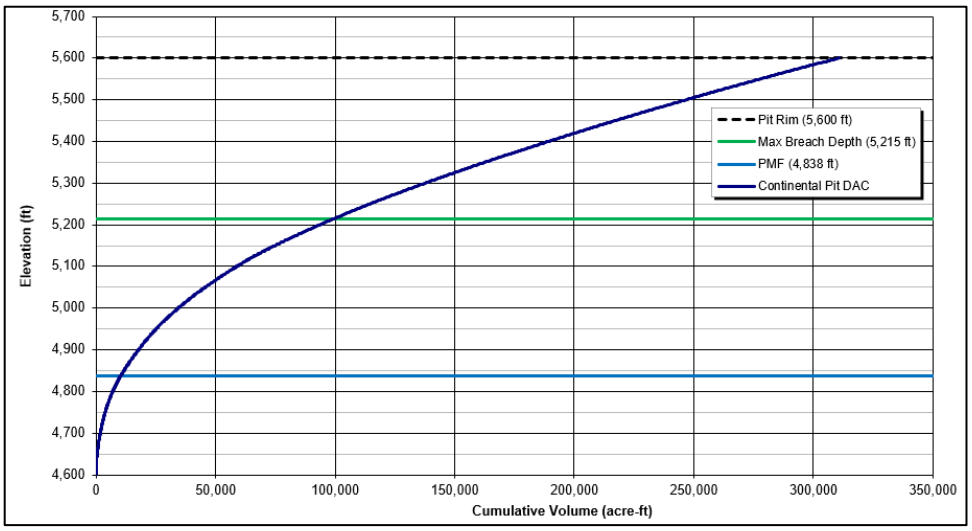

Note(s):

1. Bottom of Continental Pit is at EL. 4,600 ft.

Figure 6.5 Continental Pit Elevation-Capacity Curve with Breach Inflow

6.4 SENSITIVITY ANALYSIS

6.4.1 GENERAL

The sensitivities of the flood modeling results to the breach hydrograph, tailings rheology, and Manning's n inputs were evaluated. It is noted that the sensitivity analysis was conducted with a somewhat different preliminary configuration of the rock disposal sites, and the discussion in the following sections is based on that preliminary configuration. The sensitivity analysis indicated very limited sensitivity to the tested inputs. Consequently, it was not updated using the latest embankment and rock disposal sites configuration shown on Figure 2.1 and on Figure 6.1 to Figure 6.3.

6.4.2 BREACH HYDROGRAPH

To evaluate the sensitivity of the flood routing results to the uncertainty related to breach parameter selection and the shape and peak of the outflow hydrograph, two breach outflow hydrographs were evaluated in this study (as shown with Moderate Case and High Case hydrographs on Figure 4.5).

The inundation extent comparison shown on Figure 6.6 indicates the inundation area is not sensitive to the peak magnitude of the breach outflow hydrograph or to the hydrograph shape. This is expected considering that both scenarios have the same outflow volume.

The flood wave hydrographs shown on the same figure indicate that the High Case flood wave has a faster arrival time compared to the Moderate Case flood wave, as expected. This demonstrates that the High Case hydrograph selected as a governing case for the Flood Induced breach flood wave modeling is conservative and is considered suitable for inundation mapping and flood wave propagation evaluation, as well as for emergency planning.

Case	No.	Cross Section Name	Peak Discharge, cfs	Flood Wave Arrival Time, h:mm	Peak Discharge Arrival Time, h:mm	Maximum Depth, ft
High	1	Breach Outflow	2,140,000	0:00	0:53	112
	2	End of Buttress	2,130,000	0:18	0:54	105
	3	Continental Pit	1,980,000	0:23	0:55	34
	4	Berkeley Pit	171,000	0:25	0:56	30
Moderate	1	Breach Outflow	1,070,000	0:00	1:34	95
	2	End of Buttress	1,070,000	0:23	1:36	94
	3	Continental Pit	962,000	0:35	1:37	25
	4	Berkeley Pit	112,000	0:37	1:36	20

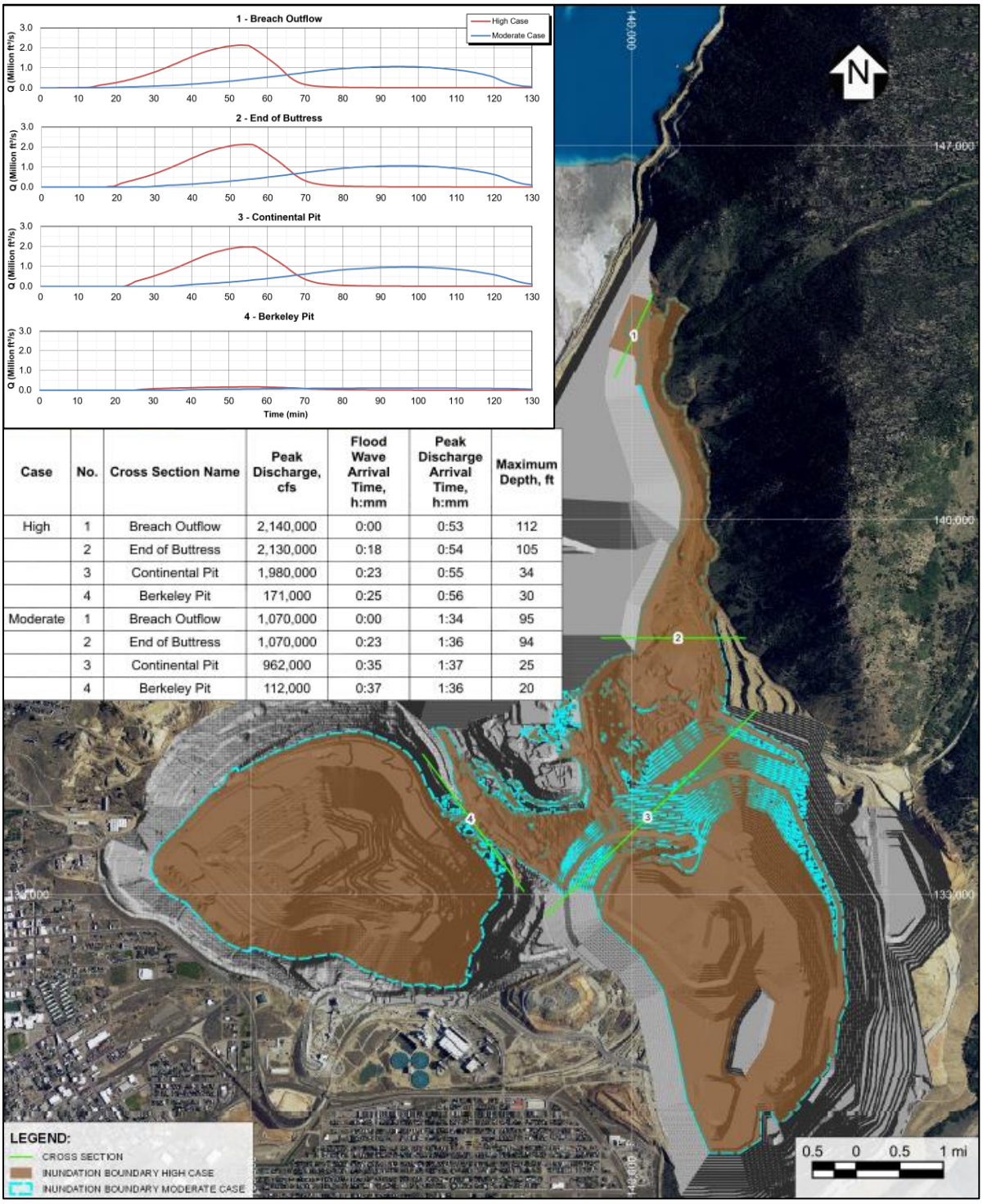

Note(s):

1. Base map provided by Montana Resources, LLC on August 7, 2024.
2. Preliminary models of the life of mine embankment and rock disposal sites were used for breach flood propagation modeling.

Figure 6.6 Flood Induced Scenario Inundation Extent – Breach Hydrograph Sensitivity

6.4.3 TAILINGS RHEOLOGY

Sensitivity that is typically evaluated for non-Newtonian flows is related to the selected rheological parameters. The three rheology ranges shown on Figure 2.13 with parameters summarized in Table 2.1 and Table 2.2 were considered for the sensitivity analysis. The Low Flowability is represented with a strong rheology having high yield stress and viscosity, while the High Flowability is represented with a weak rheology having low yield stress and viscosity. Based on the laboratory testing results, the parameters were selected to be +1.0 and -0.5 order of magnitude for the yield stress, and +0.5 and -0.25 an order of magnitude for the viscosity, as discussed in Section 2.4.4. An additional case where the flow was modeled as Newtonian (i.e., water flood) was also considered for the sensitivity analysis.

A comparison of the inundation extents for the rheology sensitivity scenarios is shown on Figure 6.7, including the flood wave hydrograph comparison for each cross section. The results indicate that the inundation extent and the flood wave arrival times are not sensitive to the selected rheological parameters. The negligible differences in the model results are considered reasonable due to the relatively low volumetric solids content of 30% in the breach outflows.

In conclusion, considering the negligible differences in the Flood Induced scenario results, the modeling is not sensitive to the rheological parameters and the selected Base Case rheology values are considered adequate.

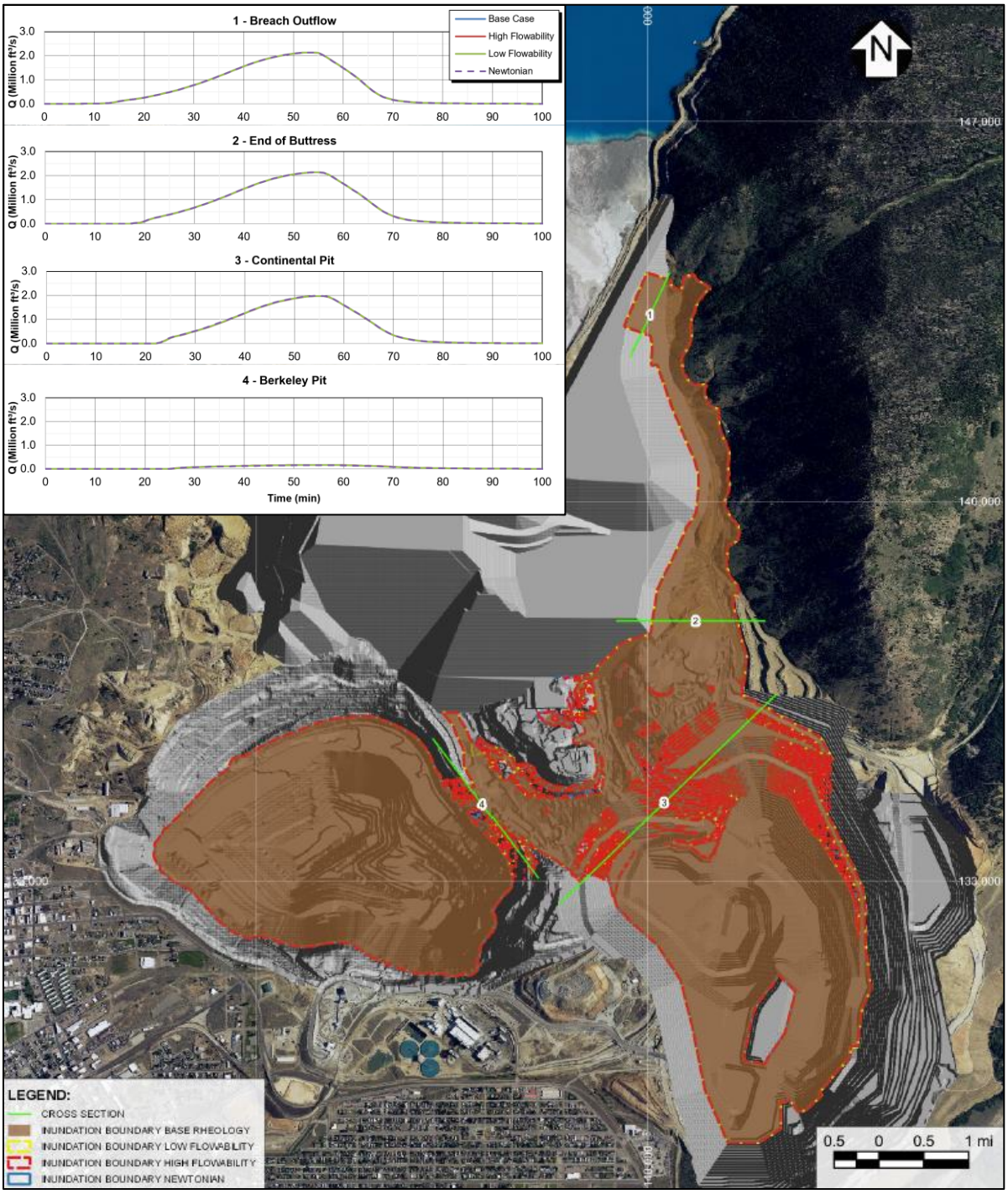

Note(s):

1. Base map provided by Montana Resources, LLC on August 7, 2024.
2. Preliminary models of the life of mine embankment and rock disposal sites were used for breach flood propagation modeling.

Figure 6.7 Flood Induced Scenario Inundation Extent – Rheology Sensitivity

6.4.4 MANNING'S n

Sensitivity of the hydrodynamic modeling results to the selected roughness parameter was completed in which the Manning's n value was changed to 0.03. This lower n value was selected to represent the lower bound value based on literature by Chow (1959) and Janssen (2016), site and aerial photographs, and professional experience. A comparison of the inundation extents for the Manning's n sensitivity analysis is shown on Figure 6.8, including the flood wave hydrographs for each cross section. The "Base Case" shown on this figure uses the High Case breach hydrograph, the Base Case rheology parameters, and a Manning's n value of 0.06. The Manning's n sensitivity case uses the same breach hydrograph and the same rheology, but a Manning's n value of 0.03 (i.e., -50% of the original value).

The inundation extent comparison shown on Figure 6.8 indicates the inundation area is not sensitive to the selected roughness value. Similarly, the flood wave arrival time shown on the hydrographs does not vary at any of the four cross sections. The resistance to flow during a dam breach event may be expected to increase rather than decrease due to the transport of eroded materials and debris; however, due to the closeness of the pits and the relatively limited extent of inundation, the variation in Manning's n does not have an impact on the results.

In conclusion, considering the negligible differences in the results that are shown not to be sensitive to the Manning's n value, the selected Manning's n value of 0.06 is considered adequate.

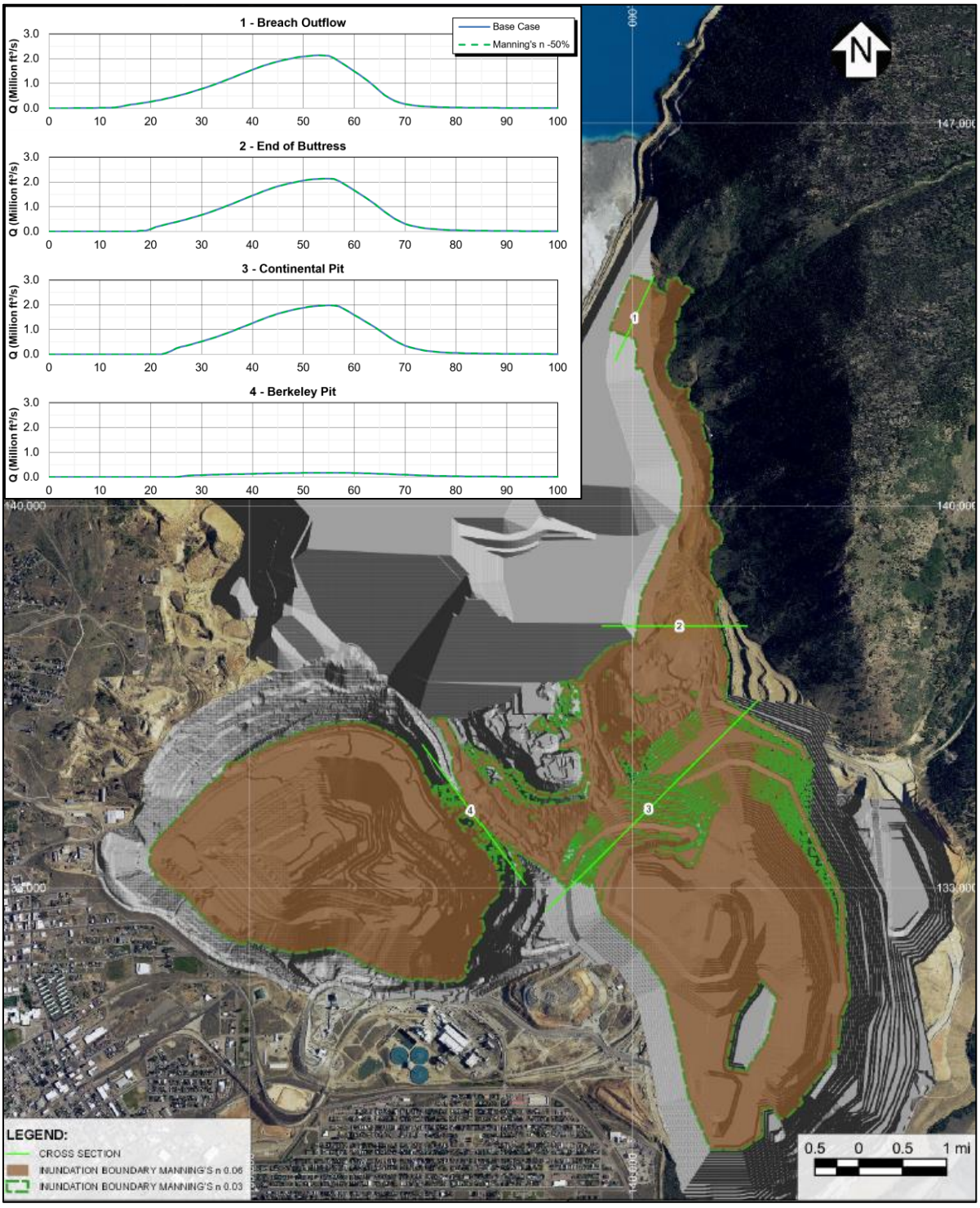

Note(s):

1. Base map provided by Montana Resources, LLC on August 7, 2024.
2. Preliminary models of the life of mine embankment and rock disposal sites were used for breach flood propagation modeling.

Figure 6.8 Flood Induced Scenario Inundation Extent – Manning's n Sensitivity

7.0 CONCLUSIONS

A dam breach inundation study was undertaken for the North-South Embankment of the YDTI for the proposed dam raise to EL. 6,560 ft to determine the potential inundation extents subsequent to a hypothetical failure at the ultimate proposed configuration (prior to closure). The modeling results are intended to assist in characterizing the potential physical impacts in terms of inundation and inform the assessment of risk of this proposed future facility arrangement. This study is not a risk assessment, and it specifically ignored the likelihood of a dam breach occurrence. The results of this analysis do not reflect upon the structural integrity or safety of the YDTI, and this study does not account for the design safety measures, management practices, or regulatory requirements implemented to prevent a breach from occurring.

This report considers the Flood Induced scenario only. The study demonstrated that the inundation limits of the Flood Induced scenario are predicted to be contained within the mine site boundary; therefore, it was considered reasonable to exclude modeling of a similar but smaller Fair Weather scenario. The dam breach outflow hydrographs were modeled using HEC-RAS Version 6.2. Ranges of breach parameters were used to understand the sensitivity of the hydrograph shape and peak discharge magnitude. The breach outflow hydrographs that corresponded to the selected breach parameters were then routed downstream using the same HEC-RAS model to evaluate the flood wave propagation and map the resulting inundation. The impacts of the tailings rheology on the breach runout characteristics were considered in the analysis by using the non-Newtonian fluid approximation.

The inundation results downstream of the YDTI were presented on maps showing maximum inundation extents, maximum and incremental inundation depths, peak discharges, and flood front and peak discharge arrival times.

Flood Induced Scenario Results

- The Flood Induced scenario assumed collapse of the North-South Embankment at the abutment location during a PMF event that could be induced due to various triggers. The embankment deformation followed by overtopping was assumed to cause an erosional failure of the dam.
- The Flood Induced scenario was modeled as a non-Newtonian fluid with a C_v of 30% in the breach outflow, which is representative of a mud flood regime.
- The natural PMF event without dam breach is contained within the YDTI, or flows into the Berkeley and Continental Pits for the catchments downstream of the YDTI.
- The entire modeled breach outflow is contained in the Berkeley and Continental Pits, with no overtopping of the pit walls and with additional capacity remaining in the pits.
- The impacts to the inundated areas upstream of the pits are expected to be severe. The maximum flooded depths are predicted to be over 12 to 24 ft, with the breach flood wave reaching the pits within 15 to 20 minutes, and with flood severity (DV) values greater than 54 ft^2/s, which would be unsafe for adults, passenger vehicles, and poorly constructed buildings.
- The mine infrastructure and facilities located between the YDTI and the open pits are predicted to be inundated and damaged or destroyed by the hypothetical breach outflow, including the HsB WTP, Precipitation Plant, HsB CS pump house, and the McQueen (tailings) booster pump house. The tailings distribution and reclaim pipelines and various access roads that are also predicted to be within the inundation limits, would be damaged or destroyed.

- The breach flood wave is not predicted to reach the Concentrator Area or the city of Butte.

Sensitivity of the Results

- The sensitivity to the breach outflow hydrograph indicates that inundation extent is not sensitive to the peak magnitude or the shape of the breach outflow hydrograph. However, the flood wave generated by the breach hydrograph with a faster and higher peak magnitude has a faster arrival time to various infrastructure and the open pits. This information is pertinent to emergency preparedness planning.
- The sensitivity to the non-Newtonian flow properties was tested by varying the rheology parameters, as well as modeling the outflow as a Newtonian fluid. The flow propagation and inundation extents are not sensitive to the non-Newtonian flow properties based on the evaluated tailings rheology, as the differences in flood extents, flood depths and arrival times were negligible.
- The sensitivity to the assumed Manning's n value was tested and the results showed negligible impact to the inundation extent and travel times. The selected Manning's n values are considered adequate.
- The findings of the sensitivity analyses do not change the outcomes of this study, and the information presented on the maps in Appendix B is considered adequate for characterizing the potential physical impacts in terms of inundation and informing the risk of this proposed future configuration of the YDTI.

8.0 REFERENCES

Adams, A., Friedman, D., Davidson, S., Characterizing and Stabilizing a Historical Tailings Facility: The Rheology to Soil Mechanics Continuum, in the Proceedings of the Tailings and Mine Waste 2017 Conference, November 5-8, Banff, Canada (2017).

Adams A., Brouwer, K.J., Robertson, P.K., and V. Martin, 2022. Evaluation of Tailings Behaviour for Dam Breach Analysis, in the Proceedings of the Tailings and Mine Waste Conference, November 7-9, 2022, Denver, CO, USA.

Adria, D., 2022. Compilation and Critical Assessment of Observations from a Selection of Historical Tailings Dam Breach Events for Numerical Breach and Runout Modeling. Master of Applied Science Thesis, University of British Columbia, Vancouver, Canada. November 2022.

Adria, D.A.M., Martin, V., McDougall, S., 2023. The Role of Sensitivity Analysis in Selecting Dam Breach Parameters. Proceedings of the CDA 2023 Annual Conference, October 22-25, Winnipeg, Canada.

Adria, D.A.M., Martin, V., Wong, H. 2024. Volume of Dam Material Mobilized by Erosion During Tailings Dam Failure Events. Proceedings of Tailings and Mine Waste 2024, November 10-13, 2024. Denver, Colorado, USA.

Canadian Dam Association (CDA), 2007. Technical Bulletin: Hydrotechnical Considerations for Dam Safety

Canadian Dam Association (CDA), 2007, revised 2013. Dam Safety Guidelines.

Canadian Dam Association (CDA), 2014, revised 2019. Technical Bulletin: Application of Dam Safety Guidelines to Mining Dams.

Canadian Dam Association (CDA), 2021. Technical Bulletin: Tailings Dam Breach Analysis.

Chow, 1959. Open-Channel Hydraulics. New York: McGraw-Hill.

Costa, J.E., 1985. Floods from Dam Failures. U.S. Geological Survey Open-File Report No. 85-560, U.S. Geological Survey, Denver, Colorado.

Días, N.A., Determinação de Propriedades Reológicas de Rejeito de Mineração por meio de Reômetro Rotacional. Universidade Federal do Espírito Santo Centro Tecnológico Programa de Pós Graduação em Engenharia Civil, (2017).

Federal Energy Regulatory Commission (FERC), 1993. Engineering Guidelines for the Evaluation of Hydropower Projects.

Federal Emergency Management Agency (FEMA), 2013. Federal Guidelines for Inundation Mapping of Flood Risks Associated with Dam Incidents and Failures. First Edition. FEMA P-946, July 2013.

Froehlich, D.C., 1995a. Peak Outflow from Breach Embankment Dam. Journal of Resources Planning and Management, vol. 121, no. 1, p.90-97.

Froehlich, D.C., 1995b. Embankment Dam Breach Parameters Revisited. Water Resources Engineering, Proceedings of the 1995 ASCE Conference on Water Resources Engineering, San Antonio, Texas, August 14-18, 1995, p. 887-891.

Froehlich, D.C., 2008. Embankment dam breach parameters and their uncertainties. Journal of Hydraulic Engineering, Vol. 134, no. 12, p. 1708-1721.

Froehlich, D.C., 2016. Predicting Peak Discharge from Gradually Breached Embankment Dam, Journal of Hydraulic Engineering, vol. 21, no. 11, http://dx.doi.org/10.1061/(ASCE)HE.1943-5584.0001424

García, M.H., R.C. MacArthur, R. French, and J. Miller. 2008. Sedimentation Hazards in Sedimentation Engineering edited by García, M.H. ASCE Manuals and Reports on Engineering Practice No. 110.

GeoLogismiki Geotechnical Software, 2019. CPeT-IT. Version 3. Serres, Greece.

Global Industry Standard on Tailings Management (GISTM, 2020). Co-convened by the International Council on Mining and Metals (ICMM), United Nations Environment Programme (UNEP), and Principles for Responsible Investment.

Hydrologic Engineering Center (HEC), 2021. HEC-RAS 2D User's Manual - Version 6.0. U.S. Army Corps of Engineers, Hydrologic Engineering Center, 609 Second Street, Davis, CA. Available: https://www.hec.usace.army.mil/confluence/rasdocs/r2dum/latest, August 2021.

International Commission on Large Dams (ICOLD), 2022, Tailings Dam Safety, Bulletin 194. Version 1.0, November 16, 2022.

Janssen. C., 2016. Manning's n Values for Various Land Covers to use for Dam Breach Analyses by NRCS in Kansas. July 12, 2016.

Jeyapalan, J., Jey K., Michael Duncan, and H. Bolton Seed, 1983. Analyses of Flow Failures of Mine Tailings Dam. Journal of Geotechnical Engineering, Vol. 109, No. 2, February, 1983.

Johnson, F.A. and P. Illes, 1976. A Classification of Dam Failures. International Water Power and Dam Construction. December 1976, p. 43-45.

Julien, P.Y., Erosion and Sedimentation (2nd ed.), Cambridge University Press (2010).

Knight Piésold Ltd. (KP), 2024a. Yankee Doodle Tailings Impoundment – Design Basis Report for 6,560 Amendment Design Document. KP Ref. No. VA101-126/24-1 Rev. 0, September 20, 2024.

Knight Piésold Ltd. (KP), 2024b. Yankee Doodle Tailings Impoundment – Life of Mine Design Report for 6,560 Amendment Design Document. KP Ref. No. VA101-126/24-1 Rev. 0, September 13, 2024.

Kulesza, R., 2011. Review of Technical Literature on Tailings Dam Failures involving Flow of Tailings. USSD Workshop on Dam Break Analysis Applied to Tailings Dams. Denver, Colorado, August 24 -26, 2011.

MacDonald, T.C., and Langridge-Monopolis, J., 1984. Breaching Characteristics of Dam Failures. Journal of Hydraulic Engineering, ASCE, vol. 110, no. 5, p. 567-586.

Machado, N.C., Retroanálise da Propagação Decorrente da Ruptura da Barragem do Fundão com Diferentes Modelos Numéricos e Hipóteses de Simulação. Universidade Federal de Minas Gerais, Programa de Pós-Graduação em Sameamento, Meio Ambiente e Recursos Hídricos, (2017).

Martin, V., Al-Mamun, M., and Small, A., 2019. CDA Technical Bulletin on Tailings Dam Breach Analyses. Proceedings of the 2019 ICOLD Conference. June. Ottawa, Ontario, Canada.

Martin, V., Fontaine, D., and Cathcart, J. G, 2015. Challenges with conducting tailings dam breach studies. October 31, 2015. doi: http://dx.doi.org/10.14288/1.0320883.

Mayne, P.W., 2007. In-situ test calibrations for evaluating soil parameters. Characterization & Engineering Properties of Natural Soils, Vol. 3, Taylor & Francis Group, London: 1602-1652.

MineBridge Software Inc., 2023. Muk3D. Version 2023.1.3.

Montana DNRC. 2010. Dam Safety Program Technical Note 2: Loss of Life Determination for Spillway Capacity Analysis. Prepared by Hydrometrics, Inc. August 2010.

O'Brien, J.S. 1986. Physical Processes, Rheology, and Modeling of Mud Flows. Ph.D. Dissertation, Colorado State University, Fort Collins, Colorado.

O'Brien and Julien, 1988. Laboratory Analysis of Mudflow Properties. Journal of Hydraulic Engineering. Vol. 114, No. 8. August 1998. ASCE, ISSN 0733-9420/88/0008^0877.

Olson, S.M., Stark, T.D, 2003. Yield Strength Ratio and Liquefaction Analysis of Slopes and Embankments. Journal of Geotechnical and Geoenvironmental Engineering. DOI: 10.1061/(ASCE)1090-02441(2003)129:8(727).

Paterson & Cooke (P&C), 2022. Montana Resources Rheology. Test Work Report. P&C Project No.: MRR-31-1295.

Pierce et al., 2010. Predicting Peak Outflow from Breached Embankment Dams. Journal of Hydrologic Engineering. ASCE, vol. 15, Issue 5. pg. 338-349.

Rana, N.M., Ghahramani, N., Evans, S.G., McDougall, S., Small, A., and W.A., Take, 2021a. Catastrophic Mass Flows Resulting from Tailings Impoundment Failures. Engineering Geology 292(2021): 1-20.

Rana, N.M., Ghahramani, N., Evans, S.G., McDougall, S., Small, A., and W.A., Take, 2021b. A comprehensive global database of tailings flows. Scholars Portal Dataverse, v1. https://doi.org/10.5683/SP2/NXMXTI.

Rico, M., Benito, G. and Diez-Herrero, A., 2007. Floods from Tailings Dam Failures. Journal of Hazard Management. pp. 79-87.

Robertson, P.K., 2010. Evaluation of Flow Liquefaction and Liquified Strength Using the Cone Penetration Test. Journal of Geotechnical and Geoenvironmental Engineering. DOI: 10.1061/(ASCE)GT.1943-5606.0000286.

Robertson, P.K. and Cabal, K.L. 2010. Estimating unit weight from CPT. Proc., 2nd Intl. Symposium on Cone Penetration Testing, Vol. 3 (CPT '10), Huntington Beach, CA.

Robertson, P.K., 2021. Evaluation Liquefied Strength Using the Cone Penetration Test: an update. Canadian Geotechnical Journal. June 18, 2021.

Seddon, K. D., 2010. Approaches to Estimation of Runout Distances of Liquefied Tailings. First Int. Seminar on the Reduction of Risk in the Management of Tailings and Mine Waste, Mine Waste 2010, Perth.

Singh, Krishan P., and Snorrason, Arni (1982). Sensitivity of Outflow Peaks and Flood Stages to the Selection of Dam Breach Parameters and Simulation Models. SWS Contract Report 288. Illinois Department of Energy and Natural Resources, State Water Survey Division, Surface Water Section at the University of Illinois. p. 179.

U.S. Army Corps of Engineers Hydrologic Engineering Center (USACE), 2014. Using HEC-RAS for Dam Break Studies. Training Document No. 39. August 2014. U.S. Army Corps of Engineers, Hydrologic Engineering Center, 609 Second Street, Davis, CA.

U.S. Bureau of Reclamation (USBR). 1988. Downstream Hazard Classification Guidelines. ACER Technical Memorandum No. 11, Assistant Commissioner-Engineering and Research, Denver, Colorado, December 1988, 57 p.

U.S. Bureau of Reclamation (USBR), 2015. RCEM – Reclamation Consequence Estimating Methodology: Guidelines for Estimating Life Loss for Dam Safety Risk Analysis.

Von Thun, J.L. and Gillette, D.R., 1990. Guidance on Breach Parameters, unpublished internal document, U.S. Bureau of Reclamation, Denver, Colorado, March 13, 1990, 17 p.

Wahl, L. Tony. 1998. Prediction of Embankment Dam Breach Parameters, A Literature Review and Needs Assessment. Dam Safety Office, Water Resources Research Laboratory, US Department of the Interior, Bureau of Reclamation, DSO-98-04.

Wahl, T. L., 2014. Evaluation of Erodibility-Based Embankment Dam Breach Equations.

Walder, J.S. and J.E. O'Connor, 1997. Methods for Predicting Peak Discharge for Floods Caused by Failure of Natural and Constructed Earth Dams. October 1997. Water Resources Research. Vol. 33, Issue 10, P. 2337-2348.

Walsh, A., 2020. Physical Modeling of Tailings Dam Breach. Master of Applied Science Thesis, Queen's University, Kingston, Canada. January 2020.

Washington State Department of Ecology (Washington). 1992, Revised October 2007. Dam Safety Guidelines Technical Note 1: Dam Break Inundation Analysis and Downstream Hazard Classification.

Xu, Y. and L.M. Zhang, 2009. Breach Parameters for Earth and Rockfill Dams. Journal of Geotechnical and Geoenvironmental Engineering. 135(12):1957-1970.

9.0 CERTIFICATION

This report was prepared and reviewed by the undersigned.

Prepared:

Daniel McGuire, EIT
Junior Engineer

Prepared:

Heleman Wong, P.Eng.
Project Engineer

Reviewed:

Violeta Martin, Ph.D., P.Eng.
Specialist Hydrotechnical Engineer
Associate

Reviewed:

Daniel Fontaine, P.E.
Specialist Engineer | Associate
YDTI Engineer of Record

This report was prepared by Knight Piésold Ltd. for the account of Montana Resources, LLC. Report content reflects Knight Piésold's best judgement based on the information available at the time of preparation. Any use a third party makes of this report, or any reliance on or decisions made based on it is the responsibility of such third parties. Knight Piésold Ltd. accepts no responsibility for damages, if any, suffered by any third party as a result of decisions made or actions based on this report. Any reproductions of this report are uncontrolled and might not be the most recent revision.

KNIGHT PIÉSOLD LTD.
PERMIT NUMBER
1001011
EGBC PERMIT TO PRACTICE

Approval that this document adheres to the Knight Piésold Quality System: DDF

APPENDIX A

Montana Resources Rheology: Test Work Report

(Pages A-1 to A-93)

Montana Resources Rheology

P&C Project No.: MRR-31-1295

Rev No.	Date	Description	Prepared	Reviewed	Reviewed
			Originator		Client
C	Jan. 13, 2022	Test Work Report – Issued to client with additional graphs	AMR/BON	-	-
B	Dec. 7, 2021	Test Work Report– Issued to client	BON	AMR	VM/RD
A	June 4, 2021	Sample Characterization - Issued to client	AMR	KAA	-

Document Title

Test Work Report

Document Number						
Office Code	Project Code	Area Code	Disc. Code	Document Type	Seq. No.	Rev No.
31	1295	00	TW	REP	0001	C

PATERSON & COOKE
Paterson & Cooke USA Ltd. +1 303 800 6280
221 Corporate Circle, Suite D, Golden, CO 80401-5637, USA
Denver@PatersonCooke.com www.PatersonCooke.com

TERMS OF REFERENCE

This work has been conducted by Paterson & Cooke for Montana Resources under Order Number 8-335112. The proposal for this work was presented in P&C Proposal 31-1295-00-PM-PRP-0001 Rev A dated March 18, 2021.

This report has been prepared by Paterson & Cooke for the exclusive use of Montana Resources for the Montana Resources Rheology Project, and no other party is an intended beneficiary of this report or any of the information, opinions and conclusions contained herein. The use of this report shall be at the sole risk of the user regardless of any fault or negligence of Montana Resources or Paterson & Cooke. Paterson & Cooke accepts no responsibility for damages, if any, suffered by any third party as a result of decisions or actions based on this report. Note that this report is a controlled document, and any reproductions are uncontrolled and may not be the most recent version.

CONTENTS

TERMS OF REFERENCE i
CONTENTS ii
1. INTRODUCTION 1
1.1 References 1
1.2 Test Work Samples 1
1.2.1 Samples Received 1
1.2.2 Sample Preparation and Usage 2
1.3 Material Characterization Scope 2
1.4 Rheology Scope 2
1.5 Symbols and Abbreviations 2
1.6 Terms and Definitions 3
1.6.1 Decant 3
1.6.2 Fully Sheared Rheology 3
1.6.3 Solids Concentration 3
2. MATERIAL CHARACTERIZATION TEST RESULTS 3
2.1 Solids Density 3
2.2 Particle Size Analysis 4
2.3 Mineralogy 9
2.4 Micro-Photographs 10
3. RHEOLOGY TEST RESULTS 12
3.1 Vane Yield Stress 12
3.1.1 Test Method and Equipment 12
3.1.2 Test Conditions 13
3.1.3 Test Results 14
3.2 Boger Slump Yield Stress 15
3.2.1 Results 15
3.3 Tube Viscometer Rheology Measurements 18
3.3.1 Method and Equipment 18
3.3.2 Conditions 19
3.3.3 Measured Data 20

3.3.4 Rheological Characterization 22
3.3.5 Slurry Rheology Correlations 22
3.3.6 Particle Size Distribution Shift During Test 24
3.4 Rheology Summary 25
APPENDIX A : MATERIAL CHARACTERIZATION TEST RESULTS A.1
APPENDIX B : RHEOLOGY TEST RESULTS B.1
APPENDIX C : TUBE VISCOMETER TEST DATA C.1

1. INTRODUCTION

Paterson & Cooke (P&C) have been retained by Montana Resources LLP to carry out tailings rheology test work.

The scope of work includes characterization, vane yield stress, and tube viscometer test work. Material characterization was completed for all six samples. Vane yield stress and tube viscometer test work was completed for two samples, DH19 56-70 and DH20-S2 162-173.

1.1 References

Table I: References

Reference	Abbreviation
Email from Violeta Martin (KP) to Ashley Rasmussen (P&C), *Subject: RE P&C Test Work Status;* dated October 14, 2021.	KP-01

1.2 Test Work Samples

1.2.1 Samples Received

The following samples were delivered to P&C's laboratory in Golden, Colorado on April 15, 2021:

Table II: Sample Notation

Sample Label	Quantity
DH19 22-32	1 x 5 gallon pail solids
DH19 56-70	1 x 5 gallon pail solids
DH20-S2 83 -92	1 x 5 gallon pail solids
DH20-S2 162-173	1 x 5 gallon pail solids
DH20 203-216	1 x 5 gallon pail solids
DDH20-S2 236-245	1 x 5 gallon pail solids
TP H_2O 1/10 to 10/10 (Process water)	10 x 5 gallon pails

The sample receipt form is available in Appendix A.1.

1.2.2 Sample Preparation and Usage

The samples, received dry, and were hydrated with the provided process water to a paste consistency.

1.3 Material Characterization Scope

The following tests were included:

- Solids density
- Particle size analysis
- Mineralogy
- Qualitative micro-photographs.

1.4 Rheology Scope

The following tests were included:

- Vane Yield stress tests were completed using P&C's Haake Viscotester using the FL-100 vane over a range of solids concentrations
- Boger slump photographs provide a visual of the sample behavior over a range of solids concentrations
- Whole slurry rheology using P&C's ¾ inch vertical tube viscometer over a range of solids concentrations.

1.5 Symbols and Abbreviations

The following symbols and abbreviations are used in this report:

M_w	mass of the liquid phase (kg)
M_s	mass of solids (kg)
M_t	total sample mass (kg)
K_{BP}	Bingham plastic viscosity (Pa·s)
PSD	particle size distribution
RPM	revolutions per minute
STP	standard temperature and pressure
T	temperature (°C)

$\dot{\gamma}$	shear rate (s^{-1})
ρ_m	slurry mixture density (kg/m^3)
ρ_s	solid phase density (kg/m^3)
ρ_w	liquid phase density (kg/m^3)
τ_y	yield stress (Pa)
τ_{yv}	vane yield stress (Pa)
τ_{yB}	Bingham yield stress (Pa)
μ_w	liquid phase Newtonian viscosity (Pa·s)

1.6 Terms and Definitions

1.6.1 Decant

The supernatant liquid recovered above the surface of a settled bed of slurry is termed decant.

1.6.2 Fully Sheared Rheology

The fully sheared rheology refers to the equilibrium rheology achieved after the slurry sample has been subjected to shearing action until there is no further change in rheology.

1.6.3 Solids Concentration

The solids mass concentration is the percentage of solids in relation to the total mass of the sample:

$$C = \frac{M_s}{M_t} , \quad (1)$$

where M_s = mass of solids in sample (kg).

M_t = total mass of the sample, i.e. both the solid and liquid phases (kg).

2. MATERIAL CHARACTERIZATION TEST RESULTS

2.1 Solids Density

The solids density of the samples was determined using a 0.001-gram accuracy balance and a helium gas pycnometer which measures solids volume. The results summarized in Table III are an average of three tests. Test details are available in Appendix A.2.

Table III: Solids Density

Sample	Solids Density
DH19 22-32	2,724 kg/m³
DH19 56-70	2,699 kg/m³
DH20-S2 83 -92	2,725 kg/m³
DH20-S2 162-173	2,688 kg/m³
DH20 203-216	2,681 kg/m³
DDH20-S2 236-245	2,663 kg/m³

2.2 Particle Size Analysis

Particle size distributions were determined by wet sieving according to the method detailed in ASTM D 422-63 (2007) “Standard Test Method for Particle Size Analysis of Soils”, and by laser diffraction using a Microtrac Model S1500.

Appendices A.3 and A.4 presents the particle size distribution analyses and Figure 1 to Figure 6 show the wet sieve and laser particle size distribution for each sample. The wet sieve particle size distribution and laser particle size distribution is compared for all samples in Figure 7 and Figure 8.

Samples DH19 22-32 and DH20-S2 83-92 had particles that were coarser than 2 mm. These particles cannot be measured using the laser particle size analyzer. The laser measurement for both samples therefore appears significantly finer than the wet sieve measurements.

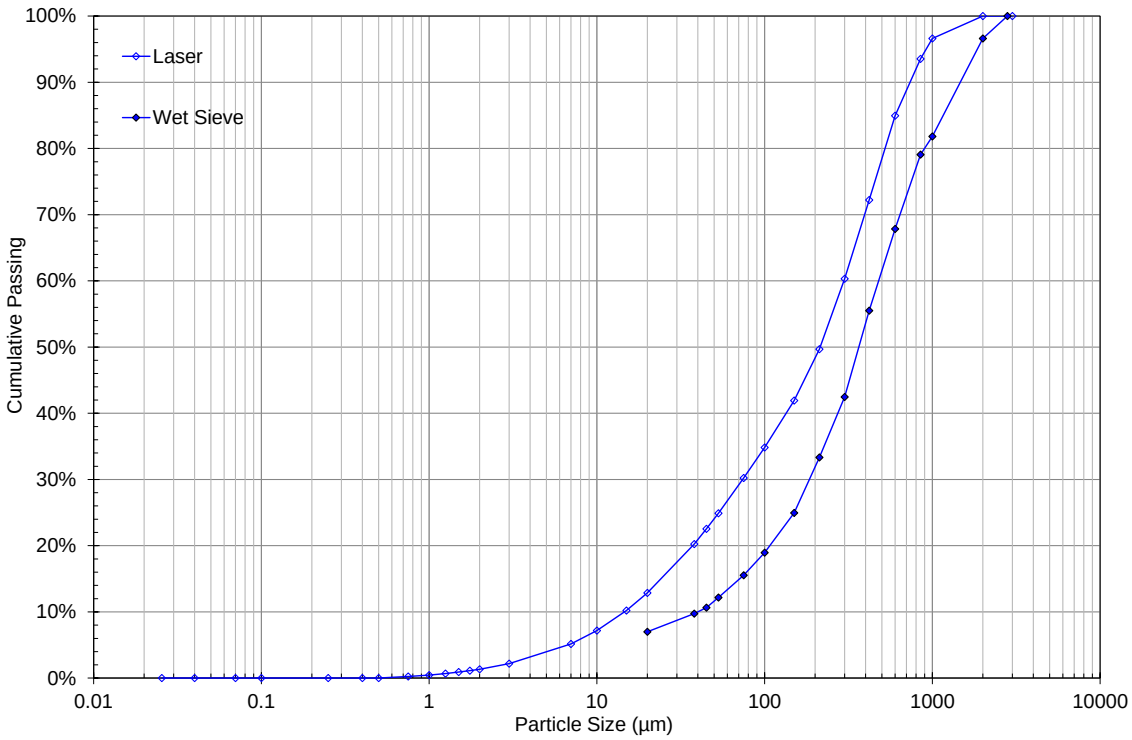

Figure 1: DH19 22-32 Particle Size Distributions

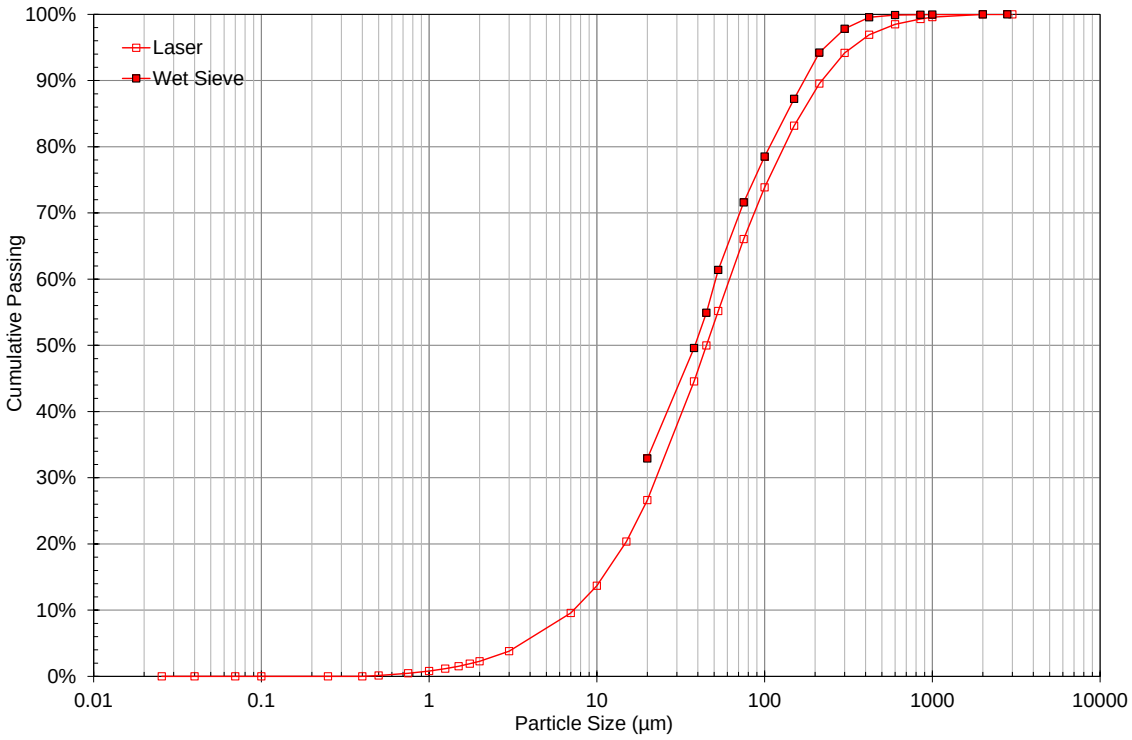

Figure 2: DH19 56-70 Particle Size Distributions

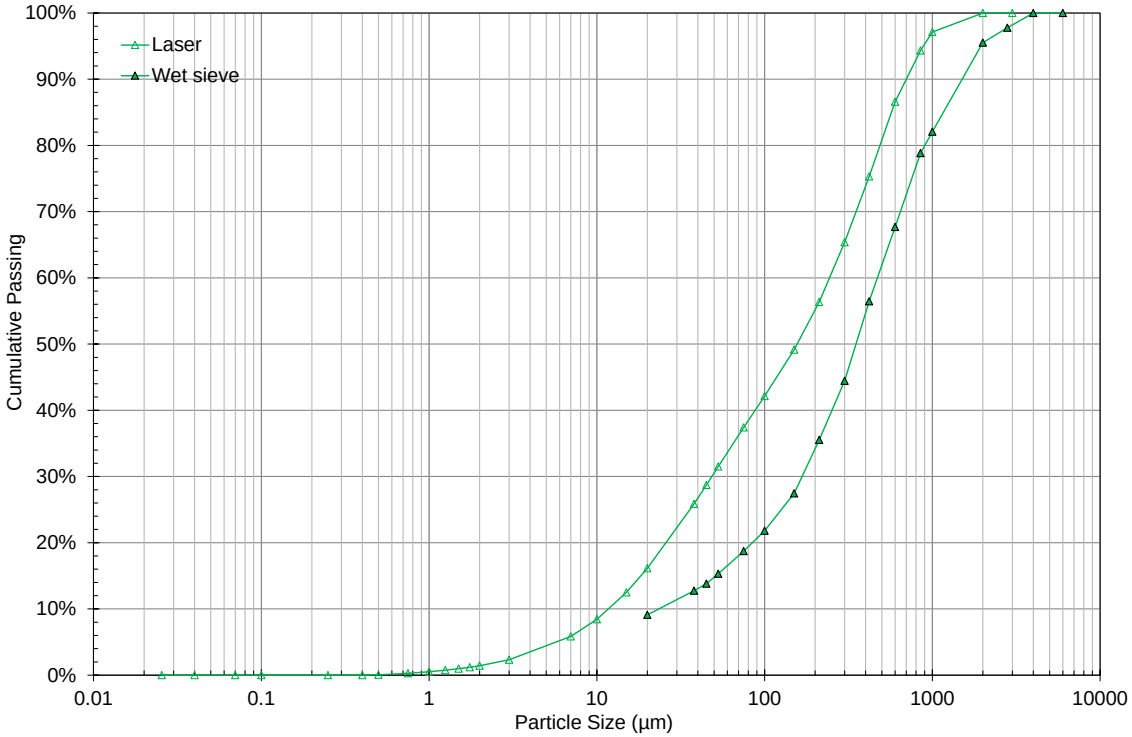

Figure 3: DH20-S2 83-92 Particle Size Distributions

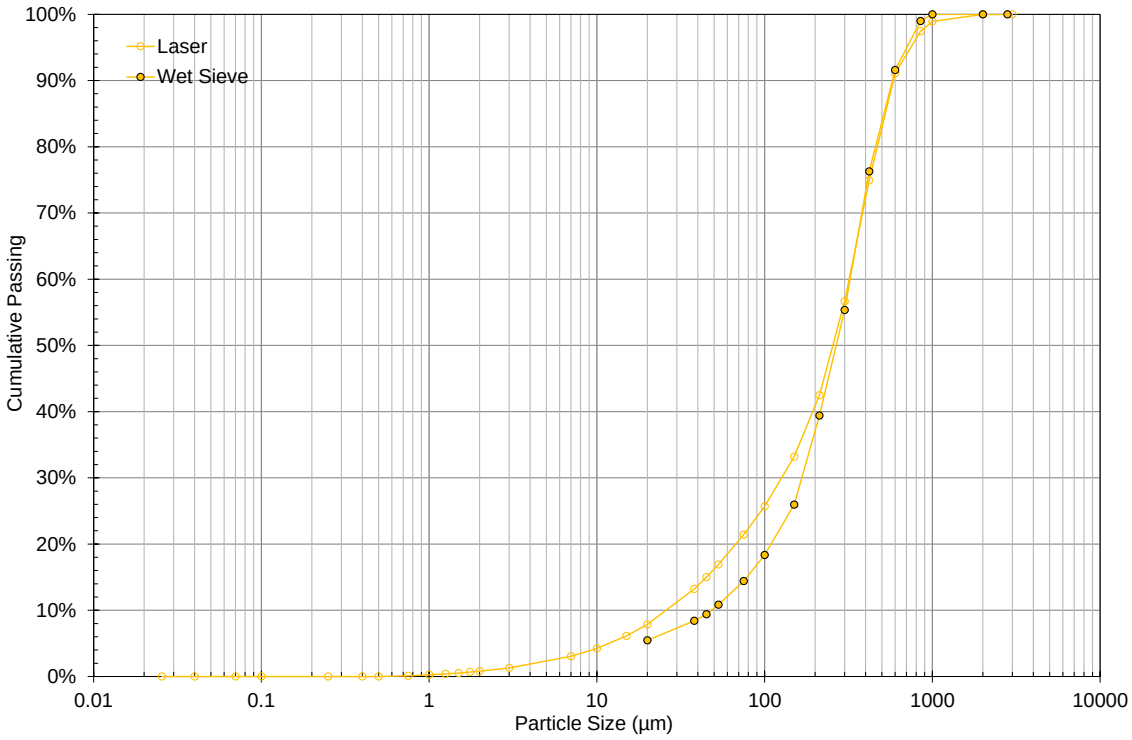

Figure 4: DH20-S2 162-173 Particle Size Distributions

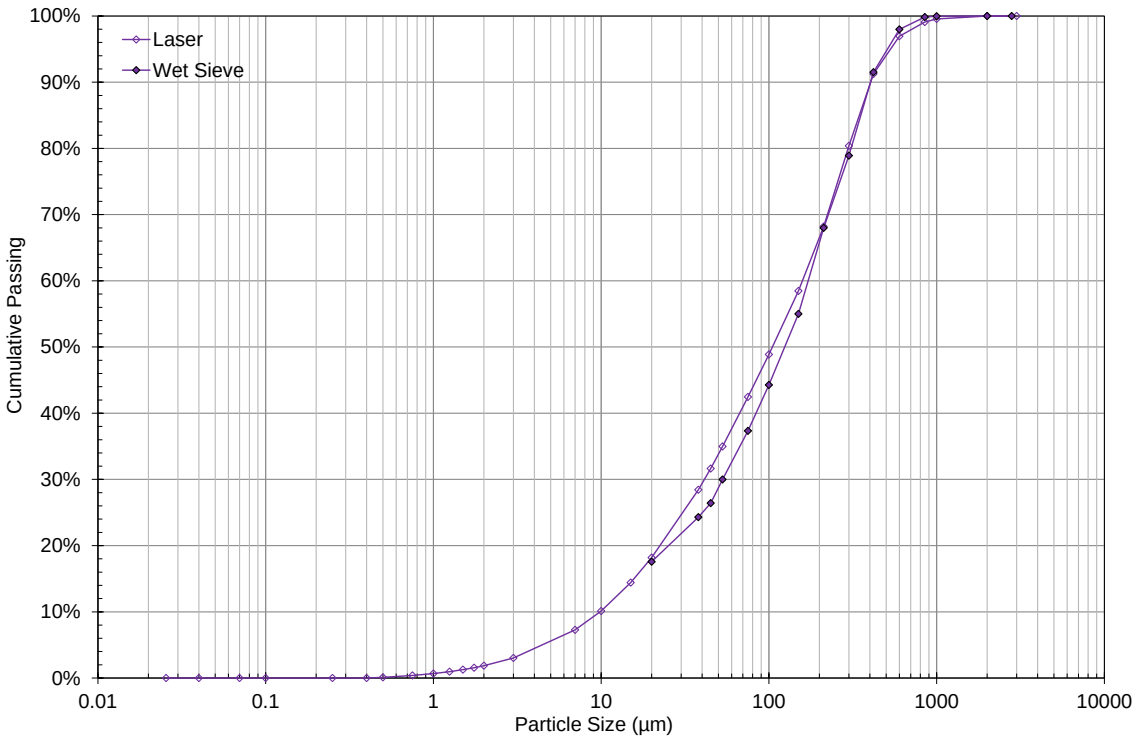

Figure 5: DH20 203-216 Particle Size Distributions

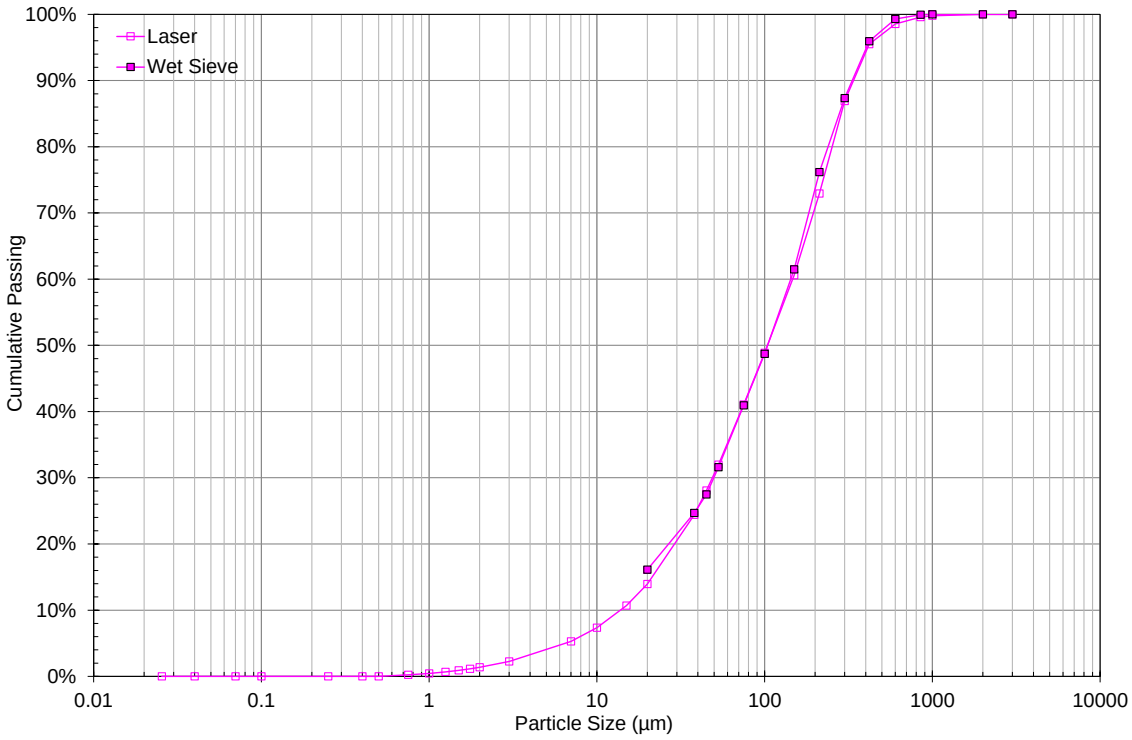

Figure 6: DDH20-S2 236-245 Particle Size Distributions

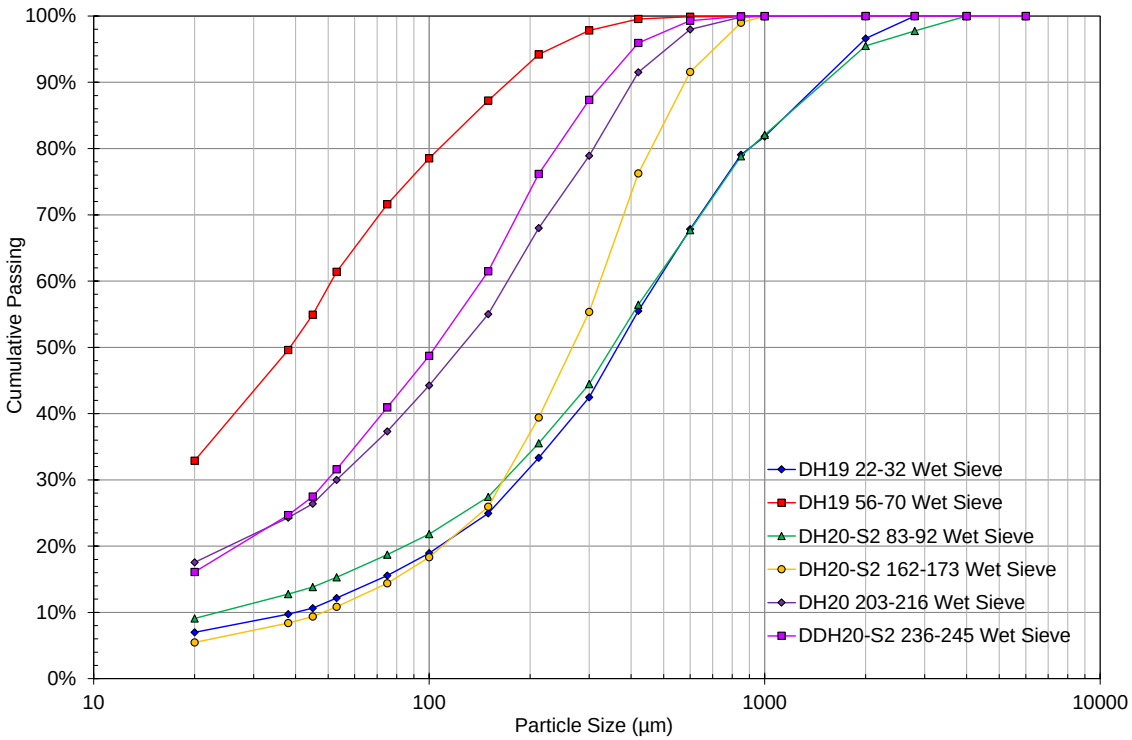

Figure 7: Wet Sieve Particle Size Distributions

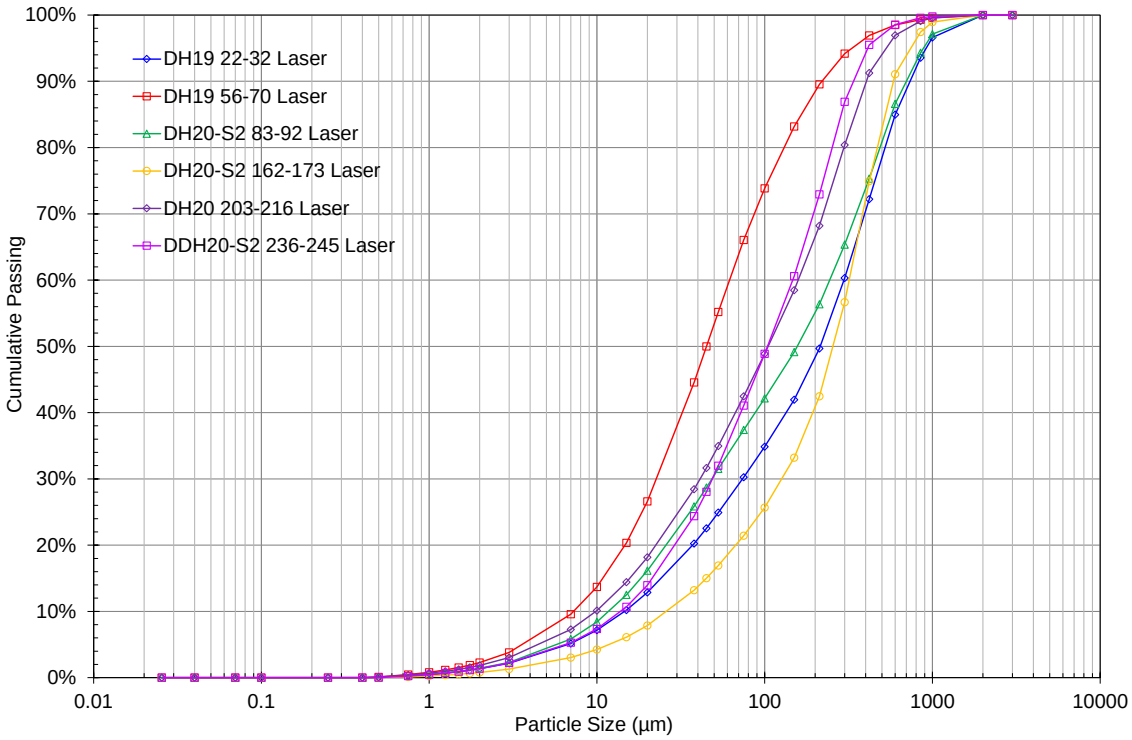

Figure 8: Laser Particle Size Distributions

2.3 Mineralogy

Sub-samples were was sent to DCM Science in Wheat Ridge, CO for mineral and clay analysis using X-ray diffraction (XRD) with reference intensity ratio (RIR). Table IV and Table V summarize the results and the DCM Science report is available in Appendix A.5.

Table IV: XRD Results

Component	**DH19 22-32**	**DH19 56-70**	**DH20-S2 83 -92**	**DH20-S2 162-173**	**DH20 203-216**	**DDH20-S2 236-245**
Calcite	5%	2%	3%	2%	2%	2%
Gypsum	-	<2%	<2%	-	<2%	-
Hematite	<2%	<2%	4%	2%	3%	-
K-Feldspar	18%	15%	19%	31%	23%	35%
Mica	21%	24%	13%	16%	18%	14%
Plagioclase	5%	7%	4%	6%	5%	11%
Pyrite	2%	3%	7%	1%	3%	2%
Quartz	24%	23%	25%	28%	28%	31%
Total clay	25%	26%	25%	14%	18%	5%
Chlorite (% of total)	-	-	-	<2%	-	-
Kaolinite (% of total)	5%	5%	6%	3%	3%	1%
Smectite (% of total)	20%	21%	19%	11%	15%	4%

Table V: XRD Analysis of Clay Fraction Within -2 µm Size Fraction

Component	**DH19 22-32**	**DH19 56-70**	**DH20-S2 83 -92**	**DH20-S2 162-173**	**DH20 203-216**	**DDH20-S2 236-245**
Chlorite	-	-	-	<2%	-	-
Kaolinite	21%	19%	23%	19%	19%	10%
Smectite	79%	81%	77%	81%	81%	90%

2.4 Micro-Photographs

Micro-photographs were taken of the sieved particle size fractions for each sample using a Leica microscope to provide a qualitative view of particle shape. Photos of the 300 µm size fraction for each sample are presented in Figure 9 to Figure 14.

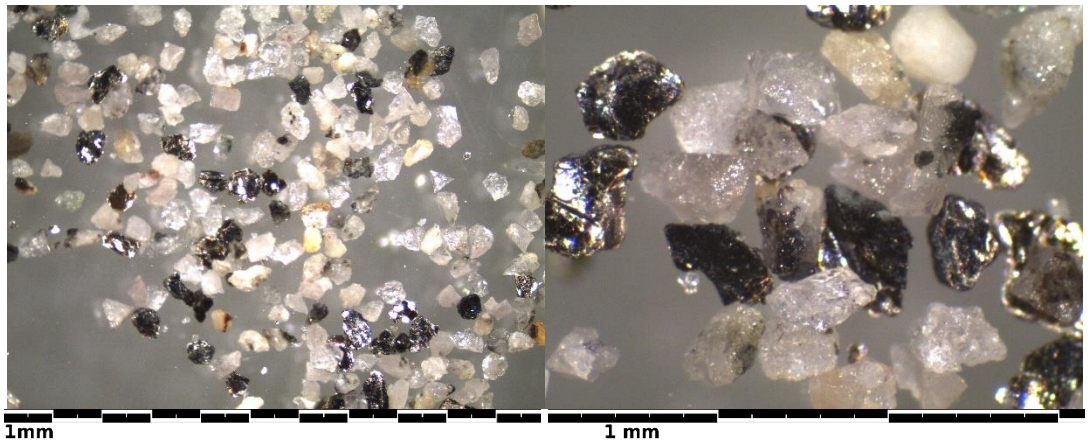

Figure 9: DH19 22-32 +300 µm size fraction (x10 magnification, x35 magnification)

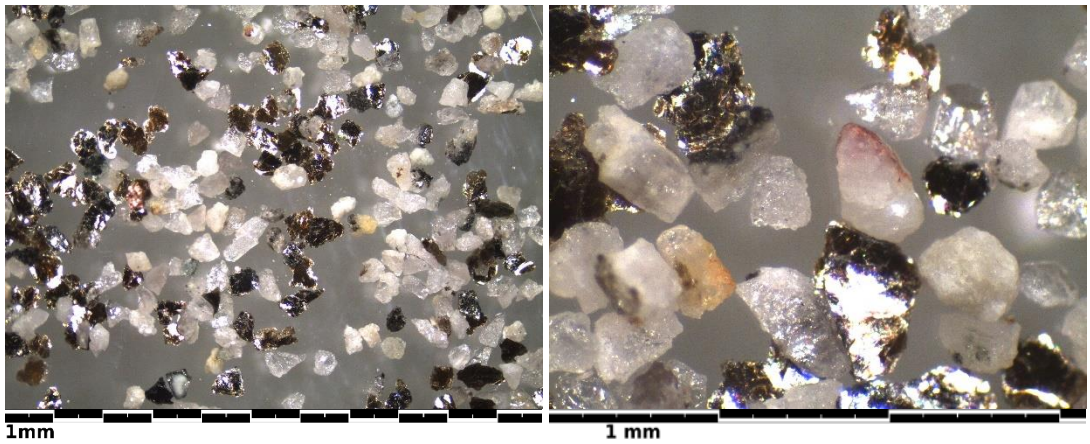

Figure 10: DH19 56-70 +300 µm size fraction (x10 magnification, x35 magnification)

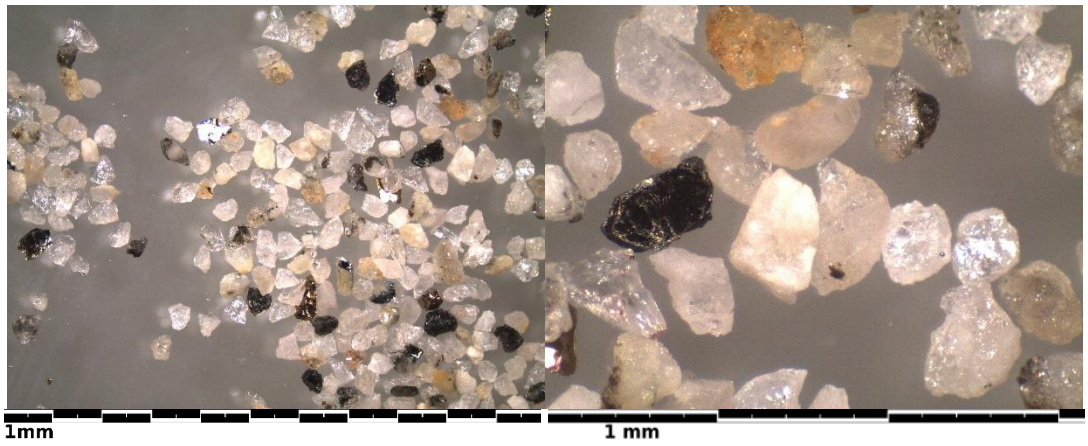

Figure 11: DH20-S2 83-92 +300 µm size fraction (x10 magnification, x35 magnification)

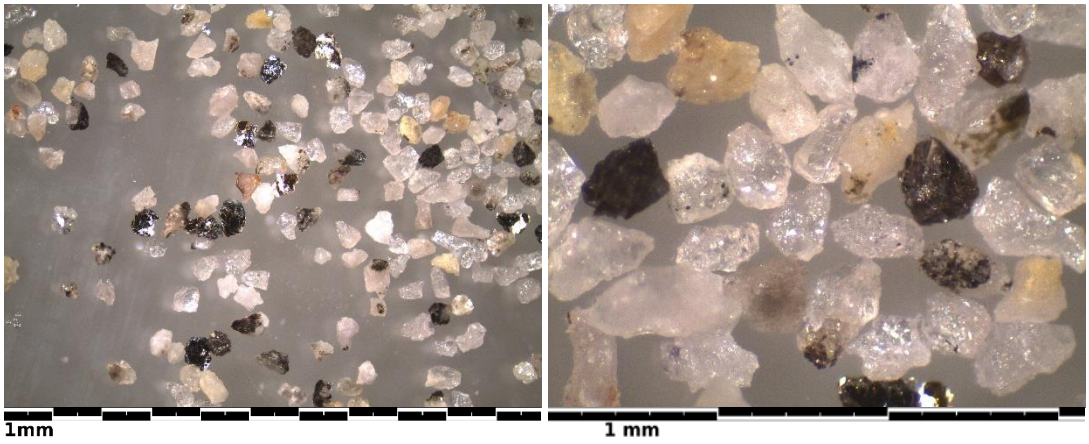

Figure 12: DH20-S2 162-173 +300 µm size fraction (x10 magnification, x35 magnification)

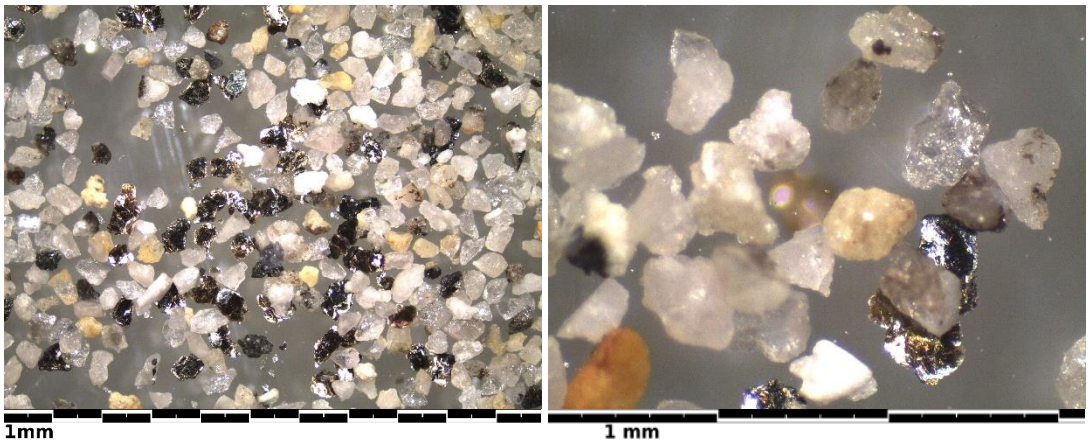

Figure 13: DH20 203-216 +300 µm size fraction (x10 magnification, x35 magnification)

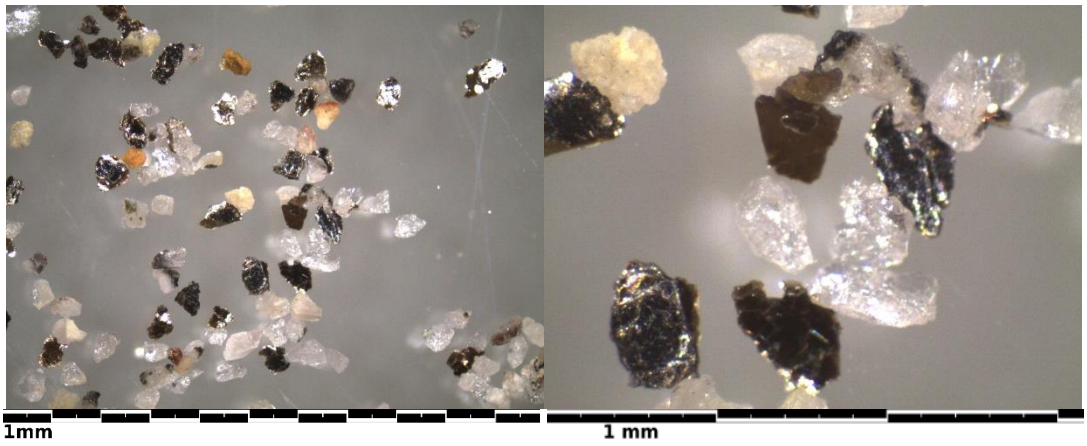

Figure 14: DDH20 236-245 +300 µm size fraction (x10 magnification, x35 magnification)

3. RHEOLOGY TEST RESULTS

Of the six received samples, two were selected for further rheology characterization. Sample DH19 56-70 and DH20-S2 162-173 as confirmed by Knight Piesold (KP-01).

3.1 Vane Yield Stress

3.1.1 Test Method and Equipment

P&C's Haake Viscotester® 550 rotational viscometer shown in Figure 15 was used for vane yield stress measurements. A FL-100 vane was used. The speed of the viscometer was held constant at 0.095 RPM resulting in a constant shear strain rate of 0.02 s^{-1}. The torque was measured throughout the test and the maximum torque was used to calculate the yield stress.

The tests were completed over a range of solids concentrations. Two vane yield stress measurements were completed at each concentration. The individual measurements at each solids concentration are presented in Appendix B. The results presented in Section 3.1.3 are an average of the two tests.

Figure 15: Haake Viscotester® 550 Rotational Viscometer

3.1.2 Test Conditions

A range of concentrations were tested for samples DH19 56-70 and DH20-S2 162-173. The tests were completed at ambient temperature and the sample pH was not adjusted. The temperature and pH were monitored throughout testing and are summarized in Table VI and Table VII.

Table VI: Rheology Test Temperature

Property	**DH19 56-70**	**DH20-S2 162-173**
Average temperature	23.7 °C	23.9 °C
Maximum temperature	24.1 °C	25.1 °C
Minimum temperature	23.4 °C	23.2 °C

Table VII: Rheology Test pH

Property	**DH19 56-70**	**DH20-S2 162-173**
Average pH	6.9	7.3
Maximum pH	7.0	7.3
Minimum pH	6.9	7.2

3.1.3 Test Results

The average vane yield stress measurements are shown in Figure 16. Detailed test results are available in Appendix B. The vane yield stress correlation parameters are detailed in Table VIII.

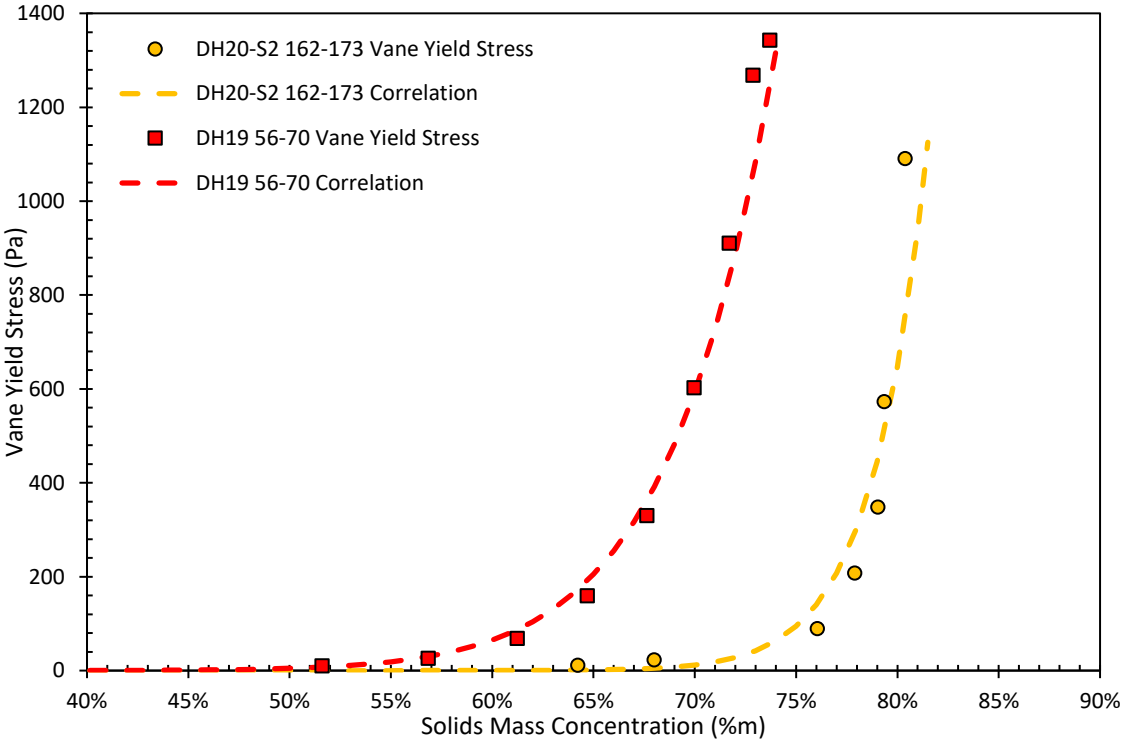

Figure 16: Vane Yield Stress Measurements

Table VIII: Vane Yield Stress Fit Parameters

Property	**DH19 56-70**	**DH20-S2 162-173**
Vane yield stress (Pa)	$\tau_{yv} = a(C)^b$	
a	98,794	500,000
b	14.3	29.8
Measured concentration range	51.6%m to 73.7%m	64.2%m to 80.4%m

3.2 Boger Slump Yield Stress

P&C's standard 73 mm diameter by 73 mm height Boger slump cylinder was used to assist in visualization of the sample behavior[1]. The tests were completed the same concentrations, temperature and pH as the vane yield tests in section 3.1.2.

The yield stress of non-Newtonian slurries is estimated from the slump obtained using a straight sided cylinder[2], as follows:

$$\frac{h}{H} = 1 - \frac{2\tau_y}{\rho_m g H}\left(1 - \ln\left(\frac{2\tau_y}{\rho_m g H}\right)\right) \quad (2)$$

where: h = measured slump height (m)

H = cylinder height (m)

ρ_m = slurry density (kg/m^3).

3.2.1 Results

The calculated Boger yield stress values are presented in Figure 17. Slump photographs of the first and last concentrations for each sample are shown in Figure 9 to Figure 14. Photographs of all the slumps are presented in Appendix B.

[1] If the Boger slump cylinder is being used in the field because a more accurate method is not available, a larger cylinder can be used to approximate the higher yield stress material.

[2]Pashias, N, Boger, D.V., Summers, J., and Glenister, D.J.. "A Fifty Cent Rheometer for Yield Stress Measurement", *J Rheology*, Vol. 40, No. 6, p. 1179-1189.

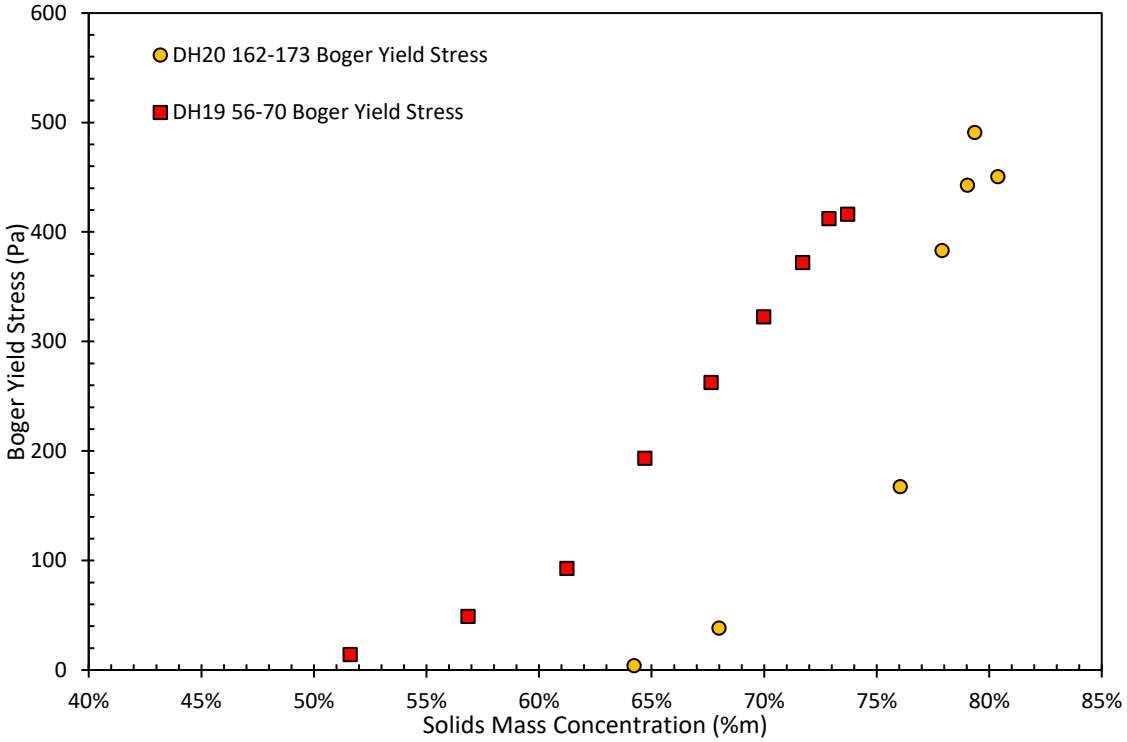

Figure 17: Boger Slump Yield Stress (Pa)

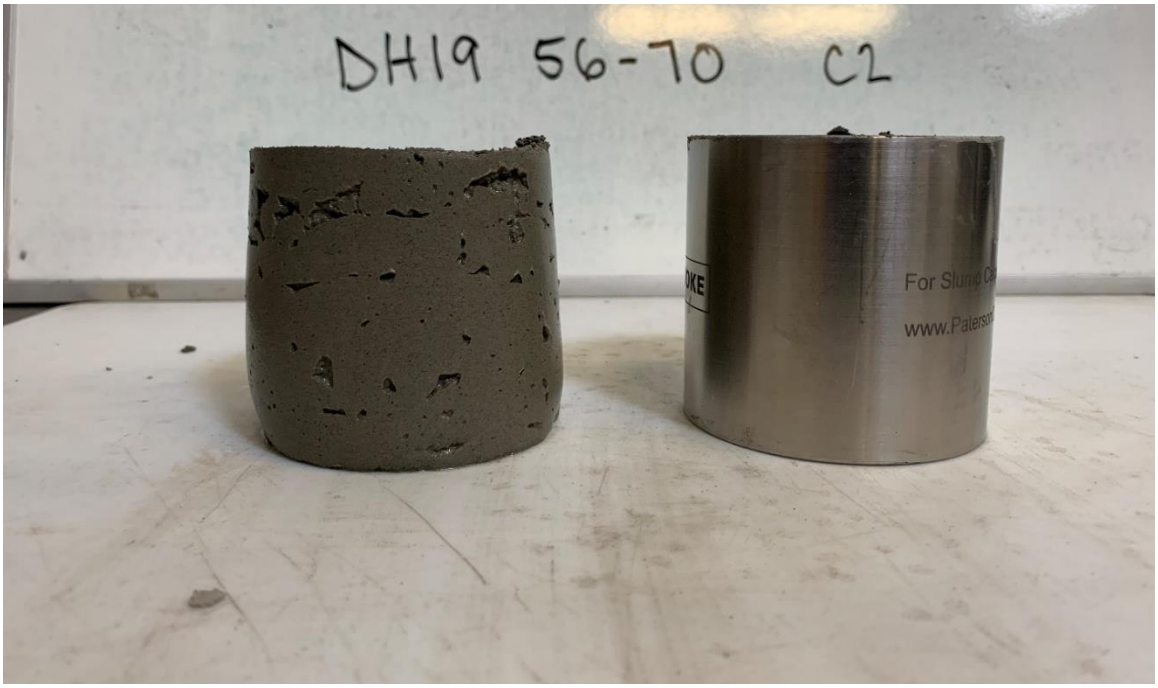

Figure 18: DH19 56-70 Boger Slump 73.7%m

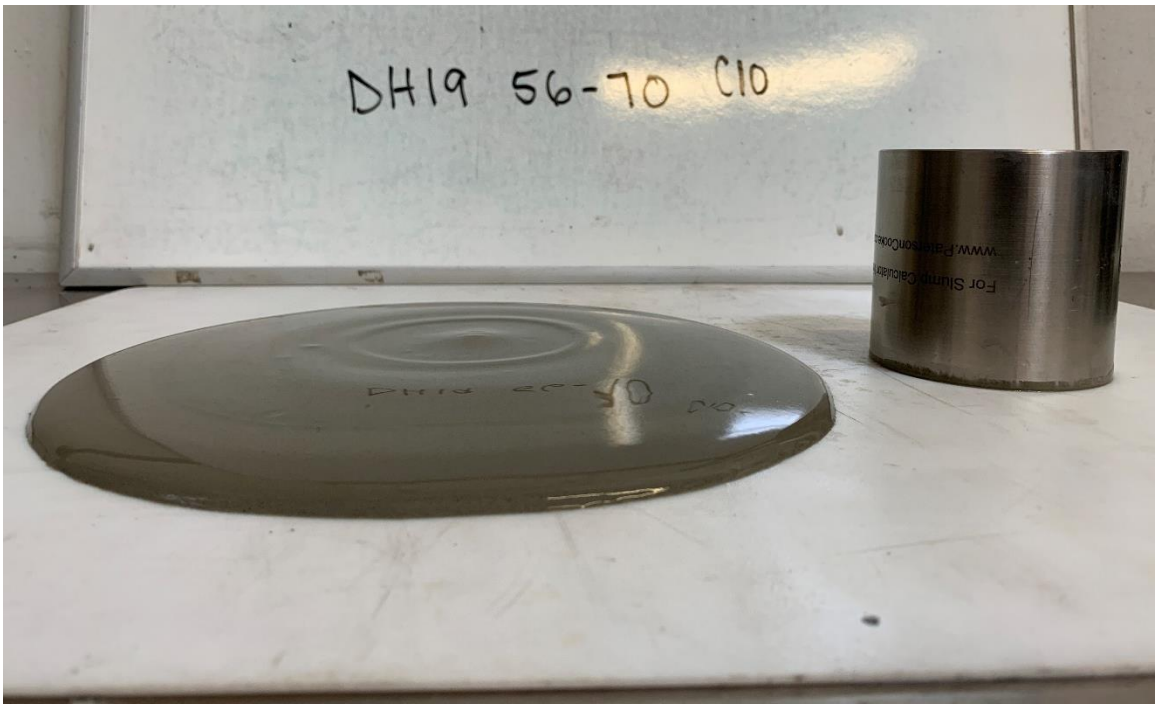

Figure 19: DH19 56-70 Boger Slump 51.6%m

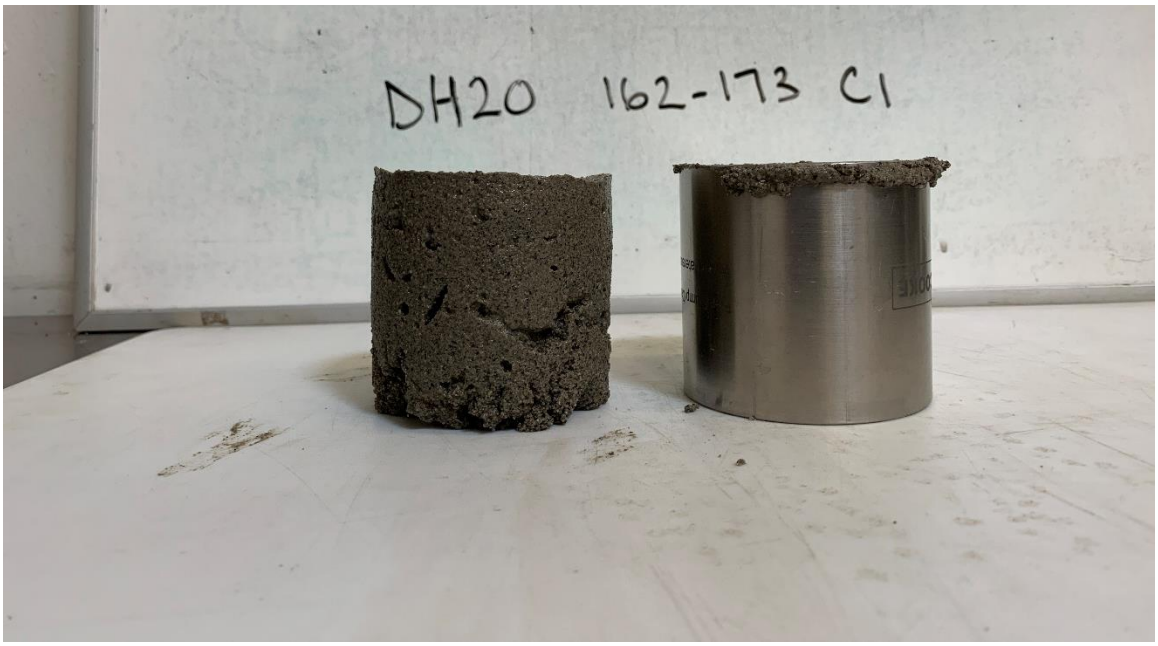

Figure 20: DH20-S2 162-173 Boger Slump 80.4%m

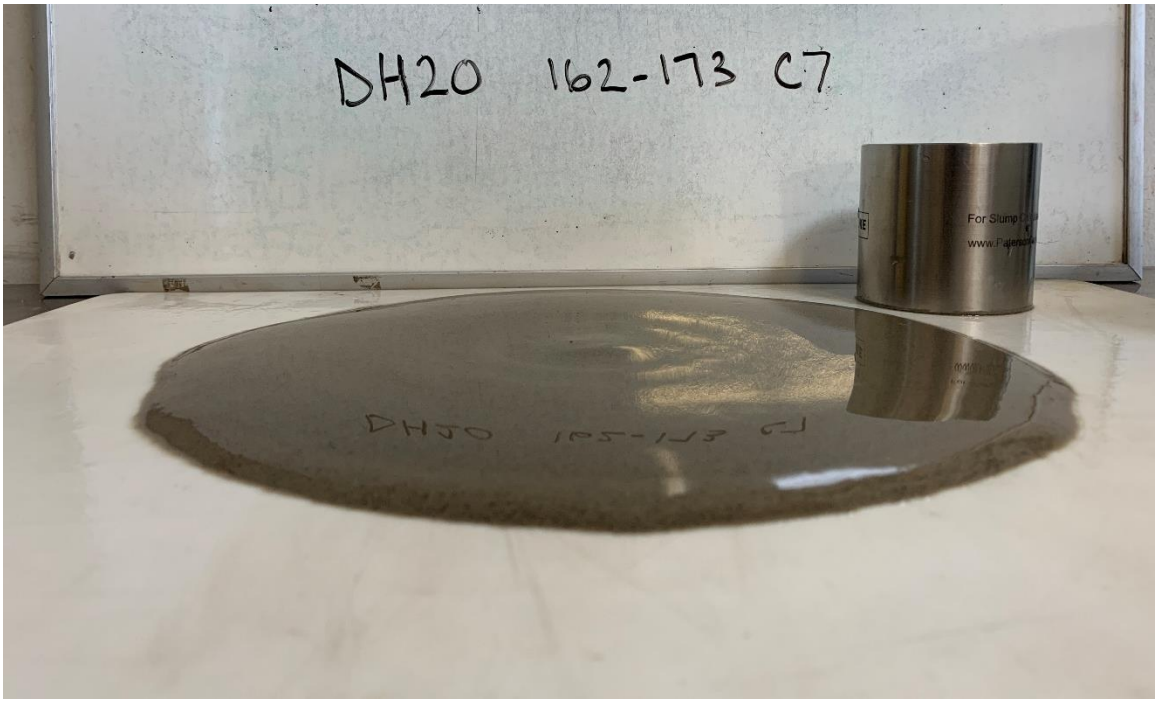

Figure 21: DH20-S2 162-173 Boger Slump 64.2%m

3.3 Tube Viscometer Rheology Measurements

3.3.1 Method and Equipment

P&C's ¾ inch (20 mm) tube viscometer has been used for the test work. An isometric sketch of the apparatus is shown in Figure 22. The viscometer comprises the following principal equipment:

- Progressive cavity pump with a variable frequency drive
- ¾ inch (20 mm) vertical up and down stainless steel measurement tubes
- Micromotion coriolis mass flow meter
- Rosemount differential pressure transmitters
- Heat exchanger to control the slurry temperature during a test.

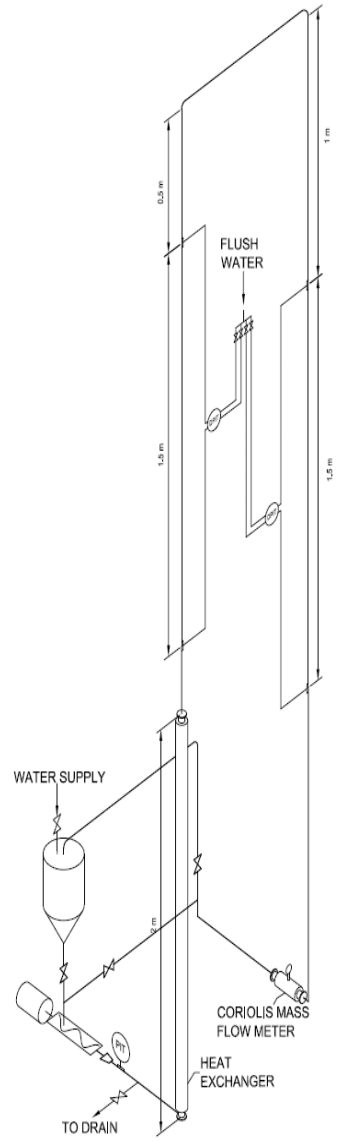

Figure 22: Isometric Sketch of P&C's ¾ inch (20 mm) Tube Viscometer

3.3.2 Conditions

Whole slurry samples of the DH19 56-70 and DH20 162-173 were used for tube viscometer test work. The samples were not flocculated. Slurry pH and temperature was monitored throughout the test work and are shown in Table IX and Table X.

Table IX: pH During Tube Viscometer Test Work

Parameter	DH19 56-70	DH20-S2 162-173
Maximum pH	7.9	8.5
Minimum pH	7.7	8.4
Average pH	7.8	8.5

Table X: Temperature During Tube Viscometer Test Work

Parameter	DH19 56-70	DH20-S2 162-173
Maximum temperature (°C)	26.8 °C	20.4°C
Minimum temperature (°C)	20.1 °C	20.2 °C
Average temperature (°C)	22.0 °C	20.3 °C

3.3.3 Measured Data

Appendix C presents the tube viscometer test data files. Each data file contains the following:

- Date, sample name and measuring system used for the tests
- Measured values of pseudo-shear rate and wall shear stress
- A pseudo-shear diagram (plot of wall shear stress versus pseudo-shear rate).

The pseudo-shear diagrams in Figure 23 and Figure 24 present the data for the DH19 56-70 and DH20 162-173. Only laminar flow data is presented on the pseudo-shear diagrams.

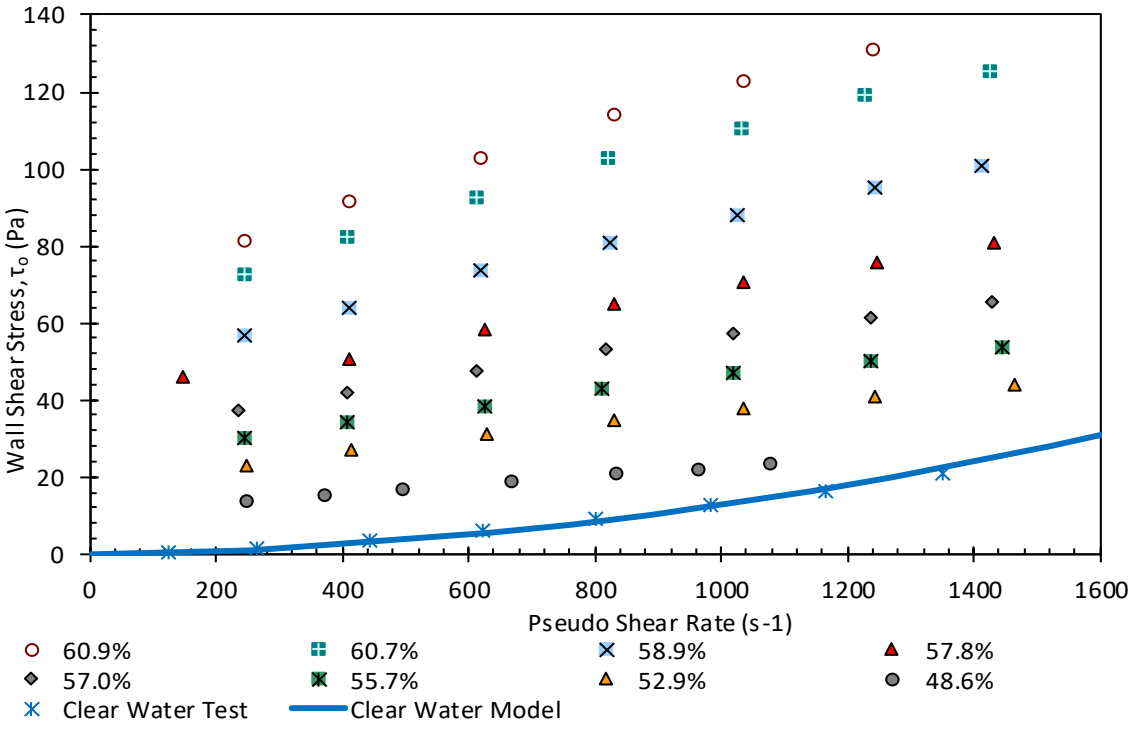

Figure 23: DH19 56-70 Pseudo-Shear Diagram

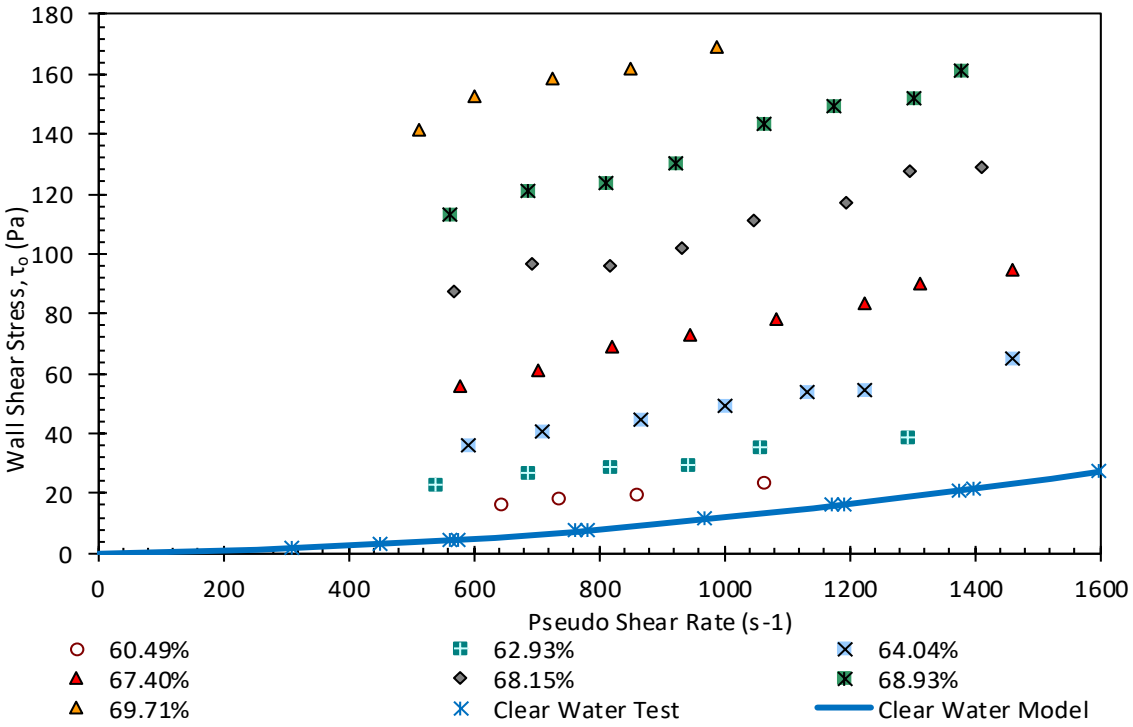

Figure 24: DH20-S2 162-173 Pseudo-Shear Diagram

3.3.4 Rheological Characterization

The laminar flow behavior of the slurry is characterized using the Bingham plastic model:

$$\tau = \tau_{yB} + K_{BP}\dot{\gamma} \quad (3)$$

where: τ = shear stress (Pa)

τ_{yB} = Bingham yield stress (Pa)

K_{BP} = plastic viscosity (Pa·s)

$\dot{\gamma}$ = shear rate (s-1).

The Bingham yield stress and plastic viscosity values are determined using the Buckingham Equation for pipe flow, which relates the Bingham model parameters to the wall shear stress and pseudo shear rate:

$$\frac{8V}{D} = \frac{\tau_0}{K_{BP}}\left[1 - \frac{4}{3}\alpha + \frac{1}{3}\alpha^4\right] \quad (4)$$

where: $\alpha = \tau_{yB}/\tau_0$

K_{BP} = Plastic viscosity (Pa·s).

3.3.5 Slurry Rheology Correlations

Table XI presents correlations for Bingham yield stress and plastic viscosity as a function of slurry mass concentration. These relationships are shown in Figure 25 and Figure 26, respectively.

Table XI: Slurry Rheological Parameters

Property	**DH19 56-70**	**DH20-S2 162-173**
Bingham yield stress (Pa)	$\tau_{yB}=a(C)^b$	
Relative plastic viscosity	$K_{BP}/\mu_{water}=(1-C/c)^{-d}$	
a	7,896.4	680,000.0
b	9.93	25.05
c	0.773	0.809
d	2.37	2.11
Measured slurry concentration range	48.6 to 60.9%m	60.5 to 69.7%m

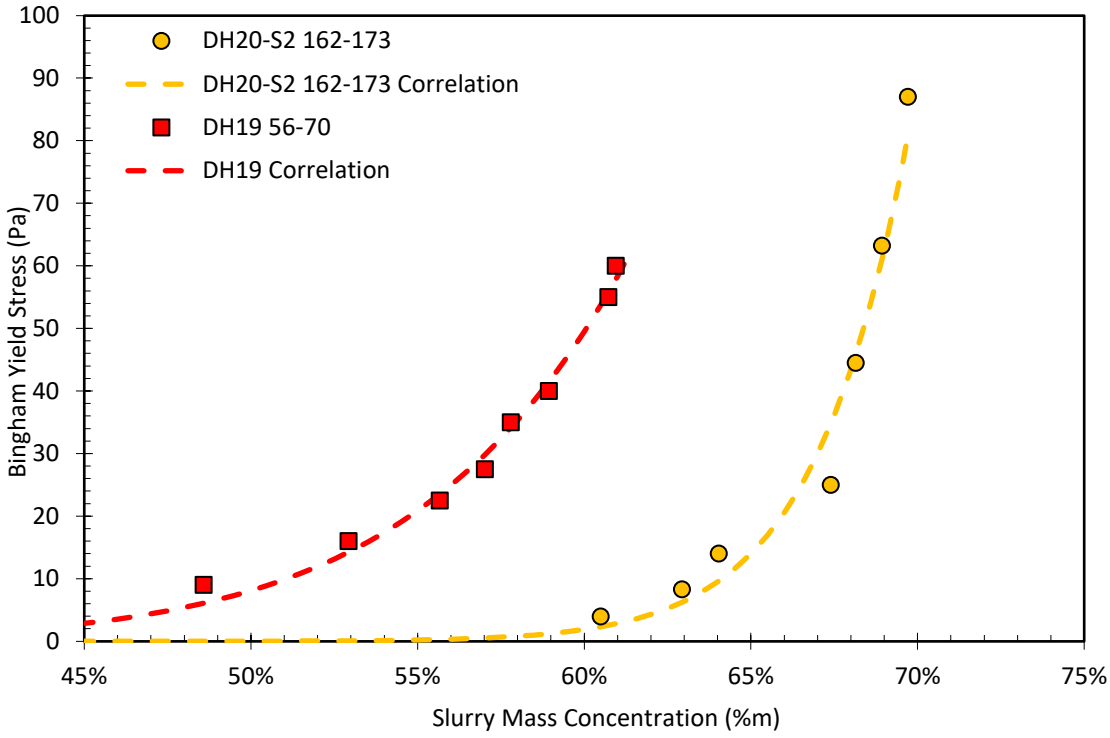

Figure 25: Bingham Yield Stress versus Slurry Mass Concentration, Test Concentration Range

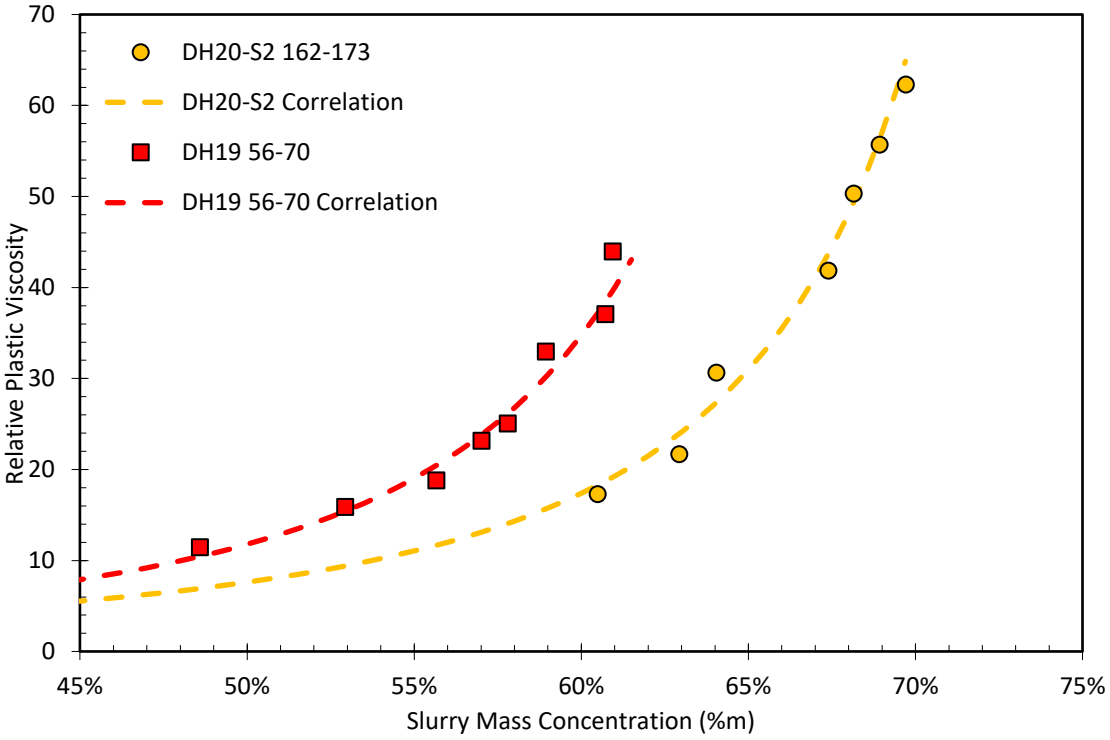

Figure 26: Relative Plastic Viscosity versus Slurry Mass Concentration, Test Concentration Range

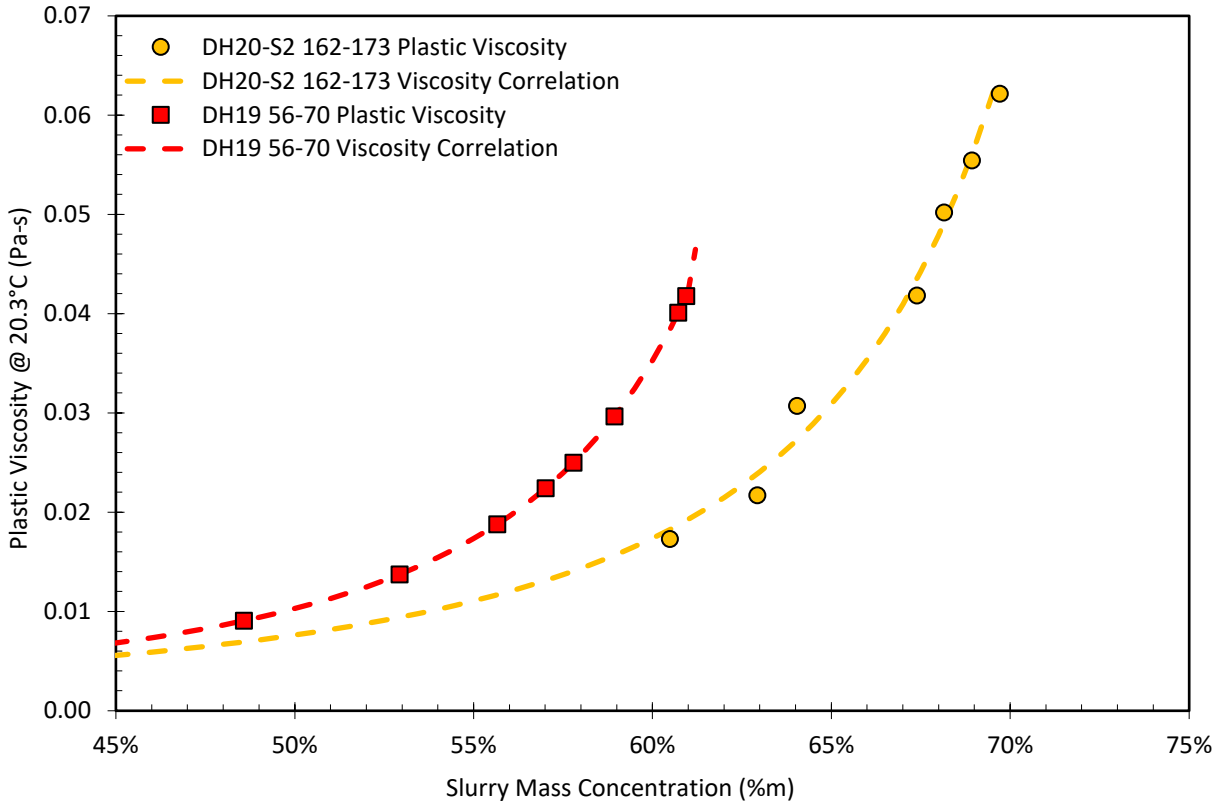

Figure 27: Viscosity versus Slurry Mass Concentration, Test Concentration Range[3]

3.3.6 *Particle Size Distribution Shift During Test*

The tube viscometer test continuously cycles sample through the pump and test loop. The pump is a progressive cavity positive displacement pump to limit the shear energy input during this process, but shear energy input is impossible to eliminate. A post tube viscometer sub-sample was collected for each sample and the particle size distribution was measured by wet sieve method. Figure 28 shows the initial and post tube viscometer particle size distributions for DH19 56-70 and DH20-S2 162-173 samples.

Sample DH19 56-70 had a relatively small shift finer over the course of the test. The test started at higher concentrations and was diluted over the course of the test, so the lowest concentrations will be most impacted by the particle size distribution shift. The impact of this shift should be minimal, but an increase in fines later in the test will raise both yield stress and viscosity for the impacted concentrations.

[3] Figure 27 has been added per client request. Please note these values are applicable for a slurry temperature of XX and XXX for DH19 56-70 and DH20-S2 162-173, respectively.

The sample DH20-S2 162-173 was visibly sandy as received. On the first high concentration attempt, the sample sanded out and the pump seized. The second test started at low concentration and added dewatered solids to cover the tested concentration range. At the end of the test the sample visibly contained more fines. The difference shown in the initial and post test particle size distributions is notable. The higher range of concentrations will have been most impacted by the shift and have higher than initial yield stress and viscosity values.

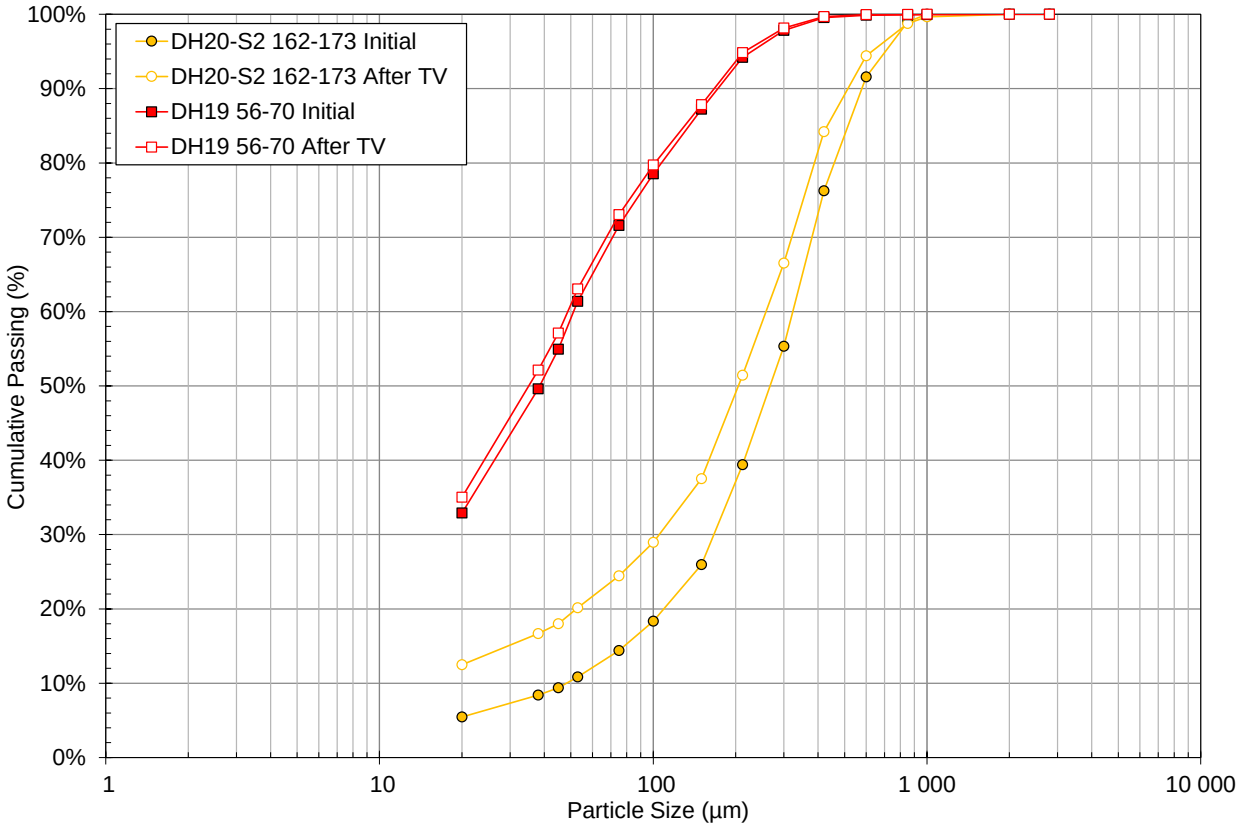

Figure 28: Wet Sieve Particle Size Distribution Before and After Tube Viscometer Test

3.4 Rheology Summary

Vane yield stress, Boger slump, and tube viscometer Bingham yield stress measurements were completed for DH19 56-70 and DH20-S2 162-173. It is not necessarily expected that the methods produce the same results. The vane yield stress is a measurement of maximum torque of the vane in a slurry that is under static conditions. The Boger yield stress measurement provides a visual indication of material yield stress and can be useful for field applications where more accurate methods are not available. Bingham yield stress is a model fit calculation under dynamic conditions. A comparison of the methods is shown in Figure 29.

The 65%m to 70%m concentrations for DH20-S2 162-273 Bingham yield stress points were likely increased by particle attrition over the course of the test as mentioned in section 3.3.6.

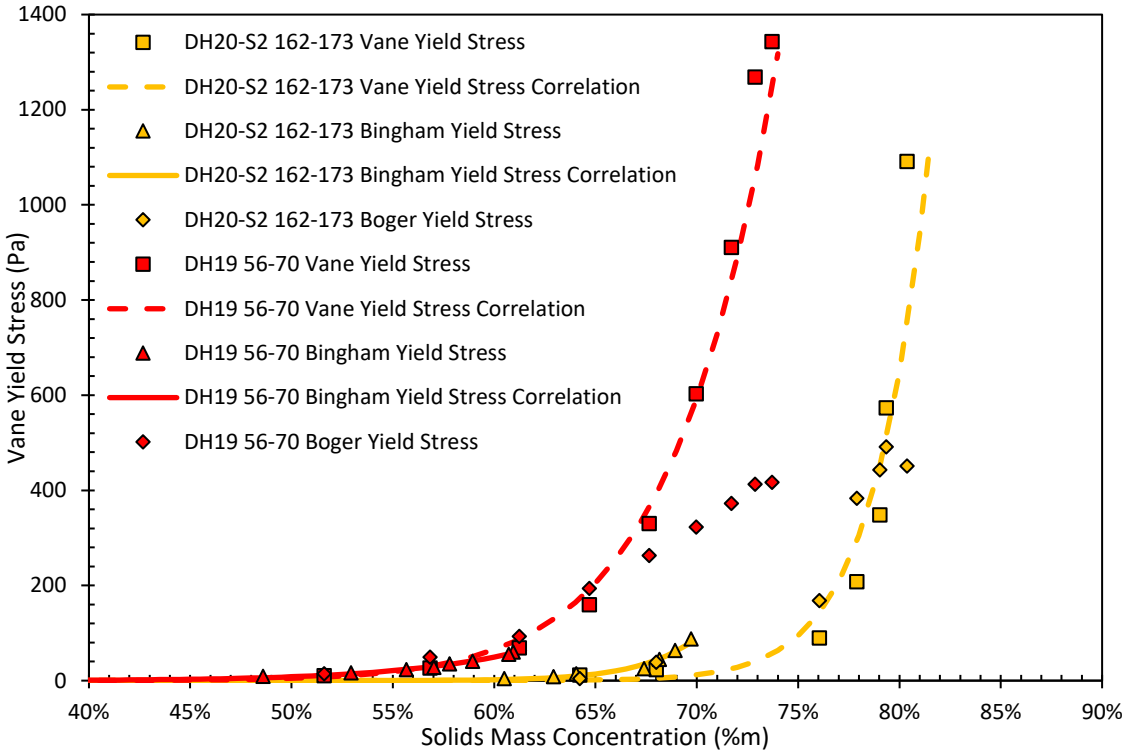

Figure 29: Vane Yield Stress, Boger Yield Stress, and Bingham Yield Stress Comparison

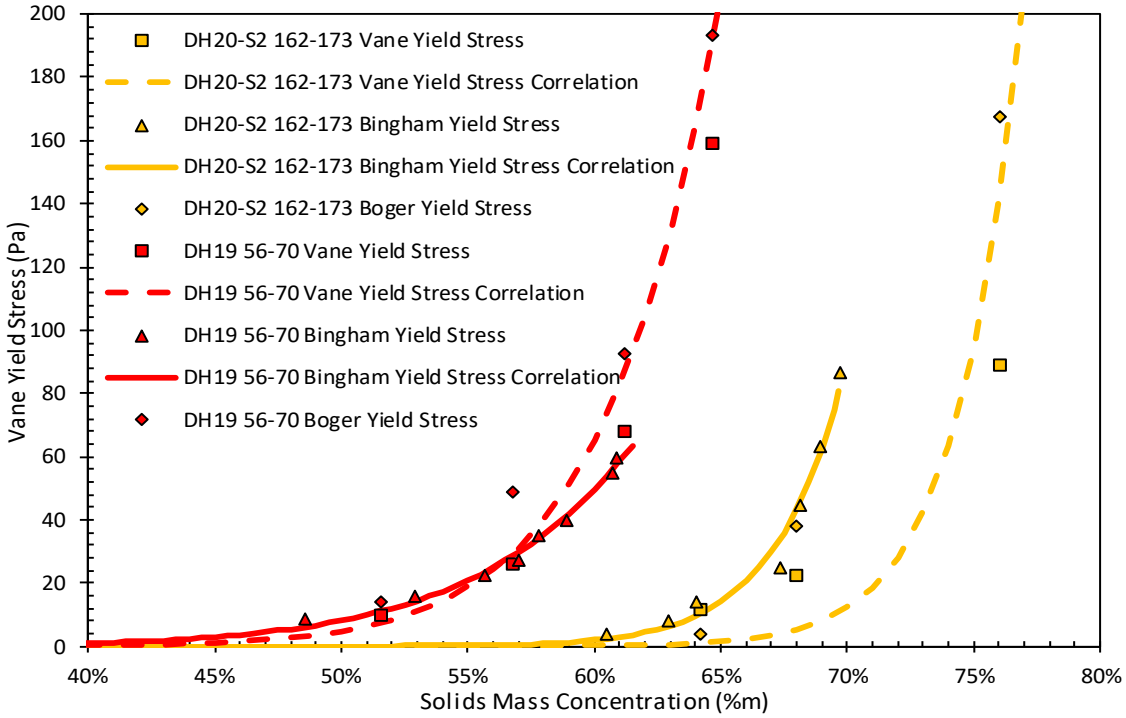

Figure 30: Vane Yield Stress, Boger Yield Stress, and Bingham Yield Stress Comparison – 200 Pa Limit

Ashley Rasmussen — Laboratory Manager

Benjamin Nicoara — Senior Laboratory Technologist

APPENDIX A : MATERIAL CHARACTERIZATION TEST RESULTS

Test
A.1 Sample Receipt
A.2 Solids Density – Pycnometer
A.3 Particle Size Analysis - Wet Sieve
A.4 Particle Size Analysis – Microtrac Laser
A.5 Mineralogy – DCM Report

A.1 Sample Receipt

PATERSON & COOKE

221 Corporate Circle, Suite D
Golden, CO 80401, USA

SAMPLE RECEIPT FORM

PROJECT NAME	Montana Resources Rheology	Date Received	April 13, 2021
PROJECT NUMBER	MRR-31-1295	Time Received	9:00 AM
PROJECT MANAGER	KA	Signature	AR

SAMPLE NAME	Tailings	Container Damage Present	No
Supplied By	AR	Sample Photo Taken	Yes
MSDS Received	Yes	Effective Gamma Dose Rate (Γ) at face of material	0.05 µSv/h
P&C Sample Code	S-31-1295-1,2,3,4,5,6		

Container Label	Container Type	pH	Conductivity (mS/cm)	Mass Estimate	% Solids Estimate	Solids Mass Calculated	Water Mass Calculated
DH20-S2 162-173	5 gallon	N/A	N/A	25.00 kg	95.0%	23.75 kg	1.25 kg
DH19 56-70	5 gallon	N/A	N/A	26.00 kg	95.0%	24.70 kg	1.30 kg
DH20 203-216	5 gallon	N/A	N/A	25.00 kg	95.0%	23.75 kg	1.25 kg
DDH20-S2 236-245	5 gallon	N/A	N/A	25.00 kg	95.0%	23.75 kg	1.25 kg
DH19 22-32	5 gallon	N/A	N/A	26.00 kg	95.0%	24.70 kg	1.30 kg
DH20-S2 83-92	5 gallon	N/A	N/A	6.00 kg	95.0%	5.70 kg	0.30 kg
TP H2O 1/10 to 10/10	5 gallon	10.2	3.0	130.00 kg	0.0%	0.00 kg	130.00 kg
					Total	126.35 kg	136.65 kg

Radiation Type	Distance from Sample	Time (min)	Total Count	Measured CPS	CPS Above Background	Dose Rate (µSv/h)
Background	2 m distance	10.0	592	0.99		
γ	At sample face	10.0	745	1.24	0.26	0.05

A.2 Solids Density – Pycnometer

PATERSON & COOKE

221 Corporate Circle, Suite D,
Golden, Colorado 80401-5637, USA
www.PatersonCooke.com

	Project No:	**MRR-31-1295**	**Client:**	**Montana Resources**
Gas Pycnometer Testing Data Form	**Sample ID:**	**DH19 22-32**	**Project Manager:**	**AMR**
	Date:	**6/1/2021**	**Operator:**	**BON**

Reference Vr (cm³) 192.2680

Without Sample

Average Vcell (cm³)	196.5501
Standard Deviation (cm³)	0.0470
Relative Standard Deviation	0.024%

With Sample

Pp (kPa)	Pd (kPa)	Pa (kPa)	Vcell (cm³)
199.10485	127.00075	82.703984	118.12
199.08701	126.98947	82.708783	118.09
199.06142	126.96022	82.702577	118.02
199.07492	126.96037	82.714657	117.97
199.0785	126.98155	82.722765	118.03

Average Vcell (cm³)	118.0439
Standard Deviation (cm³)	0.0600
Relative Standard Deviation	0.051%

Sample Density (g/cm³) = Sample Mass (g) / Sample Volume (cm³)

Sample Mass (g)	213.9530
Sample Volume (cm³)	78.5062
Sample Density (g/cm³)	2.725
Sample Density (kg/m³)	2,725

PATERSON & COOKE

221 Corporate Circle, Suite D,
Golden, Colorado 80401-5637, USA
www.PatersonCooke.com

	Project No:	**MRR-31-1295**	**Client:**	**Montana Resources**
Gas Pycnometer Testing Data Form	**Sample ID:**	**DH19 22-32**	**Project Manager:**	**AMR**
	Date:	**6/1/2021**	**Operator:**	**BON**

Reference Vr (cm³) 192.2680

Without Sample

Average Vcell (cm³)	196.5501
Standard Deviation (cm³)	0.0470
Relative Standard Deviation	0.024%

With Sample

Pp (kPa)	Pd (kPa)	Pa (kPa)	Vcell (cm³)
199.02609	126.8555	82.708658	117.61
199.00868	126.84312	82.700729	117.61
198.98937	126.84147	82.703818	117.62
198.99036	126.83605	82.698096	117.61
198.96824	126.83894	82.70488	117.64

Average Vcell (cm³)	117.6195
Standard Deviation (cm³)	0.0148
Relative Standard Deviation	0.013%

Sample Density (g/cm³) = Sample Mass (g) / Sample Volume (cm³)

Sample Mass (g)	214.9480
Sample Volume (cm³)	78.9306
Sample Density (g/cm³)	2.723
Sample Density (kg/m³)	2,723

PATERSON & COOKE

221 Corporate Circle, Suite D,
Golden, Colorado 80401-5637, USA
www.PatersonCooke.com

	Project No:	**MRR-31-1295**	**Client:**	**Montana Resources**
Gas Pycnometer Testing Data Form	**Sample ID:**	**DH19 22-32**	**Project Manager:**	**AMR**
	Date:	**6/1/2021**	**Operator:**	**BON**

Reference Vr (cm³) 192.2680

Without Sample	
Average Vcell (cm³)	196.5501
Standard Deviation (cm³)	0.0470
Relative Standard Deviation	0.024%

With Sample			
Pp (kPa)	Pd (kPa)	Pa (kPa)	Vcell (cm³)
198.93681	125.67232	82.700233	112.77
198.93554	125.6804	82.702233	112.80
198.95522	125.6871	82.702122	112.80
198.84925	125.6343	82.705859	112.73
198.8573	125.65289	82.704866	112.80

Average Vcell (cm³)	112.7816
Standard Deviation (cm³)	0.0298
Relative Standard Deviation	0.026%

Sample Density (g/cm³) = Sample Mass (g) / Sample Volume (cm³)

Sample Mass (g)	228.0770
Sample Volume (cm³)	83.7685
Sample Density (g/cm³)	2.723
Sample Density (kg/m³)	2,723

PATERSON & COOKE

221 Corporate Circle, Suite D,
Golden, Colorado 80401-5637, USA
www.PatersonCooke.com

	Project No:	**MRR-31-1295**	**Client:**	**Montana Resources**
Gas Pycnometer Testing Data Form	**Sample ID:**	**DH19 56-70**	**Project Manager:**	**AMR**
	Date:	**6/1/2021**	**Operator:**	**BON**

Reference Vr (cm³) 192.2680

Without Sample

Average Vcell (cm³)	196.5501
Standard Deviation (cm³)	0.0470
Relative Standard Deviation	0.024%

With Sample

Pp (kPa)	Pd (kPa)	Pa (kPa)	Vcell (cm³)
197.84893	131.76714	82.137621	144.40
197.83238	131.7547	82.127527	144.40
197.84373	131.76569	82.142695	144.39
197.83474	131.74706	82.127141	144.36
197.85497	131.75907	82.137676	144.34

Average Vcell (cm³)	144.3785
Standard Deviation (cm³)	0.0255
Relative Standard Deviation	0.018%

Sample Density (g/cm³) = Sample Mass (g) / Sample Volume (cm³)

Sample Mass (g)	141.0290
Sample Volume (cm³)	52.1716
Sample Density (g/cm³)	2.703
Sample Density (kg/m³)	2,703

PATERSON & COOKE

221 Corporate Circle, Suite D,
Golden, Colorado 80401-5637, USA
www.PatersonCooke.com

	Project No:	**MRR-31-1295**	**Client:**	**Montana Resources**
Gas Pycnometer Testing Data Form	**Sample ID:**	**DH19 56-70**	**Project Manager:**	**AMR**
	Date:	**6/1/2021**	**Operator:**	**BON**

Reference Vr (cm³)	192.2680

Without Sample	
Average Vcell (cm³)	196.5501
Standard Deviation (cm³)	0.0470
Relative Standard Deviation	0.024%

With Sample			
Pp (kPa)	Pd (kPa)	Pa (kPa)	Vcell (cm³)
197.81313	132.10039	82.124907	146.22
197.81985	132.09667	82.128382	146.18
197.82268	132.10207	82.119556	146.23
197.81721	132.08459	82.124369	146.13
197.80884	132.08934	82.120301	146.19

Average Vcell (cm³)	146.1897
Standard Deviation (cm³)	0.0376
Relative Standard Deviation	0.026%

Sample Density (g/cm³) = Sample Mass (g) / Sample Volume (cm³)

Sample Mass (g)	135.9690
Sample Volume (cm³)	50.3604
Sample Density (g/cm³)	2.700
Sample Density (kg/m³)	2,700

PATERSON & COOKE

221 Corporate Circle, Suite D,
Golden, Colorado 80401-5637, USA
www.PatersonCooke.com

	Project No:	**MRR-31-1295**	**Client:**	**Montana Resources**
Gas Pycnometer Testing Data Form	**Sample ID:**	**DH19 56-70**	**Project Manager:**	**AMR**
	Date:	**6/1/2021**	**Operator:**	**BON**

Reference Vr (cm³) 192.2680

Without Sample

Average Vcell (cm³)	196.5501
Standard Deviation (cm³)	0.0470
Relative Standard Deviation	0.024%

With Sample

Pp (kPa)	Pd (kPa)	Pa (kPa)	Vcell (cm³)
199.16935	132.47872	82.738471	143.40
199.14902	132.49329	82.747766	143.49
199.14479	132.49609	82.739533	143.54
199.12405	132.48396	82.733893	143.54
199.12208	132.49318	82.739795	143.57

Average Vcell (cm³)	143.5074
Standard Deviation (cm³)	0.0664
Relative Standard Deviation	0.046%

Sample Density (g/cm³) = Sample Mass (g) / Sample Volume (cm³)

Sample Mass (g)	142.9580
Sample Volume (cm³)	53.0427
Sample Density (g/cm³)	2.695
Sample Density (kg/m³)	2,695

PATERSON & COOKE

221 Corporate Circle, Suite D,
Golden, Colorado 80401-5637, USA
www.PatersonCooke.com

	Project No:	**MRR-31-1295**	**Client:**	**Montana Resources**
Gas Pycnometer Testing Data Form	**Sample ID:**	**DH20-S2 83-92**	**Project Manager:**	**AMR**
	Date:	**5/27/2021**	**Operator:**	**BON**

Reference Vr (cm³) 192.2680

Without Sample

Average Vcell (cm³)	196.5501
Standard Deviation (cm³)	0.0470
Relative Standard Deviation	0.024%

With Sample

Pp (kPa)	Pd (kPa)	Pa (kPa)	Vcell (cm³)
197.8606	126.87449	82.156319	121.12
197.87109	126.86936	82.143385	121.11
197.88038	126.87742	82.152375	121.11
197.89001	126.88892	82.146846	121.16
197.89295	126.87344	82.141564	121.10

Average Vcell (cm³)	121.1212
Standard Deviation (cm³)	0.0227
Relative Standard Deviation	0.019%

Sample Density (g/cm³) = Sample Mass (g) / Sample Volume (cm³)

Sample Mass (g)	205.5030
Sample Volume (cm³)	75.4289
Sample Density (g/cm³)	2.724
Sample Density (kg/m³)	2,724

PATERSON & COOKE

221 Corporate Circle, Suite D,
Golden, Colorado 80401-5637, USA
www.PatersonCooke.com

	Project No:	**MRR-31-1295**	**Client:**	**Montana Resources**
Gas Pycnometer Testing Data Form	**Sample ID:**	**DH20-S2 83-92**	**Project Manager:**	**AMR**
	Date:	**5/27/2021**	**Operator:**	**BON**

Reference Vr (cm³) 192.2680

Without Sample

Average Vcell (cm³)	196.5501
Standard Deviation (cm³)	0.0470
Relative Standard Deviation	0.024%

With Sample

Pp (kPa)	Pd (kPa)	Pa (kPa)	Vcell (cm³)
197.90483	126.35996	82.180341	118.73
197.90125	126.36093	82.194406	118.70
197.87714	126.34991	82.17277	118.75
197.89048	126.36005	82.181761	118.75
197.89935	126.35606	82.181044	118.72

Average Vcell (cm³)	118.7284
Standard Deviation (cm³)	0.0211
Relative Standard Deviation	0.018%

Sample Density (g/cm³) = Sample Mass (g) / Sample Volume (cm³)

Sample Mass (g)	212.0500
Sample Volume (cm³)	77.8217
Sample Density (g/cm³)	2.725
Sample Density (kg/m³)	2,725

PATERSON & COOKE

221 Corporate Circle, Suite D,
Golden, Colorado 80401-5637, USA
www.PatersonCooke.com

	Project No:	**MRR-31-1295**	**Client:**	**Montana Resources**
Gas Pycnometer Testing Data Form	**Sample ID:**	**DH20-S2 83-92**	**Project Manager:**	**AMR**
	Date:	**5/27/2021**	**Operator:**	**BON**

Reference Vr (cm³) 192.2680

Without Sample

Average Vcell (cm³)	196.5501
Standard Deviation (cm³)	0.0470
Relative Standard Deviation	0.024%

With Sample

Pp (kPa)	Pd (kPa)	Pa (kPa)	Vcell (cm³)
198.04499	128.63026	82.207382	128.58
198.03153	128.62212	82.202293	128.59
198.01407	128.61422	82.199756	128.59
198.00746	128.60954	82.202597	128.57
198.00962	128.60437	82.194558	128.57

Average Vcell (cm³)	128.5789
Standard Deviation (cm³)	0.0100
Relative Standard Deviation	0.008%

Sample Density (g/cm³) = Sample Mass (g) / Sample Volume (cm³)

Sample Mass (g)	185.1970
Sample Volume (cm³)	67.9712
Sample Density (g/cm³)	2.725
Sample Density (kg/m³)	2,725

PATERSON & COOKE

221 Corporate Circle, Suite D,
Golden, Colorado 80401-5637, USA
www.PatersonCooke.com

	Project No:	**MRR-31-1295**	**Client:**	**Montana Resources**
Gas Pycnometer Testing Data Form	**Sample ID:**	**DH20-S2 162-173**	**Project Manager:**	**AMR**
	Date:	**5/27/2021**	**Operator:**	**BON**

Reference Vr (cm³) 192.2680

Without Sample

Average Vcell (cm³)	196.5501
Standard Deviation (cm³)	0.0470
Relative Standard Deviation	0.024%

With Sample

Pp (kPa)	Pd (kPa)	Pa (kPa)	Vcell (cm³)
198.27672	127.64473	82.342064	123.32
198.27112	127.64297	82.338934	123.33
198.28203	127.64956	82.342423	123.33
198.29559	127.66358	82.356253	123.33
198.28891	127.65536	82.338424	123.35

Average Vcell (cm³)	123.3329
Standard Deviation (cm³)	0.0133
Relative Standard Deviation	0.011%

Sample Density (g/cm³) = Sample Mass (g) / Sample Volume (cm³)

Sample Mass (g)	196.8300
Sample Volume (cm³)	73.2172
Sample Density (g/cm³)	2.688
Sample Density (kg/m³)	2,688

PATERSON & COOKE

221 Corporate Circle, Suite D,
Golden, Colorado 80401-5637, USA
www.PatersonCooke.com

	Project No:	**MRR-31-1295**	**Client:**	**Montana Resources**
Gas Pycnometer Testing Data Form	**Sample ID:**	**DH20-S2 162-173**	**Project Manager:**	**AMR**
	Date:	**5/27/2021**	**Operator:**	**BON**

Reference Vr (cm³) 192.2680

Without Sample

Average Vcell (cm³)	196.5501
Standard Deviation (cm³)	0.0470
Relative Standard Deviation	0.024%

With Sample

Pp (kPa)	Pd (kPa)	Pa (kPa)	Vcell (cm³)
198.28784	127.28743	82.333708	121.73
198.26355	127.29379	82.352296	121.75
198.28297	127.3097	82.35806	121.77
198.30232	127.30278	82.348862	121.74
198.2817	127.28632	82.346325	121.71

Average Vcell (cm³)	121.7407
Standard Deviation (cm³)	0.0257
Relative Standard Deviation	0.021%

Sample Density (g/cm³) = Sample Mass (g) / Sample Volume (cm³)

Sample Mass (g)	201.1170
Sample Volume (cm³)	74.8094
Sample Density (g/cm³)	2.688
Sample Density (kg/m³)	2,688

PATERSON & COOKE

221 Corporate Circle, Suite D,
Golden, Colorado 80401-5637, USA
www.PatersonCooke.com

	Project No:	**MRR-31-1295**	**Client:**	**Montana Resources**
Gas Pycnometer Testing Data Form	**Sample ID:**	**DH20-S2 162-173**	**Project Manager:**	**AMR**
	Date:	**5/27/2021**	**Operator:**	**BON**

Reference Vr (cm³) 192.2680

Without Sample

Average Vcell (cm³)	196.5501
Standard Deviation (cm³)	0.0470
Relative Standard Deviation	0.024%

With Sample

Pp (kPa)	Pd (kPa)	Pa (kPa)	Vcell (cm³)
198.11918	126.58184	82.248323	119.15
198.11348	126.58453	82.240435	119.20
198.12948	126.5919	82.248585	119.18
198.10808	126.57622	82.23121	119.19
198.09327	126.57505	82.227363	119.22

Average Vcell (cm³)	119.1890
Standard Deviation (cm³)	0.0255
Relative Standard Deviation	0.021%

Sample Density (g/cm³) = Sample Mass (g) / Sample Volume (cm³)

Sample Mass (g)	207.9310
Sample Volume (cm³)	77.3611
Sample Density (g/cm³)	2.688
Sample Density (kg/m³)	2,688

PATERSON & COOKE

221 Corporate Circle, Suite D,
Golden, Colorado 80401-5637, USA
www.PatersonCooke.com

	Project No:	**MRR-31-1295**	**Client:**	**Montana Resources**
Gas Pycnometer Testing Data Form	**Sample ID:**	**DH20 203-216**	**Project Manager:**	**AMR**
	Date:	**5/27/2021**	**Operator:**	**BON**

Reference Vr (cm³) 192.2680

Without Sample

Average Vcell (cm³)	196.5501
Standard Deviation (cm³)	0.0470
Relative Standard Deviation	0.024%

With Sample

Pp (kPa)	Pd (kPa)	Pa (kPa)	Vcell (cm³)
198.28512	128.05628	82.355081	125.12
198.29311	128.06023	82.358308	125.11
198.28993	128.06829	82.36432	125.14
198.30097	128.07388	82.359329	125.16
198.30221	128.08458	82.359204	125.20

Average Vcell (cm³)	125.1460
Standard Deviation (cm³)	0.0370
Relative Standard Deviation	0.030%

Sample Density (g/cm³) = Sample Mass (g) / Sample Volume (cm³)

Sample Mass (g)	191.3950
Sample Volume (cm³)	71.4041
Sample Density (g/cm³)	2.680
Sample Density (kg/m³)	2,680

PATERSON & COOKE

221 Corporate Circle, Suite D,
Golden, Colorado 80401-5637, USA
www.PatersonCooke.com

	Project No:	**MRR-31-1295**	**Client:**	**Montana Resources**
Gas Pycnometer Testing Data Form	**Sample ID:**	**DH20 203-216**	**Project Manager:**	**AMR**
	Date:	**5/27/2021**	**Operator:**	**BON**

Reference Vr (cm³) 192.2680

Without Sample

Average Vcell (cm³)	196.5501
Standard Deviation (cm³)	0.0470
Relative Standard Deviation	0.024%

With Sample

Pp (kPa)	Pd (kPa)	Pa (kPa)	Vcell (cm³)
198.29826	128.7383	82.356212	128.20
198.28381	128.73968	82.359384	128.23
198.28923	128.7417	82.35948	128.23
198.2852	128.7365	82.35362	128.23
198.29157	128.74852	82.35908	128.25

Average Vcell (cm³)	128.2273
Standard Deviation (cm³)	0.0183
Relative Standard Deviation	0.014%

Sample Density (g/cm³) = Sample Mass (g) / Sample Volume (cm³)

Sample Mass (g)	183.0580
Sample Volume (cm³)	68.3228
Sample Density (g/cm³)	2.679
Sample Density (kg/m³)	2,679

PATERSON & COOKE

221 Corporate Circle, Suite D,
Golden, Colorado 80401-5637, USA
www.PatersonCooke.com

	Project No:	**MRR-31-1295**	**Client:**	**Montana Resources**
Gas Pycnometer Testing Data Form	**Sample ID:**	**DH20 203-216**	**Project Manager:**	**AMR**
	Date:	**5/27/2021**	**Operator:**	**BON**

Reference Vr (cm³) 192.2680

Without Sample

Average Vcell (cm³)	196.5501
Standard Deviation (cm³)	0.0470
Relative Standard Deviation	0.024%

With Sample

Pp (kPa)	Pd (kPa)	Pa (kPa)	Vcell (cm³)
198.24959	129.39586	82.354516	131.36
198.25416	129.39811	82.35555	131.36
198.21666	129.39704	82.355688	131.42
198.25845	129.40819	82.357894	131.39
198.27996	129.43083	82.355412	131.46

Average Vcell (cm³)	131.3987
Standard Deviation (cm³)	0.0449
Relative Standard Deviation	0.034%

Sample Density (g/cm³) = Sample Mass (g) / Sample Volume (cm³)

Sample Mass (g)	174.7780
Sample Volume (cm³)	65.1514
Sample Density (g/cm³)	2.683
Sample Density (kg/m³)	2,683

PATERSON & COOKE

221 Corporate Circle, Suite D,
Golden, Colorado 80401-5637, USA
www.PatersonCooke.com

	Project No:	**MRR-31-1295**	**Client:**	**Montana Resources**
Gas Pycnometer Testing Data Form	**Sample ID:**	**DDH20-S2 236-245**	**Project Manager:**	**AMR**
	Date:	**5/27/2021**	**Operator:**	**BON**

Reference Vr (cm³) 192.2680

Without Sample

Average Vcell (cm³)	196.5501
Standard Deviation (cm³)	0.0470
Relative Standard Deviation	0.024%

With Sample

Pp (kPa)	Pd (kPa)	Pa (kPa)	Vcell (cm³)
198.27223	129.23118	82.363093	130.52
198.26075	129.22944	82.361163	130.54
198.25685	129.21899	82.361052	130.50
198.24964	129.22425	82.352489	130.56
198.26558	129.22778	82.359342	130.53

Average Vcell (cm³)	130.5286
Standard Deviation (cm³)	0.0230
Relative Standard Deviation	0.018%

Sample Density (g/cm³) = Sample Mass (g) / Sample Volume (cm³)

Sample Mass (g)	176.1750
Sample Volume (cm³)	66.0215
Sample Density (g/cm³)	2.668
Sample Density (kg/m³)	2,668

PATERSON & COOKE

221 Corporate Circle, Suite D,
Golden, Colorado 80401-5637, USA
www.PatersonCooke.com

	Project No:	**MRR-31-1295**	**Client:**	**Montana Resources**
Gas Pycnometer Testing Data Form	**Sample ID:**	**DDH20-S2 236-245**	**Project Manager:**	**AMR**
	Date:	**5/27/2021**	**Operator:**	**BON**

Reference Vr (cm³) 192.2680

Without Sample

Average Vcell (cm³)	196.5501
Standard Deviation (cm³)	0.0470
Relative Standard Deviation	0.024%

With Sample

Pp (kPa)	Pd (kPa)	Pa (kPa)	Vcell (cm³)
198.44309	128.20859	82.417851	125.35
198.43097	128.25496	82.408998	125.61
198.39268	128.24212	82.40311	125.64
198.32922	128.24622	82.399111	125.78
198.35979	128.25933	82.392285	125.80

Average Vcell (cm³)	125.6353
Standard Deviation (cm³)	0.1794
Relative Standard Deviation	0.143%

Sample Density (g/cm³) = Sample Mass (g) / Sample Volume (cm³)

Sample Mass (g)	188.9560
Sample Volume (cm³)	70.9148
Sample Density (g/cm³)	2.665
Sample Density (kg/m³)	2,665

PATERSON & COOKE

221 Corporate Circle, Suite D,
Golden, Colorado 80401-5637, USA
www.PatersonCooke.com

	Project No:	**MRR-31-1295**	**Client:**	**Montana Resources**
Gas Pycnometer Testing Data Form	**Sample ID:**	**DDH20-S2 236-245**	**Project Manager:**	**AMR**
	Date:	**5/27/2021**	**Operator:**	**BON**

Reference Vr (cm³) 192.2680

Without Sample

Average Vcell (cm³)	196.5501
Standard Deviation (cm³)	0.0470
Relative Standard Deviation	0.024%

With Sample

Pp (kPa)	Pd (kPa)	Pa (kPa)	Vcell (cm³)
198.43241	128.53403	82.454297	126.75
198.54312	128.62849	82.443334	127.01
198.4859	128.6684	82.433778	127.32
198.50923	128.69956	82.425435	127.45
198.52411	128.70682	82.417369	127.48

Average Vcell (cm³)	127.2015
Standard Deviation (cm³)	0.3122
Relative Standard Deviation	0.245%

Sample Density (g/cm³) = Sample Mass (g) / Sample Volume (cm³)

Sample Mass (g)	184.1250
Sample Volume (cm³)	69.3486
Sample Density (g/cm³)	2.655
Sample Density (kg/m³)	2,655

A.3 Particle Size Analysis - Wet Sieve

PARTICLE SIZE DISTRIBUTION MEASUREMENT

Project No:	**MRR-31-1295**	**Sample ID:**	**DH19 22-32**	**Test Date:**	**6/1/2021**
Project Description:	**Montana Resources Rheology**	**Test:**	**Wet Sieve**	**Performed by:**	**BN**
Client Name:	**Montana Resources**	**Method:**	**Sieve**	**Date of Input (Sheet):**	**6/2/2021**

Standardized Sieve Set Sizes (µm)	Test Mass Retained (g)	Test Fraction Retained (%)	Standardized Cumulative Passing (%)
2800	0.00	0.0%	100.0%
2000	10.29	3.4%	96.6%
1000	44.90	14.8%	81.8%
850	8.29	2.7%	79.1%
600	34.11	11.2%	67.8%
420	36.09	11.9%	55.5%
300	40.91	13.5%	42.5%
212	27.73	9.1%	33.3%
150	25.46	8.4%	24.9%
100	16.09	5.3%	19.0%
75	12.43	4.1%	15.5%
53	10.23	3.4%	12.2%
45	4.67	1.5%	10.6%
38	5.56	1.8%	9.7%
20	5.52	1.8%	7.0%
-20	21.20	7.0%	

Particle Size P50 (µm)	Particle Size P80 (µm)	Particle Size P90 (µm)	% -75µm	% -45µm	% -20µm
364.4	897.7	1467.5	16%	11%	7%

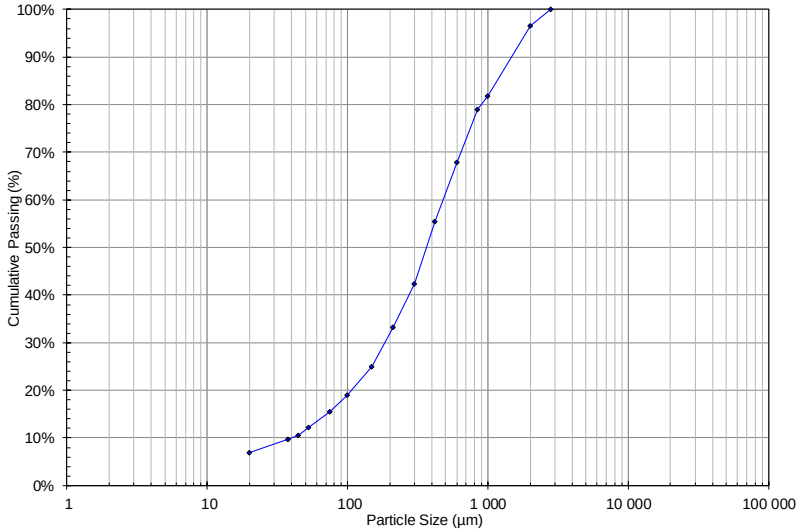

PARTICLE SIZE DISTRIBUTION MEASUREMENT

Project No:	**MRR-31-1295**	**Sample ID:**	**DH19 56-70**	**Test Date:**	**6/1/2021**
Project Description:	**Montana Resources Rheology**	**Test:**	**Wet Sieve**	**Performed by:**	**BN**
Client Name:	**Montana Resources**	**Method:**	**Sieve**	**Date of Input (Sheet):**	**6/2/2021**

Standardized Sieve Set Sizes (µm)	Test Mass Retained (g)	Test Fraction Retained (%)	Standardized Cumulative Passing (%)
2800	0.00	0.0%	100.0%
2000	0.00	0.0%	100.0%
1000	0.08	0.0%	100.0%
850	0.05	0.0%	99.9%
600	0.13	0.1%	99.9%
420	0.60	0.3%	99.6%
300	4.10	1.8%	97.8%
212	8.24	3.6%	94.2%
150	15.92	7.0%	87.2%
100	16.66	7.3%	78.5%
75	19.03	8.3%	71.6%
53	23.26	10.2%	61.4%
45	14.74	6.5%	54.9%
38	24.49	10.7%	49.6%
20	25.76	11.3%	32.9%
-20	75.03	32.9%	

Particle Size P50 (µm)	Particle Size P80 (µm)	Particle Size P90 (µm)	% -75µm	% -45µm	% -20µm
38.5	106.4	172.0	72%	55%	33%

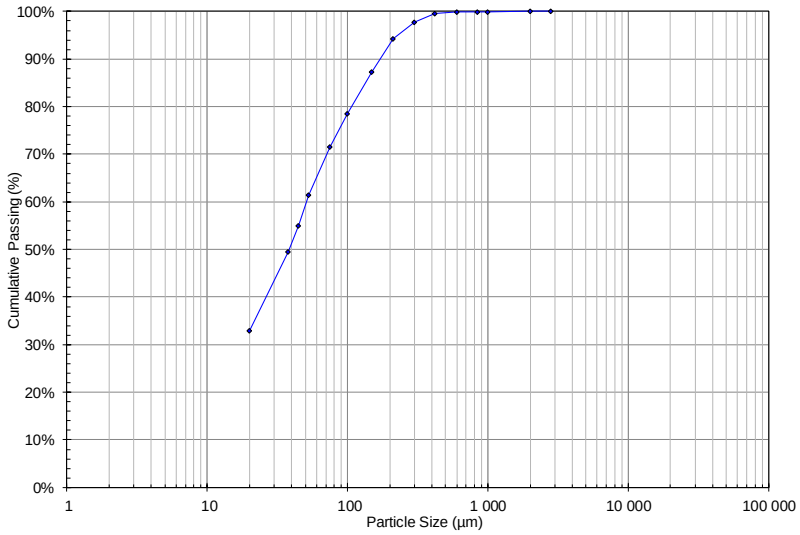

PARTICLE SIZE DISTRIBUTION MEASUREMENT

Project No:	**MRR-31-1295**	**Sample ID:**	**DH20-S2 83-92**	**Test Date:**	**5/26/2021**
Project Description:	**Montana Resources Rheology**	**Test:**	**Wet Sieve**	**Performed by:**	**AR**
Client Name:	**Montana Resources**	**Method:**	**Sieve**	**Date of Input (Sheet):**	**6/1/2021**

Standardized Sieve Set Sizes (µm)	Test Mass Retained (g)	Test Fraction Retained (%)	Standardized Cumulative Passing (%)
2800	7.55	2.3%	97.7%
2000	6.96	2.2%	95.5%
1000	43.40	13.4%	82.1%
850	10.47	3.2%	78.8%
600	35.97	11.1%	67.7%
420	34.94	10.8%	56.4%
300	40.08	12.4%	44.4%
212	28.80	8.9%	35.5%
150	26.12	8.1%	27.4%
100	16.16	5.0%	21.8%
75	12.01	3.7%	18.7%
53	11.01	3.4%	15.3%
45	4.78	1.5%	13.8%
38	6.90	2.1%	12.8%
20	8.34	2.6%	9.1%
-20	29.37	9.1%	

Particle Size P50 (µm)	Particle Size P80 (µm)	Particle Size P90 (µm)	% -75µm	% -45µm	% -20µm
350.6	901.6	1505.5	19%	14%	9%

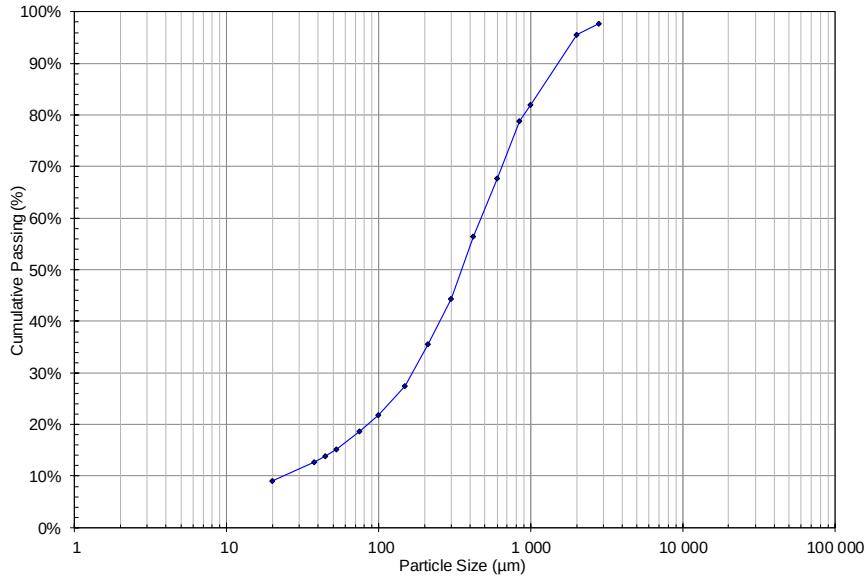

PARTICLE SIZE DISTRIBUTION MEASUREMENT

Project No:	**MRR-31-1295**	**Sample ID:**	**DH20-S2 162-173**	**Test Date:**	**6/1/2021**
Project Description:	**Montana Resources Rheology**	**Test:**	**Wet Sieve**	**Performed by:**	**BN**
Client Name:	**Montana Resources**	**Method:**	**Sieve**	**Date of Input (Sheet):**	**6/2/2021**

Standardized Sieve Set Sizes (µm)	Test Mass Retained (g)	Test Fraction Retained (%)	Standardized Cumulative Passing (%)
2800	0.00	0.0%	100.0%
2000	0.00	0.0%	100.0%
1000	0.00	0.0%	100.0%
850	2.56	1.0%	99.0%
600	18.64	7.4%	91.6%
420	36.67	14.6%	76.3%
300	54.45	21.6%	55.3%
212	40.08	15.9%	39.4%
150	33.84	13.5%	26.0%
100	17.18	6.8%	18.3%
75	11.89	4.7%	14.4%
53	8.94	3.6%	10.8%
45	3.69	1.5%	9.4%
38	4.97	2.0%	8.4%
20	4.89	1.9%	5.5%
-20	13.73	5.5%	

Particle Size P50 (µm)	Particle Size P80 (µm)	Particle Size P90 (µm)	% -75µm	% -45µm	% -20µm
267.0	456.4	578.1	14%	9%	5%

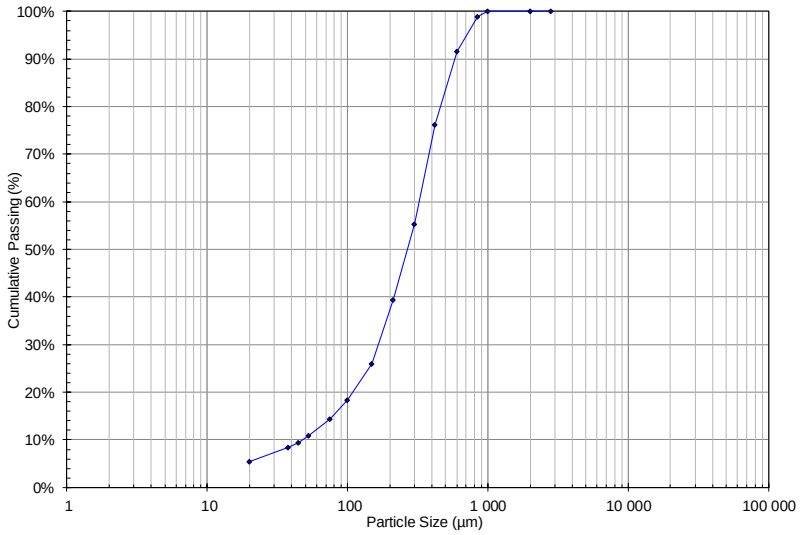

PARTICLE SIZE DISTRIBUTION MEASUREMENT

Project No:	**MRR-31-1295**	**Sample ID:**	**DH20 203-216**	**Test Date:**	**6/1/2021**
Project Description:	**Montana Resources Rheology**	**Test:**	**Wet Sieve**	**Performed by:**	**BN**
Client Name:	**Montana Resources**	**Method:**	**Sieve**	**Date of Input (Sheet):**	**6/1/2021**

Standardized Sieve Set Sizes (µm)	Test Mass Retained (g)	Test Fraction Retained (%)	Standardized Cumulative Passing (%)
2800	0.00	0.0%	100.0%
2000	0.00	0.0%	100.0%
1000	0.10	0.0%	100.0%
850	0.28	0.1%	99.8%
600	4.50	1.9%	98.0%
420	14.61	6.0%	91.5%
300	31.61	13.0%	78.9%
212	26.49	10.9%	68.0%
150	31.49	13.0%	55.0%
100	22.66	9.3%	44.3%
75	20.22	8.3%	37.3%
53	17.77	7.3%	30.0%
45	8.70	3.6%	26.4%
38	10.29	4.2%	24.3%
20	11.17	4.6%	17.6%
-20	42.56	17.6%	

Particle Size P50 (µm)	Particle Size P80 (µm)	Particle Size P90 (µm)	% -75µm	% -45µm	% -20µm
124.5	308.8	403.3	37%	26%	18%

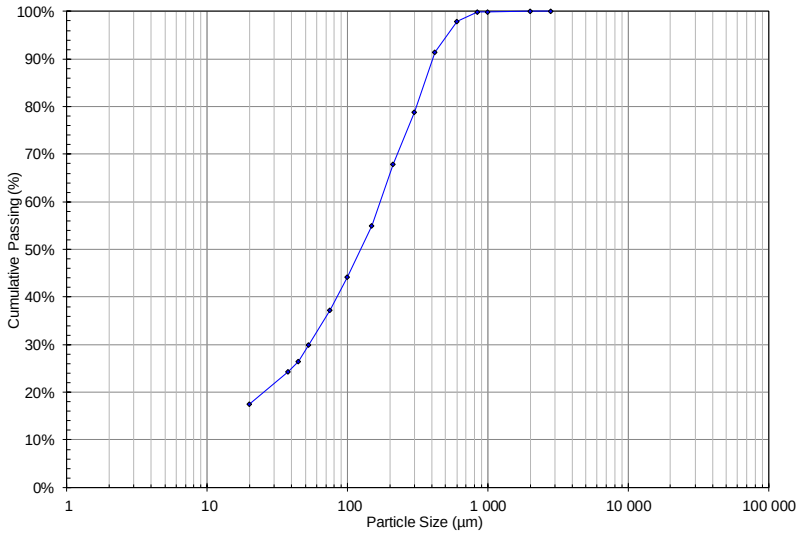

PARTICLE SIZE DISTRIBUTION MEASUREMENT

Project No:	**MRR-31-1295**	**Sample ID:**	**DDH20-S2 236-245**	**Test Date:**	**5/26/2021**
Project Description:	**Montana Resources Rheology**	**Test:**	**Wet Sieve**	**Performed by:**	**AR**
Client Name:	**Montana Resources**	**Method:**	**Sieve**	**Date of Input (Sheet):**	**6/1/2021**

Standardized Sieve Set Sizes (µm)	Test Mass Retained (g)	Test Fraction Retained (%)	Standardized Cumulative Passing (%)
3000	0.00	0.0%	100.0%
2000	0.00	0.0%	100.0%
1000	0.03	0.0%	100.0%
850	0.09	0.0%	100.0%
600	1.60	0.6%	99.3%
420	7.60	3.1%	95.9%
300	21.97	8.9%	87.3%
212	27.64	11.2%	76.2%
150	36.30	14.7%	61.5%
100	27.66	11.2%	48.7%
75	23.16	9.4%	40.9%
53	23.05	9.3%	31.6%
45	10.16	4.1%	27.5%
38	14.00	5.7%	24.7%
20	14.14	5.7%	16.1%
-20	39.83	16.1%	

Particle Size P50 (µm)	Particle Size P80 (µm)	Particle Size P90 (µm)	% -75µm	% -45µm	% -20µm
104.9	238.8	332.9	41%	27%	16%

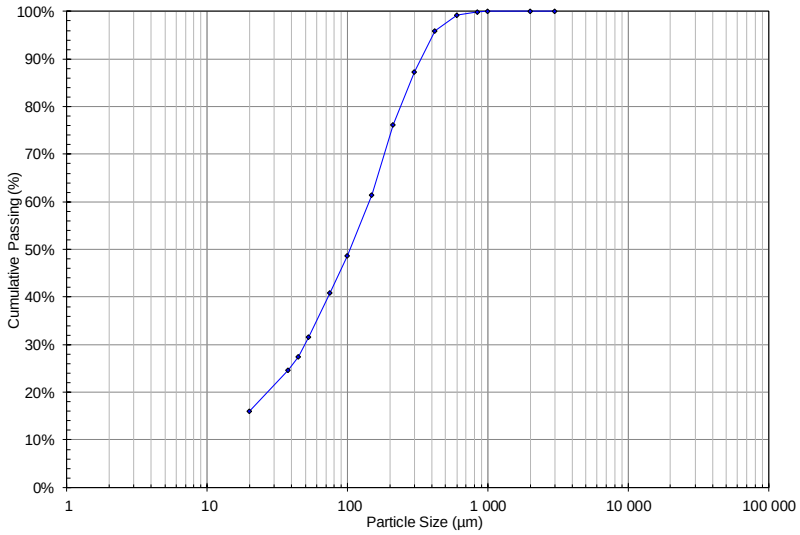

A.4 Particle Size Analysis – Microtrac Laser

PARTICLE SIZE DISTRIBUTION MEASUREMENT

Project No:	**MRR-31-1295**	**Sample ID:**	**DH19 22-32**	**Dispersant:**	**None**	**Test Date:**	**5/26/2021**
Project Description:	**Montana Resources Rheology**	**Test:**	**Laser PSD**	**Carrier Medium:**	**Water**	**Performed by:**	**BN**
Client Name:	**Montana Resources**	**Method:**	**Laser**			**Date of Input (Sheet):**	**May 26, 2021**

Standardized Sieve Set Sizes (µm)	Standardized Cumulative Passing (%)
3000	100.0%
2000	100.0%
1000	96.6%
850	93.5%
600	85.0%
420	72.2%
300	60.3%
212	49.7%
150	41.9%
100	34.8%
75	30.2%
53	24.9%
45	22.5%
38	20.2%
20	12.9%
15	10.2%
10	7.2%
7.0	5.2%
3.0	2.2%
2.0	1.3%
1.75	1.1%
1.50	0.9%
1.25	0.7%
1.00	0.5%
0.75	0.2%
0.50	0.0%
0.40	0.0%
0.25	0.0%
0.10	0.0%
0.07	0.0%
0.04	0.0%
0.026	0.0%

Particle Size P_{50} (µm)	Particle Size P_{80} (µm)	Particle Size P_{90} (µm)	% -75µm	% -45µm	% -20µm	% -3µm	% -1µm	% -0.25µm
214.2	522.2	736.2	30%	23%	13%	2%	0%	0%

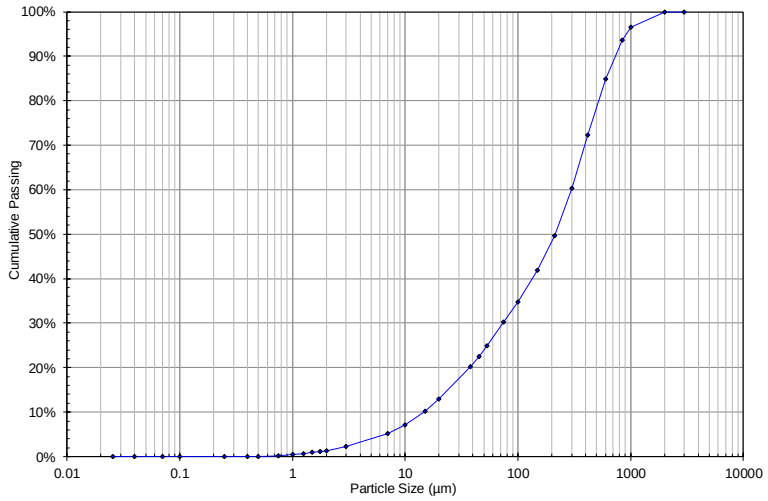

PARTICLE SIZE DISTRIBUTION MEASUREMENT

Project No:	**MRR-31-1295**	**Sample ID:**	**DH19 56-70**	**Dispersant:**	**None**	**Test Date:**	**5/26/2021**
Project Description:	**Montana Resources Rheology**	**Test:**	**Laser PSD**	**Carrier Medium:**	**Water**	**Performed by:**	**BN**
Client Name:	**Montana Resources**	**Method:**	**Laser**			**Date of Input (Sheet):**	**May 26, 2021**

Standardized Sieve Set Sizes (µm)	Standardized Cumulative Passing (%)
3000	100.0%
2000	100.0%
1000	99.6%
850	99.3%
600	98.5%
420	96.9%
300	94.2%
212	89.5%
150	83.2%
100	73.9%
75	66.1%
53	55.2%
45	50.0%
38	44.5%
20	26.6%
15	20.4%
10	13.7%
7.0	9.6%
3.0	3.8%
2.0	2.3%
1.75	1.9%
1.50	1.5%
1.25	1.2%
1.00	0.8%
0.75	0.5%
0.50	0.1%
0.40	0.0%
0.25	0.0%
0.10	0.0%
0.07	0.0%
0.04	0.0%
0.026	0.0%

Particle Size P_{50} (µm)	Particle Size P_{80} (µm)	Particle Size P_{90} (µm)	% -75µm	% -45µm	% -20µm	% -3µm	% -1µm	% -0.25µm
45.0	130.6	219.4	66%	50%	27%	4%	1%	0%

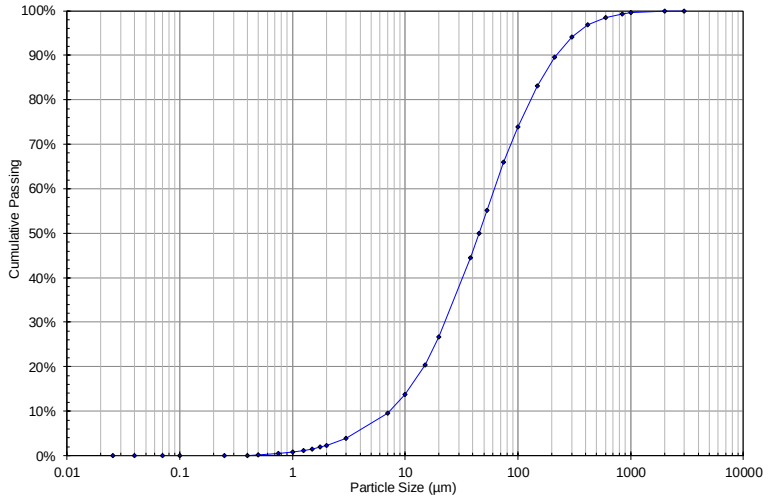

PARTICLE SIZE DISTRIBUTION MEASUREMENT

Project No:	**MRR-31-1295**	**Sample ID:**	**DH20-S2 83-92**	**Dispersant:**	**None**	**Test Date:**	**5/26/2021**
Project Description:	**Montana Resources Rheology**	**Test:**	**Laser PSD**	**Carrier Medium:**	**Water**	**Performed by:**	**BN**
Client Name:	**Montana Resources**	**Method:**	**Laser**			**Date of Input (Sheet):**	**May 26, 2021**

Standardized Sieve Set Sizes (µm)	Standardized Cumulative Passing (%)
3000	100.0%
2000	100.0%
1000	97.1%
850	94.3%
600	86.6%
420	75.3%
300	65.4%
212	56.4%
150	49.1%
100	42.1%
75	37.4%
53	31.5%
45	28.7%
38	25.9%
20	16.2%
15	12.5%
10	8.4%
7.0	5.8%
3.0	2.3%
2.0	1.4%
1.75	1.2%
1.50	1.0%
1.25	0.7%
1.00	0.5%
0.75	0.3%
0.50	0.0%
0.40	0.0%
0.25	0.0%
0.10	0.0%
0.07	0.0%
0.04	0.0%
0.026	0.0%

Particle Size P_{50} (µm)	Particle Size P_{80} (µm)	Particle Size P_{90} (µm)	% -75µm	% -45µm	% -20µm	% -3µm	% -1µm	% -0.25µm
156.3	487.2	699.7	37%	29%	16%	2%	1%	0%

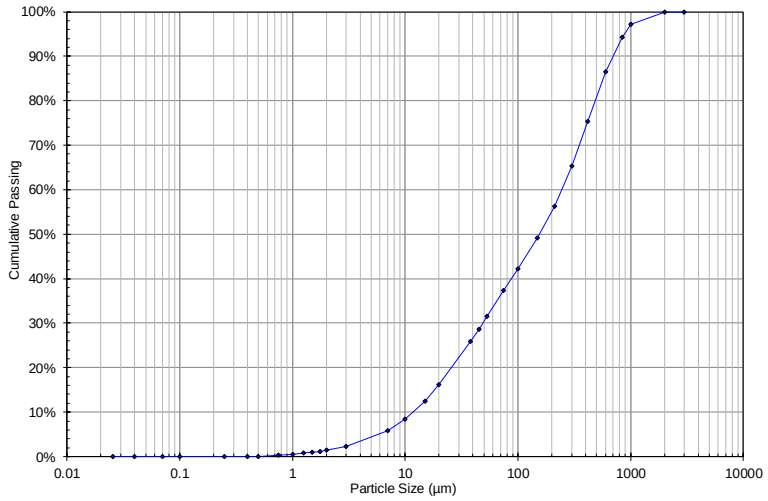

PARTICLE SIZE DISTRIBUTION MEASUREMENT

Project No:	**MRR-31-1295**	**Sample ID:**	**DH20-S2 162-173**	**Dispersant:**	**None**	**Test Date:**	**5/26/2021**
Project Description:	**Montana Resources Rheology**	**Test:**	**Laser PSD**	**Carrier Medium:**	**Water**	**Performed by:**	**BN**
Client Name:	**Montana Resources**	**Method:**	**Laser**			**Date of Input (Sheet):**	**May 26, 2021**

Standardized Sieve Set Sizes (µm)	Standardized Cumulative Passing (%)
3000	100.0%
2000	100.0%
1000	98.9%
850	97.4%
600	91.1%
420	74.9%
300	56.7%
212	42.5%
150	33.2%
100	25.7%
75	21.4%
53	16.9%
45	15.0%
38	13.2%
20	7.9%
15	6.1%
10	4.2%
7.0	3.0%
3.0	1.3%
2.0	0.8%
1.75	0.7%
1.50	0.5%
1.25	0.4%
1.00	0.2%
0.75	0.1%
0.50	0.0%
0.40	0.0%
0.25	0.0%
0.10	0.0%
0.07	0.0%
0.04	0.0%
0.026	0.0%

Particle Size P_{50} (µm)	Particle Size P_{80} (µm)	Particle Size P_{90} (µm)	% -75µm	% -45µm	% -20µm	% -3µm	% -1µm	% -0.25µm
254.9	469.8	585.9	21%	15%	8%	1%	0%	0%

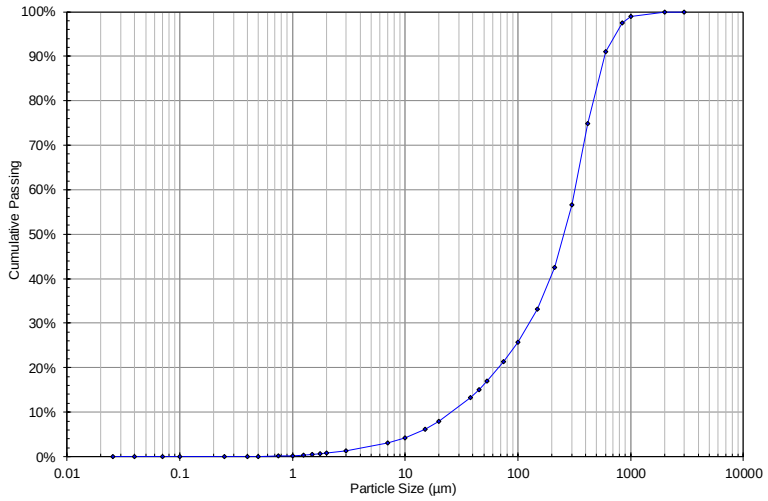

PARTICLE SIZE DISTRIBUTION MEASUREMENT

Project No:	**MRR-31-1295**	**Sample ID:**	**DH20 203-216**	**Dispersant:**	**None**	**Test Date:**	**5/26/2021**
Project Description:	**Montana Resources Rheology**	**Test:**	**Laser PSD**	**Carrier Medium:**	**Water**	**Performed by:**	**BN**
Client Name:	**Montana Resources**	**Method:**	**Laser**			**Date of Input (Sheet):**	**May 26, 2021**

Standardized Sieve Set Sizes (µm)	Standardized Cumulative Passing (%)
3000	100.0%
2000	100.0%
1000	99.6%
850	99.1%
600	97.0%
420	91.3%
300	80.4%
212	68.2%
150	58.5%
100	48.9%
75	42.5%
53	35.0%
45	31.7%
38	28.4%
20	18.2%
15	14.4%
10	10.1%
7.0	7.3%
3.0	3.0%
2.0	1.9%
1.75	1.6%
1.50	1.3%
1.25	1.0%
1.00	0.7%
0.75	0.4%
0.50	0.1%
0.40	0.0%
0.25	0.0%
0.10	0.0%
0.07	0.0%
0.04	0.0%
0.026	0.0%

Particle Size P_{50} (µm)	Particle Size P_{80} (µm)	Particle Size P_{90} (µm)	% -75µm	% -45µm	% -20µm	% -3µm	% -1µm	% -0.25µm
104.9	296.7	404.0	42%	32%	18%	3%	1%	0%

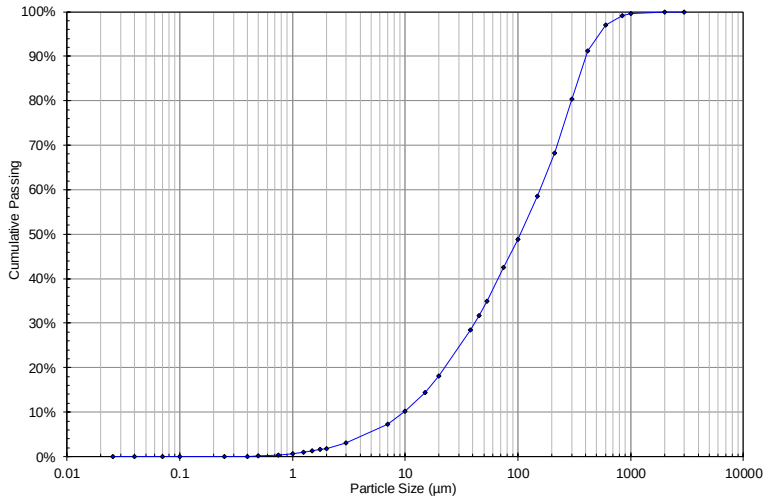

PARTICLE SIZE DISTRIBUTION MEASUREMENT

Project No:	**MRR-31-1295**	**Sample ID:**	**DDH20-S2 236-245**	**Dispersant:**	**None**	**Test Date:**	**5/26/2021**
Project Description:	**Montana Resources Rheology**	**Test:**	**Laser PSD**	**Carrier Medium:**	**Water**	**Performed by:**	**BN**
Client Name:	**Montana Resources**	**Method:**	**Laser**			**Date of Input (Sheet):**	**May 26, 2021**

Standardized Sieve Set Sizes (µm)	Standardized Cumulative Passing (%)
3000	100.0%
2000	100.0%
1000	99.8%
850	99.6%
600	98.6%
420	95.5%
300	86.9%
212	72.9%
150	60.6%
100	48.9%
75	41.1%
53	32.0%
45	28.1%
38	24.4%
20	13.9%
15	10.7%
10	7.4%
7.0	5.3%
3.0	2.2%
2.0	1.4%
1.75	1.1%
1.50	0.9%
1.25	0.7%
1.00	0.5%
0.75	0.2%
0.50	0.0%
0.40	0.0%
0.25	0.0%
0.10	0.0%
0.07	0.0%
0.04	0.0%
0.026	0.0%

Particle Size P_{50} (µm)	Particle Size P_{80} (µm)	Particle Size P_{90} (µm)	% -75µm	% -45µm	% -20µm	% -3µm	% -1µm	% -0.25µm
104.0	252.7	338.7	41%	28%	14%	2%	0%	0%

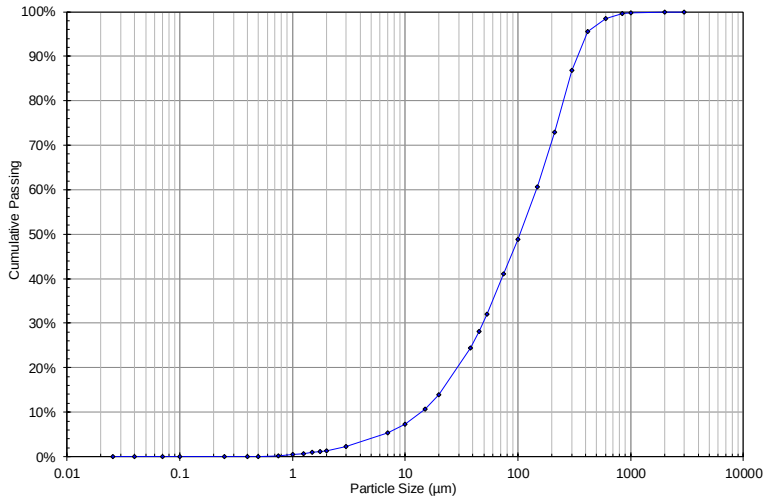

A.5 Mineralogy – DCM Report

DCM SCIENCE LABORATORY, INC.
12421 W. 49th Avenue, Unit #6
Wheat Ridge, CO 80033 (303) 463-8270

Semi-Quantitative X-Ray Diffraction Analysis
Page 1 of 3

Client:
Paterson & Cooke USA, Ltd.
221 Corporate Circle, Suite D
Golden, CO 80401

Analysis Date:	6-3-21
Reporting Date:	6-3-21
Receipt Date:	5-27-21
Client Job No.:	MRR-31-1295
Client Project:	None Given
DCMSL Project:	PCL167

Client Sample No.:	DDH20 236-245	DH20 203-216	DH20 162-173
Bulk Sample			
Calcite	2	2	2
Gypsum	-	<2*	-
Hematite	-	3	2
K-Feldspar	35	23	31
Mica	14	18	16
Plagioclase	11	5	6
Pyrite	2	3	1
Quartz	31	28	28

Client Sample No.:	DDH20 236-245	DH20 203-216	DH20 162-173
Total Clay	5	18	14
Chlorite	-	-	<2*
Kaolinite	1	3	3
Smectite	4	15	11

*May be present

DCM SCIENCE LABORATORY, INC.
12421 W. 49th Avenue, Unit #6
Wheat Ridge, CO 80033 (303) 463-8270

Semi-Quantitative X-Ray Diffraction Analysis
Page 2 of 3

Client:
Paterson & Cooke USA, Ltd.
221 Corporate Circle, Suite D
Golden, CO 80401

Analysis Date:	6-3-21
Reporting Date:	6-3-21
Receipt Date:	5-27-21
Client Job No.:	MRR-31-1295
Client Project:	None Given
DCMSL Project:	PCL167

Client Sample No.:	DH20 83-92	DH19 56-70	DH19 22-32
Bulk Sample			
Calcite	3	2	5
Gypsum	<2*	<2*	-
Hematite	4	<2*	<2*
K-Feldspar	19	15	18
Mica	13	24	21
Plagioclase	4	7	5
Pyrite	7	3	2
Quartz	25	23	24

Client Sample No.:	DH20 83-92	DH19 56-70	DH19 22-32
Total Clay	25	26	25
Kaolinite	6	5	5
Smectite	19	21	20

*May be present

The bulk samples were spiked with corundum, prepared for x-ray diffraction analysis and scanned over a range of 5° to 45° 2Θ Cu Kα radiation, 40kV, 35mA. Mineral phases were identified with the aid of computer-assisted programs accessing a powder diffraction database. Estimates of mineral concentrations are based on relative peak heights and reference intensity ratios (RIR) measured in-house.

DCM SCIENCE LABORATORY, INC.
12421 W. 49th Avenue, Unit #6
Wheat Ridge, CO 80033 (303) 463-8270

Semi-Quantitative X-Ray Diffraction Analysis
Page 3 of 3

Client:
Paterson & Cooke USA, Ltd.
221 Corporate Circle, Suite D
Golden, CO 80401

Analysis Date:	6-3-21
Reporting Date:	6-3-21
Receipt Date:	5-27-21
Client Job No.:	MRR-31-1295
Client Project:	None Given
DCMSL Project:	PCL167

Client Sample No.:	DDH20 236-245	DH20 203-216	DH20 162-173
Clay Fraction <2µm			
Chlorite	-	-	<2*
Kaolinite	10	19	19
Smectite	90	81	81

Client Sample No.:	DH20 83-92	DH19 56-70	DH19 22-32
Clay Fraction <2µm			
Kaolinite	23	19	21
Smectite	77	81	79

An oriented clay mount (<2µm) was prepared for each sample for x-ray diffration analysis and scanned over a range of 3° to 40° 2Θ Cu Kα radiation, 40kV, 25mA. The mount was analyzed air-dried RH ~25% and glycolated. Clay concentrations are based on peak areas and intensity factors measured in-house on known standards or computer calculated.

All information provided by client, including sample results, is considered proprietary and confidential. Client results and other information will not be released to anyone but the client except by client request. When the laboratory is required by law or authorized by contractual arrangement to release confidential information, the client or individual concerned shall, unless prohibited by law, be notified of the information provided.

Jason Barnes, Analyst

APPENDIX B : RHEOLOGY TEST RESULTS

Test
B.1 DH19 56-70 Vane Yield Stress and Boger Slump Test Results
B.2 DH20-S2 162-173 Vane Yield Stress and Boger Slump Test Results

B.1 DH19 56-70 Vane Yield Stress and Boger Slump Test Results

CONCENTRATION DETERMINATION DATASHEET

Project Number:	**MRR-31-1295**	**Client:**	**Montana Resources**		**Test Date:**	**7/21/2021**
Project Description:	**Rheology Test Work**	**Sample ID:**	**DH19 56-70**		**Operator:**	**AMR**

Solid Density (kg/m^3)	2699.00	Water Density (kg/m3)	1000.00	Dissolved Solids (%m)	

Trial No.	C2	C3	C4	C5	C6	C7	C8	C9	C10
(a) Slurry + Tare, g.	59.331	70.081	57.668	47.858	48.118	48.025	66.549	55.895	36.652
(b) Solids + Tare, g.	44.044	51.4	41.695	33.848	32.943	31.498	41.22	32.301	19.509
(c) Tare, g.	1.204	1.203	1.216	1.203	1.219	1.213	1.210	1.233	1.225
(d) Slurry, g.	58.127	68.878	56.452	46.655	46.899	46.812	65.339	54.662	35.427
(e) Solids, g.	42.84	50.197	40.479	32.645	31.724	30.285	40.010	31.068	18.284
(f) % Solids	73.70%	72.88%	71.71%	69.97%	67.64%	64.69%	61.23%	56.84%	51.61%
(g) % Water	26.30%	27.12%	28.29%	30.03%	32.36%	35.31%	38.77%	43.16%	48.39%
(h) Water, g.	15.29	18.68	15.97	14.01	15.18	16.53	25.33	23.59	17.14
(i) Dissolved Solids Mass	0.00	0.00	0.00	0.00	0.00	0.00	0.00	0.00	0.00
(j) Corrected % Solids	73.70%	72.88%	71.71%	69.97%	67.64%	64.69%	61.23%	56.84%	51.61%
(h) Slurry Density, kg/m3	1865.46	1847.62	1822.75	1787.19	1741.58	1687.05	1627.25	1557.10	1481.23
pH			7.03	6.9	7.04		6.94		6.91
Temperature, C			23.4	23.9	23.7		23.6		24.1
Vane Yield Stress Run 1 (Pa)	1286	1273	911.4	599	328.2	165.3	71.91	26.51	10.72
Vane Yield Stress Run 2 (Pa)	1400	1264	909.2	605.7	331.9	153.1	64.86	25.94	9.588
Average Vane Yield Stress (Pa)	1343	1268.5	910.3	602.35	330.05	159.2	68.385	26.225	10.154
% Solids:	0.00%	0.00%	0.00%	0.00%	0.00%	0.00%	0.00%	0.00%	0.00%
Slump, mm	6	6	8	11	16	23	40	51	64
Boger Yield Stress (Pa)	416.15	412.2	372.05	322.55	262.7	193.5	92.9	48.95	14.15

Notes: * C6 Boger slump measurements is an average of 3 measurements, 11 mm, 16 mm, 20 mm.

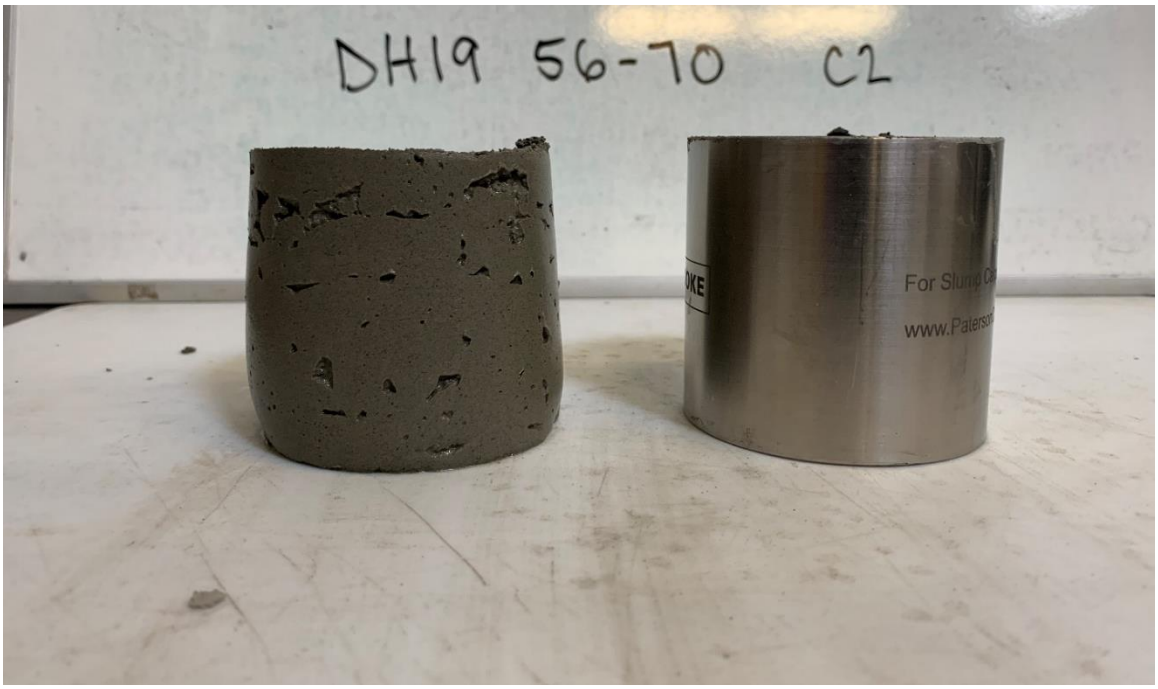

Figure 31: DH19 56-70 Boger Slump 73.7%m

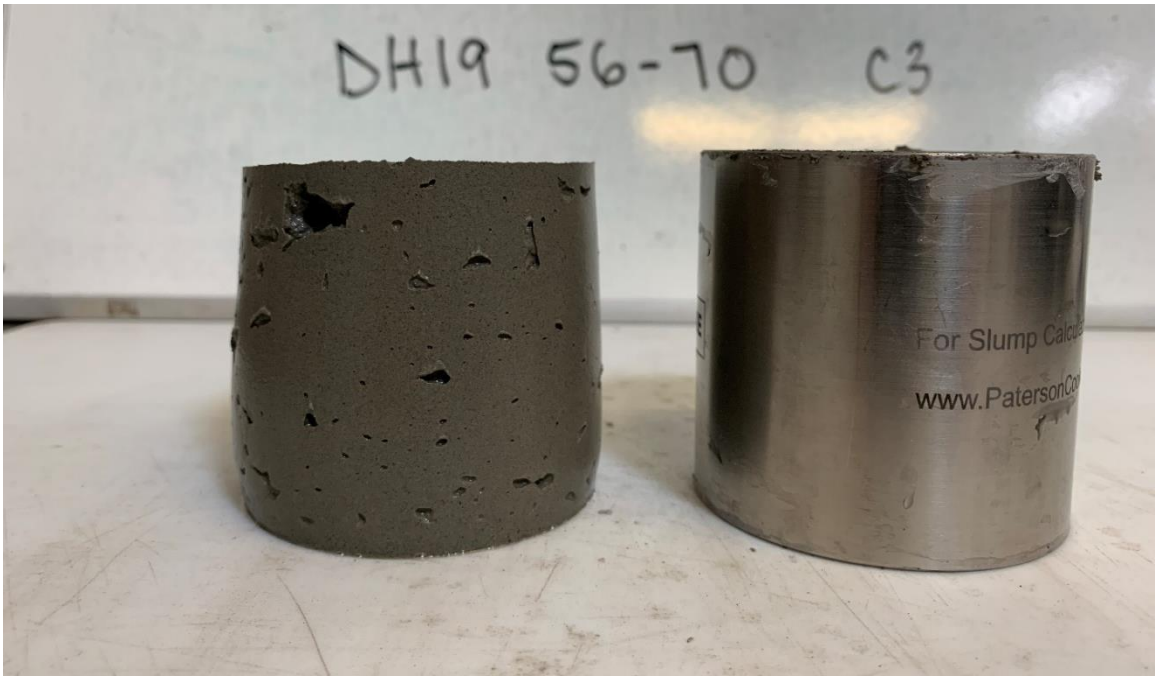

Figure 32: DH19 56-70 Boger Slump 72.9%m

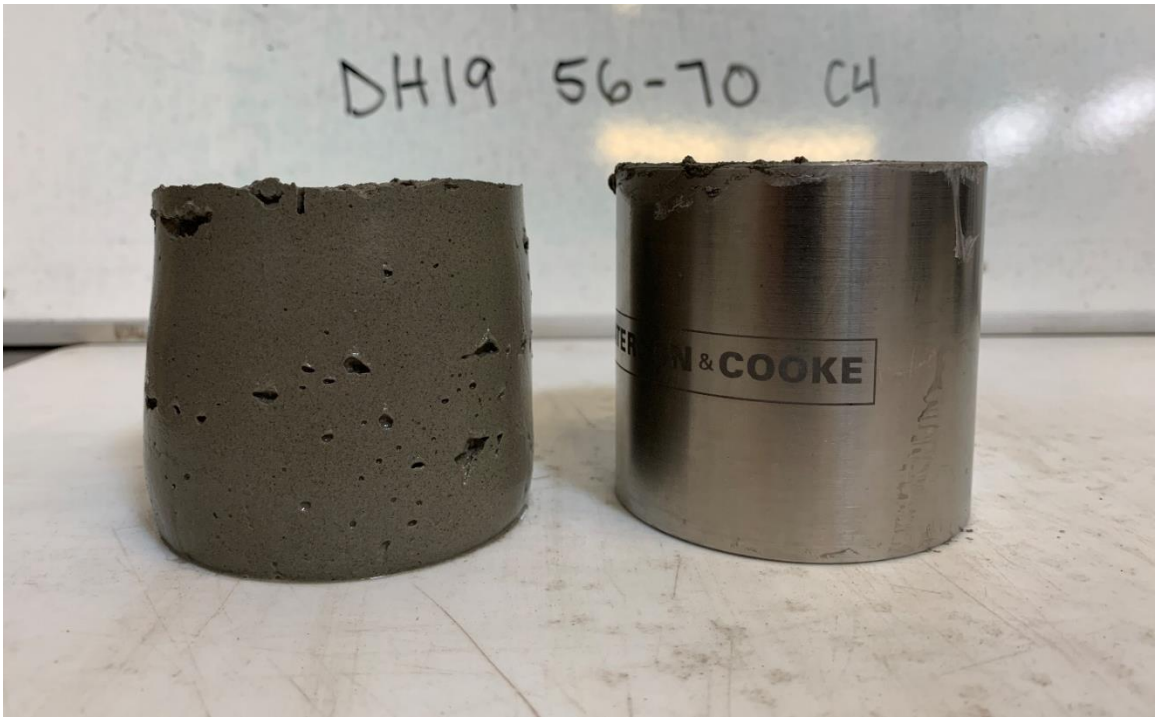

Figure 33: DH19 56-70 Boger Slump 71.7%m

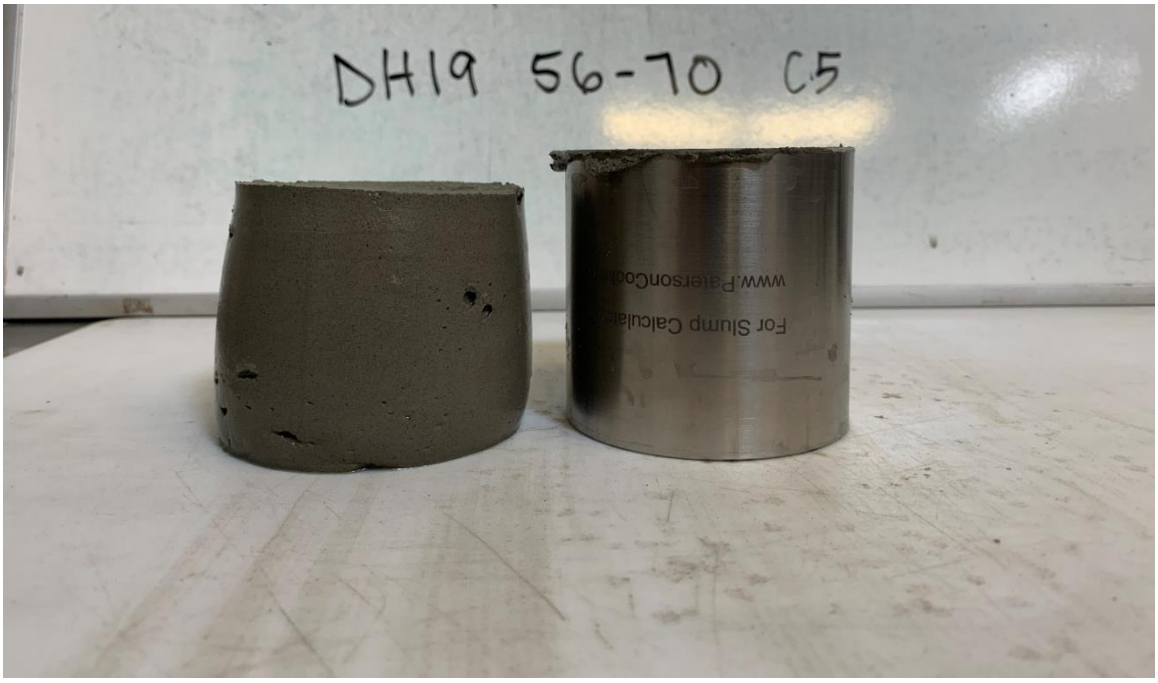

Figure 34: DH19 56-70 Boger Slump 70.0%m

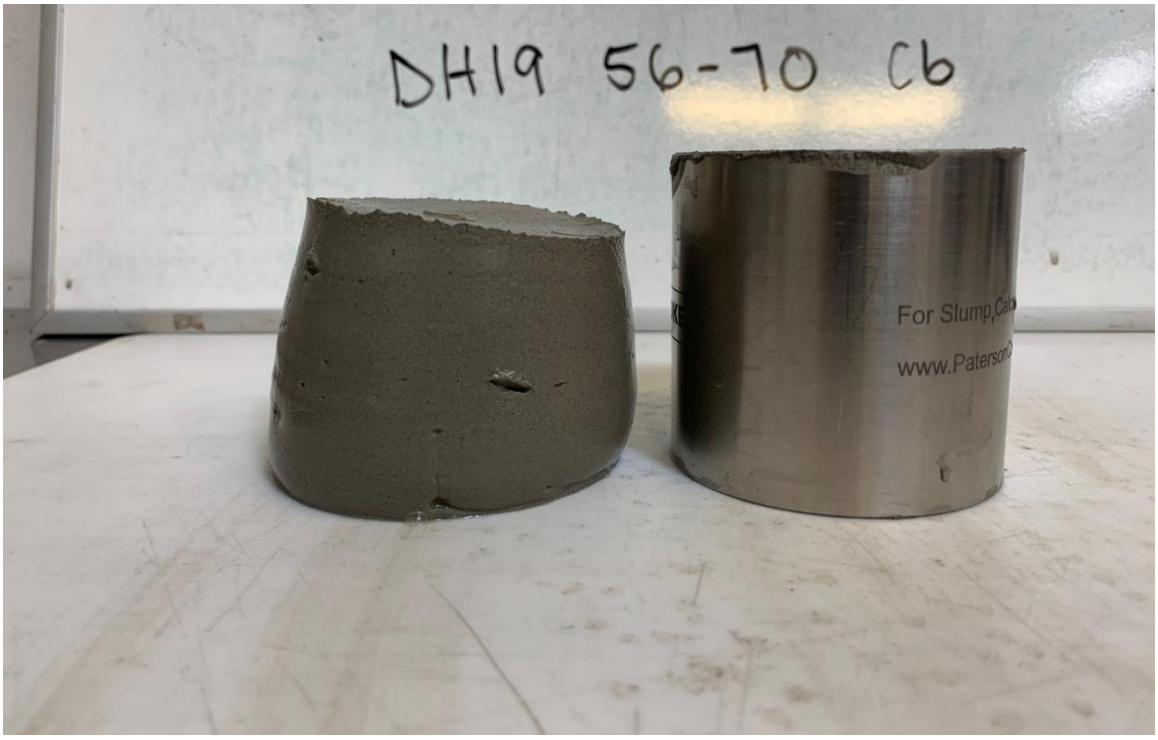

Figure 35: DH19 56-70 Boger Slump 67.6%m

Figure 36: DH19 56-70 Boger Slump 64.7%m

Figure 37: DH19 56-70 Boger Slump 61.2%m

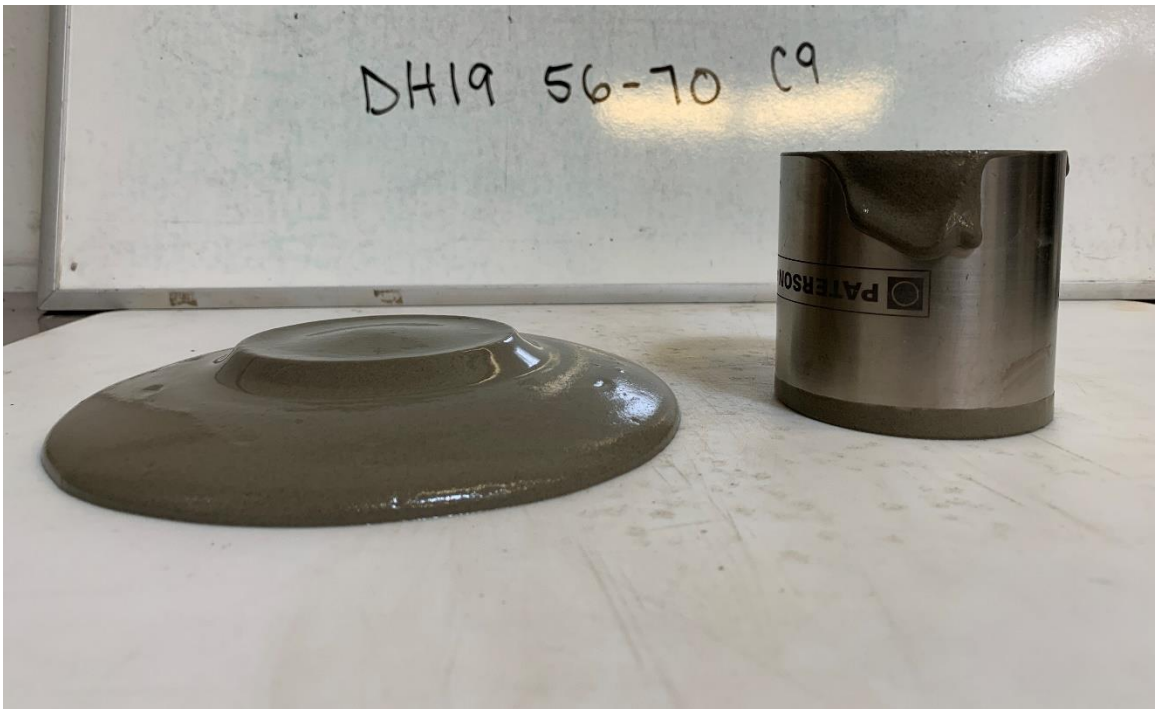

Figure 38: DH19 56-70 Boger Slump 56.8%m

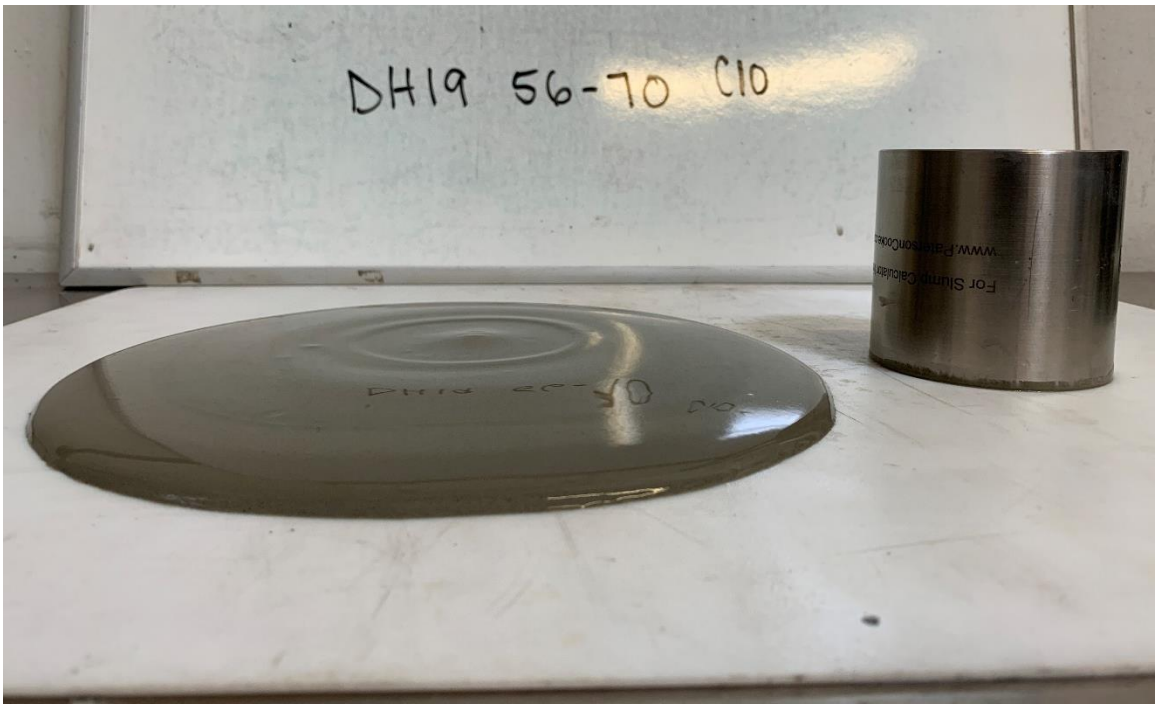

Figure 39: DH19 56-70 Boger Slump 51.6%m

B.2 DH20-S2 162-173 Vane Yield Stress and Boger Slump Test Results

CONCENTRATION DETERMINATION DATASHEET

Project Number:	**MRR-31-1295**	**Client:**	**Montana Resources**	**Test Date:**	**7/21/2021**
Project Description:	**Rheology Test Work**	**Sample ID:**	**DH20-S2 162-173**	**Operator:**	**AMR**

Solid Density (kg/m^3)	2688.00	Water Density (kg/m3)	1000.00	Dissolved Solids (%m)	

Trial No.	C1	C2	C3	C4	C5	C6	C7		
(a) Slurry + Tare, g.	58.387	69.195	69.897	76.726	47.442	36.594	62.87		
(b) Solids + Tare, g.	47.169	55.154	55.495	60.04	36.369	25.272	40.809		
(c) Tare, g.	1.224	1.213	1.208	1.23	1.214	1.224	1.213		
(d) Slurry, g.	57.163	67.982	68.689	75.496	46.228	35.37	61.657		
(e) Solids, g.	45.945	53.941	54.287	58.81	35.155	24.048	39.596		
(f) % Solids	80.38%	79.35%	79.03%	77.90%	76.05%	67.99%	64.22%		
(g) % Water	19.62%	20.65%	20.97%	22.10%	23.95%	32.01%	35.78%		
(h) Water, g.	11.22	14.04	14.40	16.69	11.07	11.32	22.06		
(i) Dissolved Solids Mass	0.00	0.00	0.00	0.00	0.00	0.00	0.00		
(j) Corrected % Solids	80.38%	79.35%	79.03%	77.90%	76.05%	67.99%	64.22%		
(h) Slurry Density, kg/m3	2019.14	1993.12	1985.34	1957.64	1914.08	1745.08	1675.84		
pH		7.23	7.28	7.3	7.34	7.22	7.21		
Temperature, C		23.2	23.4	23.44	23.3	25.1	24.9		
Vane Yield Stress Run 1 (Pa)	1057	598.4	349.4	201.9	90.24	21.43	14.1		
Vane Yield Stress Run 2 (Pa)	1125	547.1	346.9	213.8	88.55	23.69	9.024		
Average Vane Yield Stress (Pa)	1091	572.75	348.15	207.85	89.395	22.56	11.562		
% Solids:	0.00%	0.00%	0.00%	0.00%	0.00%	0.00%	0.00%		
Slump, mm	6	4	6	9	30	56	70		
Boger Yield Stress (Pa)	450.45	490.85	442.9	383.1	167.65	38.4	4.15		

Notes:

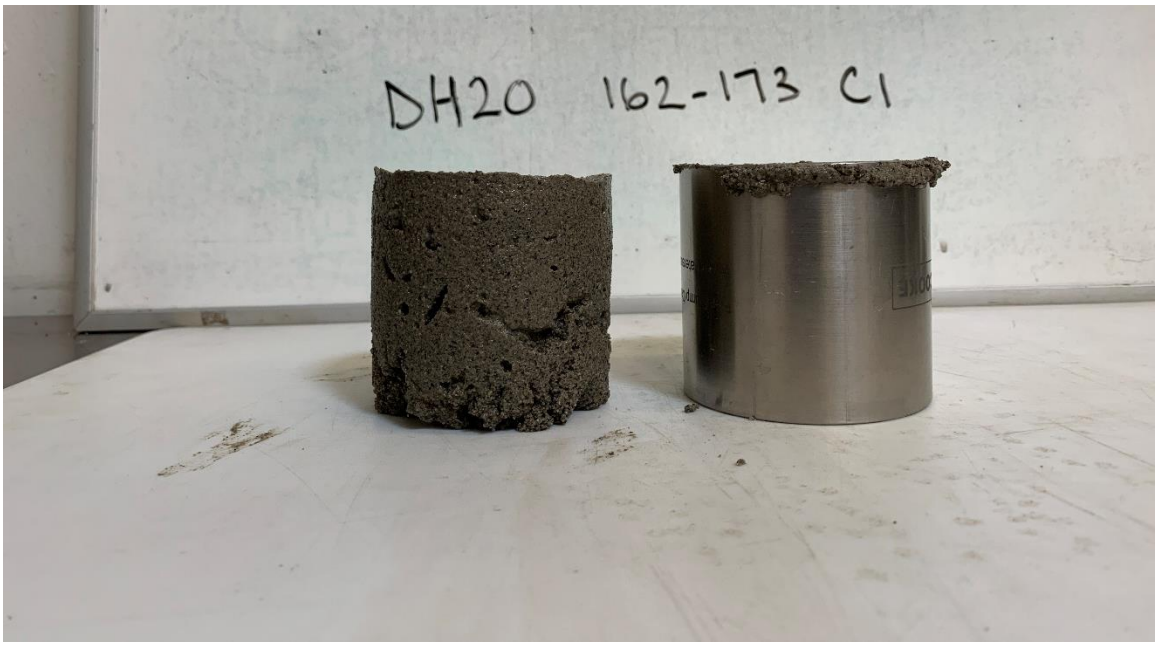

Figure 40: DH20-S2 162-173 Boger Slump 80.4%m

Figure 41: DH20-S2 162-173 Boger Slump 79.4%m

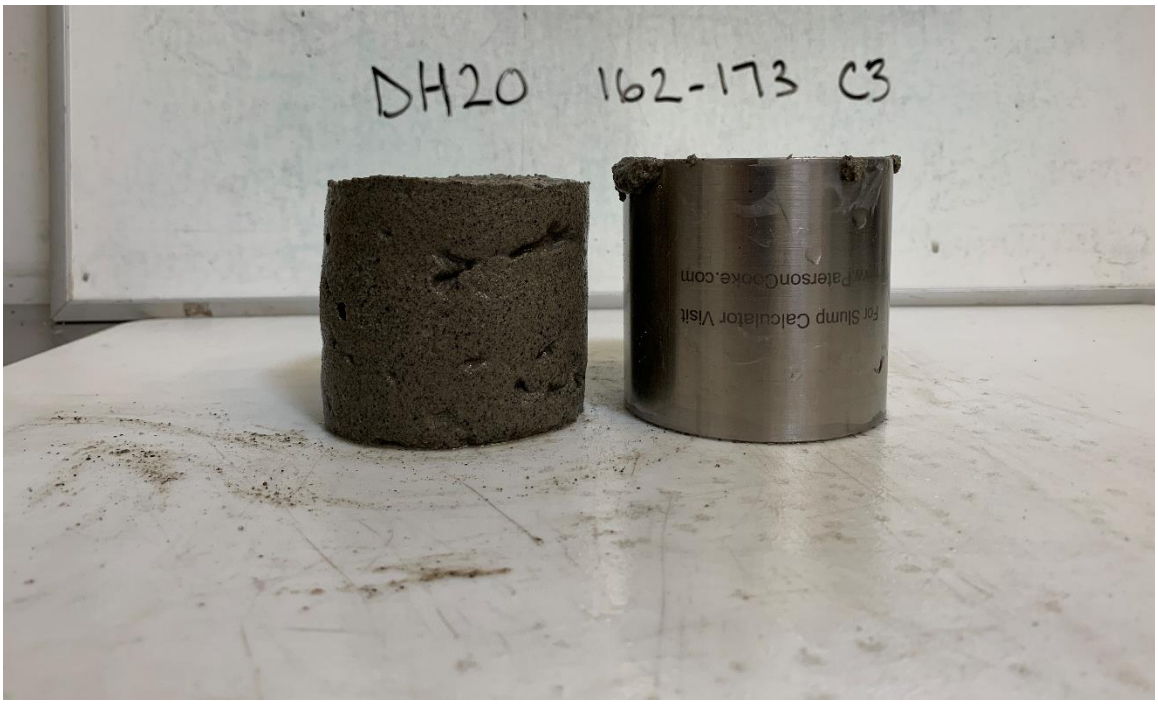

Figure 42: DH20-S2 162-173 Boger Slump 79.0%m

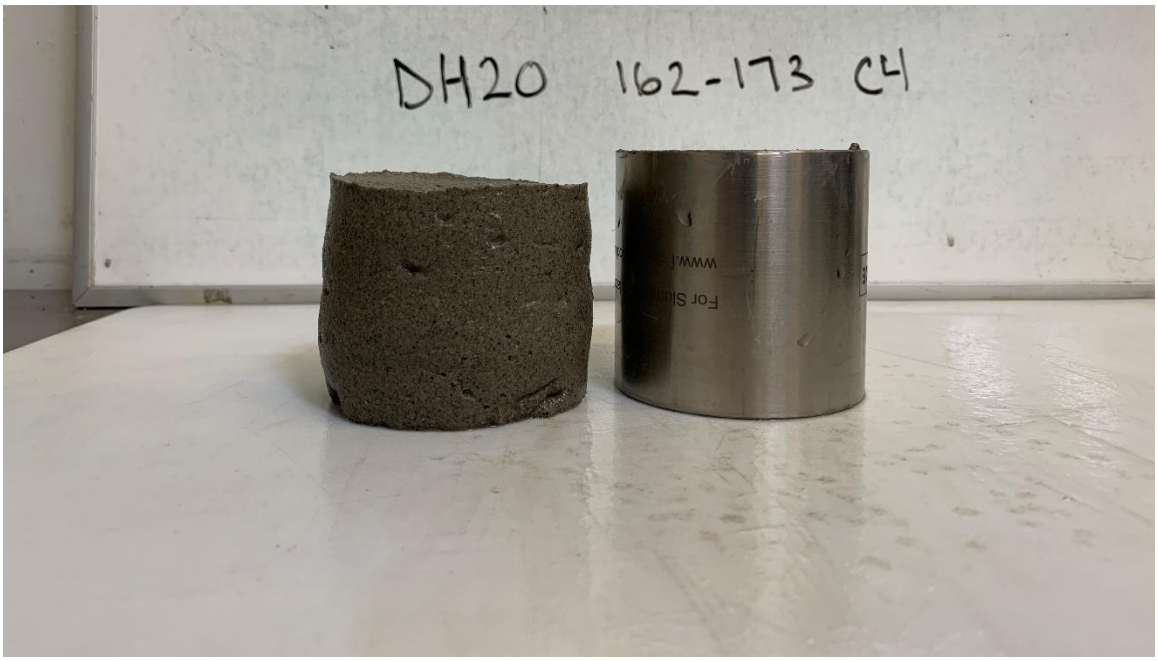

Figure 43: DH20-S2 162-173 Boger Slump 77.9%m

Figure 44: DH20-S2 162-173 Boger Slump 76.1%m

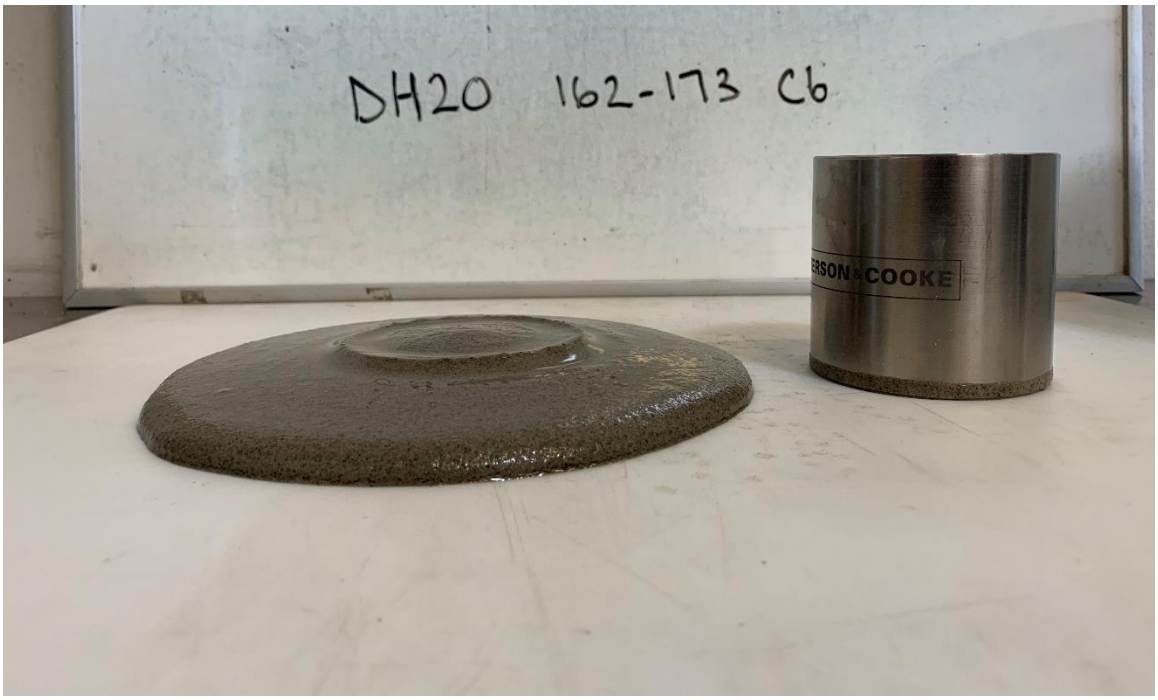

Figure 45: DH20-S2 162-173 Boger Slump 68.0%m

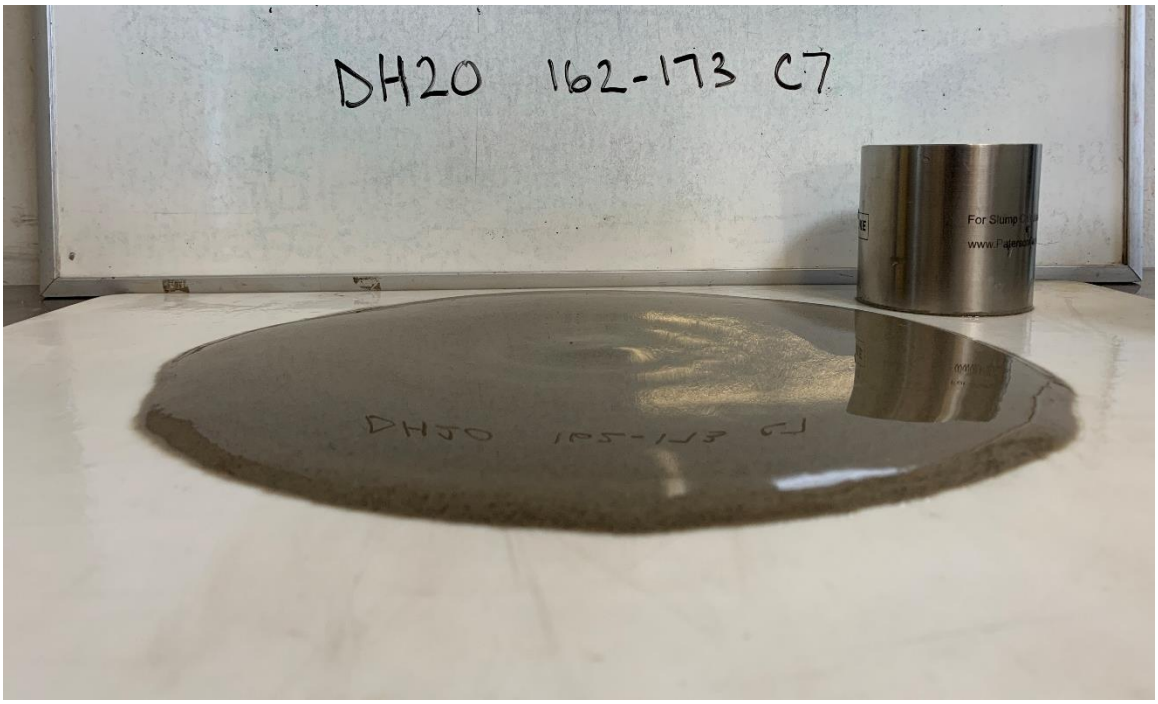

Figure 46: DH20-S2 162-173 Boger Slump 62.4%m

APPENDIX C : TUBE VISCOMETER TEST DATA

Data Sheets
DH19 56-70 TV Concentrations
DH19 56-70 TV C1
DH19 56-70 TV C2
DH19 56-70 TV C3
DH19 56-70 TV C4
DH19 56-70 TV C5
DH19 56-70 TV C6
DH19 56-70 TV C7
DH19 56-70 TV C8
DH20-S2 162-173 TV Concentrations
DH20-S2 162-173 TV C1
DH20-S2 162-173 TV C2
DH20-S2 162-173 TV C3
DH20-S2 162-173 TV C4
DH20-S2 162-173 TV C5
DH20-S2 162-173 TV C6
DH20-S2 162-173 TV C7

1. DH19 56-70 Tube Viscometer Data

CONCENTRATION DETERMINATION DATASHEET

Project Number:	**MRR-31-1295**	**Client:**	**Montana Resources**	**Test Date:**	**10/7/2021**
Project Description:	**Montana Resources Rheology**	**Sample ID:**	**DH19 56-70**	**Operator:**	**AMR**

Solid Density (kg/m^3)	2699.42	Water Density (kg/m3)	1000.00	Dissolved Solids (%m)	

Trial No.	1	2	3	4	5	6	7	8	
(a) Slurry + Tare, g.	42.59	39.261	54.673	34.581	40.75	38.873	29.266	30.361	
(b) Solids + Tare, g.	26.4	24.295	32.682	20.481	23.73	22.152	16.049	15.373	
(c) Tare, g.	1.271	1.282	1.289	1.281	1.281	1.283	1.279	1.308	
(d) Slurry, g.	41.319	37.979	53.384	33.3	39.469	37.59	27.987	29.053	
(e) Solids, g.	25.129	23.013	31.393	19.2	22.449	20.869	14.77	14.065	
(f) % Solids	60.82%	60.59%	58.81%	57.66%	56.88%	55.52%	52.77%	48.41%	
(g) % Water	39.18%	39.41%	41.19%	42.34%	43.12%	44.48%	47.23%	51.59%	
(h) Water, g.	16.19	14.97	21.99	14.10	17.02	16.72	13.22	14.99	
(i) Dissolved Solids Mass	0.00	0.00	0.00	0.00	0.00	0.00	0.00	0.00	
(j) Corrected % Solids	60.82%	60.59%	58.81%	57.66%	56.88%	55.52%	52.77%	48.41%	
(h) Slurry Density, kg/m3	1620.41	1616.73	1587.84	1569.82	1557.81	1537.30	1497.55	1438.38	

pH	7.76	7.83	7.86	7.84	7.92	7.72	7.89	7.94	
Conductivity (mS/cm)	1.4	1.46	1.55	1.8	1.65	1.72	1.66	1.81	
Temperature, C	19.5	19.5	19.5	19.5	19.5	19.5	19.5	19.5	

(h) Flask Cal wt. g									
(i) Flask + Slurry wt. g:									
(j) Sl.+Fl.+H2Og									
(k) Volume with Water									
(L) Weight of water									
(m) Slurry Vol ml.									
(n) Slurry wt. g									
(o) Slurry Density, kg/m3									

% Solids:									

Notes:

Montana Resources Rheology Sample DH 56-70 Tube Viscometer Data	**Project Manager:**	**Josh Stowe**	**Project No:**	**MRR-31-1295**
	Sample ID:	**DH 56-70**		

Date/Time	Nov-2-21 / 11:21 AM			
Sample	C1			
Operator	Zane Travis			
		D	0.015748	m
		Plastic Viscosity	0.044	Pa-s
		Bingham Yield Stress	60.0	Pa
% mass	60.9%	Slurry Density	1,620	kg/m^3
pH	7.8			
Temperature	20.2 °C			

Pseudo Shear Rate (1/s)	Wall Shear Stress (Pa)
245.7	81.6
411.4	91.4
619.6	102.9
830.0	114.0
1035.4	122.8
1240.2	130.8

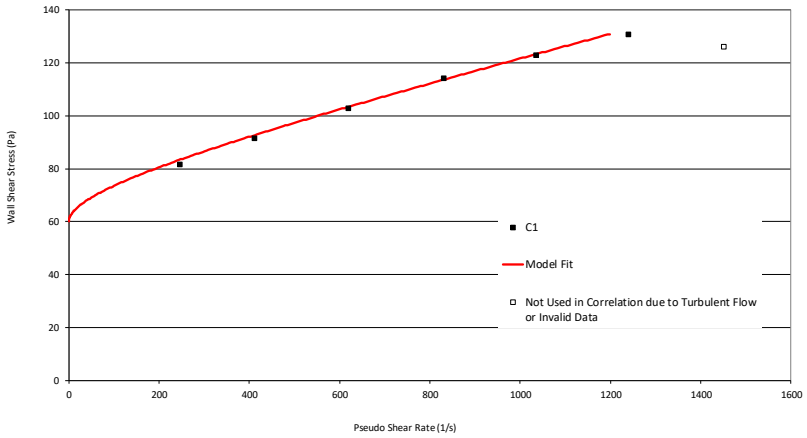

Montana Resources Rheology Sample DH 56-70 Tube Viscometer Data	**Project Manager:**	**Josh Stowe**	**Project No:**	**MRR-31-1295**
	Sample ID:	**DH 56-70**		

Date/Time	Nov-2-21 / 11:47 AM	D	0.015748	m
Sample	C2	Plastic Viscosity	0.037	Pa-s
Operator	Zane Travis	Bingham Yield Stress	55.0	Pa
% mass	60.7%	pm Slurry	1,617	kg/m^3
pH	7.8			
Temperature	20.2 °C			

Pseudo Shear Rate (1/s)	Wall Shear Stress (Pa)
1425.6	125.6
1228.4	119.4
1033.2	110.8
819.5	102.7
613.3	92.6
407.7	82.3
246.8	72.7

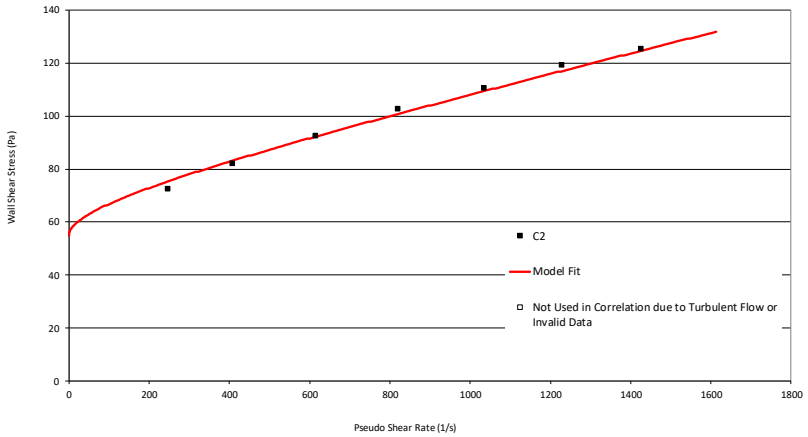

Montana Resources Rheology Sample DH 56-70 Tube Viscometer Data	**Project Manager:**	**Josh Stowe**	**Project No:**	**MRR-31-1295**
	Sample ID:	**DH 56-70**		

Date/Time	Nov-2-21 / 12:03 PM	D	0.015748	m
Sample	C3	Plastic Viscosity	0.033	Pa-s
Operator	Zane Travis	Bingham Yield Stress	40.0	Pa
% mass	58.9%	pm Slurry	1,588	kg/m^3
pH	7.9			
Temperature	20.2 °C			

Pseudo Shear Rate (1/s)	Wall Shear Stress (Pa)
1411.5	100.6
1244.1	95.1
1025.6	88.2
825.1	80.9
618.8	73.4
410.3	64.1
246.7	56.5

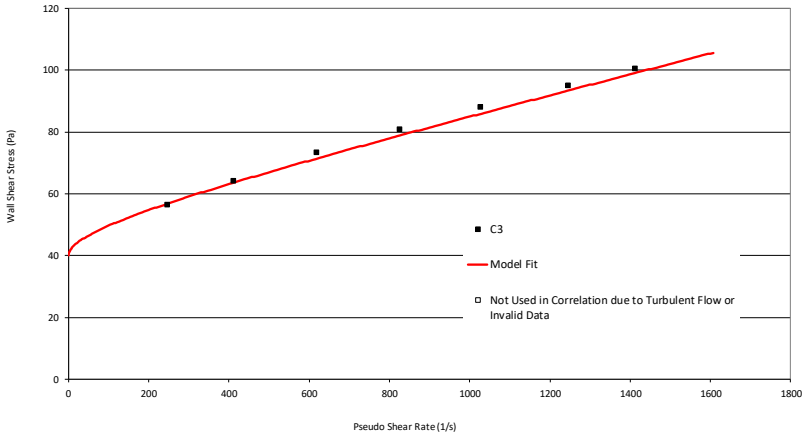

Montana Resources Rheology Sample DH 56-70 Tube Viscometer Data

Project Manager:	**Josh Stowe**	**Project No:**	**MRR-31-1295**
Sample ID:	**DH 56-70**		

Date/Time	Nov-2-21 / 1:09 PM	D	0.015748	m
Sample	C4	Plastic Viscosity	0.024	Pa-s
Operator	Zane Travis	Bingham Yield Stress	35.0	Pa
% mass	57.8%	pm Slurry	1,570	kg/m^3
pH	7.8			
Temperature	22.8 °C			

Pseudo Shear Rate (1/s)	Wall Shear Stress (Pa)
1432.2	80.7
1246.7	75.6
1034.6	70.5
831.6	64.7
626.0	58.4
410.8	50.8
148.6	45.8

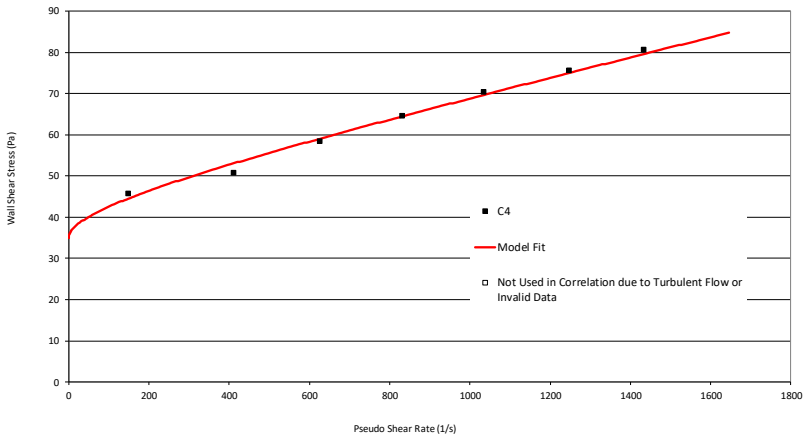

Montana Resources Rheology Sample DH 56-70 Tube Viscometer Data	**Project Manager:**	**Josh Stowe**	**Project No:**	**MRR-31-1295**
	Sample ID:	**DH 56-70**		

Date/Time	Nov-2-21 / 1:24 PM			
Sample	C5			
Operator	Zane Travis			
		D	0.015748	m
% mass	57.0%	Plastic Viscosity	0.021	Pa-s
		Bingham Yield Stress	27.5	Pa
pH	7.9	pm Slurry	1,558	kg/m^3
Temperature	25.3 °C			

Pseudo Shear Rate (1/s)	Wall Shear Stress (Pa)
1428.2	65.7
1238.5	61.3
1018.7	57.4
817.5	53.0
614.2	47.5
407.4	42.0
235.9	37.5

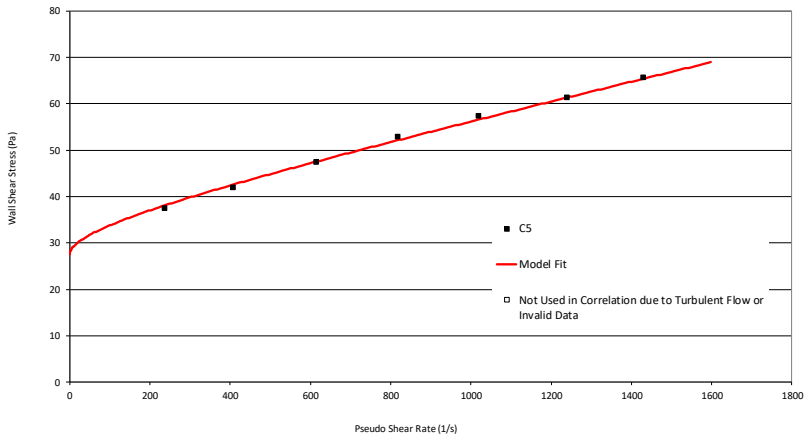

Montana Resources Rheology Sample DH 56-70 Tube Viscometer Data

Project Manager:	**Josh Stowe**	**Project No:**	**MRR-31-1295**
Sample ID:	**DH 56-70**		

Date/Time	Nov-2-21 / 1:40 PM			
Sample	C6			
Operator	Zane Travis			
		D	0.015748	m
		Plastic Viscosity	0.016	Pa-s
		Bingham Yield Stress	22.5	Pa
% mass	55.7%	pm Slurry	1,537	kg/m^3
pH	7.7			
Temperature	26.8 °C			

Pseudo Shear Rate (1/s)	Wall Shear Stress (Pa)
1444.6	53.5
1237.3	50.2
1017.7	46.8
812.2	43.0
625.3	38.5
407.5	34.0
245.3	30.0

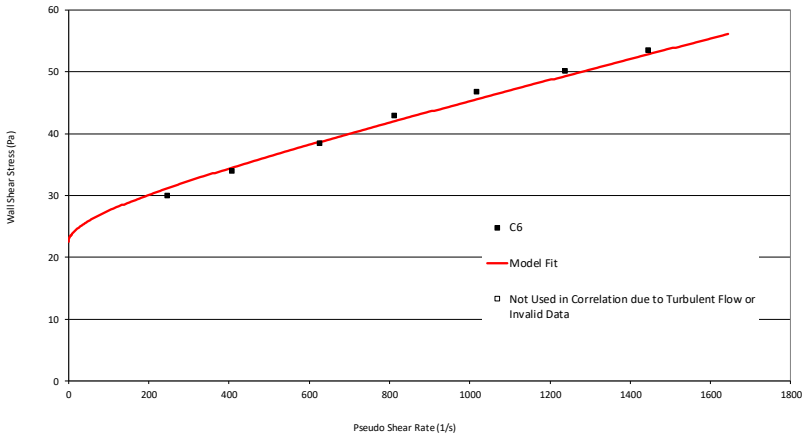

Montana Resources Rheology Sample DH 56-70 Tube Viscometer Data	**Project Manager:**	**Josh Stowe**	**Project No:**	**MRR-31-1295**
	Sample ID:	**DH 56-70**		

Date/Time	Nov-2-21 / 2:01 PM	D	0.015748	m
Sample	C7	Plastic Viscosity	0.016	Pa-s
Operator	Zane Travis	Bingham Yield Stress	16.0	Pa
% mass	52.9%	pm Slurry	1,497	kg/m^3
pH	7.9			
Temperature	20.2 °C			

Pseudo Shear Rate (1/s)	Wall Shear Stress (Pa)
1463.3	44.1
1244.9	40.9
1034.4	37.8
829.7	34.5
629.0	31.0
415.5	26.8
248.3	22.9

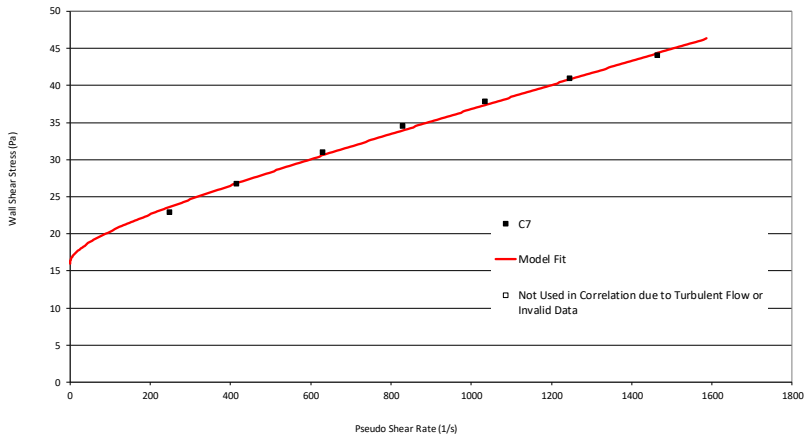

Montana Resources Rheology Sample DH 56-70 Tube Viscometer Data	**Project Manager:**	**Josh Stowe**	**Project No:**	**MRR-31-1295**
	Sample ID:	**DH 56-70**		

Date/Time	Nov-2-21 / 2:18 PM	D	0.015748	m
Sample	C8	Plastic Viscosity	0.012	Pa-s
Operator	Zane Travis	Bingham Yield Stress	9.0	Pa
% mass	48.6%	pm Slurry	1,438	kg/m^3
pH	7.9			
Temperature	20.1 °C			

Pseudo Shear Rate (1/s)	Wall Shear Stress (Pa)
247.2	13.5
371.5	15.2
497.1	16.9
666.8	19.0
835.3	20.7
964.0	22.1
1078.6	23.2

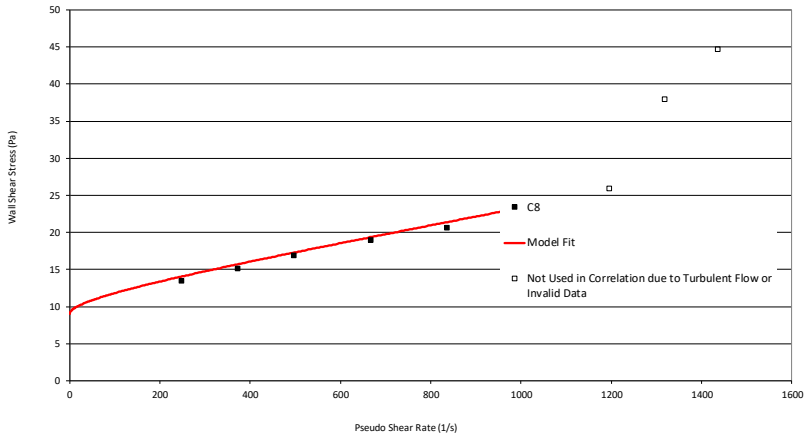

2. DH20-S2 162-173 Tube Viscometer Data

CONCENTRATION DETERMINATION DATASHEET

Project Number:	**MRR-31-1295**	**Client:**	**Montana Resources**	**Test Date:**	**11/8/2021**
Project Description:	**Montana Resources Rheology**	**Sample ID:**	**DH 162-173**	**Operator:**	**BON**

Solid Density (kg/m^3)	2688.00	Water Density (kg/m3)	1000.00	Dissolved Solids (%m)	0.10%

Trial No.	1	2	3	4	5	6	7		
(a) Slurry + Tare, g.	21.232	34.31	28.382	52.675	37.945	55.526	38.018		
(b) Solids + Tare, g.	13.368	22.088	18.657	35.939	26.281	38.699	26.906		
(c) Tare, g.	1.31	1.305	1.314	1.303	1.292	1.306	1.295		
(d) Slurry, g.	19.922	33.005	27.068	51.372	36.653	54.22	36.723		
(e) Solids, g.	12.058	20.783	17.343	34.636	24.989	37.393	25.611		
(f) % Solids	60.53%	62.97%	64.07%	67.42%	68.18%	68.97%	69.74%		
(g) % Water	39.47%	37.03%	35.93%	32.58%	31.82%	31.03%	30.26%		
(h) Water, g.	7.86	12.22	9.73	16.74	11.66	16.83	11.11		
(i) Dissolved Solids Mass	0.01	0.01	0.01	0.02	0.01	0.02	0.01		
(j) Corrected % Solids	60.49%	62.93%	64.04%	67.39%	68.15%	68.93%	69.71%		
(h) Slurry Density, kg/m3	1613.14	1654.07	1673.24	1734.29	1748.67	1763.94	1779.22		
pH	8.41	8.44	8.45	8.45	8.49	8.51	8.52		
Conductivity (mS/cm)	0.68	0.78	0.72	0.76	0.76	0.7	0.68		
Temperature, C	19.7	19.9	19.8	20.1	20.1	20.1	19.8		
(h) Flask Cal wt. g									
(i) Flask + Slurry wt. g:									
(j) Sl.+Fl.+H2Og									
(k) Volume with Water									
(L) Weight of water									
(m) Slurry Vol ml.									
(n) Slurry wt. g									
(o) Slurry Density, kg/m3									
% Solids:									

Notes:

Montana Resources Rheology Sample DH20-S2 162-173 Tube Viscometer Data	**Project Manager:**	**AR**	**Project No:**	**MRR-31-1295**
	Sample ID:	**DH20-S2 162-173**		

Date/Time	11/8/21 10:50 AM		D	0.015748	m
Sample	C1		Plastic Viscosity	0.017	Pa-s
Operator	BON/AMR		Bingham Yield Stress	4.0	Pa
% mass	60.5%		Slurry Density	1,607	kg/m^3
pH	8.4				
Temperature	20.2 °C				

Pseudo Shear Rate (1/s)	Wall Shear Stress (Pa)
642.9	16.3
734.5	18.6
860.8	19.7
1063.4	23.7

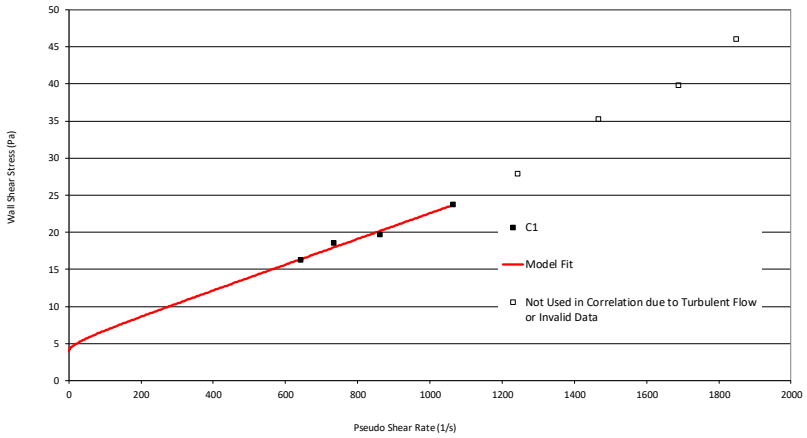

Montana Resources Rheology Sample DH20-S2 162-173 Tube Viscometer Data	**Project Manager:**	**AR**	**Project No:**	**MRR-31-1295**
	Sample ID:	**DH20-S2 162-173**		

Date/Time	11/8/21 11:10 AM		D	0.015748	m
Sample	#N/A		Plastic Viscosity	0.022	Pa-s
Operator	BON/AMR		Bingham Yield Stress	8.3	Pa
% mass	62.9%		pm Slurry	1,647	kg/m^3
pH	8.4				
Temperature	20.2 °C				

Pseudo Shear Rate (1/s)	Wall Shear Stress (Pa)
817.9	28.8
540.4	22.8
686.3	27.0
1057.8	35.5
943.1	29.6
1291.7	38.6

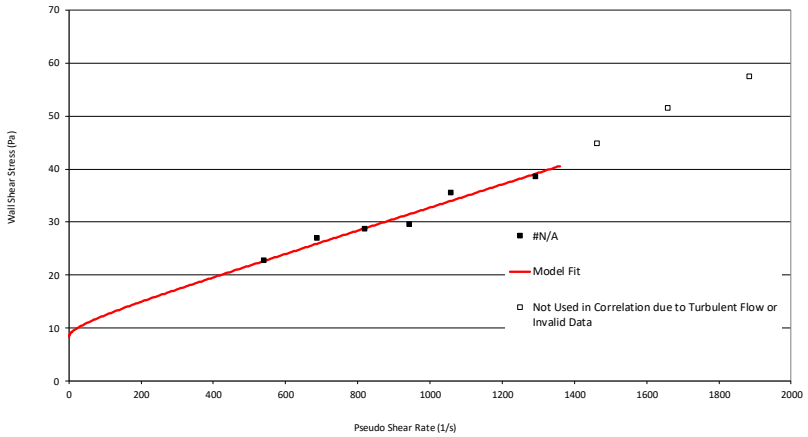

Montana Resources Rheology Sample DH20-S2 162-173 Tube Viscometer Data	**Project Manager:**	**AR**	**Project No:**	**MRR-31-1295**
	Sample ID:	**DH20-S2 162-173**		

Date/Time	11/8/21 11:30 AM		D	0.015748	m
Sample	#N/A		Plastic Viscosity	0.031	Pa-s
Operator	BON/AMR		Bingham Yield Stress	14.0	Pa
% mass	64.0%		pm Slurry	1,666	kg/m^3
pH	8.5				
Temperature	20.2 °C				

Pseudo Shear Rate (1/s)	Wall Shear Stress (Pa)
1460.1	65.1
1225.3	54.5
1133.8	54.2
1001.9	49.3
865.7	44.7
710.2	40.7
589.9	35.8

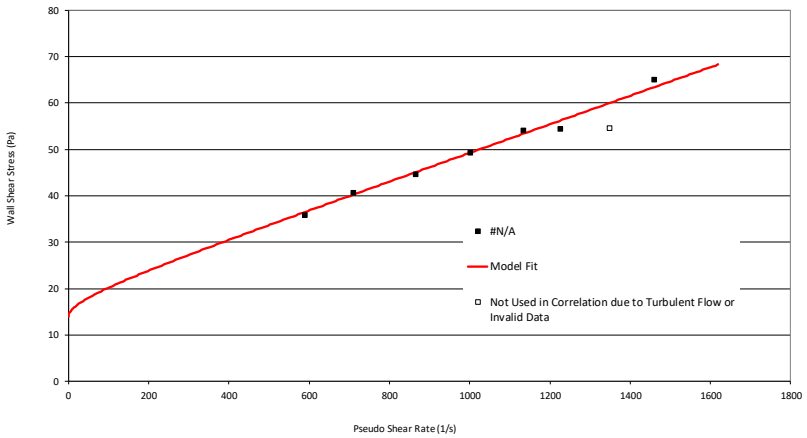

Montana Resources Rheology Sample DH20-S2 162-173 Tube Viscometer Data	**Project Manager:**	**AR**	**Project No:**	**MRR-31-1295**
	Sample ID:	**DH20-S2 162-173**		

Date/Time	11/8/21 11:54 AM		D	0.015748	m
Sample	#N/A		Plastic Viscosity	0.042	Pa-s
Operator	BON/AMR		Bingham Yield Stress	25.0	Pa
% mass	67.4%		pm Slurry	1,726	kg/m^3
pH	8.5				
Temperature	20.3	°C			

Pseudo Shear Rate (1/s)	Wall Shear Stress (Pa)
1459.6	94.5
1311.6	90.3
1224.0	83.3
1084.4	78.2
944.4	72.7
820.3	69.1
703.7	61.0
578.1	56.0

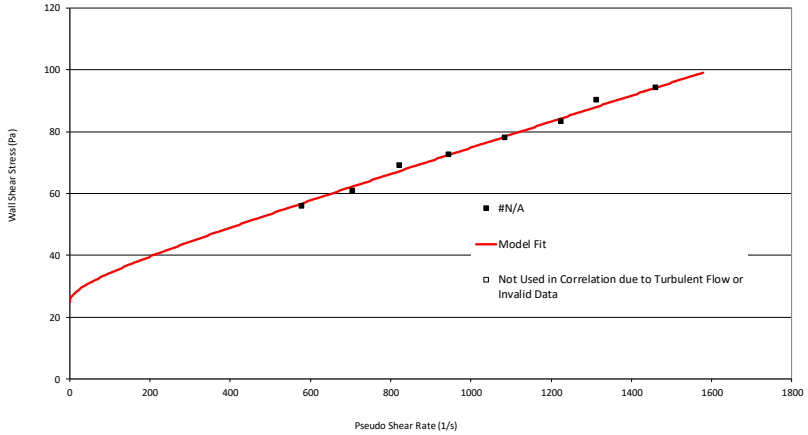

Montana Resources Rheology Sample DH20-S2 162-173 Tube Viscometer Data	**Project Manager:**	**AR**	**Project No:**	**MRR-31-1295**
	Sample ID:	**DH20-S2 162-173**		

Date/Time	11/8/21 12:33 PM		D	0.015748	m
Sample	#N/A		Plastic Viscosity	0.050	Pa-s
Operator	BON/AMR		Bingham Yield Stress	44.5	Pa
% mass	68.2%		pm Slurry	1,740	kg/m^3
pH	8.5				
Temperature	20.3	°C			

Pseudo Shear Rate (1/s)	Wall Shear Stress (Pa)
1411.8	128.8
1297.7	127.7
1194.3	117.1
1048.4	110.9
933.1	101.9
817.0	95.9
693.7	96.4
569.7	87.6

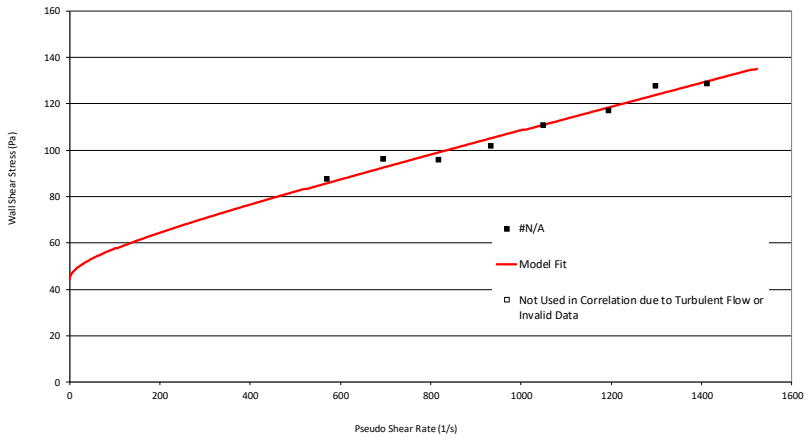

Montana Resources Rheology Sample DH20-S2 162-173 Tube Viscometer Data	**Project Manager:**	**AR**	**Project No:**	**MRR-31-1295**
	Sample ID:	**DH20-S2 162-173**		

Date/Time	11/8/21 12:55 PM		D	0.015748	m
Sample	#N/A		Plastic Viscosity	0.055	Pa-s
Operator	BON/AMR		Bingham Yield Stress	63.2	Pa
% mass	68.9%		pm Slurry	1,755	kg/m^3
pH	8.5				
Temperature	20.4 °C				

Pseudo Shear Rate (1/s)	Wall Shear Stress (Pa)
1377.7	161.4
1301.9	151.7
1176.1	149.6
1061.9	143.7
922.1	130.5
810.7	123.9
686.6	121.1
562.6	113.1

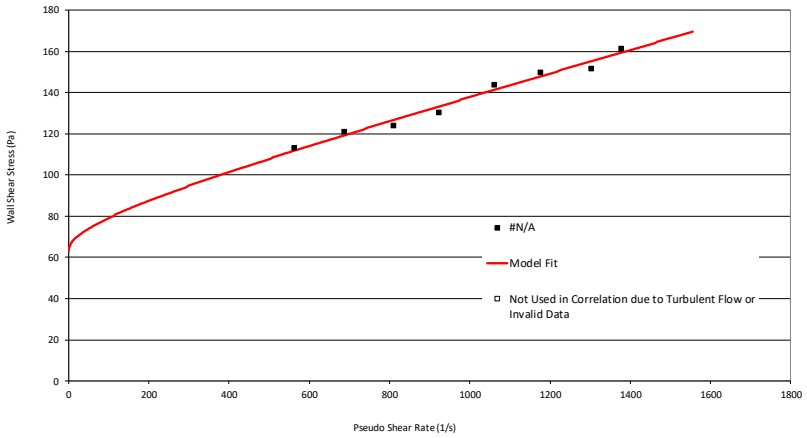

Montana Resources Rheology Sample DH20-S2 162-173 Tube Viscometer Data	**Project Manager:**	**AR**	**Project No:**	**MRR-31-1295**
	Sample ID:	**DH20-S2 162-173**		

Date/Time	11/8/21 1:17 PM		D	0.015748	m
Sample	#N/A		Plastic Viscosity	0.062	Pa-s
Operator	BON/AMR		Bingham Yield Stress	87.0	Pa
% mass	69.7%		pm Slurry	1,770	kg/m^3
pH	8.5				
Temperature	20.3 °C				

Pseudo Shear Rate (1/s)	Wall Shear Stress (Pa)
987.1	169.4
850.2	161.6
726.4	158.8
602.4	152.4
514.0	141.6

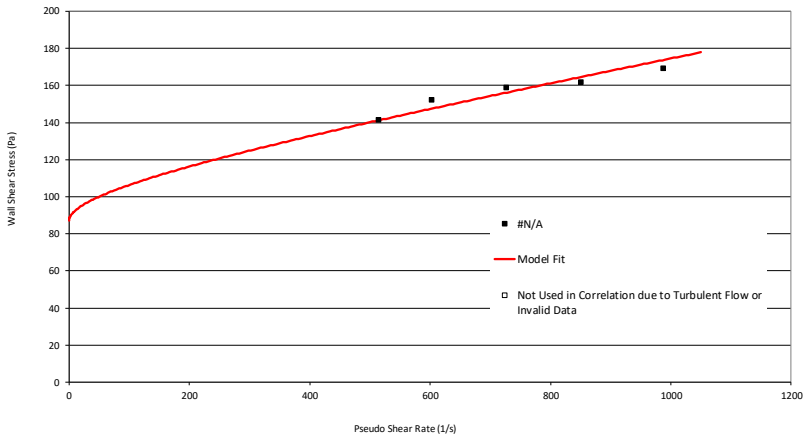

APPENDIX B

Inundation Maps for Flood Induced Dam Breach

(Figures B1 to B3)

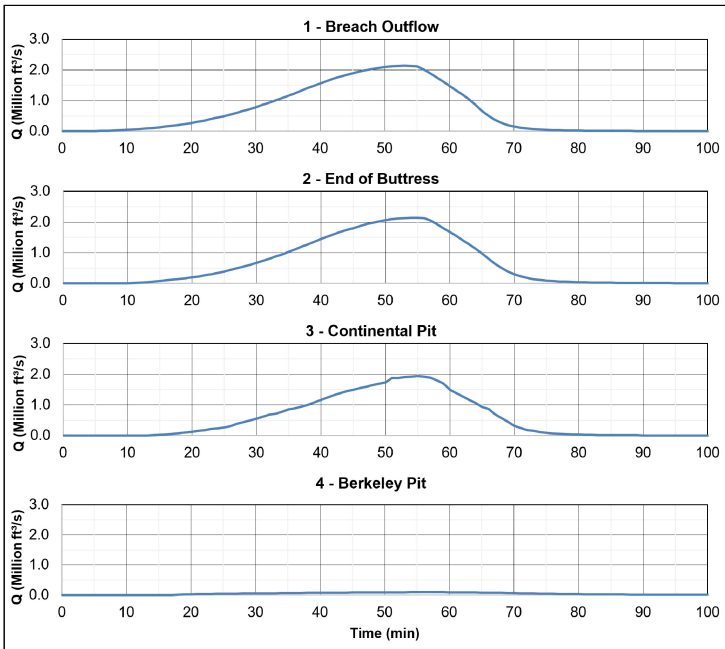

No.	Cross Section Name	Peak Discharge, ft³/s	Flood Wave Arrival Time, h:mm	Peak Discharge Arrival Time, h:mm	Maximum Depth, ft
1	Breach Outflow	2,136,000	0:00	0:53	127
2	End of Buttress	2,136,000	0:10	0:55	69
3	Continental Pit	1,940,000	0:14	0:55	43
4	Berkeley Pit	96,600	0:17	0:57	22

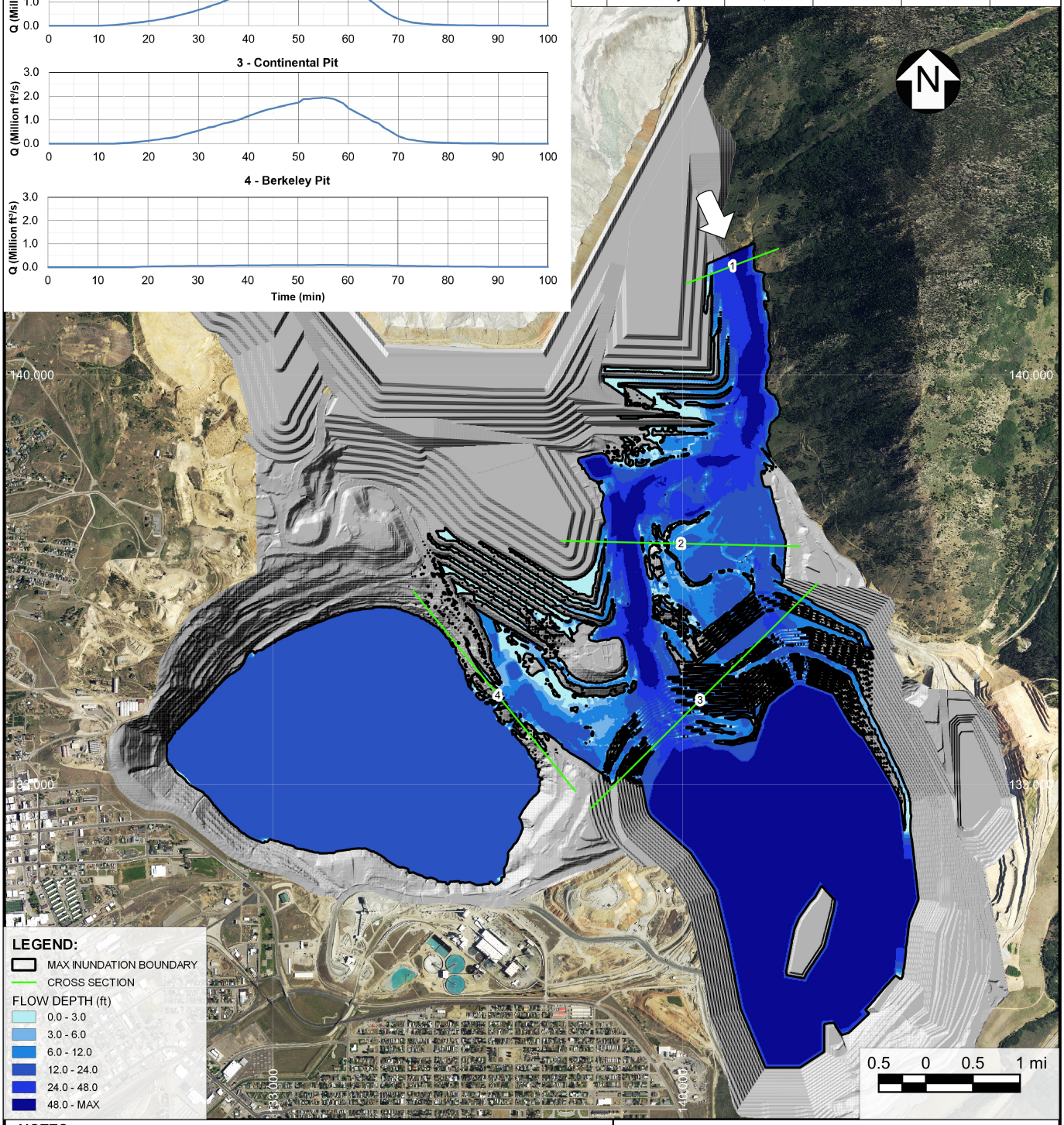

NOTES:

1. BASE MAP PROVIDED BY MONTANA RESOURCES, LLC ON AUGUST 7, 2024.
2. DAM AND ROCK DISPOSAL SITES ARE PROJECTED SURFACES AT THE TIME OF THE BREACH.
3. COORDINATE GRID IS IN FEET. COORDINATE SYSTEM: ANACONDA MINE GRID.
4. THIS FIGURE IS PRODUCED AT A NOMINAL SCALE OF 1:100,000 FOR 8.5x11 (LETTER) PAPER. ACTUAL SCALE MAY DIFFER ACCORDING TO CHANGES IN PRINTER SETTINGS OR PRINTED PAPER SIZE.
5. THIS FIGURE MUST BE READ IN CONJUNCTION WITH KP REPORT VA101-00126/24-7, DATED DECEMBER 2024.

REV	DATE	DESCRIPTION	DESIGNED	DRAWN	REVIEWED
0	19DEC'24	ISSUED WITH REPORT	DBM	DBM	VM

MONTANA RESOURCES, LLC

MONTANA RESOURCES

FLOOD INDUCED DAM BREACH INUNDATION MAP - MAXIMUM DEPTH

Knight Piésold CONSULTING

P/A NO. VA101-00126/24

REF NO. 7

FIGURE B1

REV 0

M:\101\00126\24\A\GIS\Figs\Report 7

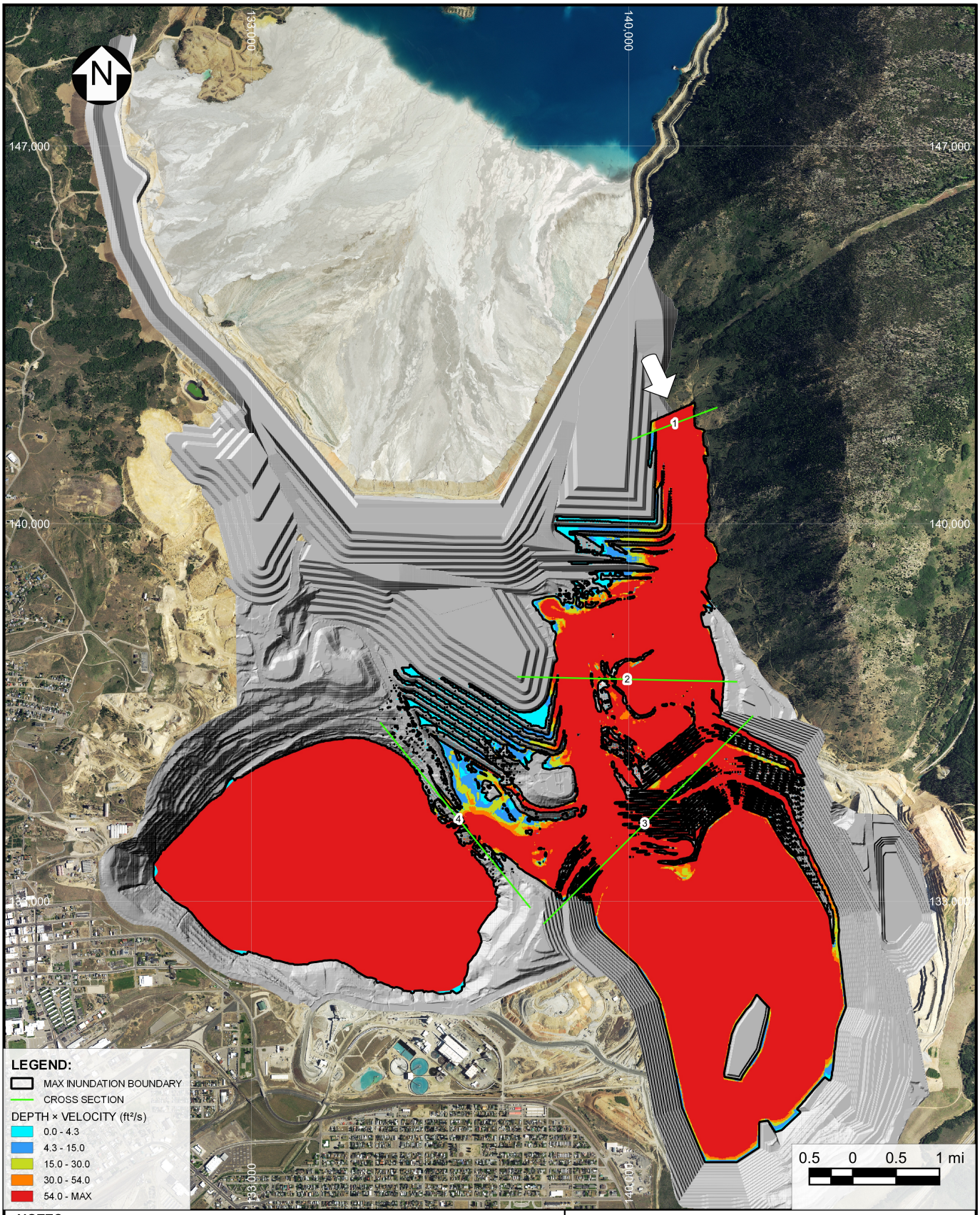

NOTES:

1. BASE MAP PROVIDED BY MONTANA RESOURCES, LLC ON AUGUST 7, 2024.
2. DAM AND ROCK DISPOSAL SITES ARE PROJECTED SURFACES AT THE TIME OF THE BREACH.
3. COORDINATE GRID IS IN FEET. COORDINATE SYSTEM: ANACONDA MINE GRID.
4. THIS FIGURE IS PRODUCED AT A NOMINAL SCALE OF 1:100,000 FOR 8.5x11 (LETTER) PAPER. ACTUAL SCALE MAY DIFFER ACCORDING TO CHANGES IN PRINTER SETTINGS OR PRINTED PAPER SIZE.
5. THIS FIGURE MUST BE READ IN CONJUNCTION WITH KP REPORT VA101-00126/24-7, DATED DECEMBER 2024.

REV	DATE	DESCRIPTION	DESIGNED	DRAWN	REVIEWED
0	19DEC'24	ISSUED WITH REPORT	DBM	DBM	VM

MONTANA RESOURCES, LLC

MONTANA RESOURCES

FLOOD INDUCED DAM BREACH MAXIMUM DEPTH × VELOCITY

Knight Piésold CONSULTING

P/A NO. VA101-00126/24

REF NO. 7

FIGURE B2

REV 0

M:\101\00126\24\A\GIS\Figs\Report 7

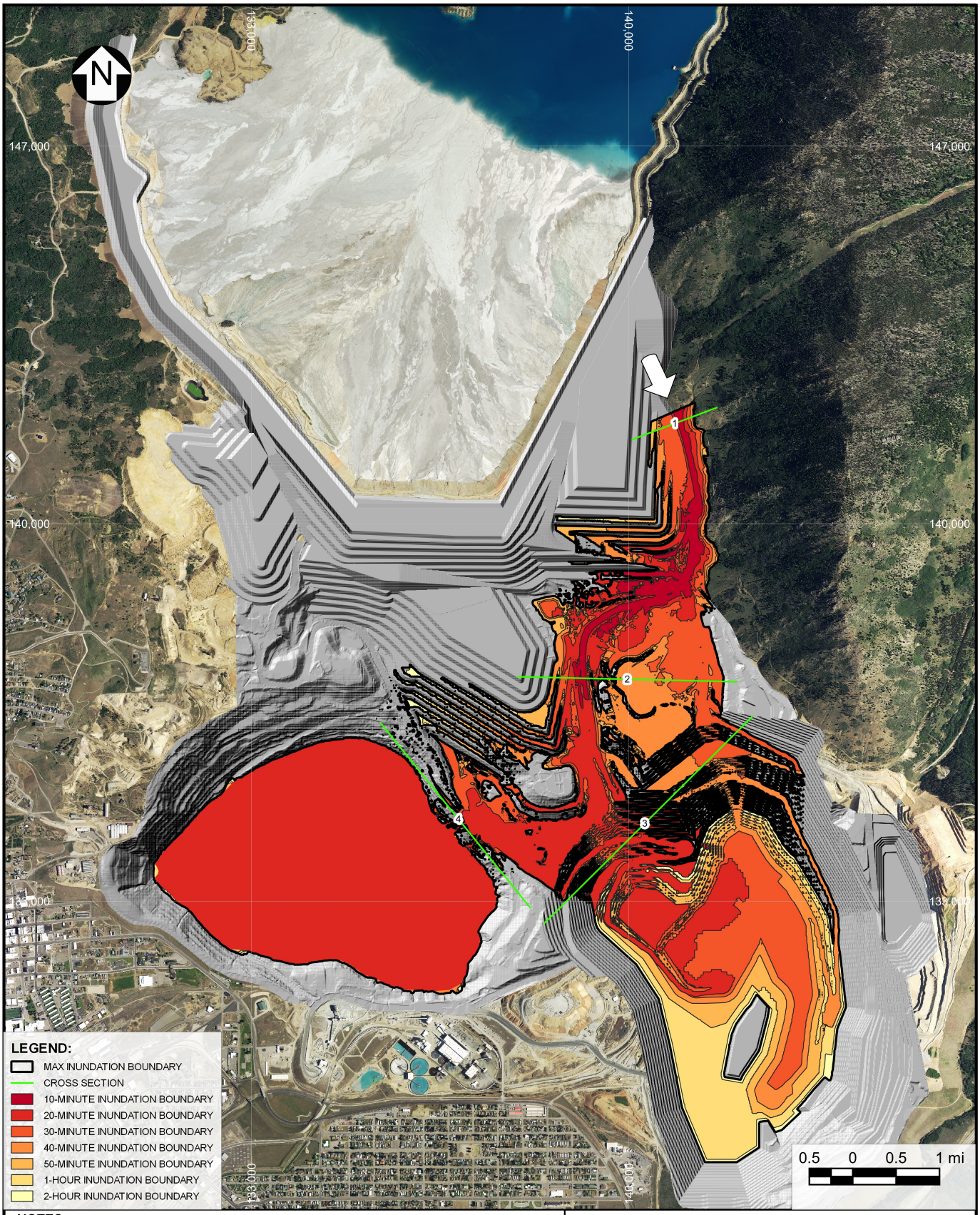

NOTES:

1. BASE MAP PROVIDED BY MONTANA RESOURCES, LLC ON AUGUST 7, 2024.
2. DAM AND ROCK DISPOSAL SITES ARE PROJECTED SURFACES AT THE TIME OF THE BREACH.
3. COORDINATE GRID IS IN FEET. COORDINATE SYSTEM: ANACONDA MINE GRID.
4. THIS FIGURE IS PRODUCED AT A NOMINAL SCALE OF 1:100,000 FOR 8.5x11 (LETTER) PAPER. ACTUAL SCALE MAY DIFFER ACCORDING TO CHANGES IN PRINTER SETTINGS OR PRINTED PAPER SIZE.
5. THIS FIGURE MUST BE READ IN CONJUNCTION WITH KP REPORT VA101-00126/24-7, DATED DECEMBER 2024.

REV	DATE	DESCRIPTION	DESIGNED	DRAWN	REVIEWED
0	19DEC'24	ISSUED WITH REPORT	DBM	DBM	VM

MONTANA RESOURCES, LLC

MONTANA RESOURCES

FLOOD INDUCED DAM BREACH FLOOD WAVE ARRIVAL TIME

Knight Piésold CONSULTING

P/A NO.	REF NO.
VA101-00126/24	7

FIGURE B3 REV 0

M:\101\00126\24\A\GIS\Figs\Report 7